BUILDING MATERIALS LABORATORY
THE TECHNICAL UNIVERSITY OF DENMARK

AALBORG PORTLAND

Technical Report 277 • 1992 ISSN 0908-3871

CBL Report no. 51

Pore Structure in Cement Based Materials

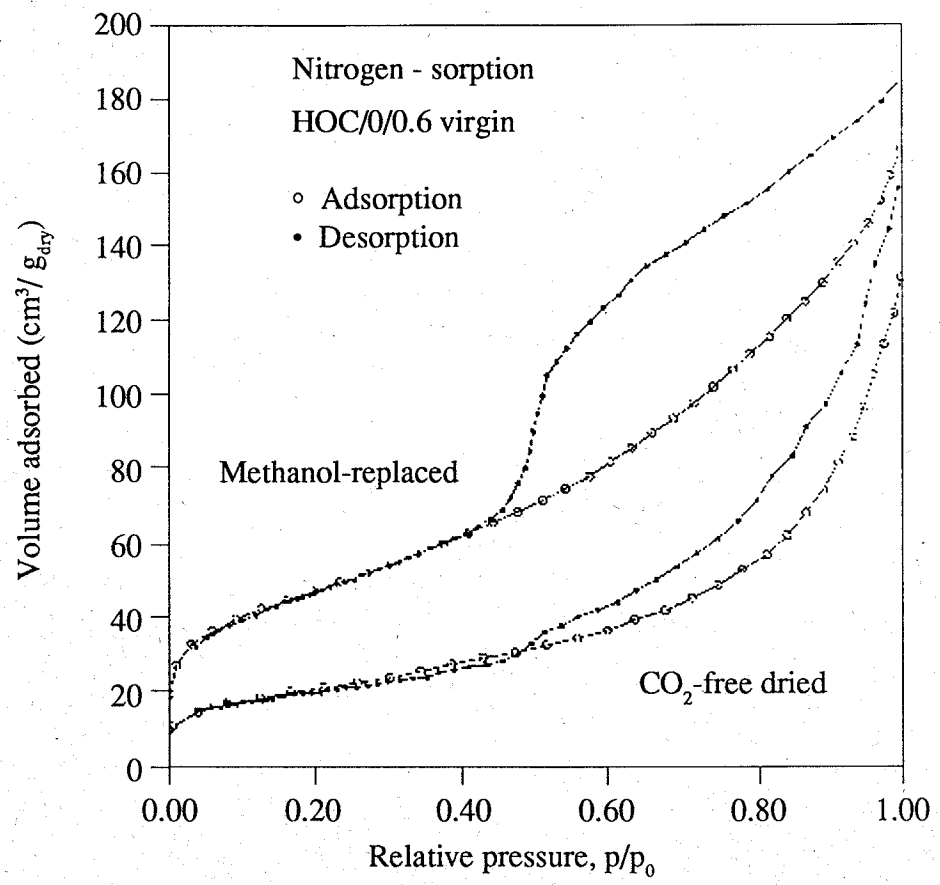

Industrial Research Education Programme
M.Sc. Jens Villadsen
Ph.D. no. 299, 05-12-1992

Committee on Industrial Research Programme, Danish Academy of Technical Science

ATV

BUILDING MATERIALS LABORATORY
THE TECHNICAL UNIVERSITY OF DENMARK

AALBORG PORTLAND

Technical Report 277 • 1992 ISSN 0908-3871

CBL Report no. 51

Pore Structure in Cement Based Materials

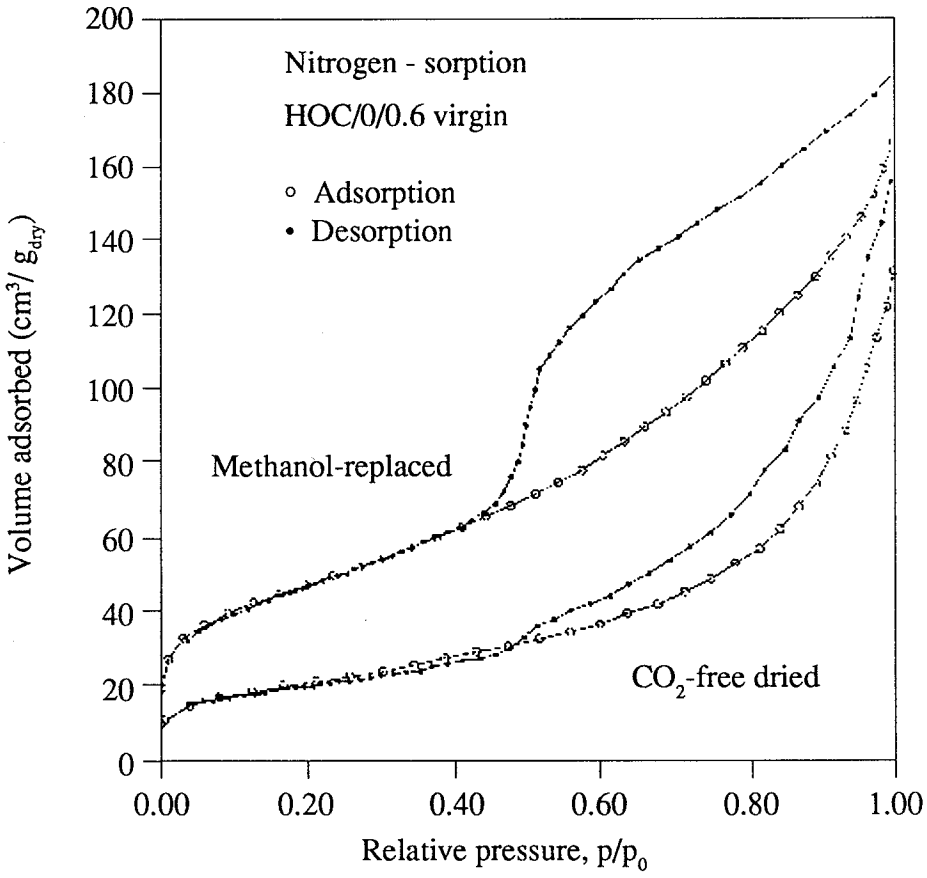

Industrial Research Education Programme
M.Sc. Jens Villadsen
Ph.D. no. 299, 05-12-1992

Committee on Industrial
Research Programme,
Danish Academy of Technical Science
ATV

LIST OF NOTATIONS

In the text, the following notations are used:

CBL	Cement and Concrete Laboratory
CZE	Technical University of Prague
LBM	Building Materials Laboratory
USA	University of Michigan
CAL	Low temperature microcalorimetry
COOL	CAL during cooling
CPSD	Cumulative pore size distribution
CUP	Inverted Cup Method
HCP	Hardened cement paste
HEAT	CAL during heating
H2O-SORP	Wateradsorption
KCC	Kelvin Capillary Condensation Analysis
MIP	Mercury intrusion porosimetry
NMR	Nuclear Magnetic Resonance
N2-SORP	Nitrogenadsorption
REM	Radioactive Emanation
SANS	Small-Angle Neutron Scattering
SAXS	Small-Angle X-ray Scattering
BILAG3	Grounded ROC ("Bilag 3 cement")
BLC	Fillercement ("Blokcement")
HOC	White cement
OPC	Ordinary Portlandcement
PFC	Portland flyash cement
P30-4A	Offshore-cement/Norway
ROC	Rapid hardening cement
SAC	Low alkali, sulfate resistant cement
HC	Hydroxycarboxylate-based plasticizer
LS	Lignosulphonate-based plasticizer
M	Sulphonated melamine formaldehyde-based superplasticizer
N	Sulphonated naphtalene formaldehyde-based superplasticizer
a	Constant (kg/s) used in CUP
A	Area (m^2)
C_{pA}	Apparent heat capacity ($J \cdot K^{-1} \cdot g_{ssd}^{-1}$)
D	Coefficient of diffusion (m^2/s)
E_i	Calorimetric output signal (μV)
Fo	Fourier number
$k_d(h)$	Water vapour diffusion coefficient calculated from CUP when $p/p_0 = h$ % in the evaporation front ($kg \cdot Pa^{-1} \cdot m^{-1} \cdot s^{-1}$)
K(h)	Water permeability coefficient from CUP when $p/p_0 = h$ % in the evaporation front ($kg \cdot Pa^{-1} \cdot m^{-1} \cdot s^{-1}$)
L	Length or thickness (m)
MT	Monolayer thickness (Å)
P	Pressure (psi), used in MIP
p/p_0	Relative vapour pressure
p_1, p_2	Water vapour pressures (Pa) used in CUP
q	Flux ($kg \cdot m^{-2} \cdot s^{-1}$) used in CUP

r_K	Kelvin radius (Å)
r_p	Pore radius (Å)
$\overline{r_p}$	Mean value (Å) of two pore radii in a temperature interval
S_{BET}	Specific BET-surface area (m^2/g_{dry})
s_M	Calorimeter sensitivity (μV/mW)
t	Adsorbed layer at surfaces, t-layer (Å)
t_{nf}	Non-frozen layer (Å) at surfaces
T	Temperature (°C)
v	Specific volume (cm^3/g_{dry})
v_{MIP} (>30 Å)	Specific volume (by MIP) of pores larger than 30 Å
v_{N2} (<30 Å)	Specific volume (by N2-SORP) of pores smaller than 30 Å
V_m	Monolayer capacity (g/g_{dry})
w_{ads}	Amount of water adsorbed (g/g_{dry})
w_{de}	Residual water content of specimen after drying at 50 °C and relative humidity of 11 % for 3 days (g/g_{dry})
w_{em}	Mean value of evaporable water content (kg/kg_{dry})
w_{es}	Total evaporable water content (g/g_{dry})
w_f	Frozen water content (g/g_{dry})
w_n	Non-evaporable water content (g/g_{ign})
w_{nf}	Non-frozen water content (g/g_{dry})
W_{cap}	Mass of water (kg) in the region of capillary suction
W_{dif}	Mass of water (kg) in the region of vapour diffusion
W_{dis}	Weight of specimen (kg) when the cup has been dismantled
W_{dry}	Weight of specimen (kg) upon drying at 105 °C (CUP)
W_{ssd}	Saturated, surface-dry weight (g_{ssd})
W_{sub}	Weight of saturated specimen (kg), submerged in water
W_3	Total mass of water (kg) in specimen used in CUP
W/C	Water-cement-ratio by weight
W/P	Water-powder-ratio by weight
$\Delta_f h$	Molar heat of fusion (J/mole)
ΔP	Difference in hydrualic pressure (Pa) used in CUP
ΔS_p	Change in pore surface area (m^2/g_{dry})
Δt_{nf}	Change in non-frozen layer (Å)
Δw_f	Change in amount of frozen water (g/g_{dry})
Δw_{kf}	Change in amount of frozen capillary condensed water (g/g_{dry})
Δw_{pf}	Change in pore volume (g/g_{dry})
Δw_{tf}	Change in amount of non-frozen water (g/g_{dry})
ε	Porosity (% by volume)
$\Sigma\Delta S_p$	Cumulative pore surface area (m^2/g_{dry})
$\Sigma\Delta w_p$	Cumulative pore volume (cm^3/g_{dry})
ρ_d	Dry density (kg_{dry}/m^3)
ρ_s	Solid density (g/cm^3)
ρ_{ssd}	Saturated, surface-dry density (g/cm^3)
$\hat{\rho}_{ssd}$	Estimated saturated, surface-dry density (g/cm^3)
ρ_w	Density of water (g/cm^3)
σ	Surface tension (N/m)
τ	Time (s)
θ	Contact angle used in MIP
υ	Molar volume (m^3/mole)
D/R	Dried/resaturated specimen
V	Virgin specimen

ADDENDUM

After printing the present report it was found necessary to add this Addendum.

In connection with the calculation of the pore size distribution curves from nitrogen sorption analysis (figures 4.2.6A-D) it is seen that the capillary pore volume (V_{CAP}) at lowest pore radius is larger than the total adsorbed volume of liquid nitrogen (V_{ADS}) from the volume-thickness (V-t) plots (figures 5.1.3.1A-D). From table A (column 2 and 3) it is seen that $V_{CAP} > V_{ADS}$ for the 4 different cement paste systems in question. This is not permissible.

Especially for the system "HOC/0/0.4 virgin" we have:
- V_{CAP} in figure 4.2.6A = 0.152 cm^3/g (at r_{pore} = 9 Å ~ p/p_0 = 0.08).
- V_{ADS} in figure 5.1.3.1A = 0.116 cm^3/g (at t = 21.3 Å ~ p/p_0 = 0.96).

The calculations, which are the basis for the nitrogen sorption curves in figures 4.2.6A-D have been made from the test reports as shown in Appendix G p. 264.

The numerical size of V_{CAP} is of course depending on how far down the calculation is continued (for "HOC/0/0.4 virgin" down to p/p_0 = 0.08). In reality and according to the V-t-analysis (figure 5.1.3.2) the calculation of the pore size distribution from nitrogen sorption based on Kelvin Capillary Condensation Analysis could **only** be applied in the pore size range (~ p/p_0 range) where capillary condensation takes place.

This means that for "HOC/0/0.4 virgin" the calculation could only take place in the p/p_0 range where capillary condensation takes place according to the appropriate V-t-plot (shown in figure 5.1.3.1A); this means from saturation (p/p_0 = 1.00) down to p/p_0 = 0.58 (~ $\hat{t}$ = 9 Å, read from figure 5.1.3.1A).

This means that a more correct estimate of the capillary pore volume is V_{CAP} = 0.115 cm^3/g read from figure 4.2.6A for $r_{pore} = \hat{r}_{pore}$ = 27 Å (~ p/p_0 = 0.58).

In table A the above mentioned calculation for "HOC/0/0.4 virgin" is shown along with similar calculations for the 3 other systems.

1	2	3	4	5	6
SYSTEM	$V_{CAP}(p/p_0)$ cm^3/g	$V_{ADS}(p/p_0)$ cm^3/g	$\hat{t}(p/p_0)$ Å	$\hat{r}_{pore}(p/p_0)$ Å	$V_{CAP}(p/p_0)$ cm^3/g
HOC/0/0.4 virgin	0.152(0.08)	0.116(0.96)	9 (0.58)	27 (0.58)	0.115(0.58)
HOC/0/0.4 D/R	0.144(0.04)	0.101(0.96)	9 (0.58)	27 (0.58)	0.108(0.58)
HOC/0/0.6 virgin	0.231(0.08)	0.177(0.97)	9 (0.58)	27 (0.58)	0.177(0.58)
HOC/0/0.6 D/R	0.220(0.08)	0.170(0.97)	7.5(0.40)	18 (0.40)	0.209(0.40)

Table A

It is seen that if a more correct (according to the V-t-analysis) estimation of V_{CAP} (shown as column 6) is applied, then a better correspondance between V_{ADS} and V_{CAP} (column 3 and 6) is observed. However the system "HOC/0/0.6 D/R" makes an unexplainable exception.

PREFACE

This report is the documentation for the work done in the Industrial Research Education Programme no. EF299 entitled "Pore structure in cement based materals", which was initiated in August 1989. In connection to the report a seperate report containing all the appendices can be ordered.

The research project has partly been financed by the Danish Academy of Technical Science and was carried out in as a formalized cooperation between the Cement and Concrete Laboratory (CBL) at Aalborg Portland A/S and the Building Materials Laboratory (LBM) at the Technical University of Denmark.

Some of the investigations carried out in the project are not mentioned in this report, since the results of these investigations are of potential commercial interest for Aalborg Portland A/S.

A full, though confidential, report comprising all investigations carried out in this project has been written and distributed to relevant parties. The present report constitutes an edited version of the confidential report. Accordingly, some sections, tables and figures are omitted.

After the public presentation of this project it was decided to extend and revise the underlying report (dated May 1992) on a few items. The present report is therefore the final report for this research project.

I wish to express my gratitude to my supervisors; Manager of the Concrete Technology Department, Ph.D. Dirch H. Bager, CBL and Associate Professor, Ph.D. Kurt Kielsgaard Hansen, LBM, who never failed to advise and support me in my work.

Furthermore, I would like to thank members of the staff at CBL and LBM, including M.Sc. students at LBM, who had helped me during the project.

Aalborg, December 1992

Jens Villadsen

TABLE OF CONTENTS

ABSTRACT

The report presented here deals with the pore structure of cement based materials, mainly hardened cement paste and mortar.

Two main investigations were carried out:

1) Pore structure stability upon drying/resaturation
2) Correlation between pore structure and water permeability

The following techniques have been used for the identification of pore structure:

- Ice formation by Low Temperature Microcalorimetry
- Mercury Intrusion Porosimetry
- Nitrogen Adsorption
- Water Adsorption

Initially, these techniques were compared using very mature, room temperature and water cured 0.4 and 0.6 water-cement-ratio pastes. Before analysis, specimens for mercury intrusion porosimetry and nitrogen adsorption were CO_2-free dried from both water-saturated and methanol-saturated states.

It was generally found that relative poor agreement existed between different techniques. In respect to cumulative pore size distributions the difference between nitrogen adsorption analysis and mercury intrusion porosimetry was found to be affected mainly by the choice of drying technique and the contact angle used for mercury intrusion porosimetry.

For specimens of comparable moisture history, pore size distribution calculated from low temperature microcalorimetry is comparable to pore size distributions optained from mercury intrusion porosimetry or nitrogen sorption analysis.

Furthermore, inter-laboratory calibration of ice formation by low temperature microcalorimetry showed good correspondance.

A systematic preliminary survey of the pore structure stability of room temperature and water cured cement pastes upon drying/resaturation was carried out for 8 commercially available cements, including the range of cements manufactured by Aalborg Portland A/S and a Norwegian offshore cement. Effects of water-cement-ratio, plasticizer and superplasticizer were investigated.

This survey revealed that especially Portland flyash cement has a stable microstructure upon drying/resaturation.

Additionally, a systematic survey was carried out on cementmortar, in order to correlate pore structure and water transport characteristics using inverted cup method. Effects of drying/resaturation, water-cement-ratio, workability, plasticizer, superplasticizer and type of cement were investigated.

It was found that Portland flyash cement mortar showed a higher degree of pore structure stability and a smaller increase in water permeability upon drying/resaturation compared to mortars made from Rapid hardening cement and Low alkali sulphate resistant cement.

RESUME

Denne rapport omhandler porestrukturen af cementbaserede materialer, især hærdnet cementpasta og cementmørtel.

Der er udført to hovedforsøgsserier:

1) Porestruktur-stabilitet overfor udtørring/genmætning
2) Sammenhæng mellem porestruktur og vandpermeabilitet

Til identifikation af porestrukturen er der benyttet følgende metoder:

- Isdannelse ved lavtemperatur mikrokalorimetri
- Kviksølvporøsimetri
- Nitrogenadsorption
- Vandadsorption

Indledningsvis blev disse metoder afprøvet og sammenlignet ved hjælp af velhydratiserede, stuetemperatur- og vand-lagrede cementpastaprøver med vand-cement-tal på 0.4 og 0.6. Før analyse blev emnerne til kviksølvporøsimetri og nitrogenadsorption udtørret. Denne tørring foregik ved CO_2-fri tørring fra både vand- og methanolmættet tilstand.

Generelt viste de forskellige metoder en relativ dårlig overensstemmelse. Med hensyn til den akkumulative porestørrelsesfordeling kan man konstatere, at forskellen mellem nitrogenadsorption og kviksølvporøsimetri især afhænger af den anvendte tørringsmetode og den kontaktvinkel, der er valgt ved kviksølvporøsimetri.

For emner med sammenlignelig fugthistorie er porestørrelsesfordelingen beregnet udfra lavtemperatur mikrokalorimetri sammenlignelig med porestørrelsesfordelinger opnået ved hjælp af kviksølvporøsimetri eller nitrogenadsorption.

Sammenlignende forsøg mellem to laboratorier af isdannelsen ved lavtemperatur mikrokalorimetri viste god overensstemmelse.

En indledende systematisk undersøgelse af porestruktur-stabiliteten af stuetemperatur- og vand-lagrede cementpastaer overfor udtørring/genmætning blev udført for 8 kommercielle cementtyper, heriblandt samtlige cementer fra Aalborg Portland A/S og en norsk off-shore cement. Indflydelse af vand-cement-tal, plastificeringsstoffer og superplastificeringsstoffer blev undersøgt.

Denne undersøgelse viste, at især Portland flyveaske cement havde en stabil mikrostruktur overfor udtørring/genmætning.

Endvidere blev der udført en systematisk undersøgelse af cementmørtler for at sammenholde porestrukturen med vandtransport-karakteristika målt med omvendt-kop metoden. Indflydelse fra udtørring/genmætning, vand-cement-tal, bearbejdelighed, plastificeringsstoffer, superplastificeringsstoffer og cementtype blev undersøgt.

Denne undersøgelse viste, at især Portland flyveaske cementmørtel ud-

viste en højere grad af porestruktur-stabilitet og en mindre stigning i vandpermeabilitet ved udtørring/genmætning sammenlignet med mørtler af Rapid og Lav alkali sulfatbestandig cement.

INTRODUCTION

Cement based materials like concrete and mortar are widely used in the building industri today. For more specific applications, also Cembrit^{R} and Densit^{R} are used.

Because of the extensive use of especially concrete, society must demand longterm durability of the constructions, in which concrete is used. This urges for fundamental research in order to understand the practical behavior of cement based materials, especially concrete.

All cement based materials are porous, i.e. they contain pores of different sizes and shapes. The simplest cement based material consists of cement and water. When cement and water are mixed the subsequent material is called hardened cement paste (HCP). Appropriate aggregates (i.e. sand, stone, microsilica, fibers etc.) are normally added in order to gain specific properties, mostly regarding strength and stiffness. These aggregates will be glued together by HCP.

Initially, HCP is a solution of cementparticles in water. As the chemical reaction - the socalled hydration proces - between cement and water proceeds, the solution gradually stiffen and transformes into a solution filled porous material. This stiffening is caused by the formation of hydration products (the socalled cement gel) growing into the solution filled pores of the porous material, thus dividing these pores (socalled capillary pores) into smaller ones as hydration proceeds.

The cement gel consists of hydrated cement (mainly calcium silicate hydrates and calcium hydroxide) in its densest state and include the socalled gel pores, located between the solid gel particles. Normally, it is assumed that the size of the gel pores are in the range of approximately 0.5 to 2 nm (10^{-9} m), while capillary pores are in the size range of approximately 2 nm to 5 μm (10^{-6} m). For comparison, the size of a water molecule is around 0.3 nm and the size of an unhydrated cement grain is around 10 μm.

In this project, the pore structure refers only to gel pores and capillary pores and does not include air pores or other larger voids in the material. The general pore structure model outlined by Powers and Brownyard /48/ is assumed to give a full description.

Knowledge of pore structure of a porous material is of great importance as a key for understanding the practical behavior of the material. It is well known, that there is a link between pore structure parameters (porosity, pore shape, pore size distribution) and the mechanical and physical behavior of the material.

The term "true pore structure" of HCP should be used only to describe the state of a pore stucture left undisturbed. Consequently, true pore structure is the pore structure of a saturated virgin (never allowed to dry) cement paste. In practice, true pore structure is almost never encountered, since the cement based material (for instance concrete) is allowed to dry and is generally susceptible to many kinds of environmental influences.

However, the term true pore structure of HCP is of value, since it designates a kind of "basic pore structure", which enable us to see the pore structure potential of an actual cement paste cured in optimal conditions in a controlled environment. This possibility is very important, since it provides us with information of the potential material behavior.

When comparing pore structure and material behavior it is off course essential that the measured pore structure will be the one of interest for the researcher, namely; the pore structure that the cement based material originally is having, when its physical or mechanical behavior is being measured.

Accordingly, this "original pore structure" seems to be well-defined on the theoretical level.

However, when it comes to the practical measurement of this original pore structure some obstacles are encountered which, especially for the structurally unstable cement based materials, have an deterioating effect on the original pore structure of interest. Consequently, it is very important to distinguish between the original and the measured pore structure.

Hence, the measured pore structure may give a complete erroneous picture of the original pore structure of interest. Furthermore, if the measured pore structure then is compared to material behavior and if a correlation between the two is established, this correlation may also be quite erroneous due to the fact that the measured pore structure does not represent the original pore structure.

Some main factors are influencing the measured pore structure. The original pore structure could be altered more or less significantly mainly by the preparation technique (mostly: complete drying), since cement based materials are structurally unstable towards drying /8,9,10/.

The methods of pore structure characterization itself may also effect the measured pore structure, since these methods are indirect, which implies that they are based on physical relationsships and geometrical models that simplifies the complexity of HCP pore structure.

Hence, a great diversity exists between the original and the measured pore structure unless the preparation (drying) of the material is omitted or at least performed in a way less damaging for the original pore structure.

A further complication is that different pore structure characterization techniques are known to produce different results for the same material.

In order to be able to understand the complicated correlation between pore structure and material behavior Bager /49/ concluded in 1983 that there is a urgent need for research work leading to a) the correlation of different methods for pore structure characterization, b) establish-

ment of standards for treatment and conditioning (comparable to the natural weathering of the material) of the material before investigation and c) establishment of a method for drying the materials in such a way that it does not mask or remove the effects optained in b).

The present project deals with a) and, to a certain extent, b). Furthermore, some examples of the relation between pore structure parameters and the physical behavior of the material are investigated.

The general idea is to take the first basic steps towards correlating pore structure and material behavior. These initial steps involve what the author finds to be the first major obstacle to overcome before any structure/behavior-correlation can take place, namely the correlation between different methods of pore structure characterization.

Bager /49/ found that these preliminary investigations were necessary in order to increase the knowledge of pore structure of hardened cement paste and other cement based materials, and thereby increase the knowledge of the correlation between the relevant pore structure (gel pores and capillary pores) and the physical and mechanical behavior of a cement based material.

The scientific basis for the innovation of this project were laid down by Sellevold, Fontenay and Bager /8,18,19,44,45/. These researchers made the first attempts to describe the fundamentals of HCP pore structure using the low temperature microcalorimetry technique.

Furthermore, these researchers mainly concentrated their efforts on the systematic mapping of ice formation (pore structure) response resulting from variations of different parameters (water/cement-ratio, degree of hydration, steam curing, moisture content, drying, microsilica).

Fontenay and Sellevold /44/ started the first investigations of ice formation measurement in HCP using the low temperature microcalorimeter. Initially, these investigations focussed on the instrumental side. Subsequently, as a routine test procedure was established, a systematic investigation was performed on virgin cured (never allowed to dry) watersaturated HCP. Pastes of different water/cement-ratios and different degrees of hydration were investigated.

Bager and Sellevold /45/ studied the influence on ice formation from steam curing of pastes having different water/cement-ratios. Before measurement these pastes were brought to equilibrium at different levels of moisture contents.

Sellevold and Bager /19/ also demonstrated that low temperature microcalorimetry could be used for pore structure analysis.

Bager /8/ studied the ice formation in mature room temperature cured HCP at different moisture levels. Furthermore, the effect of drying and resaturation (either slow or rapid) on the ice formation in mature room temperature cured HCP was investigated.

Sellevold and co-workers /58/ studied the ice formation in both virgin

and dried/resaturated pastes containing different dosages of microsilica.

Villadsen /16/ studied the ice formation in both virgin and dried/resaturated pastes with or without microsilica and cured at different levels of temperature.

The new aspects of this project compared to the investigations of Sellevold, Fontenay and Bager are that - for the first time - a systematic research project will focus on the influence of different cement types on the pore structure of HCP by low temperature microcalorimetry. Furthermore, it is also a new approach in this project that low temperature microcalorimetry - in a systematic way - is being compared to other methods of pore structure characterization. On the basis of these results low temperature microcalorimetry will be used to compare pore structure and permeability.

In this project, low temperature microcalorimetry will be used in two ways. In the qualitative use of the method the ice formation and the ice formation pattern of different cement pastes will be compared relatively to each other. In the quantitative use of the method (only used in connection with the comparison with other methods of pore structure characterization) ice formation data will be transformed into a cumulative pore size distribution curve using a specific calculation technique.

Low temperature microcalorimetry seems to be an unique method for estimating the pore structure of HCP, since analysis can take place using water saturated virgin specimens. This is in contrast to the other methods currently used (mercury intrusion porosimetry, nitrogen- and water-sorption). These methods require drying of the material before analysis. This drying will - as mentioned before - cause distortion of the pore structure and the result of the analysis may therefore show a pore structure completely different from the pore structure of interest.

The long term commercial aspect of the project is to be able to design cements having special performances with regard to physical and mechanical behavior of the cement based material as for instance low water permeability or low shrinkage upon drying. This could be done when the correlation between pore structure and permeability or between pore structure and shrinkage has been established.

1. Status and experimental series

The full description of this industrial research education programme is outlined in detail in the Education Plan (Appendix A, in Danish) by the present author and by the representatives of CBL, Aalborg Portland A/S, and LBM at The Technical University of Denmark (Dirch H. Bager and Kurt K. Hansen, respectively).

This project had the following main context:

(i) Testing and cocalibration of different methods for pore structure characterization in hardened cement paste (HCP) and cementbased materials. The methods are:

- Ice formation by Low temperature Microcalorimetry (CAL)
- Mercury Intrusion Porosimetry (MIP)
- N_2 - and H_2O-adsorption (N2-SORP and H2O-SORP)

(ii) Investigation on the influence of drying on the pore structure.

(iii) Comparison between pore structure and some physical/mechanical proporties (mainly permeability) of the material.

When comparing the goals of the Education Plan to the actual context of the project it is observed that some parts of the Education Plan were not carried out.

In the following a brief status of each of the phases described in the Education Plan (section 10: "Projektets faser") will be given.

Phase 1: "Measurement of pore structure - different techniques"

This phase was planned to include the following techniques

- ice formation by Low Temperature Microcalorimetry (CAL)
- ice formation by Nuclear Magnetic Resonance (NMR)
- Small-Angle Neutron Scattering (SANS)
- Small-Angle X-ray Diffraction (SAXS)
- Radioactive Emanation (REM)
- Mercury Intrusion Porosimetry (MIP)
- Water Adsorption (H2O-SORP)
- Nitrogen Adsorption (N2-SORP)
- Scanning Electron Microscopy (SEM)

From these techniques, only CAL, MIP, N2-SORP and H2-SORP have been used in the project.

REM was given up at an early stage, since this technique is limited to the very early ages of the hardening paste. This project deals with mature hardened cement paste.

Neither CBL nor LBM had any equipment for NMR, SANS and SAXS. Accor-

dingly, different institutions in Europe and USA were contacted in order to perform the needed experiments. Due to local closedown of activities and lack of response it was not possible, within this project, to perform any experiments using these three techniques. However, at the end of this project, contacts were finally made at Risø National Laboratory, Denmark and the Norwegian Building Research Institute (NBI), Norway for SANS and NMR, respectively. For NMR, samples were send, but results are not received at the present moment.

It was decided by the author not to introduce further techniques (thus excluding SEM, even though it is available at CBL). Instead, it was considered best to use more time on the three main techniques mentioned above, namely CAL, MIP and N2-SORP.

Hence, the main techniques used were: CAL, N2-SORP and MIP. Much time was used with these techniques. In this project, instruments for both CAL and N2-SORP were installed and calibrated at CBL, and Testing Manuals were made (Appendices B,C,D,F).
The installation and calibration of the CAL-instrument was a part of the Education Plan. At LBM, some time was spend on renovation of the MIP-instrument. At the same time, laboratory personel at both LBM and CBL was instructed in the use of the three techniques. Accordingly, a large part of the test data presented here have been generated by laboratory personel under guidance of this author.

Cocalibration of the three main techniques: CAL, N2-SORP and MIP was carried out using 8 years old, room temperature cured, 0.4 and 0.6 water-cement-ratio (W/C) cement pastes made from Danish white cement.

For CAL, the equipment at CBL was compared with similar equipment at LBM. For MIP, the equipment at LBM was compared with equipment at The University of Michigan (USA). For MIP, samples were also send to The Technical University of Prague (CZE), but comparable results are not received at the present moment.

Phase 2: "Special investigations"

This phase was planned to include

- Methods of conditioning (for achievement of the pore structure of HCP in (concrete) practice)
- Drying methods
  - D-drying (drying above dry ice)
  - P-drying (drying above magnesium perchlorate)
  - Methanol-replacement
  - Acetone-drying
  - CO_2-free drying

Only one attempt was made to estimate how virgin cured cement paste shall be treated in the laboratory, before it can be considered to be representative of cement paste in (concrete) practice.
This consisted in drying the saturated specimen at 50 °C and at 11

% r.h. for 3 days before resaturation. This has earlier been used by this author /16/ and was known to produce substantial changes in pore structure measured by CAL.

Only two methods were used in this project to dry samples before measurements (MIP, N2-SORP and H2O-SORP). They were: CO_2-free drying and methanol-replacement. Some time was used to design and construct the experimental setup for D-drying, but no experimental data were optained using this method of drying. P-drying and acetone-drying were not dealt with at all. Consequently, the main drying method used were CO_2-free drying. For comparison methanol-replacement was also introduced for some experimental series.

Phase 3: "Pore structure design"

This phase was planned to include

- An attempt to control pore structure and thereby gain special proporties concerning shrinkage, permeability and creep. Different cements and different chemical and mineralogical additives are to be used.

Initially, a survey of the pore structure characteristics of cement pastes made from different (commercially available) cements and (for some cements only) using different water-reducers, was carried out at both CBL (CAL and N2-SORP) and at LBM (CAL and MIP). The range of cements manufactured by Aalborg Portland A/S were investigated. Furthermore, a Norwegian off-shore cement was investigated.

In this preliminary survey, the effect of drying on pore structure was investigated for the different HCP-blends mentioned above.

Due to lack of time no investigations took place in order to correlate pore structure and creep.

1.1 Experimental series

The present work has involved a number of individual investigations, each having a specific purpose. These are described in the following.

1.1.1 Drying methods

Numerous studies (/1,2,3,4,5,6,7/) have shown that the method by which the evaporable water is removed from HCP has a significant effect on pore structure parameters derived from test methods where such a preliminary drying is necessary before the method can be applied. This is the case for MIP, N2-SORP and H2O-SORP.

In this serie the following drying methods are compared:

- CO_2-free drying (described in section 2.3.1)
- Methanol-replacement (described in section 2.3.2)

The comparison consisted in the estimation of total evaporable water content and pore structure characterization by N2-SORP and MIP on identical specimens using the two drying methods.

1.1.2 Pore structure characterization methods

The purpose of this serie was to compare the following methods:

- Low temperature Microcalorimetry (CAL)
- Mercury Intrusion Porosimetry (MIP)
- Nitrogenadsorption (N2-SORP)
- Wateradsorption (H2O-SORP)

CAL was performed at CBL and LBM.
MIP was performed at LBM and at the University of Michigan (USA).
N2-SORP was performed at CBL.
H2O-SORP was performed at CBL.

1.1.3 Pore structure stability (CBL-serie)

It is a well known fact that the hydrates in HCP are structurally unstable. Upon first drying (desorption) from the water saturated state large shrinkage is often seen.

Generally, it is accepted, that drying shrinkage is due to breakdown of the pore structure on the microstructural level, upon drying from the water saturated state.
This breakdown of very small pores, thus creating larger and more continuous pores (/8,9,10/), is normally accompanied by a decrease in specific BET-surface. Feldman and Swenson /11/ found, that a large BET-surface (by nitrogen) indicated a large drying shrinkage.

A possible explanation for this breakdown is shown schematically in

figure 1.1.3.1.

The purpose of this serie was to find a HCP-blend that showed a relatively high degree of pore structure stability towards a drying/resaturation treatment (as described in section 2.3.3).

For this reason, both virgin (never allowed to dry) and dried/resaturated specimens of the same HCP-blend were tested by the methods of CAL, MIP and N2-SORP. For MIP and N2-SORP the drying of the specimens before analysis could in fact mask the effects of the drying/resaturation treatment.

1.1.4 Pore structure stability (LBM-serie)

For practical reasons the author was not able to be engaged in prolonged experimental work at LBM. Instead, it was decided to carry out the needed experimental series as part of the work required for M.Sc.-students.

The purpose of this serie was the same as described in section 1.1.3. Furthermore, the influence of plasticizers and superplasticizers on pore structure, were investigated.

Pore structure was characterized by CAL and drying test were performed in order to calculate relative water vapour diffusion coefficients.

The results from this serie were previously reported by Holland /12/. This main part of this serie was carried out under guidance of the present author as a part of this project. At LBM, Kurt K. Hansen had the formal responsibility, and some of the experimental work was carried out under his guidance.

1.1.5 Additional investigations (LBM)

In connection with this project, and especially in connection with the activities described in section 1.1.4, additional investigations took place at LBM.

These investigations were partly supervised by the present author, and the practical studies were performed by M.Sc.-students at LBM. The results from the investigations have previously been reported by Holland /12/ and by Rosenbom and Waldstrøm /13/.

Holland investigated the permeability of cementmortars using CUP (see section 3.7).

Rosenbom and Waldstrøm also investigated the permeability of cement mortars using CUP. Furthermore, the pore structure of some of the mortars were characterized by CAL.

The main purpose was to get further information of pore structure in cementbased materials. Special interest was taken into the pore structure and the permeability of cementmortars as compared to HCP.

It is well known, that HCP in mortar has a pore structure different from that of plain cement paste, mainly due to the contact zone between cement paste and aggregate.

Sellevold and Bager /14/ found that the primary ice formation by CAL of mortars was greater than that of plain cement paste. This was believed to be caused by the existence of larger pores in the cement-paste/aggregate-interface.

Winslow and Liu /15/ found that cement paste in concrete was more porous than in plain, i.e. without aggregate, cement paste. Furthermore, they found that the pore structure in mortar were much closer to that of concrete than to the structure of plain cement paste.

2. Materials and sample preparation

In this chapter the applied materials and the experimental procedures involved for the different series are described along with details on the sample preparation for different methods of pore structure characterization.

2.1 Materials

2.1.1 Cements

The following types of cement have been used in the project:

Description:	Type:	Abbreviation:
Aalborg Portland:		
Portland flyash cement	PFC(A/MS/MA/G)*	PFC
Rapid hardening cement	PC(R/IS/MA/G)*	ROC
Sulfate resistent cement	PC(A/HS/EA/G)*	SAC
White cement	PC(R/HS/EA/W)*	HOC
Fillercement ("Blokcement")	DPC(D/IS/HA/G)*	BLC
Ordinary Portlandcement	PC(A/IS/MA/G)*	OPC
Grinded ROC ("Bilag 3 cement")	PC(E/IS/MA/G)*	BILAG3
Norway:		
Offshore-cement	P30-4A	P30-4A

*According to /41/

The chemical and mineralogical composition and some physical characteristics of the cements are shown in table 2.1.1.1.

2.1.3 Additives

In this project two plasticizers and two superplasticizers have been used. They are described in table 2.1.3.1.

2.1.4 Aggregate

Only quarts sand of the type normally used at CBL has been used as aggregate. It consists of three fractions. The sand is described in table 2.1.4.1.

2.2 Specimen fabrication

2.2.1 General

Fabrication of specimens for the methods used in the project, took place at both LBM and CBL.
Except for the specimens used for the cocalibration of different methods (see section 2.2.2), all the samples were made within this project.

Fabrication of cementmortar-specimens for the additional investigations at LBM (section 2.2.5) were described in detail by Holland /17/ and by Rosenbom and Waldstrøm /13/.

At LBM, mixing of pastes was performed by a vacuum-mixer (Whip-Mix). Mixing of pastes at CBL was performed by a ordinary DIN-mortar mixer.

During mixing, casting and setting special effort was made to avoid entrapped air and segregation in the fresh and hardening paste.

This included evacuation of the mixing water and the paste. The latter was carried out in a special apparatus (figure 2.2.1.1). Through an outlet in the bottom of this apparatus, cement paste specimens were cast in cylindrical teflon moulds while being vibrated. The moulds had diameters of either 14.5 or 22.6 mm and a length of approximately 100 mm.

The moulds were sealed and slowly rotated to avoid segregation for approximately 16 h before demoulding. This resulted in homogeneous specimens.

After demoulding, the specimens were placed in sealed containers filled with saturated lime water and cured at room temperature.

The equipment for the fabrication of the HCP-specimens at CBL is shown in figure 2.2.1.1 (photos).

The procedure for the fabrication of specimens at LBM were described in detail by Villadsen /16/ and by Holland /17/.

The fabrication of specimens at CBL was performed according to CBL Testing Manual no. 1.11.3 (Appendix B, in danish). (Preparation of this manual was included in the Education Plan).

Each HCP-blend was identified by a name: X/Y/Z, where X was the type of cement, Y was the type of admixture (chemical, mineralogical or none (0)) and Z was the water-powder-ratio (W/P) by weight.

In this way, for instance ROC/0/0.4 designated a plain ROC cement paste with no admixture and with W/P = water-cement-ratio, W/C = 0.4.

2.2.2 Specimens for cocalibration of different methods

Specimens mentioned here were used for the cocalibration of both drying methods and methods for pore structure characterization.

8 years old mature virgin hardened cementpastes made from Danish white cement were used. Water-cement-ratios were 0.4 and 0.6. The specimens were stored in sealed containers with saturated lime water.

The two different pastes were tested in both virgin and dried/resaturated states (according to section 2.3.3).
In this way, 4 different specimens were tested by each of the characterization methods.

When comparing different methods for pore structure characterization it is often seen in the literature that researchers are using porous vycor glass (PVG). In this project the above mentioned mature hardened cementpastes were used for practical reasons: Relevant relation to concrete practice and the fact that these pastes already had been been made by D. Bager in connection with a planned similar RILEM project which for a number of reasons never was initiated.

When it was necessary to dry the specimens before applying the method (as was the case for MIP, N2-SORP and H2O-SORP), this was done either by CO_2-free drying or by methanol-replacement according to the below mentioned scheme:

Method (place)	Drying method
MIP (LBM)	Both CO_2-free and methanol-replacement
MIP (USA)	CO_2-free
MIP (CZE)	CO_2-free
N2-SORP	Both CO_2-free and methanol-replacement
H2O-SORP	Methanol-replacement

2.2.3 Specimens for pore structure stability tests (CBL-serie)

The HCP-blends tested were made from 7 different commercial cements. They were (according to section 2.1.1): ROC, SAC, HOC, BLC, OPC, BILAG3 and P30-4A.

Normally, W/C was 0.4. Additionally, W/C of 0.3 and 0.2 were used for ROC and SAC. To achieve sufficient workability, a superplastisizer of the sulphonated melamine formaldehyde type (table 2.1.3.1) was used for the pastes with W/C = 0.2. A dosage of 4 and 6 % by weight of cement were used for SAC and ROC, respectively.

Cylindrical specimens of both 14.5 and 22.6 mm in diameter and approximately 100 mm in length were made. The specimens were cured in saturated lime water at room temperature for at least 82 days before being used.

2.2.4 Specimens for pore structure stability tests (LBM-serie)

The HCP-blends tested were made from 3 different commercial cements: ROC, SAC and PFC (according to section 2.1.1), using W/C = 0.4.

The water reducers used were two commercial superplasticizers based on sulphonated melamine formamaldehyde (M) and sulphonated naphtalene formaldehyde (N) condensates (table 2.1.3.1), one commercial lignosulphonate-based (LS) plasticizer and one "laboratorymade" hydroxycarboxylate-based (HC) plasticizer (table 2.1.3.1).
The used dosages of M, N, LS and HC were 2.0, 2.0, 0.4 and 0.07 % by weight of cement, respectively.

Cylindrical specimens of both 14.5 and 22.6 mm in diameter and approximately 100 mm in length were made. The specimens were cured in lime water at room temperature for at least 79 days before being used.

2.2.5 Specimens for additional investigations (LBM)

The cementmortars used by Holland /12/ were proportioned according to the Danish Standard (DS 411, /42/). This was not very successfull since it resulted in stiff mortars with a low workability. Hence, the results from the CUP-permeability studies using these specimens may show the effect of a low workability instead of the effect of different cement types.

For this reason, a different approach was taken when preparing the mix proportions for cementmortars to be used by Rosenbom and Waldstrøm /13/. These cementmortars were proportioned according to TI-B51, /43/, which is a Danish test method for alkali-aggregate reactivity of sand. A slump of 60 - 100 mm was aimed for, since almost equal workability was considered to be a necessity when comparing different mortars.

The mix-proportions and slumps for the various cementmortars mentioned above, are shown in table 2.2.5.1.

The mortars were moulded in 100x200 mm cylinder moulds while being vibrated. After demoulding, the cylinders were water-cured at 20 °C for at least 2 months.

The cementmortars tested were made from 3 different commercial cements: ROC, SAC and PFC.
Holland tested virgin cementmortars with W/C of 0.4 and with 4 different additives (according to table 2.1.3.1): M, N, LS, and HC.
The dosages were the same as the ones used for the plain cement pastes (section 2.2.4).
Rosenbom and Waldstrøm tested both virgin and dried/resaturated cementmortars with W/C of 0.4 and 0.6.

2.2.7 Specimens for Low temperature Microcalorimetry (CAL)

The specimens for CAL were made from cylinders (diameter = 14.5 mm).

They were cut to a lenght of 65 mm using a watercooled diamantsaw.

2.2.8 Specimens for Mercury Intrusion Porosimetry (MIP)

2.2.8.1 Specimens for MIP at LBM

Specimens for MIP at LBM were dried according to sections 2.2.8.1.1 and 2.2.8.1.2.
Just before testing predried specimens were roughly crushed and pieces of about 3 mm (equivalent diameter) were manually selected for the analysis. These pieces were degassed at room temperature using a vacuum pump and finally an oil diffusionpump.

2.2.8.1.1 Cocalibration of different methods

The specimens were made from the specimens used for CAL at LBM. These specimens were cut into four pieces along with and perpendicular to the cylinder axis. Drying was carried out at LBM using either CO_2-free drying or methanol-replacement, see section 2.3.1 and 2.3.2. The samples were kept in a vacuum desiccator over silica gel until testing.

2.2.8.1.2 Pore structure stability tests (CBL-serie)

These specimens were cylindrical (diameter = 22.6 mm and 2-3 mm in thickness) discs. They were dried by CO_2-free drying at CBL and kept in a vacuum desiccator over silica gel until testing.

2.2.8.2 Specimens for MIP at USA

The specimens were made from the specimens used for CAL at CBL. These were cut into pieces as described in section 2.2.8.1.1 and dried by CO_2-free drying. No further crushing was carried out before analysis.

2.2.9 Specimens for Nitrogenadsorption (N2-SORP)

The samples for N2-SORP were made from cylinders (diameter = 22.6 mm). Discs (2-3 mm in thickness) were cut from the cylinders using a water cooled diamantsaw.

The discs were then dried (either by CO_2-free drying or by methanol-replacement) and kept in a vacuum desiccator over silica gel at room temperature until testing.

Just before the analysis, discs were transferred from the desiccator to a glove box containing silica gel and sodium hydroxide ("Ascarite II") to keep a dry and almost CO_2-free atmosfere.
The disc were ground by a mortar and pestle. The fraction between 150 µm and 500 µm were used for the analysis.

Finally, vacuumdrying at 50 °C was performed in the sorptionapparatus, just before the adsorption measurements were carried out. This final drying in the sorptionsapparatus is an integrated part

of the test procedure when N2-SORP is performed at CBL.

2.2.10 Specimens for Wateradsorption (H2O-SORP)

The samples for H2O-SORP were prepared in the same way as samples for N2-SORP. Only methanol-replacement was used as drying method for these specimens.

2.3 Sample preparation

2.3.1 CO_2-free drying

This method has previously been described by Fontenay and Sellevold /44/.

Water saturated specimens were placed in a vacuum desiccator over silica gel at room temperature for 2 days, while pumping by means of a vacuum pump. This predrying was carried out in order to remove the main part of the evaporable water before introducing the specimen to high temperature. In this way, further hydration due to high temperature conditioning is avoided.

Subsequently, the specimens were placed in a vacuum oven at 92.5 °C for 7 days. The oven was connected to a saturated solution of LiCl ("wet crystals") kept at room temperature, thus creating a relative water vapour pressure of 0.11. Finally, the oven was evacuated to 2.4 torr (320 Pa).

Experiments (Appendix E) have shown that CO_2-free drying is similar to drying at 105 °C in a ventilated oven, since the same degree of drying was optained. The CO_2-free drying method was found to be more reproducible, probably because no carbonation took place. The experimental setup is illustrated in figure 2.3.1.1.

The application of CO_2-free drying was carried out according to CBL Testing Manual no. 1.10.3 (Appendix F, in Danish).

2.3.2 Methanol-replacement

Water saturated specimens with a thickness of approximately 3 mm were used to ensure a quick replacement of methanol in the pores.

The thin specimens were placed in sealed containers with relatively large volumes of technical grade methanol. The methanol was replaced by fresh methanol seven times within 14 days. Finally, the methanol-replaced specimens were dried by CO_2-free drying (section 2.3.1).

It was assumed, that the method of CO_2-free drying also could be used for methanol-replaced specimens. Observations indicates, that methanol-replacement has a limited effect (a slightly lower degree of drying as compared to CO_2-free drying from water-saturated state). In this context, this lower degree of drying is negligible.

2.3.3 Drying/resaturation treatment

The drying/resaturation treatment described here is an attempt to expose the material to a drying environment which can be related to practice.

The drying took place at 50 °C at a relative water vapour pressure of 11 % (a saturated LiCl-solution at 2.4 torr (320 Pa)) for 3 days Resaturation was carried out gradually. Final saturation took place in a pressure tank at 150 atm (15.2 MPa).

The standard scheme for drying and resaturation is shown in table 2.3.3.1.

3. Methods

In this chapter details are given concerning measurement technique, theory and calculation procedures for the different methods employed in this project.

3.1 Lowtemperature microcalorimetry (CAL)

Ice formation by CAL at both LBM and CBL were carried out by a low temperature Calvet microcalorimeter (SETARAM), using a differential scanning mode of operation.

The method has previously been described by Sellevold et al./44,45/.

The experimental setup for CAL at CBL is shown at figure 3.1.1A. The microcalorimeter is shown in figure 3.1.1B.

By applying CAL on saturated or partly saturated porous specimens, information of pore structure can be optained /19/.

During ice formation the liberated amount of heat is measured as heat flow. From figure 3.1.1B the principle of measurement could be seen. The calorimeter contains two cylindrical cell introduction tubes. These are identical and are placed symmetrically in the aluminium calorimeter block. Each of the two thinwalled tubes are connected to the calorimeter block by 516 termopiles connected in series. The thermopiles are spaced evenly on the tube surface.

The tubes contains the measurement cell (M) and the reference cell (R). During the experiment the saturated, surface dry sample was contained in the airtight measurement cell. Before the experiment a few mg of AgI was sprinkled at the sample surface to minimize supercooling of the water.

Heat flow was measured as the differential output signal (E_i) from the two seperate sets of thermopiles.

While cooling at a rate of 3.3 °C/h at LBM (3.6 °C/h at CBL) and heating at a rate of 4.1 °C/h at LBM (4.2 °C/h at CBL), simultaneous measurements of time, τ(s), temperature, T(°C), and calorimeter output signal, E_i (μV), took place in the temperature range from approximately 15 °C to -60 °C.

From these measurements the apparent heat capacity, C_{pA}, can be calculated as:

$$C_{pA} = \frac{E_i}{s_M \cdot (dT/d\tau) \cdot W_{ssd}} \qquad (J \cdot K^{-1} \cdot g_{ssd}^{-1})$$

where

s_M is the calorimeter sensitivity (μV/mW)
(dT/dt) is the rate of temperature change (°C/s)
W_{ssd} is the saturated surface dry weight (g_{ssd})

From curves showing temperature versus apparent heat capacity, the ice formation in the saturated specimen can be calculated, as it is proportional to the area below the the curve and above an estimated baseline. The methods used for estimation of this baseline, and hence the calculation of ice formation have previously been outlined by Fontenay et al. /18,44/.

Investigations /18/ have shown that the results optained by CAL are very reproducible. Accordingly, only one test is necessary to gain precise data on ice formation. This is also due to the appropriate specimen fabrication technique (section 2.2.1) securing highly homogenious specimens.

Typical heat capacity curves optained during both cooling (COOL) and heating (HEAT) for CAL at CBL are shown in figure 3.1.2.

The observed hysteresis between cooling and heating indicates the continuity of the pore system. During cooling, the propagation of the ice front is controlled by the narrowest necks in the pore system. Accordingly, the ice formation during cooling is comparable to mercury intrusion (section 3.2) and nitrogen desorption (section 3.3).

The qualitative interpretation of these temperature-heat capacity-curves is quite simple. The peaks indicates concentrated ice formation. With the help of these curves the porestructure i.e. poresize can be estimated, since water held in small pores freezes at lower temperatures than water held in greater pores /19/.

Since no ordinary ice forms below -55 °C /44/, the amount of non-frozen water at -55 °C, $w_{nf}(-55)$, represents water in very small pores or physically adsorbed water at surfaces.

A Manual for carrying out CAL at LBM is written by Holland et al. /20/. This Manual was partly prepared by this author.

The application of CAL at CBL was done according to CBL Testing Manuals no. 1.11.1, 1.11.2 and appendix (these are shown at Appendix C, in Danish). (Preparation of these manuals was included in the Education Plan).

3.1.1 Cumulative pore size distribution

Cumulative pore size distribution (CPSD) can be calculated from CAL-results by means of a method similar to Kelvin Capillary Condensation analysis (KCC) used to calculate CPSD from sorption isotherms.

Like in KCC, the pore water is assumed to be dividable into two

parts:

[a]) Capillary condensed water
[b]) Surface adsorbed water

Considering circularly cylindrical pores, the pore radius, r_p, could be written as:

$$r_p = r_K + t_{nf} \qquad (Å)$$

where r_K = Kelvinradius of the solid/liquid (ice/water) meniscus.
t_{nf} = Adsorbed surface layer. Consists of very strongly bound water, unable to freeze at ordinary temperatures.

Defay et al. /21/ describes the growth of an ice crystal into a narrow capillary. The relation between temperature and r_K of the narrow capillary was given by the equation

$$r_K = - \frac{2 \cdot \upsilon^l \cdot \sigma^{sl}}{\Delta_f h \cdot \ln(T/T_0)} \qquad (Å)$$

where υ^l = molar volume of water = $18 \cdot 10^{-6}$ m^3/mole
σ^{sl} = surface tension of the water/ice interface
= 0.030 N/m
$\Delta_f h$ = heat of fusion of ice
= 6012 + 40.4 · $(T_0 - T)$ J/mole, calculated from data of Radjy given by Fontenay et al. /18,44/.
T = actual temperature (K)
T_0 = 273.2 K

Hence, r_K could be calculated for different freezing point depressions $(T_0 - T)$:

$(T_0 - T)$	K	0	1	3	5	7	10	20	30	40	50	60
r_K	Å	∞	493	166	101	73	52	27	19	16	13	12

Figure 3.1.1.1 shows the calculated relation between r_K and $(T_0 - T)$.

One of the assumptions for the use of this equation is that the ice/water- and not the vapour/water-interface controls the formation of ice in the narrow capillaries. According to /18/ this is a reasonable assumption, since all pore entrances (with possible va-

pour/water-interface) will be filled with ice, when the largest capillaries have frozen, at relatively high temperatures.

For pores of very small width in the order of a few molecular diameters the application of capillary theory can hardly be extrapolated, since no ordinary meniscus seems likely under these circumstances. However, other methods, using capillary theory (nitrogen- and water-sorption) have similar uncertainties. For comparative purposes the application of capillary theory on small pores therefore seems permissible.

The applied values for $\Delta_f h$ assumes that both the ice and the non-frozen water are at atmosferic pressure. This is a rather crude assumption, since freezing will create different pressures on each side of an interface.

Several researchers /18,44,45,52,53,54,55,56,57,59/ interpreted - as the present author - the freezing point depression as the result of the existence of pore water freezing in smaller capillaries and they advocated a relationship between freezing point depression and pore size similar to the equation of Defay et al. /21/ shown above.

Furthermore, CAL immediately can provide us with detailled information of frost resistance of the material tested. Frost resistance is a very important practical property.

MIP and N2-SORP implies that specimens are dried totally before testing in contrast to CAL where totally saturated and never dried specimens could be used. However, MIP and N2-SORP have been used extensively by cement paste researchers for many decades and it would therefore be very appropriate to compare these methods to CAL.

The non-frozen layer (t_{nf}) at surfaces could, as a first approximation, be assumed to be of constant value throughout the temperature range of relevance. However, this would mean that the pore size distribution calculated from calorimetric ice formation will be a rather steep curve. Most likely, however, it would be expected that t_{nf} depends on temperature . Accordingly, the non-frozen layer becomes thinner as temperature decreases in the same way as the surface adsorbed t-layer becomes thinner as the relative vapour pressure decreases.

Fagerlund /52/ gave an estimate on the temperature dependency of t_{nf}. By this, t_{nf} (Å) could be calculated from the freezing point depression, (T_0-T) (°C), by the equation

$$t_{nf} = 19.7 \cdot (T_0-T)^{-1/3}$$

To the knowledge of the author no other researcher has established such a relation. Consequently, in the absence of other estimates on t_{nf}, the values of Fagerlund are used.

Pore sizes ($2 \cdot r_p$) from about 40 Å to about 300 Å are detectable using the above mentioned calculation technique.

3.2 Mercury Intrusion Porosimetry (MIP)

MIP-data at LBM were generated by a mercury porosimeter (Micromeritics Instr. Corp.). A diagram of the apparatus is shown in figure 3.2.1. The porosimeter was operated manually.

The pore radius, r_p, was calculated from the Washburn equation

$$r_p = - \frac{2 \cdot \sigma \cdot \cos \theta}{p}$$

where θ = contact angle between mercury (Hg) and dry paste (117° are normally used at LBM)
σ = surface tension of Hg = 0.484 N/m (at 20 °C)
p = applied pressure (psi)

Bager and Sellevold /22/ and Fontenay /18/ both used drying procedures quite similar to the CO_2-free drying method used in this project, and they operated with a contact angle of 117°, citing the experimental work of Winslow and Diamond /23/ on oven dried samples. Accordingly, this value is used as a standard value in this project.

The predried material was placed in the sample holder (part A in figure 3.2.2) of the MIP-sample cell, and assembled to the mating cap (part B in figure 3.2.2). The sample cell was then prefilled with Hg under high vacuum conditions and placed in the pressure chamber of the porosimeter. The pressure on the mercury was generated through the hydraulic oil surrounding the sample cell. Pressure was then increased stepwise.

The amount of Hg forced into the pores at each step was measured using a precision bore tube and an electrical displacement counter (figure 3.2.3). The cap (part B in figure 3.2.2) contained a cup with a platinum feed through, creating electrical connection between Hg in the cup and in the sample cell.

In the porosimeter the sample cell was assembled with the top part of the pressure chamber. This part contained a fixed electrical contact that dipped into the cup of the sample cell, and a movable electrical contact (figure 3.2.3).

As pressure was increased, Hg was pressed into the pores and the Hg-level in the precision bore tube decreased. The movable contact followed until contact was reached. This movement was measured by the electrical displacement counter and was proportional to the penetrated volume.

At each pressure, equilibrium was said to be reached when 2 minutes had elapsed since the last count on the electrical diplacement counter.

MIP-runs with only Hg in the sample cell (blank-runs) were used to compensate for the compressibility of the Hg itself.

The apparatus has been described in general by Orr /24/, and the specific porosimeter at LBM has previously been used and described by Bager and Sellevold /22/ and by Sørensen /25/.

A Manual for carrying out MIP at LBM is written by Nielsen et al. /26/. This Manual was partly prepared by this author.

MIP at USA was carried out using an Autoscan 60 Porosimeter (Quantachrome Corporation).

Pore sizes ($2 \cdot r_p$) from about 30 Å to about 40 µm are detectable using this method, depending mainly on the maximum pressure capacity of the porosimeter and on which contact angle is chosen.

3.3 Nitrogen adsorption (N2-SORP)

Nitrogen adsorption and -desorption data were generated by an automated nitrogen sorption apparatus (Sorptomatic 1900, Carlo Erba).

The apparatus is shown in figure 3.3.1.

The isotherms were determined by the volumetric method, in which stepwise introduction of known volumes of gas to the predried sample is applied.

After each introduction a certain amount of the gas is adsorbed by the sample. The amount not adsorbed by the sample at equilibrium create a partial pressure above the sample. This equilibrium pressure is measured by a pressure transducer. The volume of adsorbed nitrogen (in liquid state) and the companion equilibrium gas pressure above the sample gives one adsorption point at the adsorption isotherm.

The criteria of equilibrium at each pressure step is chosen by the user. The pressure is measured continiously. When the pressure difference of two consecutive readings is below a certain value, equilibrium is considered to be reached. Both the time interval between two consecutive readings and the pressure difference are decided by the user. For these measurements, 3 minutes and 0.5 torr (67 Pa) have been chosen, respectively.

When both the volume of gas introduced and the equilibrium pressure of the gas is known, the amount of gas adsorbed by the sample can be calculated using the known introduced volume of nitrogen gas, and the relation between volume of gas and gas pressure above the sample. The latter relation is established by simply introducing successive and known volumes of gas to an empty sample burette

while recording the respective equilibrium pressures (blank-run).

Pore size distribution and cumulative volume was calculated from the desorption branch of the isotherm by application of the Kelvin equation and making corrections for the t-layer adsorbed at surfaces. The relevant calculations are performed automatically by a computer software programme, supplied with the Sorptomatic 1900 instrument. This programme uses the procedures described by Barrett, Joyner and Halenda /27/.

These authors considered the pore structure to be a system of open ended, non-intersecting, circularly cylindrical pores. Pore radius is calculated from

$$r_p = r_K + t \ ,$$

thus dividing the adsorbed gas into two categories:

[a]) Physically adsorbed on the pore walls
(t-layer; $t = t(p/p_0)$)
[b]) Capillary condensed in the inner capillary volume
(Kelvin radius; $r_K = r_K(p/p_0)$)

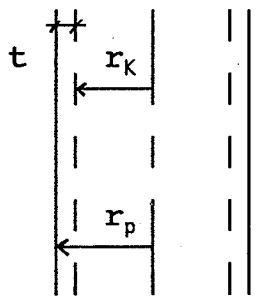

The applied Kelvin equation is

$$r_K = - \frac{2 \cdot \sigma \cdot \upsilon}{R \cdot T} \cdot \frac{1}{\ln (p/p_0)}$$

where σ = surface tension of liquid nitrogen = 0.00885 $N \cdot m^{-1}$
υ = liquid molar volume of nitrogen = $34.65 \cdot 10^{-6}$ $m^3 \cdot mole^{-1}$
T = temperature at which σ and υ were calculated
= 77.3 K
R = gas constant = 8.316 $J \cdot K^{-1} \cdot mole^{-1}$

(Numerical data are taken from /27/)

Hence, r_K is calculated /27/ from

$$r_K = -\frac{9.53}{\ln(p/p_0)} \quad (Å)$$

The t-layer is calculated /27/ from

$$t = MT \cdot \left(\frac{-5}{\ln(p/p_0)}\right)^{1/3} \quad (Å)$$

where MT = monolayer thickness = 4.3 Å

This t-curve was constructed /27/ from experimental data of Schull /28/ based on the assumption that each adsorbed nitrogen molecule in a given layer is vertically above its neighbour in the previous adsorbed layer as pointed out by Gregg and Sing /29/.

Pore sizes ($2 \cdot r_p$) from about 20 Å to about 600 Å are detectable using this apparatus. Thus, the mesopores (20 Å < porewidth < 500 Å) according to IUPAC-conventions, could be measured.

The application of N2-SORP at CBL was carried out according to CBL Testing Manuals no. 1.10.1, 1.10.2 and appendix (these are shown at Appendix D, in Danish). These manuals were prepared by this author.

A typical test report from a complete adsorption/desorption analysis is shown at Appendix G. The procedures for the calculation of cumulative pore size distribution from the desorption branch of the isotherm are also shown.

3.4 Water adsorption (H2O-SORP)

Predried and crushed samples (section 2.2.10) were placed in small weighing bottles in a vacuum desiccator over a saturated solution of LiCl, maintaining a relative humidity (r.h.) of 11 % in the desiccator.
The desiccator was evacuated to a partial pressure of 2.4 torr (320 Pa), and kept at room temperature.

After more than 3 months of adsorption at 11 % r.h. the amount of adsorbed water was calculated.

Subsequently, the weighing bottles containing the samples were placed in a vacuum desiccator over saturated solution of $MgCl_2$, maintaining 33 % r.h. in the desiccator. The desiccator was evacuated to a partial pressure of 5 torr (667 Pa) and kept at room temperature.

After 3 weeks at 33 % r.h., the amount of adsorbed water was calculated.

The determination was performed in triplicates in a single desiccator.

The specific surface area according to the BET-method /30/, S_{BET}, is calculated from

$$S_{BET} = \frac{V_m}{M} \cdot N \cdot \delta$$

where
S_{BET} = specific BET-surface area (m^2/g_{dry})
δ = area covered by one molecule of water (m^2)
N = Avogadros number
M = molecule weight of water (g/mole)
V_m = monolayer volume (g/g_{dry})

Taking $\delta = 11.4 \cdot 10^{-20}$ m^2, $N = 6.024 \cdot 10^{23}$ and M = 18 g/mole the following equation is gained:

$$S_{BET} = 3815 \cdot V_m \quad (m^2/g_{dry})$$

The monolayer capacity, V_m, was calculated from the linearized BET-equation /30/

$$\frac{(p/p_0)}{w_{ads} \cdot (1 - (p/p_0))} = \frac{1}{V_m \cdot C} + \frac{C - 1}{V_m \cdot C} \cdot (p/p_0)$$

where
p/p_0 = relative vapour pressure
w_{ads} = adsorbed water content (g/g_{dry})
C = constant, indicating the reactivity of the surface

Plotting $(p/p_0)/(w_{ads} \cdot (1-(p/p_0)))$ versus (p/p_0) in the region of $0.05 < p/p_0 < 0.35$ gives a straight line (BET-plot) with an intercept (I) and a slope (α).

Thus, V_m and C could be calculated as follows

$$V_m = \frac{1}{\alpha+I} \quad \text{and} \quad C = \frac{\alpha+I}{I}$$

Using the amounts of adsorbed water at p/p_0 = 0.11 and 0.33, S_{BET} is calculated from two points of the adsorption isotherm.

3.6 Inverted cup method (CUP)

Using this type of cup (see figure 3.6.1 for principle and experimental setup) both water permeability coefficients (K) and water vapour diffusion coefficients (k_d) could be calculated according to Thorsen /31/.

A water saturated specimen was assembled with the other components of the cup (as shown in figure 3.6.1). The assembled cup was then placed in a climate chamber with well defined relative humidity, temperature and ventilation (r.h. = 60 ± 5 % , temperature = 22 ± 2 °C, continious flow of air was created at specimen surfaces using a ventilator).

Simultaneous measurements of weight loss and time were carried out regularly. A typical weight loss curve is shown in figure 3.6.2.

The drying could be separated into three phases (as shown in figure 3.6.2).

Phase I:

In this phase (see figure 3.6.1) the saturated specimen loose weight relatively fast. This is mainly due to evaporation from the initially saturated surface of the specimen. Water is transported from the wet side to the evaporation front by capillary suction. Since capillary suction is slower than vaporisation from meniscii surfaces, the evaporation front (figure 3.6.2) moves towards the wet side of the cup and relative humidity gradually increases at the evaporation front.

Phase II:

In this phase water is transported by diffusion from meniscii surfaces at a much slower rate compared to phase I. The evaporation front moves towards the wet side of the cup.

Phase III:

The evaporation front is no longer moving, indicating that equilibrium is reached between amount of water transported by capillary suction and by vapour diffusion.

The flux of water, q, through the specimen is calculated from the weight loss curve as

$$q = a/A \qquad (kg \cdot m^{-2} \cdot s^{-1})$$

where
- a = the slope of the weight loss curve (kg/s) in phase III, where steady state has been reached
- A = exposed area (m^2) of the specimen

Water transport by capillary suction can, assuming one-dimensional laminar flow in circular cylindrical tubes, be calculated using Darcy's law:

$$q = K \cdot \frac{\Delta P}{L}$$

where
- K = coefficient of permeability (kg/Pa·m·s)
- ΔP = difference in hydraulic pressure (Pa) due to the low pressure under a meniscus surface
- L = capillary suction length (m)

Water transport by water vapour diffusion can, under steady-state conditions, be calculated using Ficks law:

$$q = k_d \cdot \frac{p_1 - p_2}{L}$$

where
- k_d = water vapour diffusion coefficient (kg/Pa·m·s)
- p_1 = vapour pressure (Pa) in evaporation front
- p_2 = vapour pressure (Pa) in climate chamber
- L = vapour diffusion length (m)

For steady-state conditions (phase III) the evaporation front is fixed at a distance x from the dry side of the cup (see figure 3.6.2). This means that water is transported by capillary suction in the distance (L-x) and by vapour diffusion in the distance x.

When steady state conditions were optained, values of x, K and k_d can be calculated using the procedures outlined by Thorsen /31/.

The distance x can be calculated from considerations concerning mass of water in the different regions corresponding to (L-x) and x.

Thus, the total mass of water in the specimen when the test was completed (W_3) may be written as

$$W_3 = W_{dis} - W_{dry}$$

where W_{dis} = weight of specimen (kg) when the cup has been dismantled
W_{dry} = weight of specimen (kg) after drying at 105 °C

Mass of water in the region of capillary suction (W_{cap}) may be written as

$$W_{cap} = \left(\frac{L-x}{L}\right) \cdot V \cdot \varepsilon \cdot \rho_w$$

where V = volume of the specimen (m^3)
ε = (open) porosity (m^3/m^3)
ρ_w = density of water (kg/m^3) = 1000 kg/m^3

Mass of water in the region of vapour diffusion (W_{dif}) may be written as

$$W_{dif} = \left(\frac{x}{L}\right) \cdot V \cdot w_{em} \cdot \rho_d$$

where w_{em} = mean value of the evaporable water content (kg/kg_{dry}) in the region of vapour diffusion
ρ_d = dry density (kg_{dry}/m^3)

Since

$$W_3 = W_{cap} + W_{dif}$$

$$\varepsilon = \frac{(W_{ssd} - W_{dry})/\rho_w}{(W_{ssd} - W_{sub})/\rho_w}$$

$$\rho_d = \frac{W_{dry}}{V} = \frac{W_{dry}}{(W_{ssd} - W_{sub})/\rho_w}$$

the distance x can be calculated from (taking ρ_w = 1000 kg/m^3)

$$x = L \cdot \frac{(W_{dis} - W_{dry}) - (W_{ssd} - W_{dry})}{w_{em} \cdot W_{dry} - (W_{ssd} - W_{dry})}$$

where W_{ssd} = saturated, surface dry weight (kg_{ssd})
W_{sub} = weight of saturated specimen (kg), submerged in water

Hence, knowing L, the distance x is calculated from gravimetry.

The mean value of evaporable water content in the region of vapour diffusion, w_{em}, is found from the sorption isotherm of the actual specimen, as the amount of adsorbed water at a relative vapour pressure, p/p_0, which is the mean value of $p/p_0 = p_2/p_0$ in the climate chamber and an assumed $p/p_0 = p_1/p_0$ at the evaporation front (p_1/p_0 = 0.90 or 0.98 is normally assumed). The present calculations has been carried out for both these values.

Knowing x, both K and k_d can be calculated from the equations

$$q = K \cdot \frac{\Delta P}{L - x}$$

$$q = k_d \cdot \frac{p_1 - p_2}{x}$$

Since

$$q = \frac{a}{A}$$

$$\Delta P = - \frac{2 \cdot \sigma}{r_K}$$

σ = surface tension of water (N/m)
r_K = Kelvin radius (m)
= $r_K (p_1/p_0)$
p_1/p_0 = p/p_0 in the evaporation front

the following equations for the determination of K and k_d are gained

$$K = \frac{(L - x) \cdot a \cdot r_K (p_1/p_0)}{2 \cdot \sigma \cdot A}$$

$$k_d = \frac{x \cdot a}{A \cdot p_0 \cdot (p_1/p_0 - p_2/p_0)}$$

It is observed, that both K and k_d depends on the assumed water vapour pressure, $p/p_0 = p_1/p_0$, in the evaporation front.

3.7 Relative water vapour diffusion coefficients

5 saturated, surface dry discs (Ø22.6 mm and 3 ± 0.5 mm in thickness) were placed on a brass specimen holder and weighed. The holder were constructed in such a way that the discs were able to dry freely from both sides. Furthermore, the concept of weighing 5 discs at a time improved the reliability of the method. Placing the discs in the holder facilitated the weighing procedure.

The discs were placed in a vacuum desiccator above a saturated solution of LiCl, maintaining a relative humidity of 11 % .
The desiccator was evacuated to approximately 2.4 torr (320 Pa) and kept at room temperature. Measurements of weight loss from the initial saturated, surface dry weight were carried out regularly during a period of 35 days. After each measurement the desiccator was evacuated again.

During drying, the moisture content of the material is a function of time. The theory of non-steady state moisture transport is to be used when describing the moisture content of the specimen during drying. This theory has been outlined in generel terms in /32/.

The relative coefficient of diffusion, D/D_0, can be calculated when the actual specimen, and an arbitrary chosen reference (0) specimen have reached the same degree of drying.

The degree of drying (expressed as cumulative weight loss relative to total cumulative weight loss at equilibrium with the actual relative vapour pressure, here 0.11) is a function of drying time, which is expressed as the Fourier number

$$Fo = \frac{D \cdot \tau}{L^2}$$

where
D = coefficient of diffusion (m^2/s)
τ = drying time (s)
L = drying length (m)

When the actual and the reference (0) specimen have reached the same degree of drying their Fourier numbers are the same, thus

$$\frac{D \cdot \tau}{L^2} = \frac{D_0 \cdot \tau_0}{L^2{}_0}$$

Since the specimens are geometrical identical, $L = L_0$, the relative diffusion coefficient could be calculated as

$$\frac{D}{D_0} = \frac{\tau_0}{\tau} \quad <=> \quad D = D_0 \cdot \frac{\tau_0}{\tau}$$

where τ_0 and τ are the drying times required to reach the same degree of drying.

This method can be used for the estimation of diffusion characteristics only when the specimens, which are compared, display the same kind of moisture transport mechanisms during drying as pointed out by Nilsson /46/.

4. Results

4.1 Drying methods

Results from this serie are given along with the results presented in section 4.2, since the effect of drying method on pore structure characteristics is investigated there.

4.2 Pore structure characterization methods

Physical characteristics of the CAL-specimens used at both CBL and LBM are given in table 4.2.1.

Figures 4.2.1A-D shows temperature versus heat capacity (ice formation) during cooling for each of the 4 different HCP-specimens. Results are shown for CAL at both LBM and CBL.

The quantitative results from the CAL-tests at both CBL and LBM are given in table 4.2.2. Here, the frozen water (w_f) and the non-frozen water (w_{nf}) contents are given at different temperatures.
w_{nf} is calculated as $w_{es} - w_f$ from COOL INCR.

Physical characteristics of the MIP-specimens used at LBM, USA and CZE are given in table 4.2.3.

Cumulative pore size distributions from MIP performed at LBM, USA and CZE are shown in figures 4.2.2A-D.

Figure 4.2.2E shows cumulative pore size distribution from MIP performed at LBM for hardened cement paste (HOC/0/0.6 virgin). The paste was analysed by 3 independent repetitions.

Physical characteristics of the N2-SORP-specimens used are given in table 4.2.4.

Nitrogen adsorption- and desorption-isotherms are shown in figures 4.2.3A-D. The effect of using either methanol-replacement or CO_2-free drying as drying method is shown.

Cumulative pore size distribution from N2-SORP on CO_2-free dried samples are shown in figure 4.2.4.

Specific BET-surface area optained by N2-SORP and H2O-SORP are shown in table 4.2.5.

In tables 4.2.6A-D CAL-data, optained from figures 4.2.1A-D (CBL-curves), are transformed into cumulative pore size distributions using the temperature depending non-frozen layer thickness of Fagerlund (section 3.1.1).

In figures 4.2.6A-D cumulative pore size distributions are compared for the methods of CAL, N2-SORP and MIP. For MIP, a contact angle of 117° was used.

In figures 4.2.7A-D cumulative pore size distributions are compared for the methods of CAL, N2-SORP and MIP. For MIP, a contact angle of 140° was used.

In figure 4.2.8 the effect on cumulative pore size distribution from changing the contact angle, θ, from 117° to 140° is shown.

4.3 Pore structure stability (CBL-serie)

Physical characteristics of the CAL-specimens are given in table 4.3.1.

Figures 4.3.1A-J,L shows heat capacity versus temperature during cooling for the different cementpastes in both virgin and dried/ resaturated states.

The quantitative results from CAL are given in table 4.3.2. Here, the frozen water (w_f) and the non-frozen water (w_{nf}) contents are given at different temperatures.

Cumulative pore size distribution calculated from MIP are given in figures 4.3.2A-I. Figure 4.3.2A shows the effect of different HCP-blends, while figures 4.3.2B-I shows the effect of a drying/re-saturation treatment for each HCP-blend (apart from OPC, P30-4A and ROC/M/0.2)

Cumulative pore size distribution calculated from N2-SORP are given in figures 4.3.3A-J. Figure 4.3.3A shows the effect of different HCP-blends, while figures 4.3.3B-J shows the effect of a drying/re-saturation treatment for each HCP-blend (apart from OPC and P30-4A).

Table 4.3.3 shows values of specific BET-surface calculated from N2-SORP. Results are given for different HCP-blends, dried by CO_2-free drying prior to analysis. For ROC, HOC and P30-4A the effect of methanol-replacement is also shown.

4.4 Pore structure stability (LBM-serie)

The results of this serie were previously reported by Holland /12/.

Physical characteristics of the CAL-specimens are given in table 4.4.1.
Figure 4.4.1 shows temperature versus heat capacity (ice formation) during cooling for virgin HCP-specimens using 3 different cements and no admixtures.

Figures 4.4.2A-C shows ice formation during cooling for virgin HCP-specimens using either none or 4 different admixtures, for the following types of cement: A) ROC, B) SAC and C) PFC.

Figures 4.4.3A-C shows ice formation during cooling for both virgin and dried/resaturated, pure HCP-specimens, for the following types of cement: A) ROC, B) SAC and C) PFC.

The quantitative results from the CAL-tests are given in table 4.4.2. Here, the frozen water (w_f) and the non-frozen water (w_{nf}) contents are given at different temperatures.

Figure 4.4.4 shows relative water vapour diffusion coefficients calculated from drying test results at 11 % r.h. Results are given for virgin HCP-specimens using 3 different types of cement and 4 types of admixtures. Furthermore, the effect of drying/resaturation for pure HCP is shown.

4.5 Additional investigations (LBM)

In table 4.5.1 are shown the permeability results by CUP for the different mortars investigated by Holland /12/ and Rosenbom and Waldstrøm /13/.

In figure 4.5.1A-B results are shown for water vapour diffusion coefficients, $k_d(90)$, by CUP of cementmortars of A) Holland /12/ and B) Rosenbom and Waldstrøm /13/.

In figure 4.5.2A-B results are shown for water permeability coefficients, K(90), by CUP of cement mortars of A) Holland /12/ and B) Rosenbom and Waldstrøm /13/.

In figure 4.5.3A-C are shown curves of heat capacity versus temperature during cooling for the various mortars investigated by Rosenbom and Waldstrøm. In table 4.5.2 are shown the results from ice formation measurements by CAL. Data are given on frozen (w_f), non-frozen (w_{nf}) and total evaporable (w_{es}) water contents.

5. Discussion

5.1 Methods of drying and pore structure characterization

5.1.1 CAL at LBM and CBL

From heat capacity curves during cooling (figures 4.2.1A-D) it is observed, that the level of heat capacity for tests carried out at LBM is higher than at CBL. This is explained by the fact that the vessel in the reference cell at LBM was empty, while at CBL, this vessel was filled with approximately 11 g of calcined alumina. According to SETARAM calcined alumina is inert in the temperature range used.

Filling the reference vessel with an inert material, as it is done at CBL, causes the level of the signal from the reference cell, E_R, to increase as shown in figure 5.1.1.1. This means that the differential output signal, E_i, calculated as the difference between the output signal from the measurement cell, E_M, and E_R, is lowered accordingly. Since the apparent heat capacity, C_{pA}, of the specimen (see section 3.1) is proportional to E_i, C_{pA} is also lowered. This explains the different levels of heat capacity optained on nominally identical specimens at LBM and CBL.

Off course, the two different levels of C_{pA} could be reduced to approximately the same level by means of a supplementary test run at CBL. In this test, the vessel in the measurement cell should be empty (no specimen) and the vessel in the reference cell should be filled with inert alumina (as usual).

The heat capacity signal from this "zero-test" could then be subtracted from the heat capacity signal of the ordinary tests where the vessel in the measurement cell contains a specimen.
This procedure - although quite simple to perform - is not used here, since the author consider the level difference to be of no relevance when comparing numerically the test results of the same material from the two different laboratories: CBL and LBM.

From figure 4.2.1A it is observed that ice formation is taking place around -10 °C for the CBL-specimen. For the companion LBM-specimen no ice is formed above -20 °C. The observed ice formation around -10 °C can not be correlated to freezing in any specific pore size range since it takes place in large waterfilled cavities (air bubbles) situated mainly at the surface of the specimen, or represents water evaporated from the sample and condensed either at the inner surface of the vessel or at the small AgI-particles. This ice formation is very small (normally around 0.001 g/g_{dry}) and have therefore no influence for the interpretation of the overall ice formation.

From calculated ice formation (table 4.2.2) good correspondance between the two laboratories was observed.

Although the optained ice formation data are in good correspondance

the following points could be able to contribute to differences in the shape of the temperature-heat capacity curve and have influence on the amount of calculated ice.

a) Method of data sampling.
b) The determination of the total evaporable water content.
c) Cooling/heating rates.

Re a)

At LBM and CBL, the criteria for sorting af data are approximately the same and are chosen in accordance with the criteria used by Fontenay /18/.

In this way a set of data (consists of simultaneous measured values of time, temperature and differential output signal) will be stored if any of the following criteria is fulfilled:

[a]) Time criterion:
A certain amount of time has elapsed since the last set of data was stored

[b]) Temperature criterion:
The temperature is an integer

[c]) Output signal criterion:
The output signal is changed by a certain amount since the last set of data was stored

At LBM the data are progressively collected, processed and stored in a datafile. Hence, when the test is finished the data to be used for calculation of the ice formation are processed.

At CBL, a certain interval of time passes between two consecutive data collections. These intervals have a lower time limit set by the storage capacity of the control software programme (5000 sets of data), and by the time required for analysis (depending on initial and final temperatures, and temperature rate). A typical time interval was approximately 20 sec. (during cooling) and 15 sec. (during heating).

After each test at CBL, the 5000 sets of data are converted from hexadecimal code to real numbers. Subsequently, the 5000 sets of data are sorted by the above mentioned criteria. The sorted file typically consists of 100-150 sets of data, which is of the same magnitude as the number of data sets upon CAL at LBM.
Furthermore, a data file of this size is readily used in a worksheet software programme as LOTUS 1-2-3 for additional data handling.
From this file ice formation data can be calculated. Both converting and sorting of the data were performed automatically by computer, using a programme (Turbo-Pascal) developed at CBL, under guidance of this author.

The criteria used in the sorting procedure of this programme at CBL are shown as a flow diagramme in figure 5.1.1.2A.

The criteria used in the sorting procedure of the programme at LBM are shown as a flow diagramme in figure 5.1.1.2B.

The advantage of the LBM-method is that immidiately after storing a set of data, a new data collection is performed, while at CBL the time interval between two sets of data is at least 15 sec. Especially in temperature ranges of concentrated ice formation (peaks), this means that the CBL-method collects fewer sets of data than the LBM-method. This could result in more uneven CBL-curves (as seen from figures 4.2.1A-D) as compared to LBM-curves.

This unevenness of the curve has a certain influence on the calculation of ice, since the ice formation is proportional to the area below the temperature-heat capacity curve and above an estimated baseline. Since the calculated amount of ice at the two laboratories are in good correspondance, the difference in methods of data sampling at LBM and CBL is not considered to be of significance.

Re b)

The determination of the total evaporable water content, w_{es}, has been determined by CO_2-free drying at both laboratories. From table 4.2.2 it is observed, that w_{es} is higher at LBM than at CBL. Because of high paste homogenity, this difference is believed mainly to be caused by differences of the saturated LiCl-solutions used at LBM and CBL.

The volume of the commercial oven used at CBL is at least 20 times that of the non-commercial oven used at LBM. Hence, the CBL-oven was used to dry many samples of different water contents at the same time. CO_2-free drying at LBM is observed to be more severe than CO_2-free drying at CBL. This can be explained by the fact, that the LiCl-solution at CBL relatively quickly becomes less saturated and less homogeneous unless the solution is checked regularly.

Obviously, the degree of saturation of the LiCl-solution at CBL has not been checked as regularly as the one at LBM. This should have been done in order not to add any unnecessary uncertainty to this drying procedure.

It is very important, that the solution mainly consisted of "wet crystals". If this is not the case, the water vapour pressure above the solution will increase beyond 0.11 and the severity and reproducibility of the drying method will decrease as seen in the case of CO_2-free drying at CBL.

The total evaporable water content, w_{es}, is used in the ice formation calculations to bring the calculated ice on a dry weight basis. Hence, to high a value of w_{es} gives to high a value of calculated ice on a dry weight basis.

It can be argued, that w_{es}(LBM)-values are more precise than w_{es} (CBL)-values, since drying at LBM evaporates more water from nominally the same specimens than drying at CBL.

Re c)

The nominal cooling rates were 3.3 °C/h (LBM) and 3.6 °C/h (CBL). The nominal heating rates were 4.1 °C/h (LBM) and 4.2 °C/h (CBL).

The rates used at LBM have been used as standard rates at the laboratory for many years, and are applied here for comparison purposes. The rates at CBL were established according to the rates used at LBM. The difference in rates between LBM and CBL is caused by the fact that the control software programme at CBL only permits rates as a multiple of 0.06 °C/h.

According to Fontenay /18/, such small differences in rates will not cause any measureable difference in ice formation.

5.1.2 MIP at LBM and USA

5.1.2.1 Effect of drying method

From figures 4.2.2A-C it is seen that methanol-replacement tends to give a finer pore structure compared to CO_2-free drying from the watersaturated state.

This is in line with observations of other researchers /7,33/. Some of these authors /33/ investigated HCP of various W/C hydrated for 240 days, and compared MIP-results for pastes, which had been either methanol-replaced before drying (above concentrated sulphuric acid) with results for pastes, which were dried directly from saturated surface dry (ssd) water state.

Thus, it could be concluded that a coarsening of the pore structure takes place, when the pastes were dried by CO_2-free drying from the ssd-water state. Furthermore, at ultimate pressure, the intruded volume is larger for specimens, which are dried directly from ssd-water state than for specimens, which are dried from ssd-methanol state.

In figure 4.2.2D this effect is not seen, since the two drying procedures seems to give almost identical cumulative pore size distributions. The two distributions are not distinguisable, since deviations are almost the same as optained from triplicate MIP-test on identical samples (figure 4.2.2E).

It is seen, that the effect of drying method is significant for both the 0.4 W/C-pastes and the virgin cured 0.6 W/C-paste, while the effect is absent for the dried/resaturated 0.6 W/C-paste. Since methanol-replacement is known to preserve the (water-saturated) original pore structure /5/, especially the finer part of the pore structure as pointed out by Bager /47/ using CAL, and since the first drying/

resaturation stabilizes the pore structure /34/, it is believed that CO_2-free drying is less severe to pastes, which have been exposed to drying/resaturation treatment prior to complete drying.

Furthermore, it appears that for dried/resaturated specimens, the effect of drying method decreases when W/C increases (figures 4.2.2B and 4.2.2D).

From figures 4.2.2A and 4.2.2C and table 4.2.3 it can be seen that around 55 % and 80 % of the total volume (water porosity) is penetrated by mercury at final pressure at LBM for virgin, mature, CO_2-free dried HOC-pastes of 0.4 and 0.6 W/C, respectively.

For very mature ROC-paste of 0.4 W/C Bager and Sellevold /22/ found that only 48 % of total water porosity was penetrated by mercury at final pressure, using the same apparatus.

As W/C increases from 0.4 to 0.6 a larger part of the total (water) porosity seems to be penetrable to mercury. This is in agreement with observations of other researchers /18,33/.

5.1.2.2 Effect of different laboratories

From figures 4.2.2A-D deviations between the two laboratories are observed. The deviations seems significant, since they are larger than deviations optained from triplicate MIP-test on identical samples (figure 4.2.2E).

Bager and Sellevold found that the cumulative pore size distribution (from MIP) depended on the size of the MIP specimen. The difference was considerable when using powders (particle size less than 0.5 mm) compared to chunks of several mm. Since the specimens used in this investigation were nearly same size the difference between LBM and USA could not be explained by differences of specimen size.

For all four specimens, MIP at USA intruded a significant lower volume at final pressure, even though final pressure at USA (60000 psi (413.7 MPa)) was larger than at LBM (50000 psi (344.7 MPa)).

The deviations between curves of USA and LBM is most significant in the high pressure (small pore radius) region. In this region the USA-curves flattens out, while the LBM-curves proceeds upwards, indicating further intrusion (pore volume).

The phenomena was also reported by Sørensen /25/, and Bager and Sellevold /22/, using the same apparatus.

The observed further intrusion at LBM might be caused by alteration in the contact zone between mercury and hydraulic oil giving an amalgamated material having a lower electrical conductance than bulk mercury. This phenomena is not observed at USA, possibly because another principle is used for measurement of intruded volume.

This phenomena is more likely caused by the way equilibrium is being established at each pressure step. At LBM, equilibrium is assumed, when 2 minutes has elapsed and no further intrusion is observed. Typically, 30 pressure steps is used at LBM to reach the ultimate pressure. At USA, the intruded volume is measured almost continiously, since continious pressure generation is applied.

Even though the observed deviation between the two laboratories seems significant the author would not consider this to be conclusive, since uncertainties other than the purely instrumental ones may have contributed.

As mentioned previously, HCP pore structure is very sensitive to changes in moisture conditions. Accordingly, the apparent difference between the two laboratories should be tested using a material, in which the pore structure is stable towards changes in moisture conditions as for instance porous vycor glass (PVG). Hence, it could be concluded that a difference between laboratories seems to exist using HCP, but no definitive conclusion can be made unless a comparative test is performed using PVG.

However, one of the most important purposes of this project is the comparison of CAL to other relevant methods using commercially available equipment and thus not the ultimative comparison between different MIP-equipment.

5.1.3 N2-SORP and H2O-SORP

For all four pastes investigated, the influence of drying method on the adsorption-/desorption isotherms is clearly seen from figures 4.2.3A-D.

Hence, it is observed that drying from the methanol saturated state seems to have at least two effects on the sorption isotherm compared to drying from water saturated state.

Firstly, at low values of p/p_0 the amount of adsorbed nitrogen is remarkably larger for specimens which are dried from methanol saturated state. This is indicative of a larger specific surface of the methanol replaced specimens compared to specimens which have been dried directly from the water saturated state.

Secondly, the hysteresis between the adsorption- and the desorption-isotherm is much more pronounched for the methanol replaced specimens. This means that methanol replacement compared to drying from the water saturated state to a larger degree preserves the inkbottle pores of the original pore structure.

From volume-thickness (V-t) plots detailed knowledge of pore structure can be extracted /2,33,35,36/.

In figure 5.1.3.2a three different and representative V-t-plots are shown (curves A, B and C).

Accordingly, the initial straight line - common for A, B and C - of the V-t-plot indicates adsorption at free surfaces and the slope of this straight line is equal to total surface area (S_{Vt}).

Furthermore, an upward deviation from the initial straight line indicates capillary condensation (curve A and partly curve B), while a downward deviation indicates the presence of micropores (curve C and partly curve B).

In the pore size range of capillary condensation, KCC-analysis (as described in section 3.3) is appropriate.

In figure 5.1.3.2b is shown how the volume of micropores could be estimated graphically from a V-t-plot indicating the presence of micropores.

In figures 5.1.3.1A-D the effect of different drying methods on the V-t-plot, from the adsorption branch of the nitrogen isotherm, is shown for each of the 4 pastes. In table 4.2.5 S_{Vt} is shown.

For all four pastes it is observed from figures 5.1.3.1A-D that methanol-replacement seems to preserve the micropores, while CO_2-free drying from the water saturated state seems to cause a collapse of micropores, since only capillary condensation is observed.

From table 4.2.5 it is observed that BET-surface area by nitrogen, $S_{BET}(N_2)$, and total surface area, S_{Vt}, are in good correspondance. According to /50/ this means that the applied t-curve is reliable. Both $S_{BET}(N_2)$ and S_{Vt} increases when specimens are dried from ssd-methanol state, compared to drying from ssd-water state. $S_{BET}(N_2)$ and S_{Vt} also increases when W/C increases from 0.4 to 0.6, but decreases when specimens are submitted to drying/resaturation.

It is also observed that BET-surface area to water, $S_{BET}(H_2O)$, is larger than $S_{BET}(N_2)$. The reason for this can be explained by the higher accessibility of H_2O-vapour molecules into the narrow pore entrances due to the fact that the H_2O-molecule is smaller than the N_2-molecule. Furthermore, the H_2O-molecule has a strong dipole moment in contrast to the N_2-molecule; water can therefore enter narrower pores than nitrogen.

5.2 Pore structure stability

5.2.1 CAL at LBM and CBL

In this section, ice formation of different HCP-blends measured by CAL are compared qualitatively. In section 5.5 the ice formation measured by CAL will be used in a more direct way to make quantitative calulations of pore size distributions in such a way that pore size distributions calculated by CAL (according to section 3.1.1) could be compared to those optained from MIP and N2-SORP.

In this section, the correlation between freezing point depression and pore size will only be used qualitatively. Thus, freezing at

low temperatures will indicate the presence of small pores and freezing at higher temperatures will indicate the presence of larger pores in the pore system.

From figure 4.4.1 (CAL at LBM) it is observed that less ice is formed at higher temperatures for virgin mature ROC-paste compared to virgin mature SAC- and PFC-paste. Thus, virgin ROC-paste has a relatively smaller amount of larger pores compared to virgin SAC- and PFC-paste.

For ROC-paste, the addition of different plasticizers or superplasticizers (figure 4.4.2A) have almost no effect on ice formation, although the superplasticizer of the naphthalene sulphonated type seems to increase the amount of ice formed at higher temperatures and decrease the amount of ice formed at lower temperatures compared to both the reference (without additive) and other additives. This seems to indicate that this superplasticizer produces larger pores in ROC-paste compared to the other additives investigated.

For SAC-paste, the addition of different plasticizers or superplasticizers (figure 4.4.2B) seems to increase the amount of ice formed at higher temperatures and decrease the amount of ice formed at lower temperatures. This indicates, that larger pores are formed when plasticizers and superplasticizers are added to SAC-paste.

For the PFC-paste, the effect of adding different plasticizers and superplasticizers can be seen in figure 4.4.2C. The addition of superplasticizer of the naphthalene sulphonate type seems to produce larger pores compared to both the reference and the other additives investigated.

The main features of figures 4.4.1 and 4.4.2A-C are that the pore structure is more influenced by the type of cement than by the type of plasticizer or superplasticizer used. Furthermore, virgin cured ROC-paste has a relatively smaller amount of larger pores compared to both SAC- and PFC-paste.
The superplasticizer of the naphthalene sulphonate type seems to give an increased amount of coarser pores compared to both the reference paste and the other additives investigated, especially when used with ROC and PFC.

From figures 4.4.3A-C it is seen that a drying/resaturation treatment increased the amount of ice formed at higher temperatures at the expense of the amount of ice formed at lower temperatures, indicating a coarsening of the pore structure upon drying. It is also observed, that the effect of a drying/resaturation treatment is less pronounced for the PFC-paste (figure 4.4.3C) compared to both ROC- and SAC-paste, since a large part of the ice formed at lower temperatures in the virgin cured specimens also formed when the PFC-paste had been dried/resaturated. This indicates, that PFC-paste has preserved the fine part of the pore structure better than both ROC- and SAC-pastes.

Normally, as seen for the other HCP-blends investigated here (figu-

res 4.3.1A-J and L), calorimetric ice formation at low temperares (corresponding to the peak at approximately -42 °C) decreases, and ice formation at higher temperatures (corresponding to the amount of frozen water at -20 °C) increases, when a virgin mature specimen has been exposed to a drying/resaturation treatment prior to freezing. This was, as mentioned earlier (section 1.1.3) interpreted in terms of a structural collapse of smaller pores upon drying from the water saturated state, thus creating a more continious pore system of larger pores.

5.2.2 MIP

From MIP-results (figure 4.3.2A) it is observed, that blends made from different cements and with different W/C show different pore size distribution.

The following points should be made with respect to 0.4 W/C pastes: For pore sizes less than approximately 180 Å BLC-paste had a markedly higher porosity to Hg than other 0.4 W/C pastes investigated, especially when compared to the BILAG3-paste, which displayed the lowest porosity of all 0.4 W/C pastes.

The higher porosity of BLC-paste compared to other pastes investigated is expected, since BLC contains inert filler.
The observed low porosity of BILAG3-paste could to some extend be explained by a higher degree of hydration of this paste compared to the other pastes (as indicated from weight loss upon ignition, w_n, for CAL-specimens shown in table 4.3.1).

As expected, lowering of W/C from 0.4 to 0.3 and 0.2 lowered the porosity of the paste.

Details on the intrusion of each paste are easily seen on figures 4.3.2B-J, where the effect of drying/resaturating the specimen before preparation (drying and outgassing) for MIP also can be seen.

From the intrusion curves (figures 4.3.2B-J), apparently no systematic effect of drying/resaturation is observed.

According to the CAL-results (section 5.2.1), it might be expected, that MIP-specimens, which have been dried/resaturated would display a coarser pore structure compared to virgin cured MIP-specimens.

This is true for some of the HCP-blends investigated by MIP. Other dried/resaturated blends display a finer pore structure compared to the companion virgin cured specimen. This is the case for SAC/0/0.3 and SAC/M/0.2, although the observed deviations between mature virgin and dried/resaturated specimens could, to some extent, be explained by the deviations observed from the triplicate testing of identical samples (figure 4.2.2E).

However, it must be remembered, that CAL is performed on saturated specimens and MIP is performed on completely dried specimens. In this way, specimens, which are conditioned (dried/resaturated) befo-

re analysis are dried twice before MIP and only once before CAL.

Normally, the first drying of hardened cement pastes affects the pore structure more than subsequent drying/rewetting.

5.2.3 N2-SORP

N2-SORP-results (figure 4.3.3A) display almost the same features as already pointed out from the MIP-results.

The 0.4 W/C pastes are quite similar to each other, apart from the BLC-paste, which is significantly more open to N_2-molecules, and therefore has a higher porosity than the other pastes.

Again, as observed from the MIP-results, lowering of W/C from 0.4 to 0.3 for ROC- and SAC- pastes also lowered the porosity of these pastes.

A further decrease in W/C from 0.3 to 0.2 decreased the porosity of the SAC-paste but had apparently no effect for the ROC-paste.

Details of the N2-SORP-results for each blend are easily seen on figures 4.3.3B-K, where the effect of drying/resaturating the specimen before preparation (drying and outgassing) also can be seen.

As for the MIP-results no systematic effect of drying/resaturation is observed, but some dried/resaturated blends displayed a finer pore structure compared to the companion virgin cured blend. This is the case for BLC/0/0.4.

5.2.4 Final discussion

Results from these preliminary studies on pore structure stability towards a drying/resaturation treatment investigated by the various techniques of CAL, MIP and N2-SORP seems to indicate, that certain blends are preferable to others.

From the investigations at LBM, PFC-paste is found to have preserved a rather large part of the finer pores. This is probably caused by the incorporation of the relatively large volume of flyash particles in the cement.

Norwegian investigations /40/ have found that concrete made from a special Off-shore cement (P30-4A) displayed good pore structure resistivity towards drying/resaturation.

This cement was also tested in this project (figure 4.3.1L).

Compared to the other cement pastes (figures 4.3.1A-K), the P30-4A paste does not show any outstanding resistivity towards drying/resaturation.

However, on the basis of the promising results reported in /40/ it was decided to investigate this type of cement further.

The main features of this preliminary survey of commercial available cements are that the incorporation of flyash seems to improve the ability of the material (hardened cement paste) to withstand a rather strong pseudo-climatic influence (50 °C and 11 % r.h for 3 days).

The description and the results of the investigations that have been carried out on the basis of these preliminary studies are contained in a confidential report.

5.3 Additional investigations

From figure 4.5.1A it is observed that the water vapour diffusion coefficient, $k_d(90)$, is not largely influenced by the type of additive, although it seems that adding superplasticizer of the naphthalene sulphonate type to PFC-mortar gives significantly higher $k_d(90)$

It is seen from figures 4.5.1A-B, that 0.4 W/C mortars without additives, shoved almost the same $k_d(90)$, despite of differences in workability.

Figure 4.5.1B shows that both drying/resaturation and increasing W/C from 0.4 to 0.6 seems to increase $k_d(90)$. The effect of increasing W/C seems to be larger than the effect of drying/resatution, when looking at 0.4 W/C mortar. Furthermore, it can be seen that drying/resaturation of the 0.4 W/C ROC-mortar causes an increase in $k_d(90)$, which is about twice the increase observed when PFC- and SAC-mortars are dried/resaturated.

From figure 4.5.2A it is observed that the water permeability coefficient, K(90), is not largely influenced by the type of additive, although adding of superplasticizer to SAC-mortar seems to increase K(90).

From figure 4.5.2B it is seen, that increasing W/C from 0.4 to 0.6 increases K(90). It is also observed that drying/resaturation of the 0.4 W/C mortars increases K(90) for ROC- and SAC-mortar, while K(90) for PFC-mortar is nearly unaffected by the drying/resaturation treatment.

From table 2.2.5.1 it could be calculated that the volume of paste in the 0.4 W/C mortar investigated by Rosenbom and Waldstrøm /13/ is greater than the volume of paste in the 0.4 W/C mortar investigated by Holland /12/.

In table 4.5.1 it is observed that apparently comparable mortars from these two investigations on permeability nevertheless displays consistent differences. The 0.4 W/C mortar of low paste volume (and very low workability, /12/) displays a smaller water permeability (K(90)) than apparently comparable 0.4 W/C mortars of relatively higher paste volume (and normal workability, /13/).

Because of the complexity of the concrete technology it seems almost impossible to relate the pore structure of plain cement paste to the

practical behavior of concrete, the latter naturally being of primary importance in the building industry.

In practical concrete the pore structure of the plain cement paste volume is modified by aggregates (sand, stone, fibres etc.). Around each aggregate a transition zone is formed, having an anisotropic and most often less dense pore structure than bulk plain cement paste.

When comparing ice formation in 0.4 W/C mortars (figures 4.5.3A-C) to ice formation in comparable 0.4 W/C cement pastes (figures 4.4.3A-C) it is observed that even in virgin cured mortars ice is formed at higher temperatures (above -10 °C). For virgin cured 0.4 W/C HCP no ice is formed until around -20 °C. This means that the ice formed in mortar at higher temperatures represents the volume of pores associated to the transition zone, having a larger porosity than the bulk plain cement paste.

From figures 4.5.3A-C on calorimetric ice formation of 0.4 W/C mortars it is observed that the ability of PFC-paste to preserve the fine part of pore structure upon drying/resaturation (discussed in section 5.2.1) also holds for PFC-mortar when compared to ROC- and SAC-mortars.

Thus, a certain consistency of the results is revealed: Upon drying/ resaturation, PFC-mortar displays high degree of pore structure stability (a relatively high amount of small pores were preserved) and therefore only a small increase in water transport, as expected.

5.5 Cocalibration of CAL, MIP and N2-SORP

In this section the possibility of comparing low temperature microcalorimetry to MIP and N2-SORP in a more direct and quantitative way (as described in section 3.1.1) will be discussed using the very mature (8 years) HOC-pastes.

In this project and in the past CAL has primarily been used as a tool for the relative comparison between ice formation of different hardened cement pastes.

Except on single occations /19/ in the past, CAL-data has not been used to actually calculate the pore size distribution. By cement paste researchers this distribution has most frequently been measured by the extensive use of MIP and N2-SORP.

Even though the techniques of MIP and N2-SORP have been used for many decades and the precision and automatisation rapidly proceeds on the instrumental side, it could be argued that these techniques from an objective point of view still have some shortcomings on the theoretical side.

The MIP-model assumes the pore system to be a number of circular tubes connected in series with the tube near the surface of the material. The open pore system in hardened cement paste is highly com-

plex with a high amount of "bottlenecks" representing narrowings of characteristic sizes in the pore system.

Consequently, as the analyzis is performed and as the Hg-pressure is increased yet smaller pores are penetrated. As the bottlenecks are penetrated the pore volume behind the bottleneck is penetrated too and this volume will be taken into account as representing the pore volume of pores having a pore diameter corresponding to the diameter of the bottleneck.

In this way MIP overestimates the volume of smaller pores due to bottlenecks in the pore system.

Another source of uncertainty of the MIP-model rests in the problem of estimating the contact angle, θ, between mercury and the pore wall. Even though that values of 117° or 140° often are used in the literature, at least two factors may contribute to the uncertainty of optaining a precise estimate for θ.

Firstly, the necessary drying before measurement most likely alters the properties of the pore wall and therefore θ must depend on how the material has been dried before measurement. Secondly, it also seems likely that the properties of the mercury (and perhaps also the pore wall) changes as pressure is increased during an analyzis. Therefore θ might also depend on Hg-pressure.

On the other hand, CAL also have some shortcomings. As both MIP and N2-SORP, CAL is an indirect method of pore structure characterization and - as it was mentioned in INTRODUCTION - such methods only measures a substitutional property and this property is then transformed into pore size by means of a theoretical equation. Measured properties as Hg-pressure, nitrogen relative vapour pressure and freezing point depression is transformed into pore size for MIP, N2-SORP and CAL, respectively.

The different assumptions for the theoretical equation linking pore size and freezing point depression were discussed previously in section 3.1.1. In addition, it should be mentioned, that CAL during cooling overestimates the volume of the smaller capillaries since water held in bottleneck pores freezes in accordance to the size of the bottleneck. This type of overestimation is also seen when MIP (intrusion) and N2-SORP (desorption) are applied.

It can be seen from figure 4.2.6A, that for very mature virgin 0.4 W/C paste there seems to be bad accordance between the pore size distribution calculated from CAL-data and those calculated from MIP and, especially, N2-SORP.

The CAL-derived curve is both steeper and covers a more narrow pore size range than the curves derived from MIP and N2-SORP.

However, it does not seem reasonable and realistic to compare the pore size distribution of the virgin (never allowed to dry) CAL-specimen to the pore size distribution of both MIP- and N2-SORP-speci-

mens, which have been dried totally from the virgin water saturated state (or dried from methanol-saturated state) before the measurement.

A more realistic comparison is displayed in figure 5.5.1A, in which the MIP- and N2-SORP-curves are identical to the ones in figure 4.2.6A. However, the CAL-curve displayed represents a specimen, which have been dried (3 days at 50 °C and 11 % relative humidity) and then resaturated.

In figure 5.5.1A it is observed that the CAL-derived curve seems to be in relatively good accordance with the MIP-curve (LBM), representing a specimen, which have been totally dried from the water saturated state. Furthermore, it seems that CAL is in much more agreement with MIP than with N2-SORP. However, CAL seems comparable to both MIP and N2-SORP.

It is also observed that for very mature 0.4 W/C paste N2-SORP displays a much coarser pore size distribution than MIP when CO_2-free drying from the water saturated state is used as drying method.

In figure 5.5.1B the pore size distribution calculated from relevant CAL-data (for a dried/resaturated specimen) are compared to MIP- and N2-SORP-derived curves for very mature 0.6 W/C pastes.

It is observed that the pore size distribution derived from CAL-data seems comparable with the curves of both MIP and N2-SORP.

For very mature, dried/resaturated 0.4 W/C paste (figure 4.2.6B) the pore size distribution calculated from calorimetric ice formation during cooling is not as steep as for the companion virgin specimen (figure 4.2.6A), since ice formation for the dried/resaturated specimen is more gradual and covers a wider range of temperatures (i.e. poresizes) compared to the virgin specimen.

In contrast to 0.4 W/C pastes it is observed for the very mature, virgin cured 0.6 W/C paste (figure 4.2.6C) that MIP displays a coarser pore size distribution than N2-SORP. This is also seen for the dried/resaturated 0.6 W/C paste (figure 4.2.6D).

Figure 4.2.7A-D exemplifies that pore size distribution curves are highly sensitive towards changes in the parameters of the different techniques (contact angle, surface tension, thickness of adsorbed or unfrozen layer at surfaces).

The only difference between figures 4.2.6A-D and figures 4.2.7A-D is that the contact angle θ used in the transformation of MIP-pressure to pore size is changed from 117° to 140°, the latter being used as frequently as 117° in the literature.

This increase in contact angle moves the MIP-curves shown in figure 4.2.6A-D to the right. Figure 4.2.8 shows this effect more clearly.

It is seen, that this decreases (for 0.4 W/C pastes) and increases

(for 0.6 W/C) the difference between MIP- and N2-SORP curves for specimens, which have been CO_2-free dried from the water saturated state.

It has been shown that CAL-derived pore size distributions could be made using a calculation technique comparable to Kelvin Capillary Condensation Analysis. However, for comparable specimens, the best agreement between CAL and other methods was observed for 0.4 W/C pastes and then only when compared to MIP.

It is also obvious that CAL cannot estimate the distribution of pores above a certain size, since for higher temperatures (large pore sizes) the measurement of ice formation cannot be performed in any greater detail using the current test procedure.

In this project it has been tried, for very mature HCP, to compare CAL directly with MIP and N2-SORP by means of cumulative pore size distributions.

From this comparison (figures 5.5.1A-B) it is observed that some agreement was observed, mainly between CAL and MIP.
Although the best agreement was observed for very mature 0.4 W/C HOC-paste, and even if some disagreement was observed for the larger pores (pore diameter larger than approximately 80 Å) it must be concluded from figures 5.5.1A-B that pore size distribution calculated from CAL are comparable to the pore size distributions optained from MIP and N2-SORP, when comparable specimens are used.

Furthermore, in this context, CAL has the great advantage compared to both MIP and N2-SORP that it could be used to describe the original (and undisturbed) pore structure of primary interest - the true pore structure.

However, CAL is restricted to the lower pore size range and should be combined with other relevant methods to give a complete picture of the pore structure.

5.6 Total porosity

In this section the total porosity of very mature (8 years) HOC-pastes will be discussed.

At high degree of hydration as is the case for these specimens (8 years) MIP alone cannot measure the total pore volume of HCP (especially not for W/C = 0.4 or below). Despite of the very high pressure applied, Hg cannot enter the micropores. To describe the micropores it is necessary to use N2-SORP and subsequently V-t-analysis as shown in section 5.1.3 and figure 5.1.3.2.

Hansen and Almuhaideem /33/ have tried to account for the pore volume missing when MIP is used alone. These researchers estimated and measured the bulk density, ρ_{ssd}, of well hydrated Portland cement pastes by application of solvent (methanol) replacement and by combining the pore volumes optained by N2-SORP (miropore volume) and

MIP. They assumed that the pore volume of pores having a diameter/ size larger than 40 Å could be measured by MIP (using a contact angle, θ, of 140°).

Hansen and Almudaiheem found that the estimated and the measured bulk density agreed very well and they concluded on the basis of these findings that the misssing pore volume could be accounted for by using methanol replacement and N2-SORP for the estimation of the micropore volume.

This author has performed similar estimates of ρ_{SSD} (see table 5.6.1) and subdivides the pore volume at 30 Å in pore diameter, although it is possible to reach approximately 26 Å when performing MIP at LBM (using θ = 117°). The diameter of 30 Å was chosen, since V-t-analysis (figure 5.1.3.1A-D) seems to indicate that micropore-filling stops at this stage. Consequently, the microporevolume is taken as the intercept at the V-axis of the tangent line going through t = 30/2 = 15 Å in the V-t-plot (figures 5.1.3.1A-D) in accordance with /35,36/ and figure 5.1.3.2.

From table 5.6.1 it is observed that the measured and estimated bulk densities are in agreement (with the unexplainable exception of the values for the 0.6 W/C dried/resaturated paste).

Thus, it has been shown that the total porosity of these very mature HOC-pastes only can be accounted for by the application of methanol replacement and by subsequently combining the pore volumes optained by MIP and N2-SORP.

The present findings are in agreement with the previous and original results of Hansen and Almudaiheem /33/.

6. Conclusion

In this Industrial Research Education Programme the following main goals have been reached:

a. Pore structure characterization techniques:

- Facilities for CAL and N2-SORP have been established at CBL.
- Different techniques have been tested and compared (MIP, CAL, N2-SORP and H2O-SORP).
- Testing Manuals have been made at CBL and LBM (co-author).

b. Drying techniques:

- Facility for CO_2-free drying has been established at CBL.
- Different techniques have been tested and compared (CO_2-free drying from water- or methanol-saturated states).
- Testing Manual has been made at CBL.

c. A systematic survey on pore structure characteristics of different cements:

- Effects of drying/resaturation, water-cement-ratio, plasticizer, superplasticizer and flyash have been investigated.

d. A systematic survey on pore structure and water transport characteristics of mortars:

- Effects of drying/resaturation, water-cement-ratio, workability, plasticizer, superplasticizer and type of cement have been investigated.

From these investigations the main conclusions are:

6.1 Methods of drying and pore structure characterization

a. Pore size distributions calculated from low temperature microcalorimety are comparable to pore size distributions optained from either mercury intrusion porosimetry or nitrogen sorption analysis when comparable specimens are used.

b. Measurements of ice formation by low temperature microcalorimetry at both CBL and LBM showed good correspondance.

c. From volume-thickness plots (nitrogen sorption analysis) it was found that drying from the methanol-saturated state preserves the micropores, while drying from the water-saturated state destroyed the micropores.

d. Drying from the methanol-saturated state caused less disturbance of the pore structure than drying from the water-saturated state. This was shown by mercury intrusion porosimetry and nitrogen

sorption analysis.

e. Total porosity of very mature 0.4 and 0.6 W/C HOC-pastes can be accounted for by the application of methanol replacement and by subsequently combining the pore volumes optained by MIP and N2-SORP.

6.2 Pore structure stability

a. In a systematic survey of the pore structure features of different cement pastes made from 8 different commercial cements it was observed using low temperature microcalorimetry that especially Portland flyash cement (PFC) displayed a high degree of pore structure stability upon drying/resaturation.

6.3 Additional investigations

a. In a survey on the possible correlation between pore structure (characterized by lowtemperature microcalorimetry) and water permeability (characterized by inverted-cup method) of cement mortars it was established, that PFC-mortar showed a higher degree of pore structure stability and a lower increase in water permeability upon drying/resaturation as compared to both ROC- and SAC-mortar.

7. References

/1/ Köster, H., and Odler, I.:
"Investigations on the Structure of Fully Hydrated Portland Cement and Tricalcium Silicate Pastes. I. Bound Water, Chemical Shrinkage and Density of Hydrates". Cement and Concrete Research Vol. 16, pp. 207-214, 1986.

/2/ Abdel-Jawad, Y., and Hansen, W.:
"Pore Structure of Hydrated Cement Determined by Mercury Porosimetry and Nitrogen Sorption Techniques". Mat.Res.Soc. Symp., Proceedings, Vol. 137, 1989.

/3/ Day, R.L., and Marsh, B.K.:
"Measurement of Porosity in Blended Cement Pastes". Cement and Concrete Research Vol. 18, pp.63-73, 1988.

/4/ Feldman, R.F., and Beaudoin, J.J.:
"Pretreatment of Hardened Hydrated Cement Pastes for Mercury Intrusion Measurements". Cement and Concrete Research Vol. 21, pp.297-308, 1991.

/5/ Litvan, G.G.:
"Variability of the Nitrogen Surface Area of Hydrated Cement Paste". Cement and Concrete Research Vol. 6, pp.139-144, 1976.

/6/ Moukwa, M., and Aitcin, P.-C.:
"The Effect of Drying on Cement Pastes Pore Structure as Determined by Mercury Porosimetry". Cement and Concrete Research Vol. 18, pp.745-752, 1988.

/7/ Marsh, B.K., Day, R.L., Bonner, D.G., and Illston, J.M.:
"The Effect of Solvent Replacement upon the Pore Structure Characterization of Portland Cement Paste". Proceedings, Principles and Applications of Pore Structural Characterization, Milan, Italy, 1983.

/8/ Bager, D.H.: "Ice Formation in Hardened Cement Paste", Ph.D.-Thesis, Technical Report 141/84, Building Materials Laboratory, Technical University of Denmark, 1984.

/9/ Parrott, L.J.; Hansen, W., and Berger, R.L.:
"Effect of First Drying upon the Pore Structure of Hydrated Alite Paste". Cement and Concrete Research Vol. 10, No. 5, pp.647-655, 1980.

/10/ Sabri, S., and Illston, J.M.:
"Isothermal Drying Shrinkage and Wetting of Hardened Cement Paste". "Fundamental Research of Creep and Shrinkage of Concrete". Martinus Nijhoff Publishers, The Hague/Boston/London, 1982.

/11/ Feldman, R.F., and Swenson, E.G.:
"Volume Change on First Drying of Hydrated Portland Cement with and without Admixtures". Cement and Concrete Research Vol.5, pp.25-35, 1975.

/12/ Holland, A.D.:
"Porestructure of Hardened Cement Paste and Mortar with Different Types of Cement and Admixtures", Lab. for Bygn. Mat., Danmarks Tekn. Højskole, 1990. (In Danish).

/13/ Rosenbom, K., and Waldstrøm, M.:
"Permeability Measured by CUP-method and AASTHO T277-841, and Pore Structure Measured by Low Temperature Microcalorimetry", Lab. for Bygn. Mat., Danmarks Tekniske Højskole (In Danish).

/14/ Sellevold, E.J., and Bager, D.H.:
"Some Implications of Calorimetric Ice Formation Results for Frost Resistance Testing of Cement Products". Beton & Frost. Dansk Betonforening. Publikation nr. 22:85, 1985.

/15/ Winslow, D., and Liu, D.:
"The Pore Structure of Paste in Concrete". Cement and Concrete Research Vol. 20, pp.227-235, 1990.

/16/ Villadsen, J.:
"The influence of Curing Temperature on Pore Structure of Hardened Cement Paste", Lab. for Bygn. Mat., Danmarks Tekn. Højskole, 1989 , Technical Report 218/90. (In Danish).

/17/ Holland, A.D.:
"Casting report: Hardened Cement Pastes and Mortars for Pore Structure Analysis and Permeability-tests", Kursus 6126. LBM. DTH. Sommer 1990 (In Danish).

/18/ Fontenay, le Sage de, C.:
"Ice Formation in Hardened Cement Paste", Ph.D.-Thesis, Technical Report 101/82, Building Materials Laboratory, Technical University of Denmark, 1982. (In Danish).

/19/ Sellevold, E.J., and Bager, D.H.:
"Low Temperature Microcalorimetry as a Pore Structure Probe". Proceedings, 7th International Congress on the Chemistry of Cement, Vol.4, pp.349-354, Paris, 1980.

/20/ Holland, A.D., Villadsen, J., Nielsen, A.M., and Hansen, K.K.:
"Manual for microcalorimeter. Version KL3", Lab. for Bygn. Mat., Danmarks Tekn. Højskole 1991, Technical Report 230/91 (In Danish).

/21/ Defay, R., Prigogine, I., Bellemans, A., Everett, D.H.:
"Surface Tension and Adsorption", Longmans, 1966.

/22/ Bager, D.H., and Sellevold, E.J.:
"Mercury Porosimetry of Hardened Cement Paste: Influence of Particle Size". Cement and Concrete Research. Vol. 5, pp.171-178, 1975.

/23/ Winslow, D.N., and Diamond, S.:
"A Mercury Porosimetry Study of the Porosity in Portland Cement". Journal of materials, JMLSA, Vol.5, no.3, pp.564-585, 1970.

/24/ Orr, C.: "Application of Mercury Penetration to Materials Analysis". Powder Technology, 3, pp.117-123, 1969/70

/25/ Sørensen. E.V.:
"Water Vapour Permeability of Hardened Cement Paste". Ph.D.-Thesis. Technical Report 83/80. Building Materials Laboratory. Technical University of Denmark. 1980.

/26/ Nielsen, A.M., Villadsen, J., and Hansen, K.K.:
"Manual for Mercury Porosimeter", Lab. for Bygn. Mat. Danmarks Tekn. Højskole 1991, Technical Report 232/91 (In Danish).

/27/ Barrett, E.P., Joyner, L.G., and Halenda, P.P.:
"The Determination of Pore Volume and Area Distributions in Porous Substances. I. Computations from Nitrogen Isotherms". J. Amer. Chem. Soc., 73, pp. 373-380, 1951.

/28/ Schull, C.G. in J. Amer. Chem. Soc. 70, 1410, 1948.

/29/ Gregg, S.J., and Sing, K.S.W.:
"Adsorption, Surface Area and Porosity", Academic Press, London and New York, 1967.

/30/ Brunauer,S., Emmett, P.H., and Teller, E.:
"Adsorption of Gases in Multimolecular Layers". Journal of American Chemical Society, vol. 60, p.309 1938.

/31/ Thorsen, T.: "Inverted Cup Method". Proceedings, Symposium of Building Physics, Lund, Sweden, August, 1987.

/32/ Herholdt et al.:
"Betonbogen", 2. ed., CtO, Aalborg Portland, 1985. (In Danish).

/33/ Hansen, W., and Almudaiheem, J.:
"Pore Structure of Hydrated Portland Cement Pastes by Nitrogen Sorption and Mercury Intrusion Porosimetry". Mat.Res.Soc. Symp., Proceedings, Vol. 85, 1987.

/34/ Helmuth, R.A., and Turk, D.H.:
"The Reversible and Irreversible Drying Shrinkage of Hardened Portland Cement and Tricalcium Silicates Pastes". J. Portland Cement Assoc., R & D Labs., pp. 8-21, 1967.

/35/ Radjy, F., and Sellevold, E.J.:
"A Phenomenological Theory for the t-Method of Pore Structure Analysis. I. Slit-Shaped Pores". J. of Colloid Interface Sci., Vol. 39, pp. 367-378, 1972.

/36/ Sellevold, E.J., and Radjy, F.:
"A Phenomenological Theory for the t-Method of Pore Structure Analysis. II. Circularly Cylindrical Pores". J. of Colloid Interface Sci., Vol. 39, pp. 379-387, 1972.

/37/ Reinhardt, H.W., and Gaber, K.:
"From Pore Size Distribution to an Equivalent Pore Size of Cement Mortar". Materiaux et Constructions, 23, pp.3-15, 1990.

/38/ Odler, I., and Hinrichs, W.:
"Investigation of the Hydration of Portland Blastfurnace Slag Cement: Composition, Structure and Properties of the Hydrated Material". Advances in Cement Research, 2, no.5, pp. 15-20, 1989.

/39/ Mehta, P.K.: "Pozzolanic and Cementitious By-Products in Concrete - Another Look". Proceedings, Third Canmet Int. Conference on fly ash, silica fume, slag and natural pozzolans in concrete. ACI, SP-114, 1989.

/40/ Hammer, T.A, and Sellevold, E.J.:
"Frost Resistance of High Strength Concrete". Second International Symposium on Utilization of High-Strength Concrete. May 20-23, 1990. California, USA.

/41/ Danish Standardization Board:
"Special regulations for certification 227, SBC 227". (In Danish).

/42/ Dansk Ingeniørforening:
"Danish Code of Practice for the Structural Use of Concrete". DS411, 3. edition, 1984 (In Danish).

/43/ Teknologisk Institut:
"Test Method for Alkali-Aggregate Reactivity of Sand". TI-B51, 2. edition, 1985 (In Danish).

/44/ Fontenay, le Sage de, C., and Sellevold, E.J.:
"Ice Formation in Hardened Cement Pastes - I.Mature Water-Saturated Pastes". Durability of Building Materials and Components. ASTM STP 691, pp.425-438, 1980.

/45/ Bager, D.H., and Sellevold, E.J.:
"Ice Formation in Hardened Cement Pastes - II. Steam Cured Pastes with Variable Moisture Contents". Durability of Building Materials and Components. ASTM STP 691, pp.439-454, 1980.

/46/ Nilsson, L.O.:
"Moisture Problems at Concrete Floors", Report TVBM-3002/1-188/1977. Technical University of Lund. 1977.(In Swedish).

/47/ Bager, D.H.: "Discussion of session 7". Proceedings, Principles and Applications of Pore Structural Characteristics, Milan, Italy, 1983.

/48/ Powers, T.C., and Brownyard, T.L.:
"Studies of the Physical Properties of Hardened Portland Cement Paste". Journal of the American Concrete Institute. Proceedings. Vol. 43. 1947.

/49/ Bager, D.H.: "Hardened Cement Paste and Concrete as a Living Material from the Point of View of Pore Structure". Intl. Coll. on Materials Science and Restauration. Esslingen, Germany. 1983.

/50/ Mikhail, R.SH., Brunauer, S., and Bodor, E.E.:
"Investigations of a Complete Pore Structure Analysis I. Analysis of Micropores". J. of Cooloids Interface Sci., Vol. 26, pp. 45-53. 1968.

/51/ Hansen W.: Personal communication on results from Helium Pycnometry at University of Michigan, 1991.

/52/ Fagerlund, G.:
"Determination of Pore Size Distribution from Freezing Point Depression". Materiaux et Constructions. Vol.6, No. 33. 1973.

/53/ Stockhausen, N., Dorner, H., Zech, B., and Setzer, M.J.:
"Untersuchung von Gefriervorgängen in Zementstein mit Hilfe der DTA". Cement and Concrete Research. Vol. 9, pp. 783-794, 1979. (In German).

/54/ Dorner, H.W., and Setzer, M.J.:
"Tieftemperatur-DTA-Untersuchungen des Zementsteingefüges bei Untersciedlichem Hydratationsgrad". Cement and Concrete Research. Vol. 10, pp. 403-411, 1980. (In German).

/55/ Dorner, H.W.:
"Mikrokalorimetrische Studie über die Eisbildung in Chloridhaltigem Zementstein". Cement and Concrete Research. Vol. 14, pp. 807-815, 1984. (In German).

/56/ Beddoe, R.E. and Setzer, M.J.:
"Phase Transformation of Water in Hardened Cement Paste A Low-Temperature DSC Investigation". Cement and Concrete Research. Vol. 20, pp. 236-242, 1990.

/57/ Brun, M., Quinson, J.F., and Benoist, L.:
"Determination of Pore Size Distribution by Setaram DSC 101 (Thermoporometry)". Thermochimica Acta. 49, pp. 49-52, 1981.

/58/ Sellevold, E.J., Bager, D.H., Klitgaard Jensen, E., and Knudsen, T.: "Silica Fume - Cement Pastes: Hydration and Pore Structure". Preprint from the Proceedings of Nordisk Miniseminar on Silica in Concrete, 1981.

/59/ Gunnink, B.W.:
"New Method for Measuring Pore Size Distributions in Concrete". Journal of Materials in Civil Engeneering. Vol.3, No.4, 1991.

TABLES

	TYPE OF CEMENT							
	ROC[B]	SAC[B]	HOC[B]	PFC[B]	BLC	OPC	BILAG3	P30-4A
SiO_2 %	21.69	23.71	24.58	28.56	17.62	21.15	20.97	22.18
Al_2O_3 %	5.17	3.26	1.78	8.86	3.71	4.95	4.99	3.94
Fe_2O_3 %	2.85	2.72	0.32	4.24	2.41	2.89	2.90	3.22
CaO %	63.42	65.82	69.24	49.76	56.85	64.83	64.18	64.21
MgO %	0.82	0.68	0.54	0.87	0.70	0.77	0.80	1.51
SO_3 %	3.03	1.95	2.12	2.70	2.98	2.95	3.28	2.55
K_2O acid %	0.53	0.22	0.03	0.43	0.93	0.46	0.55	0.55
Na_2O acid %	0.24	0.22	0.13	0.22	0.38	0.24	0.27	0.23
Na_2O eq. %	0.59	0.36	0.15	0.50	0.99	0.54	0.63	0.59
Flyash %	2	0	0	23	0	0	-	0
L.O.I. %	1.51	1.00	0.92	1.95	12.36	1.14	1.30	1.00
C_3S %	-	54.3	66.5	-	-	55.2	52.2	50.6
C_2S %	-	27.0	20.3	-	-	19.0	20.7	25.5
C_3A %	-	4.0	4.2	-	-	8.2	8.3	5.0
C_4AF %	-	8.3	1.0	-	-	8.8	8.8	9.8
$CaSO_4$ %	-	2.51	3.3	-	-	3.8	4.19	4.4
Free CaO %	1.33	0.85	2.62	1.28	0.77	1.02	1.23	0.95
Density, kg/m^3	3176	3195	3148	2897	3027	3152	3161	3170
Blaine, m^2/kg	414	333	439	447	777	372	547	409
Residuals:								
0.2 mm %	0.07	0.03	0.02	0.31	0.07	-	0.03	
0.09 mm %	0.46	0.65	0.03	2.21	0.21	-	0.07	0.65*

Table 2.1.1.1: Chemical and mineralogical composition and physical properties of the cements.

* the number is the residual on the 0.063 mm - sieve.
B these are "Basis-cements", normally used at CBL. They are homogenized from dayly samples of seven months plant production.
\- data not available

Product name	Active components	Dry-matter	Abbreviation
Conplast 212	Lignosulphonate	36 % by wt.	LS
Sodium glukonate	Hydroxycarboxylate	38 % by wt.	HC
Sikament-NA	Naphthalene sulphonate	41 % by wt.	N
Sikament-FF	Melamine sulphonate	30 % by wt.	M

Table 2.1.3.1: Chemical additives.
LS and HC are plastisizers.
N and M are superplastisizers.

	FRACTIONS (mm)		
	0 - 1/4	1/4 - 1	1 - 4
Amount passing (%) the screen (mm):			
32.000	100.0	100.0	100.0
16.000	100.0	100.0	100.0
8.000	100.0	100.0	100.0
4.000	100.0	100.0	100.0
2.000	100.0	100.0	35.7
1.000	100.0	29.0	0.4
0.500	100.0	0.1	0.1
0.250	98.0	0.0	0.0
0.125	8.0	0.0	0.0
0.075	0.0	0.0	0.0
Grain density, dry kg/m^3	2647	2638	2597
Absorption, %	0.1	0.21	0.38

Table 2.1.4.1: Sieve analysis, density and absorption of quartssand from CBL.

For optaining a sand grading within zone 2 (British Standard), the fractions were (% by weight):

0 - 1/4 mm: 16.67 %
1/4 - 1 mm: 33.33 %
1 - 4 mm: 50.00 %

		W/C = 0.4		W/C = 0.6
		A/C[b] = 4.6	A/C = 2.5	A/C = 4.5
		Holland /12/	R & W /13/	R & W /13/
Cement (PFC)	kg/m^3	400.0	591.0	377.4
Additive[a]				
Water	kg/m^3	160.0	239.71	230.2
Aggregate:				
0 - 1/4 mm	kg/m^3	307.6	246.1	282.8
1/4 - 1 mm	kg/m^3	614.9	491.7	565.0
1 - 4 mm	kg/m^3	922.5	736.4	846.6
Slump	mm	-	83	90
Cement (ROC)	kg/m^3	400.0	598.3	380.5
Additive[a]				
Water	kg/m^3	160.0	242.6	232.1
Aggregate:				
0 - 1/4 mm	kg/m^3	311.4	249.1	285.1
1/4 - 1 mm	kg/m^3	622.4	497.9	569.9
1 - 4 mm	kg/m^3	934.0	745.6	853.5
Slump	mm	-	78	72
Cement (SAC)	kg/m^3	400.0	600.9	381.3
Additive[a]				
Water	kg/m^3	160.0	243.6	232.7
Aggregate:				
0 - 1/4 mm	kg/m^3	312.4	250.1	285.8
1/4 - 1 mm	kg/m^3	624.6	499.9	571.1
1 - 4 mm	kg/m^3	937.0	748.6	855.3
Slump	mm	-	100	60

Table 2.2.5.1: Mix-proportions and slumps for cementmortars.

[a] Additives, if any, were used in the same dosages as for HCP-specimens (section 2.5.4)

[b] A/C = Aggregate-cement-ratio by weight

	Drying	Resaturation					
Exposure	50 °C and 11 % r.h.	Water (vapour)		Water (liquid)			Saturated limewater
Pressure	2.4 torr	atm.	17.5 torr	atm.	17.5 torr	150 atm.	atm.
Time of exposure, days	3	3	4	3	3	1	until testing (> 2)

Table 2.3.3.1: Standard scheme for drying and resaturation of HCP-specimens.

W/C	(Laboratory) Specimen	ρ_{ssd}	w_{de}	w_{es}	ε
		g/cm^3	g/g_{dry}	g/g_{dry}	% by vol.
0.4	(LBM)				
	#1.3 V	1.999	-	0.226	36.8
	#1.5 D/R	1.997	0.057	0.226	36.8
	(CBL)				
	#1.4 V	1.999	-	0.203	33.7
	#1.6 D/R	2.001	0.046	0.207	34.3
0.6	(LBM)				
	#7.3 V	1.774	-	0.405	51.1
	#7.1 D/R	1.774	0.066	0.414	51.9
	(CBL)				
	#7.5 V	1.773	-	0.384	49.2
	#7.2 D/R	1.773	0.048	0.392	49.9

Table 4.2.1: Physical characteristics for CAL-specimens

V are virgin specimens
D/R are dried/resaturated specimens

ρ_{ssd} = saturated, surface dry density
w_{de} = residual water content after drying at 50 °C and 11 % r.h. for 3 days
w_{es} = total evaporable water content
ε = porosity

W/C	(Laboratory) Specimen	ICE FORMATION (w_f)								w_{es}	NON-FROZEN WATER (w_{nf})				
		-55°C				-35°C	-20°C	-10°C	-10°C		-55°C	-35°C	-20°C	-10°C	-10°C
		COOL		HEAT		COOL			HEAT		COOL				HEAT
		TOT	INCR	TOT	INCR										
0.4	(LBM)														
	#1.3 V	44	41	53	55	17	0	0	18	226	185	209	226	226	208
	#1.5 D/R	64	61	75	75	51	33	5	44	226	165	175	193	221	182
	(CBL)														
	#1.4 V	36	39	46	50	15	0	0	17	203	164	188	203	203	186
	#1.6 D/R	59	64	63	63	44	26	4	39	207	143	163	181	203	168
0.6	(LBM)														
	#7.3 V	164	189	-	-	139	86	51	-	405	216	266	319	354	-
	#7.1 D/R	196	200	203	193	183	173	138	182	414	214	231	241	276	232
	(CBL)														
	#7.5 V	170	184	170	165	129	82	50	113	384	200	255	302	334	271
	#7.2 D/R	193	194	204	198	173	164	128	181	392	198	219	228	264	211

Table 4.2.2: Data on ice formation and water content (given in mg/g_{dry}) from CAL-test at both CBL and LBM. Water contents were optained by CO_2-free drying (table 4.2.1).

V are virgin specimens - not available
D/R are dried/resaturated specimens

W/C	(MIP-laboratory) Specimen	ρ_{ssd}	w_{de}	w_{es} [b]	ε
		g/cm^3	g/g_{dry}	g/g_{dry}	% by vol.
0.4	(LBM)				
	#1.3 V	2.00	-	0.226	36.9
	#1.5 D/R	2.00	0.057	0.226	36.9
	(LBM) [a]				
	#1.3 V	2.00	-	0.217	35.7
	#1.5 D/R	2.00	0.057	0.220	36.1
	(USA)				
	#1.4 V	2.00	-	0.203	33.7
	#1.6 D/R	2.00	0.044	0.207	34.3
	(CZE)				
	#1.4 V	2.00	-	0.205	34.0
	#1.6 D/R	2.00	0.048	0.204	33.9
0.6	(LBM)				
	#7.3 V	1.77	-	0.405	51.0
	#7.1 D/R	1.77	0.066	0.414	51.8
	(LBM) [a]				
	#7.3 V	1.77	-	0.381	48.8
	#7.1 D/R	1.77	0.067	0.415	51.9
	(USA)				
	#7.5 V	1.77	-	0.384	49.1
	#7.2 D/R	1.77	0.048	0.392	49.8
	(CZE)				
	#7.5 V	1.77	-	0.371	47.9
	#7.2 D/R	1.77	0.065	0.414	51.8

Table 4.2.3: Physical characteristics for MIP-specimens.
[a] Dried by methanol-replacement prior to MIP
[b] Specimens for MIP at LBM are dried at LBM, the rest are dried at CBL.
ρ_{ssd}, w_{de}, w_{es} and ε are defined in table 4.2.1

Specimen	Drying method	ρ_{ssd}	w_{es}	w_{de}	ε
		g/cm^3	g/g_{dry}	g/g_{dry}	% by vol.
HOC/0/0.4 V	CO_2-free	2.00	0.203	-	33.7
	Methanol	1.99	0.201	-	33.3
HOC/0/0.4 D/R	CO_2-free	2.00	0.207	0.046	34.3
	Methanol	1.99	0.203	0.056	33.6
HOC/0/0.6 V	CO_2-free	1.77	0.384	-	49.1
	Methanol	1.79	0.349	-	46.3
HOC/0/0.6 D/R	CO_2-free	1.77	0.392	0.048	49.8
	Methanol	1.77	0.389	0.053	49.6

Table 4.2.4: Physical charateristics for N2-SORP-specimens

- not available

ρ_{ssd} = saturated, surface dry density
w_{de} = residual water content after drying at 50 °C and 11 % r.h. for 3 days
w_{es} = total evaporable water content
ε = porosity

Specimen	Drying method	$S_{BET}(N_2)$	$S_{BET}(H_2O)$	$S_{Vt}(N_2)$
		m^2/g_{dry}	m^2/g_{dry}	m^2/g_{dry}
HOC/0/0.4 V	CO_2-free	45.5	-	48.7
	Methanol	129.0	142.7	122.8
HOC/0/0.4 D/R	CO_2-free	33.4	-	32.5
	Methanol	75.6	133.9	79.7
HOC/0/0.6 V	CO_2-free	73.7	-	82.9
	Methanol	169.1	142.8	184.2
HOC/0/0.6 D/R	CO_2-free	62.8	-	51.1
	Methanol	113.1	138.1	111.8

Table 4.2.5: Specific surface area according to the BET-method for both nitrogen- and water adsorption. Total surface area, S_{Vt}, according to the V-t-plot from nitrogen adsorption.

$S_{BET}(H_2O)$ is calculated from the water adsorption at 11 and 33 % r.h.

- Not measured.

T °C	W_f g/g$_{dry}$	r_K Å	t_{nf} Å	r_p Å	$\overline{r_p}$ Å	Δt_{nf} Å	ΔW_f g/g$_{dry}$	ΔW_{tf} g/g$_{dry}$	ΔW_{Kf} g/g$_{dry}$	ΔW_{pf} g/g$_{dry}$	ΔS_p $10^4 \cdot m^2$/g$_{dry}$	$\sum \Delta S_p$ $10^4 \cdot m^2$/g$_{dry}$	$\sum \Delta W_p$ cm^3/g$_{dry}$
-20	0	27	7.3	34.3								0	0
-24	0.004	23	6.8	29.8	32.1	0.5	0.004	0	0.004	0.006	0.00040	0.00040	0.006
-28	0.007	20	6.5	26.5	28.1	0.3	0.003	0.000	0.003	0.005	0.00036	0.00076	0.011
-32	0.012	18	6.2	24.2	25.4	0.3	0.005	0.000	0.005	0.009	0.00069	0.00145	0.020
-36	0.016	17	5.9	22.9	23.6	0.3	0.004	0.000	0.004	0.007	0.00061	0.00206	0.027
-40	0.021	16	5.8	21.8	22.4	0.1	0.005	0.000	0.005	0.009	0.00081	0.00287	0.036
-44	0.026	14	5.6	19.6	20.7	0.2	0.005	0.000	0.005	0.009	0.00090	0.00377	0.045
-48	0.031	13	5.5	18.5	19.1	0.1	0.005	0.000	0.005	0.010	0.00103	0.00480	0.055
-52	0.035	13	5.3	18.3	18.4	0.2	0.004	0.000	0.004	0.008	0.00088	0.00568	0.063
-55	0.039	12	5.2	17.2	17.8	0.1	0.004	0.000	0.004	0.008	0.00089	0.00657	0.071

Table 4.2.6A: Calculation sheet for the transformation of CAL-data (very mature, virgin 0.4 W/C HOC-paste during cooling) into cumulative pore size distribution.
Assumption: $t_{nf} = 19.7 \cdot (T_0 - T)^{-1/3}$
See next page for further information.

T °C	W_f g/g$_{dry}$	r_K Å	t_{nf} Å	r_p Å	$\overline{r_p}$ Å	Δt_{nf} Å	ΔW_f g/g$_{dry}$	ΔW_{tf} g/g$_{dry}$	ΔW_{Kf} g/g$_{dry}$	ΔW_{pf} g/g$_{dry}$	ΔS_p $10^4 \cdot m^2$/g$_{dry}$	$\sum \Delta S_p$ $10^4 \cdot m^2$/g$_{dry}$	$\sum \Delta W_p$ cm^3/g$_{dry}$
-3	0	166	13.7	179.7								0	0
					119.9	4.6	0.004	0.000	0.004	0.005	0.00008		
-10	0.004	51	9.1	60.1								0.00008	0.005
					56.4	1.5	0.005	0.000	0.005	0.007	0.00025		
-12	0.009	44	8.6	52.6								0.00033	0.012
					48.3	0.6	0.006	0.000	0.006	0.009	0.00036		
-15	0.015	36	8.0	44.0								0.00069	0.021
					41.9	0.3	0.005	0.000	0.005	0.007	0.00036		
-17	0.020	32	7.7	39.7								0.00105	0.028
					37.0	0.4	0.006	0.000	0.006	0.009	0.00050		
-20	0.026	27	7.3	34.3								0.00155	0.037
					31.5	0.6	0.006	0.000	0.006	0.010	0.00061		
-25	0.032	22	6.7	28.7								0.00216	0.047
					27.0	0.4	0.006	0.000	0.006	0.010	0.00076		
-30	0.038	19	6.3	25.3								0.00292	0.057
					24.2	0.3	0.006	0.000	0.006	0.011	0.00088		
-35	0.044	17	6.0	23.0								0.00380	0.068
					22.4	0.2	0.005	0.000	0.005	0.009	0.00082		
-40	0.049	16	5.8	21.8								0.00462	0.077
					20.7	0.3	0.005	0.001	0.004	0.007	0.00072		
-45	0.054	14	5.5	19.5								0.00534	0.084
					18.9	0.2	0.005	0.001	0.004	0.008	0.00082		
-50	0.059	13	5.3	18.3								0.00616	0.092
					18.3	0.1	0.005	0.000	0.005	0.010	0.00108		
-55	0.064	13	5.2	18.2								0.00724	0.102

Table 4.2.6B: Calculation sheet for the transformation of CAL-data (very mature, dried/resaturated 0.4 W/C HOC-paste during cooling) into cumulative pore size distribution.
Assumption: $t_{nf} = 19.7 \cdot (T_0 - T)^{-1/3}$
See next page for further information.

T °C	w_f g/g$_{dry}$	r_K Å	t_{nf} Å	r_p Å	$\overline{r_p}$ Å	Δt_{nf} Å	Δw_f g/g$_{dry}$	Δw_{tf} g/g$_{dry}$	Δw_{Kf} g/g$_{dry}$	Δw_{pf} g/g$_{dry}$	ΔS_p $10^4 \cdot m^2/g_{dry}$	$\sum \Delta S_p$ $10^4 \cdot m^2/g_{dry}$	$\sum \Delta W_p$ cm^3/g$_{dry}$
-4	0	125	12.4	137.4								0	0
					110.4	2.1	0.028	0	0.028	0.034	0.00061		
-7	0.028	73	10.3	83.3								0.00061	0.034
					71.7	1.2	0.022	0.000	0.022	0.029	0.00080		
-10	0.050	51	9.1	60.1								0.00141	0.063
					54.8	0.7	0.009	0.001	0.008	0.011	0.00041		
-13	0.059	41	8.4	49.4								0.00182	0.074
					45.6	0.6	0.010	0.001	0.009	0.013	0.00057		
-16	0.069	34	7.8	41.8								0.00239	0.087
					38.1	0.5	0.013	0.001	0.012	0.018	0.00094		
-20	0.082	27	7.3	34.3								0.00333	0.105
					31.5	0.5	0.015	0.002	0.013	0.021	0.00133		
-25	0.097	22	6.7	28.7								0.00466	0.126
					27.0	0.4	0.016	0.002	0.014	0.024	0.00176		
-30	0.113	19	6.3	25.3								0.00642	0.150
					24.2	0.3	0.016	0.002	0.014	0.025	0.00205		
-35	0.129	17	6.0	23.0								0.00847	0.175
					22.4	0.2	0.013	0.002	0.011	0.020	0.00180		
-40	0.142	16	5.8	21.8								0.01027	0.195
					20.7	0.3	0.014	0.003	0.011	0.020	0.00197		
-45	0.156	14	5.5	19.5								0.01224	0.215
					18.9	0.2	0.014	0.002	0.012	0.023	0.00243		
-50	0.170	13	5.3	18.3								0.01467	0.238
					18.3	0.1	0.014	0.001	0.013	0.026	0.00284		
-55	0.184	13	5.2	18.2								0.01751	0.264

Table 4.2.6C: Calculation sheet for the transformation of CAL-data (very mature, virgin 0.6 W/C HOC-paste during cooling) into cumulative pore size distribution.
Assumption: $t_{nf} = 19.7 \cdot (T_0 - T)^{-1/3}$
See next page for further information.

T °C	W_f g/g$_{dry}$	r_K Å	t_{nf} Å	r_p Å	$\overline{r_p}$ Å	Δt_{nf} Å	ΔW_f g/g$_{dry}$	ΔW_{tf} g/g$_{dry}$	ΔW_{Kf} g/g$_{dry}$	ΔW_{pf} g/g$_{dry}$	ΔS_p $10^4 \cdot m^2$/g$_{dry}$	$\sum \Delta S_p$ $10^4 \cdot m^2$/g$_{dry}$	$\sum \Delta W_p$ cm^3/g$_{dry}$
-3	0	166	13.7	179.7								0	0
-5	0.040	101	11.5	112.5	146.1	2.2	0.040	0	0.040	0.047	0.00064	0.00064	0.047
-7	0.075	73	10.3	83.3	97.9	1.2	0.035	0.000	0.035	0.043	0.00089	0.00153	0.090
-10	0.128	51	9.1	60.1	71.7	1.2	0.053	0.002	0.051	0.066	0.00185	0.00338	0.156
-15	0.146	36	8.0	44.0	52.1	1.1	0.018	0.004	0.014	0.019	0.00073	0.00411	0.175
-20	0.164	27	7.3	34.3	39.2	0.7	0.018	0.003	0.015	0.022	0.00112	0.00523	0.197
-25	0.167	22	6.7	28.7	31.5	0.6	0.003	0.003	0	0	0	0.00523	0.197
-30	0.170	19	6.3	25.3	27.0	0.4	0.003	0.002	0.001	0.002	0.00013	0.00536	0.199
-35	0.173	17	6.0	23.0	24.2	0.3	0.003	0.002	0.001	0.002	0.00015	0.00551	0.201
-40	0.178	16	5.8	21.8	22.4	0.2	0.005	0.001	0.004	0.007	0.00065	0.00616	0.208
-45	0.183	14	5.5	19.5	20.7	0.3	0.005	0.002	0.003	0.006	0.00054	0.00670	0.214
-50	0.189	13	5.3	18.3	18.9	0.2	0.006	0.001	0.005	0.010	0.00103	0.00773	0.224
-55	0.194	13	5.2	18.2	18.3	0.1	0.005	0.000	0.005	0.010	0.00108	0.00881	0.234

Table 4.2.6D: Calculation sheet for the transformation of CAL-data (very mature, dried/resaturated 0.6 W/C HOC-paste during cooling) into cumulative pore size distribution.
Assumption: $t_{nf} = 19.7 \cdot (T_0 - T)^{-1/3}$
See next page for further information.

Explanatory text for tables 4.2.6A-D

T : Temperature (°C)

$T_0 - T$: Freezing point depression (°C)

w_f : Amount of frozen water (g/g_{dry}) read from the cumulative ice formation curve

r_K : Kelvinradius (Å) of the solid/liquid meniscus (from section 3.1.1)

t_{nf} : The unfrozen layer (Å) at surfaces (from section 3.1.1 or section 5.5)

r_p : Pore radius (Å) = $r_K + t_{nf}$

$\overline{r_p}$: Mean value (Å) of two pore radii in a temperature interval

Δt_{nf} : Change in unfrozen layer (Å) in the temperature interval

Δw_f : Change in amount of frozen water (g/g_{dry}) in a temperature interval

Δw_{tf} : Change in amount of unfrozen water (g/g_{dry}) in a temperature interval:

$$\Delta w_{tf} = \Delta t_{nf} \cdot \Sigma \Delta s_p$$

Δw_{kf} : Change in amount of frozen capillary condensed water (g/g_{dry}) in a temperature interval.
Assuming circular cylindrical pores:

$$\Delta w_{kf} = \Delta w_f - \Delta w_{tf}$$

Δw_{pf} : Change in pore volume (g/g_{dry}) in a temperature interval.
Assuming circular cylindrical pores:

$$\Delta w_{pf} = \Delta w_{kf} \cdot (r_p / r_K)^2$$

Δs_p : Change in pore surface area ($g/g_{dry}/Å \sim 10^4 \cdot m^2/g_{dry}$, assuming $\rho = 1\ g/cm^3$).
Assuming circular cylindrical pores:

$$\Delta s_p = 2 \cdot (\Delta w_{pf} / \overline{r_p})$$

$\Sigma \Delta s_p$: Cumulative pore surface area ($10^4 \cdot m^2/g_{dry}$). Initially, $\Sigma \Delta s_p = 0$.

$\Sigma \Delta w_p$: Cumulative pore volume ($g/g_{dry} \sim cm^3/g_{dry}$, assuming $\rho = 1\ g/cm^3$)

Specimen		no.	Age*	ρ_{ssd}	w_{de}	w_{es}	ε	w_n
			days	g/cm^3	g/g_{dry}	g/g_{dry}	% by vol.	g/g_{ign}
ROC/0/0.4	V	1.1	211	2.02	-	0.234	38.3	0.204
ROC/0/0.4	D/R	1.6	(104)	1.99	0.078	0.231	37.3	0.216
SAC/0/0.4	V	3.12	200	2.02	-	0.244	39.6	0.177
SAC/0/0.4	D/R	3.10	(92)	2.01	0.075	0.250	40.3	0.185
HOC/0/0.4	V	2.19	201	2.01	-	0.231	37.6	0.196
HOC/0/0.4	D/R	2.11	(99)	1.98	0.090	0.247	39.2	0.202
BLC/0/0.4	V	5.2	205	1.96	-	0.271	41.8	0.313
BLC/0/0.4	D/R	5.4	(83)	1.96	0.071	0.270	41.8	0.318
OPC/0/0.4	V	7.5	201	2.02	-	0.219	36.4	0.209
OPC/0/0.4	D/R	7.3	(90)	2.02	0.044	0.212	35.3	0.218
BILAG3/0/0.4	V	6.5	200	2.01	-	0.220	36.3	0.220
BILAG3/0/0.4	D/R	6.2	(82)	2.01	0.078	0.217	35.9	0.232

Table 4.3.1: Physical characteristics for CAL-specimens (CBL-serie)

V are virgin specimens
D/R are dried/resaturated specimens

- not available
* Age:
For virgin specimens, this is the age for CAL.
For dried/resat. specimens, this is the age for initiation of the drying/resaturation treatment.

Specimen		no.	Age*	ρ_{ssd}	w_{de}	w_{es}	ε	w_n
			days	g/cm^3	g/g_{dry}	g/g_{dry}	% by vol.	g/g_{ign}
ROC/0/0.3	V	8.1	204	2.18	-	0.165	30.8	0.176
ROC/0/0.3	D/R	8.4	(89)	2.17	0.046	0.155	29.1	0.193
ROC/M/0.2	V	9.4	204	2.29	-	0.134	27.0	0.150
ROC/M/0.2	D/R	9.6	(84)	2.29	0.075	0.158	31.2	0.177
SAC/0/0.3	V	10.6	203	2.19	-	0.165	31.0	0.161
SAC/0/0.3	D/R	10.2	(85)	2.17	0.010	0.122	23.6	0.164
SAC/M/0.2	V	11.3	205	2.34	-	0.123	25.7	0.132
SAC/M/0.2	D/R	11.2	(83)	2.34	0.038	0.112	23.6	0.144
P30-4A/0/0.4	V	12.2	259	2.08	-	0.221	37.6	0.204
P30-4A/0/0.4	D/R	12.4	(248)	2.01	0.115	0.228	37.3	0.207

Table 4.3.1: Continued

ρ_{ssd} = saturated, surface dry density
w_{de} = residual water content after drying at 50 °C and 11 % r.h. for 3 days
w_{es} = total evaporable water content
ε = porosity
w_n = non-evaporable water content

Specimen		ICE FORMATION (w_f)								w_{es}	NON-FROZEN WATER (w_{nf})				
		-55°C				-35°C	-20°C	-10°C	-10°C		-55°C	-35°C	-20°C	-10°C	-10°C
		COOL		HEAT		COOL			HEAT		COOL				HEAT
		TOT	INCR	TOT	INCR										
ROC/0/0.4	V	42	49	47	52	16	0	0	28	234	185	218	234	234	206
ROC/0/0.4	D/R	67	61	71	67	51	46	27	61	231	170	180	185	204	170
SAC/0/0.4	V	57	61	-	-	29	4	0	-	244	183	215	240	244	-
SAC/0/0.4	D/R	77	75	80	78	61	55	36	69	250	175	189	195	214	181
HOC/0/0.4	V	31	35	44	47	10	0	0	23	231	196	221	231	231	208
HOC/0/0.4	D/R	64	63	66	64	50	41	21	55	247	184	197	206	226	192
BLC/0/0.4	V	90	100	98	100	42	3	0	60	271	171	229	268	271	211
BLC/0/0.4	D/R	101	103	107	104	76	64	41	92	270	167	194	206	229	178
OPC/0/0.4	V	37	41	45	50	18	2	0	26	219	178	201	217	219	193
OPC/0/0.4	D/R	58	55	63	64	43	31	13	49	212	157	169	181	199	163
BILAG3/0/0.4	V	28	30	31	36	8	0	0	14	220	190	212	220	220	206
BILAG3/0/0.4	D/R	58	54	57	55	41	30	12	45	217	163	176	187	205	172

Table 4.3.2: Data on ice formation and water content (given in mg/g_{dry}) from CAL-tests performed at CBL. Water content were optained by CO_2-free drying (table 4.3.1).

V are virgin specimens
D/R are dried/resaturated specimens

- data not available

Specimen		ICE FORMATION (w_f)								w_{es}	NON-FROZEN WATER (w_{nf})				
		-55°C				-35°C	-20°C	-10°C	-10°C		-55°C	-35°C	-20°C	-10°C	-10°C
		COOL		HEAT		COOL			HEAT		COOL				HEAT
		TOT	INCR	TOT	INCR										
ROC/0/0.3	V	15	14	18	20	3	1	0	7	165	151	162	164	165	158
ROC/0/0.3	D/R	28	29	30	30	19	4	1	20	155	126	136	151	154	135
ROC/M/0.2	V	0	5	0	0	0	0	0	0	134	129	134	134	134	134
ROC/M/0.2	D/R	7	12	12	12	2	0	0	6	134	127	132	134	134	128
SAC/0/0.3	V	24	13	23	23	3	0	0	10	122	109	119	122	122	112
SAC/0/0.3	D/R	30	32	56	35	21	10	1	25	122	90	101	112	121	97
SAC/M/0.2	V	0	5	0	0	0	0	0	0	123	118	123	123	123	123
SAC/M/0.2	D/R	12	6	12	12	2	0	0	6	112	106	110	112	112	106
P30-4A/0/0.4	V	38	36	41	42	9	0	0	21	221	185	212	221	221	200
P30-4A/0/0.4	D/R	59	60	64	60	45	40	26	51	207	147	162	167	181	156

Table 4.3.2: Continued

Specimen		$S_{BET(N_2)}$, m^2/g_{dry}	
		CO_2-free dried	Methanol-replaced
ROC/0/0.4	V	29.3	58.7
ROC/0/0.4	D/R	23.7	57.9
SAC/0/0.4	V	31.9	-
SAC/0/0.4	D/R	27.9	-
HOC/0/0.4	V	15.3	67.4
HOC/0/0.4	D/R	17.5	62.9
BLC/0/0.4	V	26.3	-
BLC/0/0.4	D/R	21.2	-
OPC/0/0.4	V	20.8	-
OPC/0/0.4	D/R	-	-
BILAG3/0/0.4	V	53.3	-
BILAG3/0/0.4	D/R	27.5	-
ROC/0/0.3	V	6.3	-
ROC/0/0.3	D/R	9.1	-
ROC/M/0.2	V	11.3	-
ROC/M/0.2	D/R	5.3	-
SAC/0/0.3	V	16.5	-
SAC/0/0.3	D/R	13.8	-
SAC/M/0.2	V	3.6	-
SAC/M/0.2	D/R	10.9	-
P30-4A/0/0.4	V	-	28.7
P30-4A/0/0.4	D/R	-	28.1

Table 4.3.3: Specific BET-surface area, calculated from the adsorption branch of the nitrogen isotherm for specimens dried by either CO_2-free drying or methanol-replacement.

- not measured

Specimen		no.	Age*	ρ_{ssd}	w_{de}	w_{es}	ε	w_n
			days	g/cm^3	g/g_{dry}	g/g_{dry}	% by vol.	g/g_{ign}
PFC/0/0.4	V	2.11	89	1.94	-	0.261	40.1	0.187
PFC/0/0.4	D/R	2.16	(90)	1.95	0.095	0.269	41.4	0.208
PFC/N/0.4	V	14.1	79	1.93	-	0.288	43.1	0.203
PFC/N/0.4	D/R	14.2	(90)	1.93	0.069	0.282	42.5	0.216
PFC/M/0.4	V	9.5	92	1.94	-	0.262	40.3	0.217
PFC/M/0.4	D/R	9.4	(90)	1.94	0.067	0.273	41.5	0.207
PFC/LS/0.4	V	8.2	96	1.93	-	0.256	39.4	0.211
PFC/LS/0.4	D/R	8.4	(90)	1.96	0.067	0.258	40.1	0.196
PFC/HC/0.4	V	11.23	145	1.96	-	0.273	42.0	0.201
PFC/HC/0.4	D/R	11.12	(90)	1.95	0.071	0.264	40.7	0.209
ROC/0/0.4	V	1.24	99	2.03	-	0.229	37.8	0.207
ROC/0/0.4	D/R	1.13	(90)	2.02	0.078	0.231	37.9	0.205
ROC/N/0.4	V	7.15	94	2.00	-	0.237	38.3	0.211
ROC/N/0.4	D/R	7.13	(90)	2.00	0.134	0.242	39.0	0.211

Table 4.4.1: Physical characteristics for CAL-specimens (LBM-serie)

V are virgin specimens
D/R are dried/resaturated specimens

- not available
* Age: see table 4.3.1

Specimen		no.	Age*	ρ_{ssd}	w_{de}	w_{es}	ε	w_n
			days	g/cm^3	g/g_{dry}	g/g_{dry}	% by vol.	g/g_{ign}
ROC/M/0.4	V	5.4	177	2.01	-	0.246	39.7	0.209
ROC/M/0.4	D/R	5.6	(90)	2.00	0.078	0.237	38.3	0.208
ROC/LS/0.4	V	4.12	94	2.02	-	0.235	38.4	0.204
ROC/LS/0.4	D/R	4.5	(90)	2.01	0.094	0.237	38.5	0.209
ROC/HC/0.4	V	6.12	166	2.03	-	0.237	39.0	0.206
ROC/HC/0.4	D/R	6.15	(90)	2.02	0.075	0.233	38.1	0.209
SAC/O/0.4	V	3.22	167	2.03	-	0.250	40.6	0.171
SAC/O/0.4	D/R	3.21	(90)	2.02	0.086	0.244	39.8	0.179
SAC/N/0.4	V	15.11	134	2.01	-	0.265	42.0	0.178
SAC/N/0.4	D/R	15.2	(90)	2.00	0.069	0.264	41.8	0.176
SAC/M/0.4	V	10.23	88	2.01	-	0.260	41.5	0.176
SAC/M/0.4	D/R	10.21	(90)	2.00	0.067	0.256	40.7	0.179
SAC/LS/0.4	V	13.2	80	2.02	-	0.260	41.6	0.168
SAC/LS/0.4	D/R	13.13	(90)	2.01	0.067	0.251	40.4	0.175
SAC/HC/0.4	V	12.6	94	2.03	-	0.255	41.1	0.166
SAC/HC/0.4	D/R	12.2	(90)	2.02	0.066	0.245	39.8	0.173

Table 4.4.1: Continued

Specimen		ICE FORMATION (w_f)								w_{es}	NON-FROZEN WATER (w_{nf})				
		-55°C				-35°C	-20°C	-10°C	-10°C		-55°C	-35°C	-20°C	-10°C	-10°C
		COOL		HEAT		COOL			HEAT		COOL				HEAT
		TOT	INCR	TOT	INCR										
PFC/0/0.4	V	90	101	109	114	65	5	0	64	261	160	196	256	261	197
PFC/0/0.4	D/R	110	105	143	134	75	55	21	83	269	164	194	214	248	186
PFC/N/0.4	V	95	114	167	170	81	31	0	75	288	174	207	257	288	213
PFC/N/0.4	D/R	117	113	137	131	88	61	7	90	282	169	194	221	275	192
PFC/M/0.4	V	98	97	146	146	65	10	0	67	262	165	197	252	262	195
PFC/M/0.4	D/R	115	106	138	131	78	52	8	86	273	167	195	221	265	187
PFC/LS/0.4	V	93	81	162	163	52	2	0	63	256	175	204	254	256	193
PFC/LS/0.4	D/R	105	100	119	112	69	43	3	77	258	158	189	215	255	181
PFC/HC/0.4	V	96	93	144	141	52	1	0	58	273	180	221	272	273	215
PFC/HC/0.4	D/R	110	107	128	123	77	54	25	85	264	157	187	210	239	179
ROC/0/0.4	V	56	47	73	74	17	0	0	27	229	182	212	229	229	202
ROC/0/0.4	D/R	75	71	123	113	60	49	31	59	231	160	171	182	200	172
ROC/N/0.4	V	47	46	72	75	25	1	0	30	237	191	212	236	237	207
ROC/N/0.4	D/R	62	57	63	61	45	37	23	45	242	185	197	205	219	197

Table 4.4.2: Data on ice formation and water content (given in mg/g_{dry}) from CAL-tests performed at LBM. Water content were optained by CO_2-free drying at LBM (table 4.4.1).

V are virgin specimens
D/R are dried/resaturated specimens

Specimen	ICE FORMATION (w_f)								w_{es}	NON-FROZEN WATER (w_{nf})				
	-55°C				-35°C	-20°C	-10°C	-10°C		-55°C	-35°C	-20°C	-10°C	-10°C
	COOL		HEAT		COOL			HEAT		COOL				HEAT
	TOT	INCR	TOT	INCR										
ROC/M/0.4 V	48	45	59	59	19	0	0	25	246	201	227	246	246	221
ROC/M/0.4 D/R	75	72	94	90	60	49	25	59	237	165	177	188	212	178
ROC/LS/0.4 V	51	45	60	60	19	0	0	26	235	190	216	235	235	209
ROC/LS/0.4 D/R	73	68	89	85	56	46	30	56	237	169	181	191	207	181
ROC/HC/0.4 V	47	37	85	84	13	0	0	23	237	200	224	237	237	214
ROC/HC/0.4 D/R	75	74	85	80	62	49	24	59	233	159	171	184	209	174
SAC/0/0.4 V	69	62	96	91	30	2	0	38	250	188	220	248	250	212
SAC/0/0.4 D/R	89	88	108	103	76	68	52	75	244	156	168	176	192	169
SAC/N/0.4 V	72	87	91	87	47	10	2	41	265	178	218	255	263	224
SAC/N/0.4 D/R	93	94	104	100	81	68	36	78	264	170	183	196	228	186
SAC/M/0.4 V	85	81	138	134	51	5	0	55	260	179	209	255	260	205
SAC/M/0.4 D/R	100	98	121	116	86	76	39	84	256	158	170	180	217	172
SAC/LS/0.4 V	78	83	186	180	47	7	1	50	260	177	213	253	259	210
SAC/LS/0.4 D/R	92	91	122	117	78	67	40	74	251	160	173	184	211	177
SAC/HC/0.4 V	74	73	106	102	39	4	0	44	255	183	216	251	255	211
SAC/HC/0.4 D/R	90	89	96	93	76	65	38	73	245	156	169	180	207	172

Table 4.4.2: Continued

	MORTAR CHARACTERISTICS				K(90)	s	k_d(90)	s	K(98)	s	k_d(98)	s
	Cement	Additive	W/C	Moisture history	10^{-16} kg/Pa·m·s		10^{-12} kg/Pa·m·s		10^{-16} kg/Pa·m·s		10^{-12} kg/Pa·m·s	
Data from /12/	ROC	0	0.4	V	1.05	0.21	2.60	0.90	4.15	0.78	2.12	0.73
		N			1.18	0.10	3.44	0.27	4.75	0.40	2.80	0.22
		M			1.25	0.10	3.07	0.18	5.05	0.37	2.50	0.14
		LS			0.93	0.17	3.15	0.16	3.77	0.75	2.56	0.13
		HC			1.33	0.12	3.38	0.53	5.23	0.47	2.75	0.44
	SAC	0	0.4	V	1.40	0.34	3.17	0.25	5.63	1.34	2.57	0.21
		N			2.10	0.08	4.44	0.17	8.43	0.38	3.61	0.13
		M			2.18	0.36	3.60	0.63	8.65	1.44	2.92	0.52
		LS			1.68	0.15	3.69	0.33	6.73	0.66	3.00	0.27
		HC			1.33	0.17	2.95	0.37	5.38	0.72	2.40	0.30
	PFC	0	0.4	V	1.43	0.22	2.36	0.28	5.73	0.82	1.92	0.23
		N			1.53	0.26	6.18	0.45	6.15	0.95	5.03	0.37
		M			1.24	0.30	3.25	0.46	5.08	1.29	2.65	0.37
		LS			1.33	0.22	2.79	0.26	5.23	0.89	2.27	0.22
		HC			1.17	0.15	2.25	0.16	4.70	0.53	1.83	0.13
Data from /13/	ROC	0	0.4	V	2.09	0.18	2.45	0.09	7.06	0.58	2.48	0.13
			0.4	D/R	11.00	1.02	8.78	0.57	41.19	4.23	8.05	0.51
			0.6	V	12.55	1.47	10.81	0.48	49.93	5.87	8.46	0.37
	SAC	0	0.4	V	4.50	0.47	3.57	0.23	17.30	1.82	3.11	0.21
			0.4	D/R	14.00	2.50	6.46	0.67	54.74	9.94	5.56	0.56
			0.6	V	19.23	2.59	9.59	1.11	76.29	10.4	7.69	0.88
	PFC	0	0.4	V	2.07	0.15	4.32	0.26	7.38	0.60	3.74	0.20
			0.4	D/R	2.31	0.37	6.80	0.54	8.13	1.52	5.76	0.43
			0.6	V	16.71	1.22	14.35	1.03	63.81	4.81	12.48	0.84

Table 4.5.1: Results from permeability tests on mature mortar by CUP, performed at LBM. Data from Holland /12/ and Rosenbom and Waldstrøm /13/.

K(90), K(98) = Water permeability coefficients (p/p_0 in evaporation front).
k_d(90), k_d(98) = Water vapour diffusion coefficients (p/p_0 in evaportion front).
s = Standard deviation

V virgin specimen
D/R dried/resaturated specimen

Cement	W/C	Moisture history	ICE FORMATION (w_f)				w_{es}	NON-FROZEN WATER (w_{nf})			
			-55°C	-35°C	-20°C	-10°C		-55°C	-35°C	-20°C	-10°C
ROC	0.4	V	19	11	6	6	78	59	67	72	72
		D/R	34	31	29	24	77	43	46	48	53
SAC		V	27	18	9	5	77	50	59	68	72
		D/R	35	34	31	27	79	44	45	48	52
PFC		V	30	16	5	4	84	54	68	79	80
		D/R	41	31	23	13	85	44	54	62	72

Table 4.5.2: Data on ice formation during cooling, and water content mg/g_{dry} mortar) from CAL-tests at LBM on mature mortars. Water content was optained by drying at 105 °C for 7 days. Data from /13/.

V virgin specimens
D/R dried/resaturated specimens

		W/C = 0.4		W/C = 0.6	
		V	D/R	V	D/R
$v_{N2}(<30\ Å)$	(cm^3/g_{dry})	0.089	0.030	0.093	0.030
$v_{MIP}(>30\ Å)$	(cm^3/g_{dry})	0.079	0.103	0.266	0.374
$v = v_{N2} + v_{MIP}$	(cm^3/g_{dry})	0.168	0.133	0.359	0.404
$\hat{\rho}_{ssd}$	(g/cm^3)	2.01	2.00	1.78	1.70
ρ_{ssd}	(g/cm^3)	2.00	2.00	1.77	1.77
ρ_s	(g/cm^3)	2.42	2.31	2.47	2.38

Table 5.6.1:

Estimated and measured bulk densities for very mature (8 years) HOC-pastes. Specimens for MIP (LBM) and N2-SORP (CBL) were CO_2-free dried from methanol saturated state.

$v_{N2}(<30\ Å)$ = specific volume (by N2-SORP) of pore smaller than 30 Å. Reading (micropore volume) from figures 5.1.3.1A-D.

$v_{MIP}(>30\ Å)$ = specific volume (by MIP) of pores larger than 30 Å. Reading from figures 4.2.2A-D (MIP LBM (Methanol)).

v = specific volume

ρ_{ssd} = saturated, surface-dry density. From table 4.2.3.

$\hat{\rho}_{ssd}$ = estimated saturated, surface-dry density.

$$\hat{\rho}_{ssd} = \rho_s - (\rho_s - \rho_w) \cdot (v \cdot \rho_s / (1 + v \cdot \rho_s))$$

ρ_s = solid density. Optained by Helium pycnometry, /51/.

ρ_w = density of water. Assumed 1 g/cm^3.

V virgin specimen

D/R dried/resaturated specimen

FIGURES

Figure 1.1.3.1:

Schematic illustration of the effects on pore structure upon drying and rewetting.

(1) A saturated pore system with two structural elements.

(2-3) Two phases during drying. Capillary tension stresses are building up in pore liquid.

(4) Small pores have collapsed, more or less permanently.

(5) Upon rewetting some of the new bonds will remain, thus creating:

(a) irreversible shrinkage
(b) a coarsening of the pore structure

(c) a decrease in total surface area

$$D_5 \approx D_A + D_B + D_C$$

$$(p/p_0)_2 < (p/p_0)_1$$

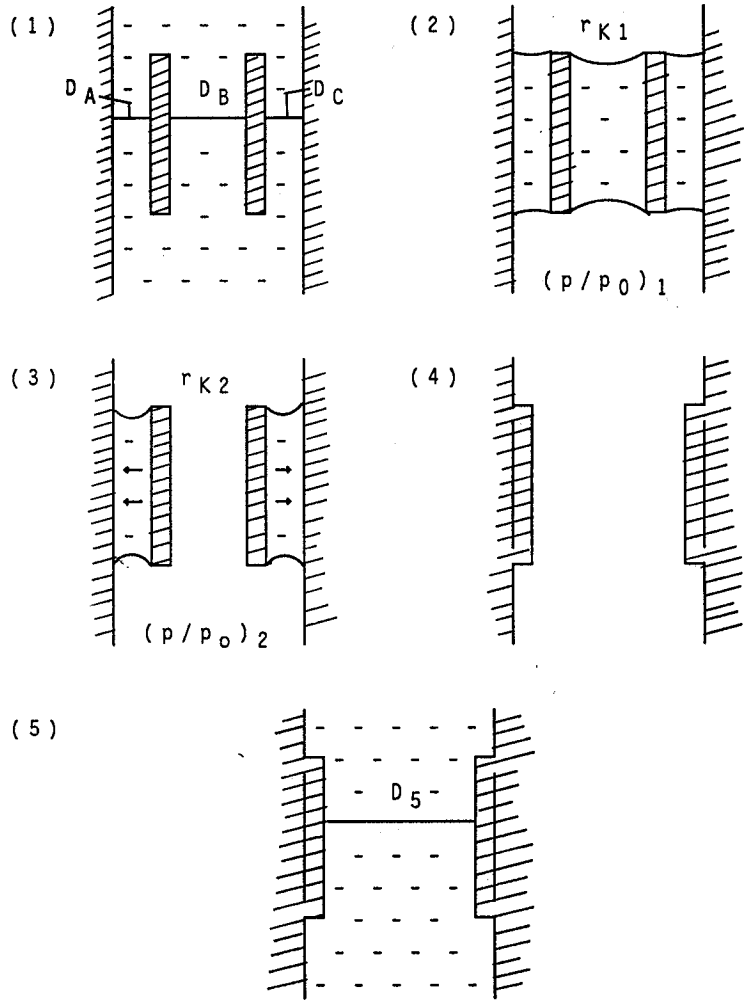

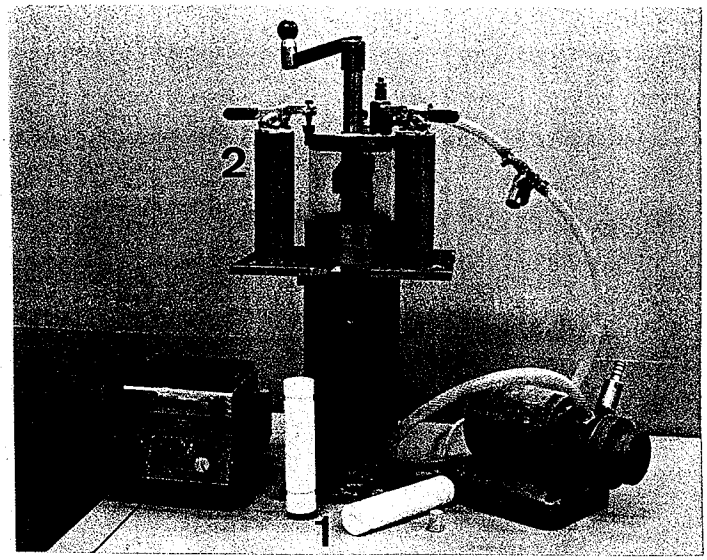

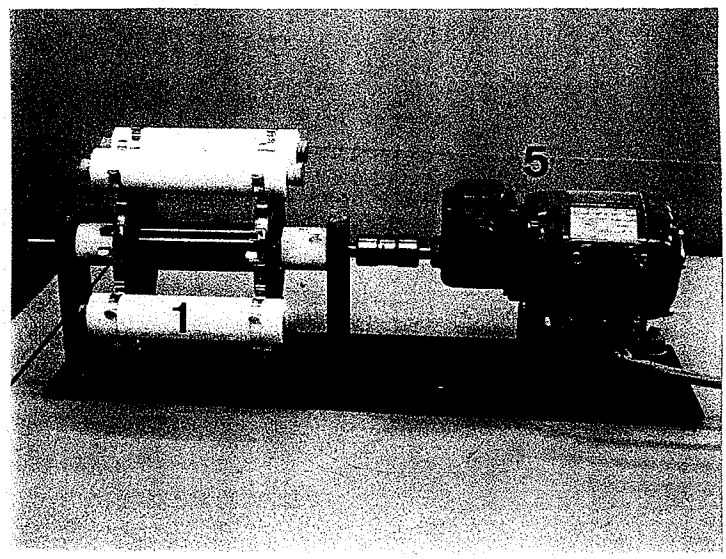

Figure 2.2.1.1 : Setup for the fabrication of HCP-specimens. Main components are:

1. Teflon moulds
2. Apparatus for deairing and subsequent casting of the paste
3. Vacuum pump
4. Vibrating plate
5. Electrical mould rotator

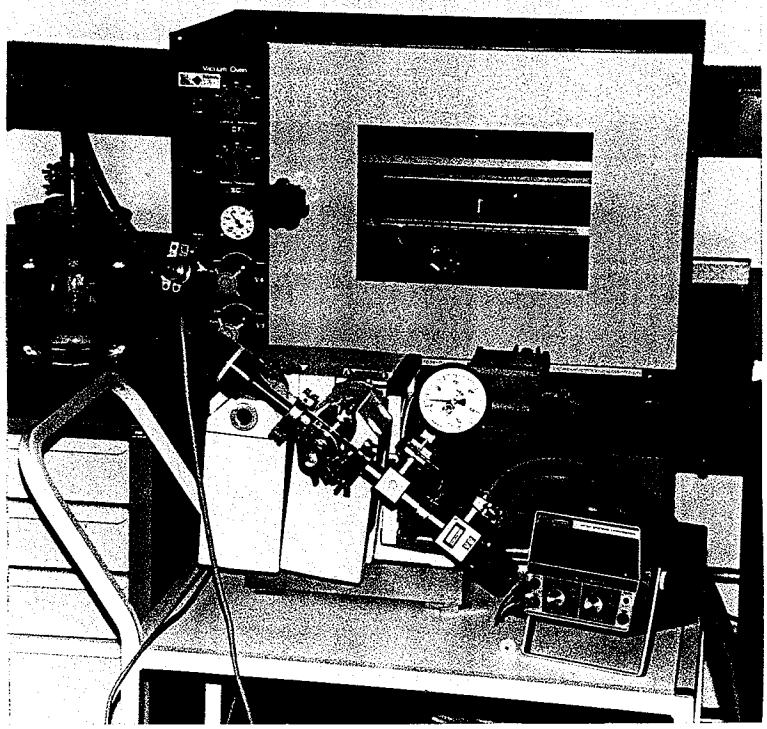

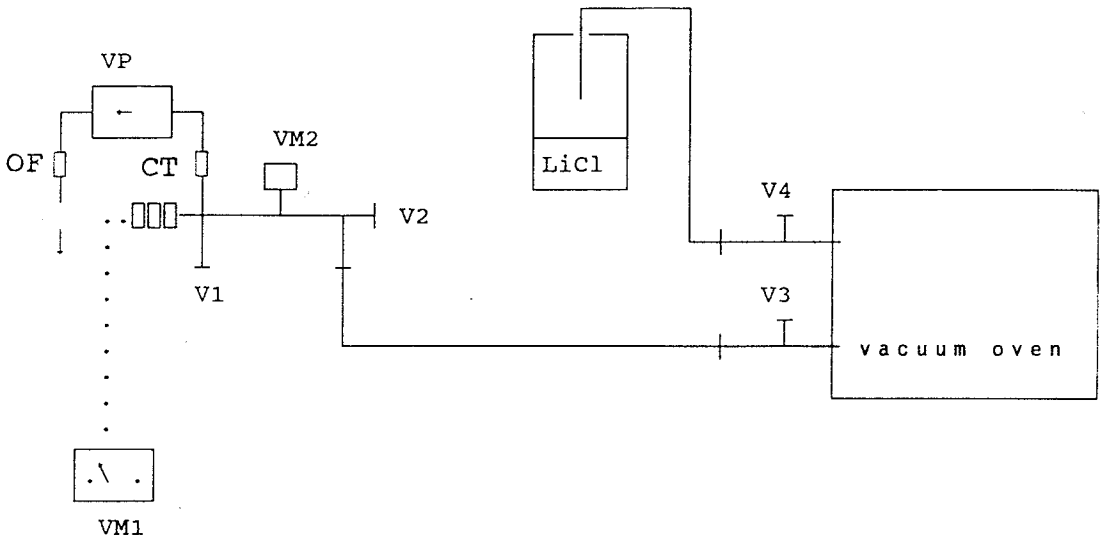

Figure 2.3.1.1: Experimental setup for CO_2-free drying.

V1-V4	:	Valves
OF	:	Oil mist filter
CT	:	Condensate trap
VM1,VM2	:	Vacuum meters
VP	:	Vacuum pump
LiCl	:	Saturated solution of LiCl

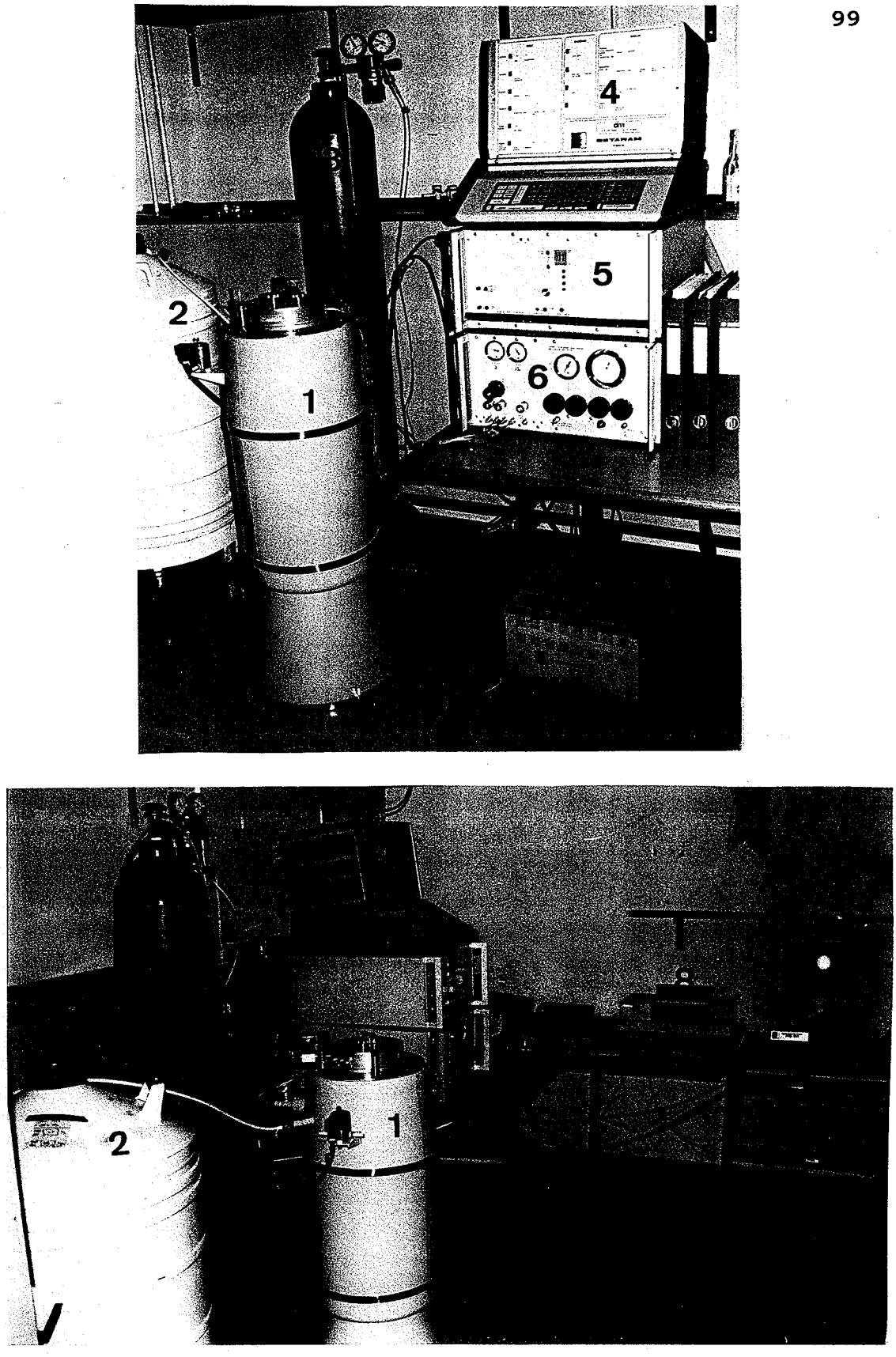

Figure 3.1.1A: Experimental setup for CAL at CBL.

Main components are:

1. Calvet microcalorimeter
2. Reservoir (100 l) for liquid nitrogen
3. N_2-gas
4. G11 Controller
5. Calibration unit
6. Gas circulation unit
7. PC
8. Plotter
9. Vacuum pump

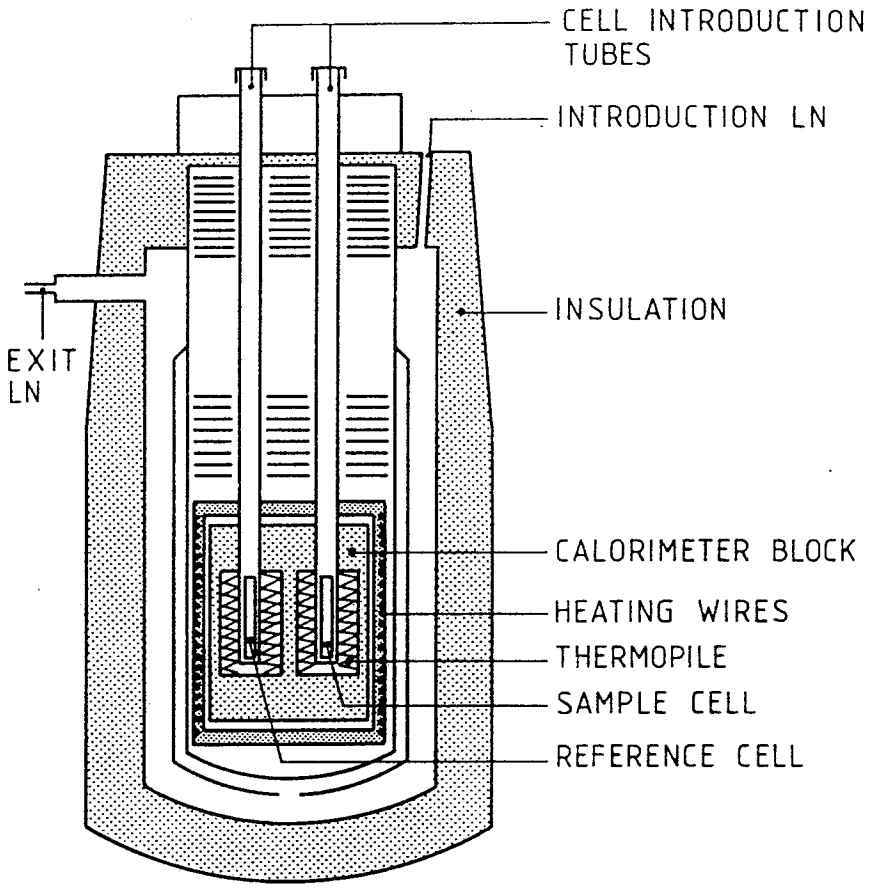

Figure 3.1.1B: Calvet lowtemperature microcalorimeter

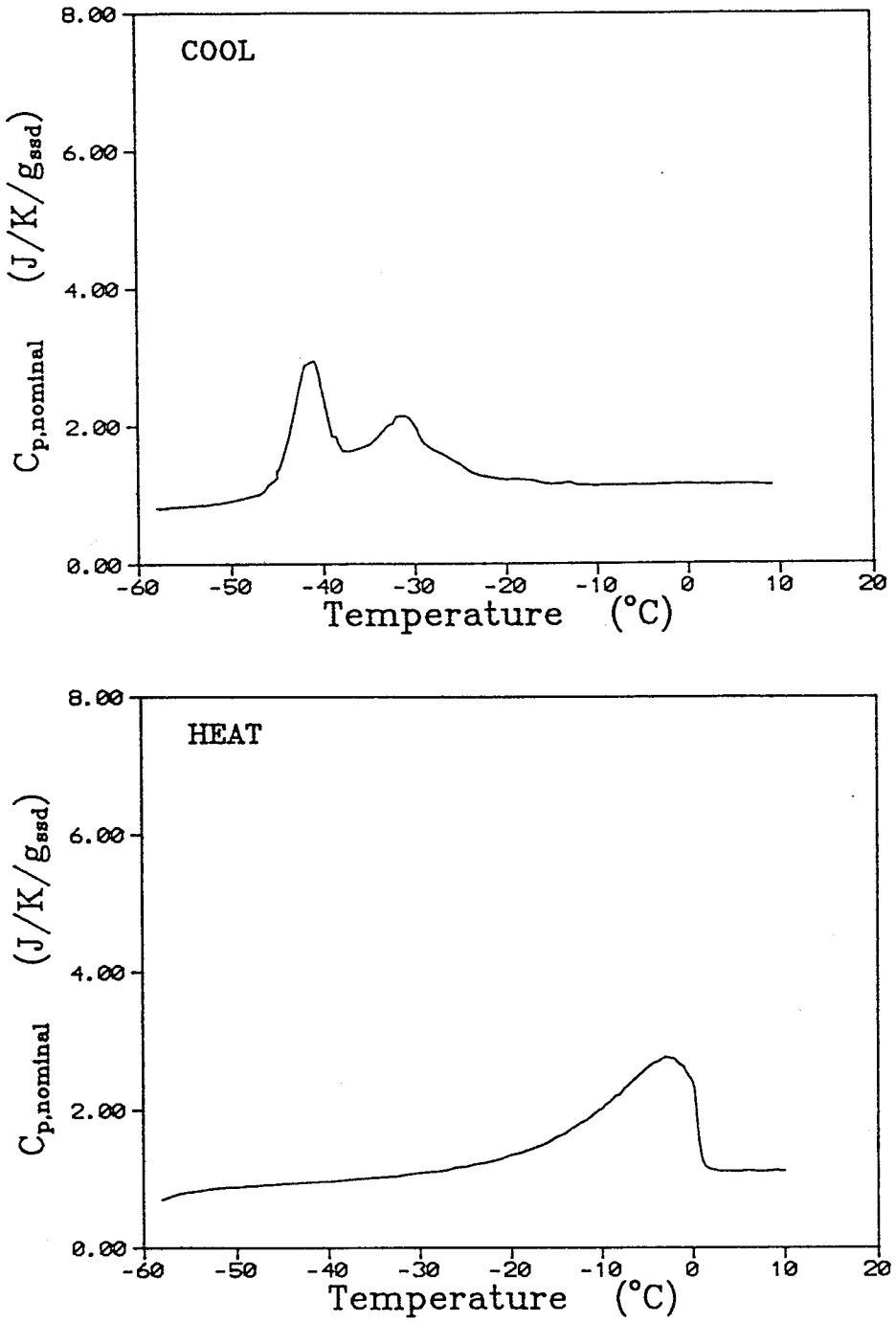

Figure 3.1.2: Example of heat capacity curves optained during both cooling (COOL) and heating (HEAT) for CAL.

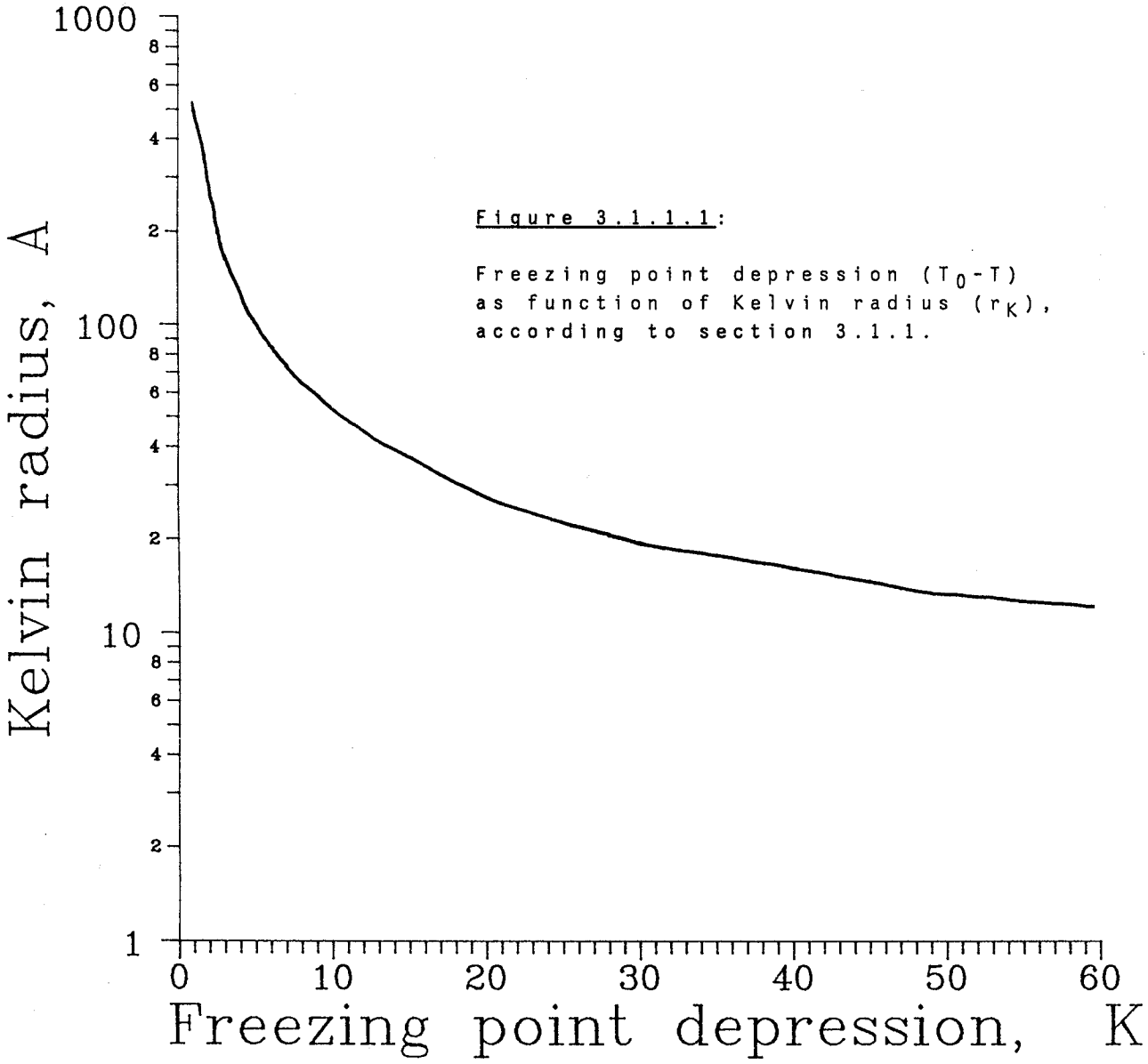

Figure 3.1.1.1:

Freezing point depression (T_0-T) as function of Kelvin radius (r_K), according to section 3.1.1.

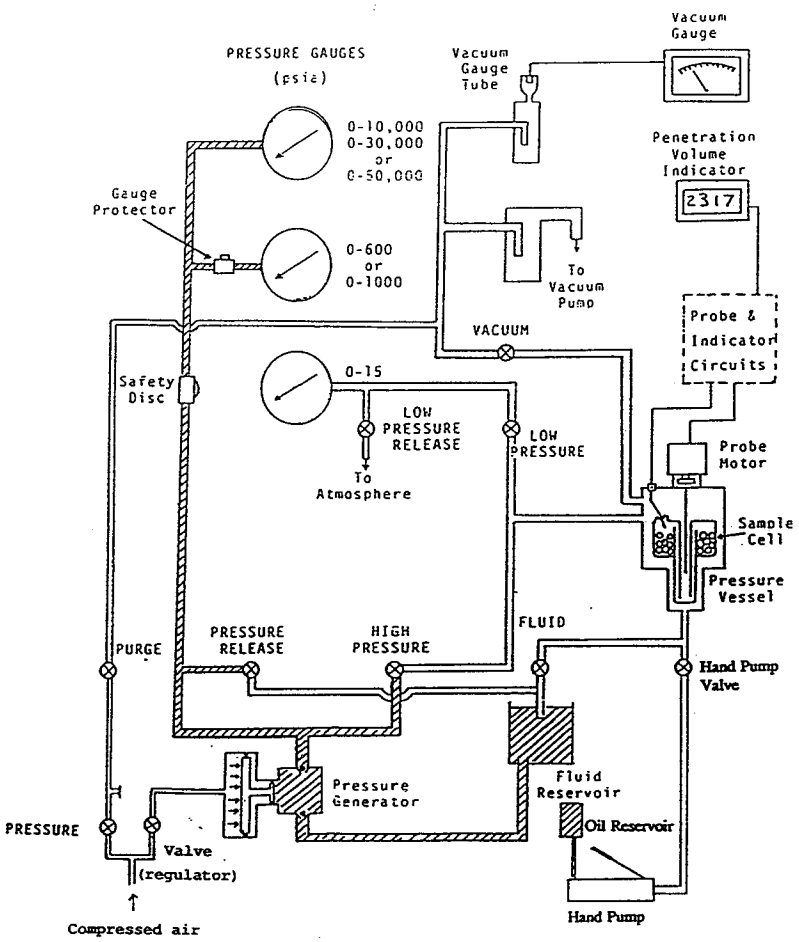

Figure 3.2.1: Diagram of porosimeter at LBM. From /20/.

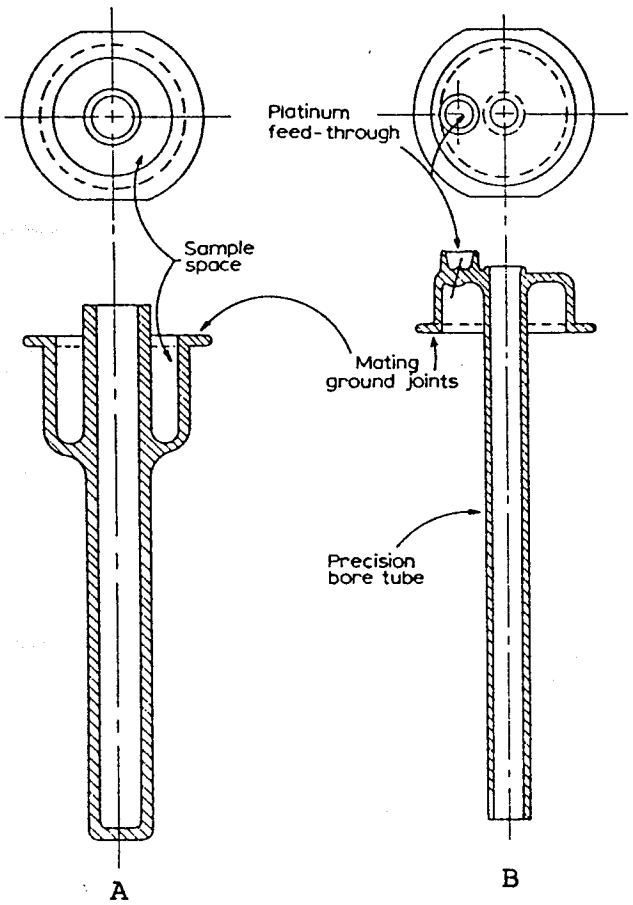

Figure 3.2.2: Sample cell of the porosimeter. Consists of sample holder (A) and cap (B). From /24/.

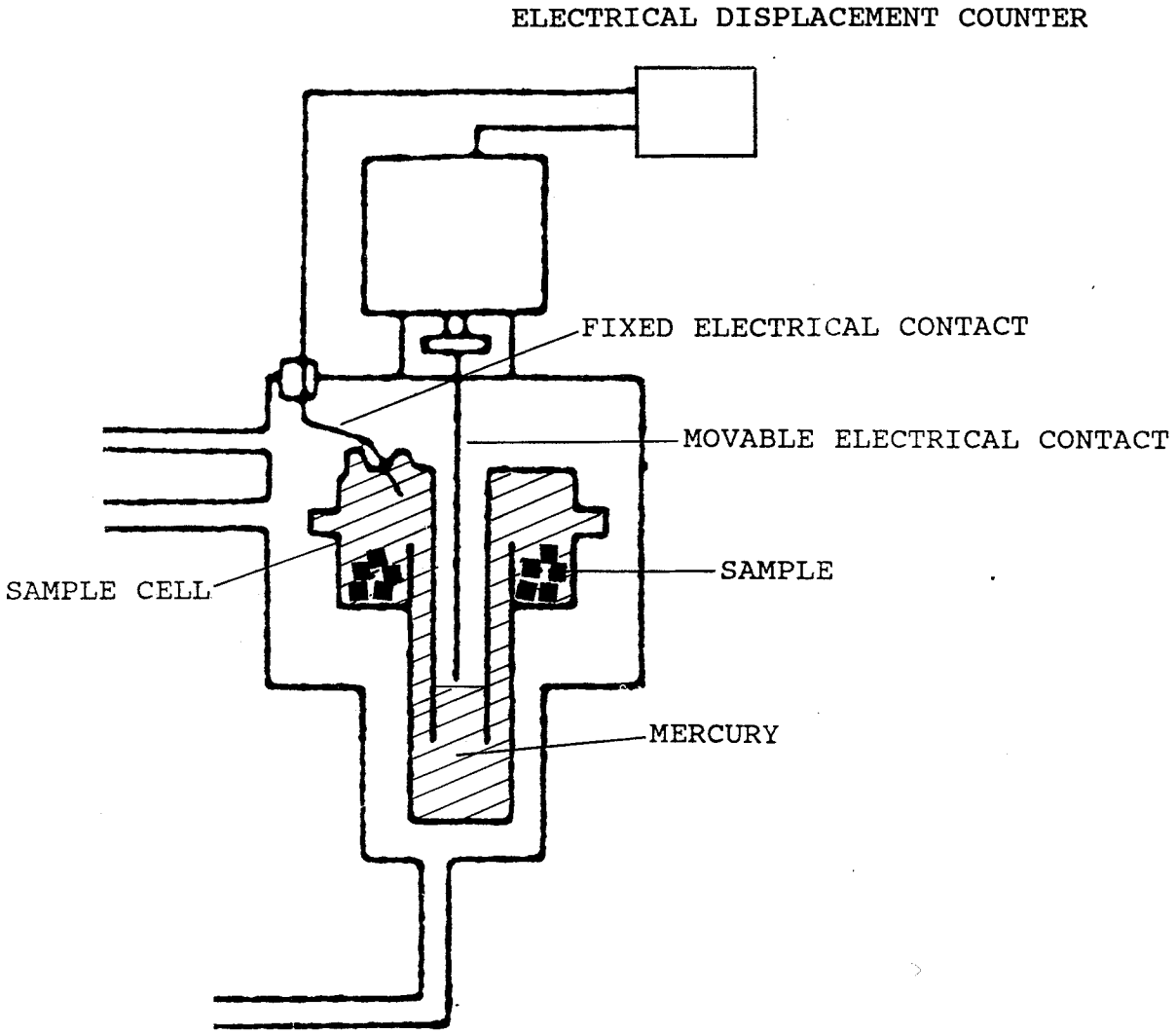

Figure 3.2.3: Measurement of intruded mercury volume.

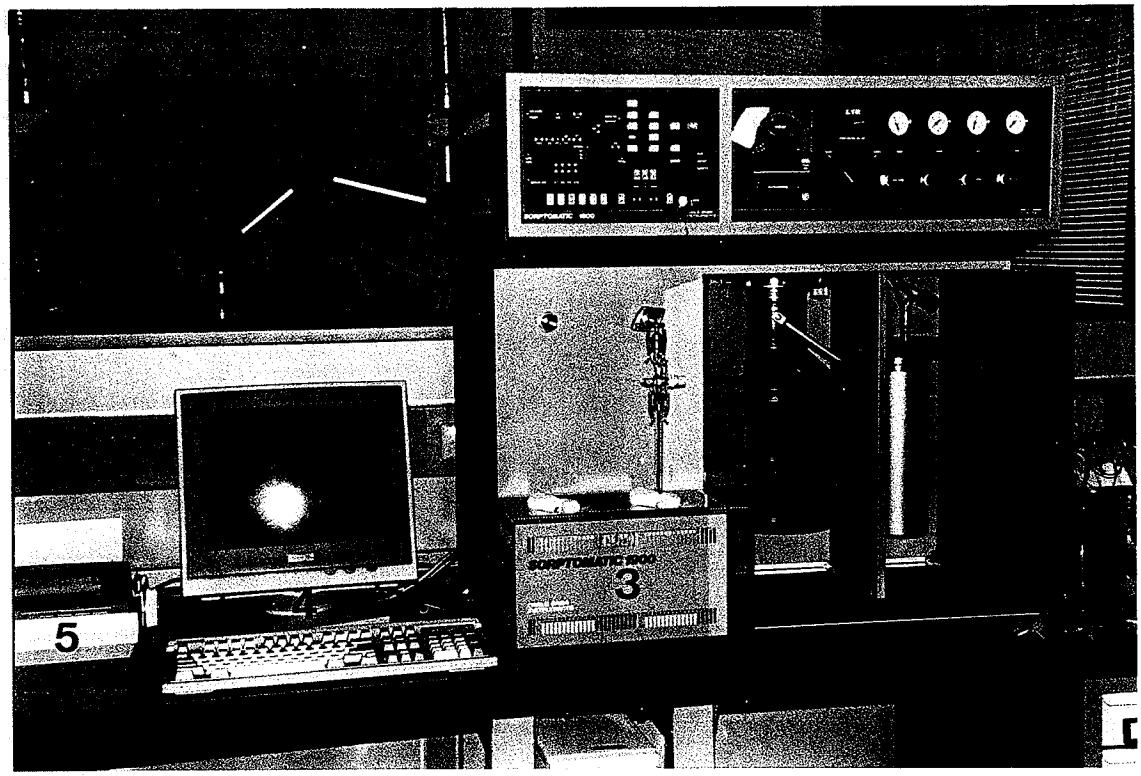

Figure 3.3.1: Nitrogen sorption apparatus.

Main components are:

1. Test chamber with cooling bath and sample container (burette)
2. Reservoir for liquid nitrogen
3. Heating box for outgasssing
4. PC
5. Plotter

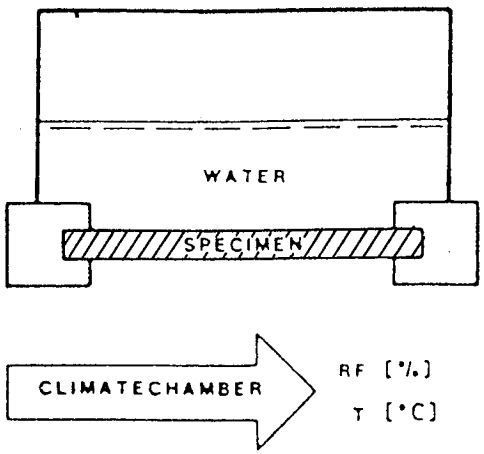

Principle

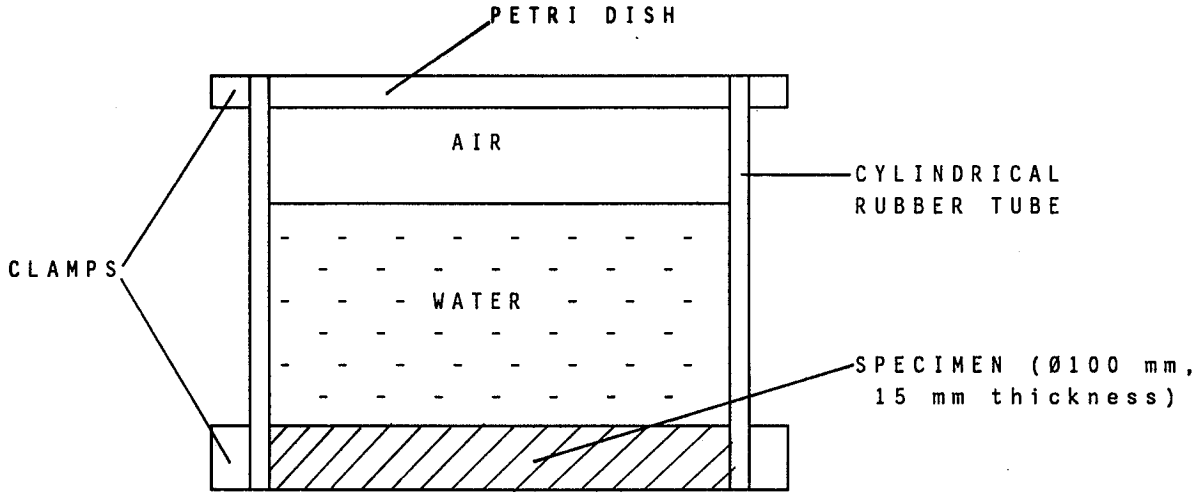

Assembled cup

Figure 3.6.1: Principle and experimental setup for inverted cup method (CUP).

Figure 3.6.2: Three phases of the weight loss curve

---------- Evaporation front

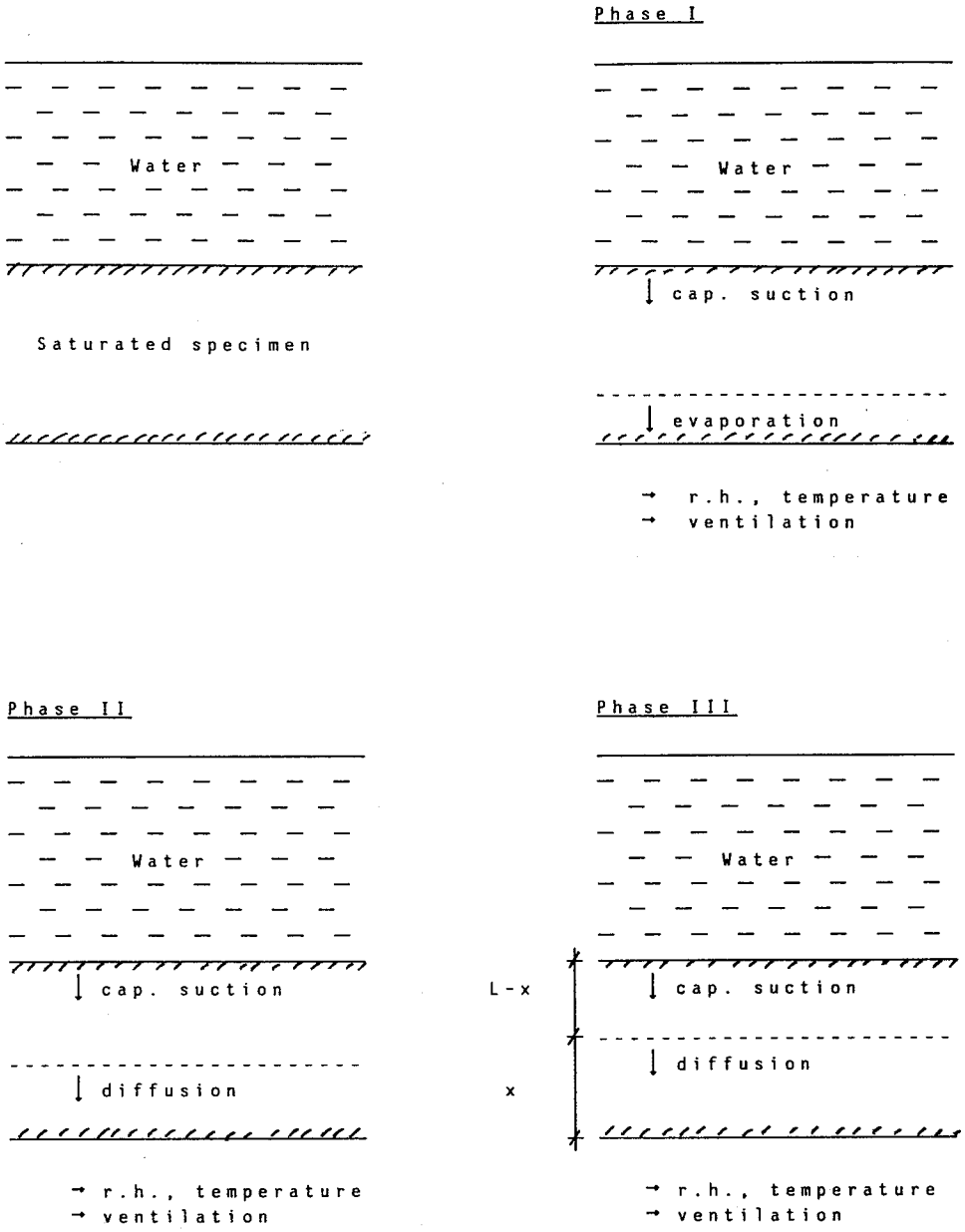

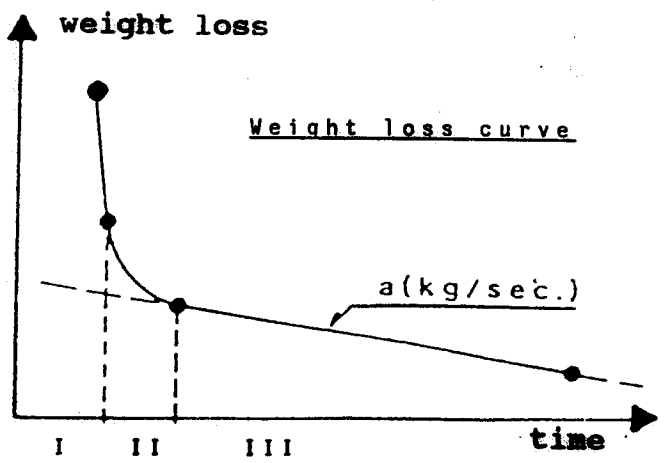

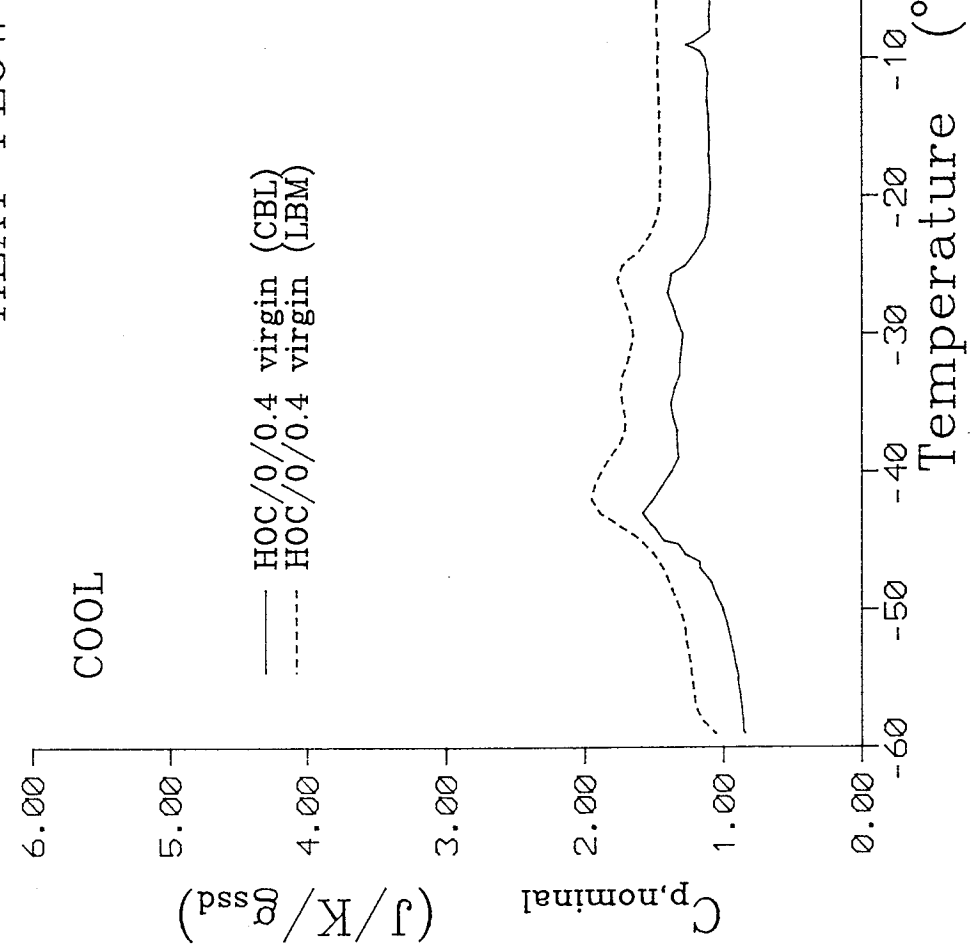

Figure 4.2.1A: Heat capacity during cooling for very mature virgin, 0.4 W/C HOC-paste. Cocalibration of CAL at CBL and LBM.

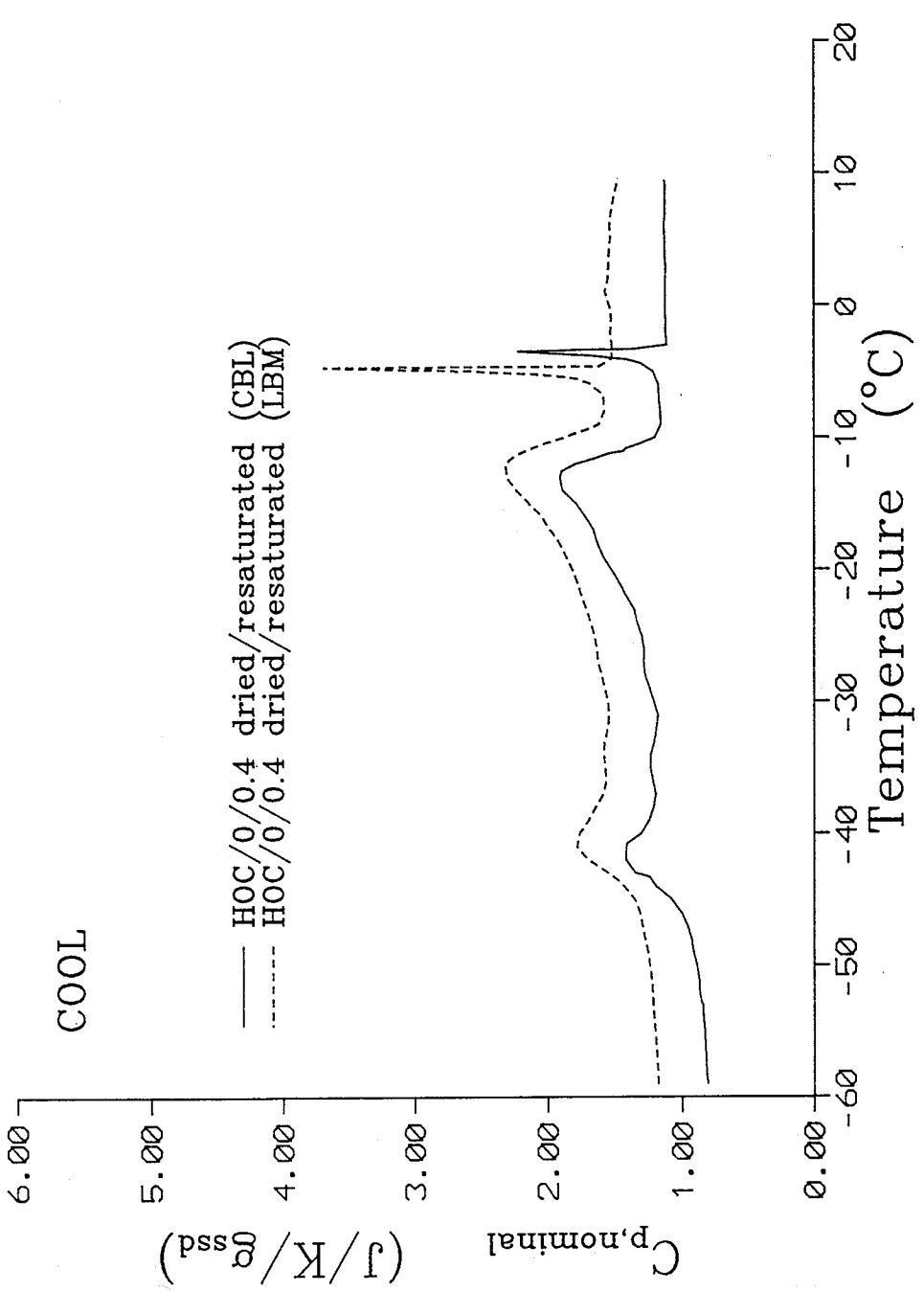

Figure 4.2.1B: Heat capacity during cooling for very mature, dried/resaturated 0.4 W/C HOC-paste. Cocalibration of CAL at CBL and LBM.

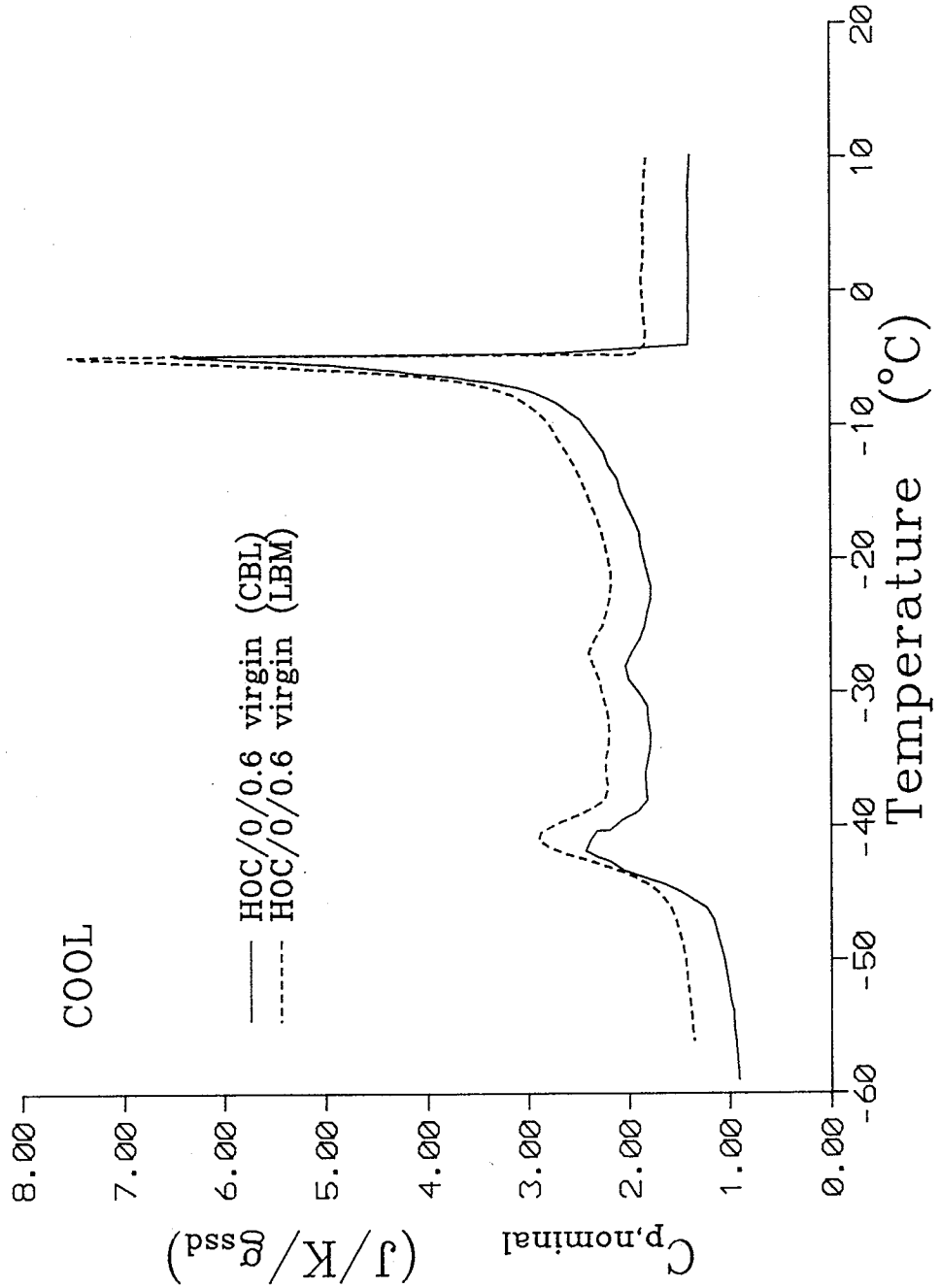

Figure 4.2.1C: Heat capacity during cooling for very mature virgin, 0.6 W/C HOC-paste. Cocalibration of CAL at CBL and LBM.

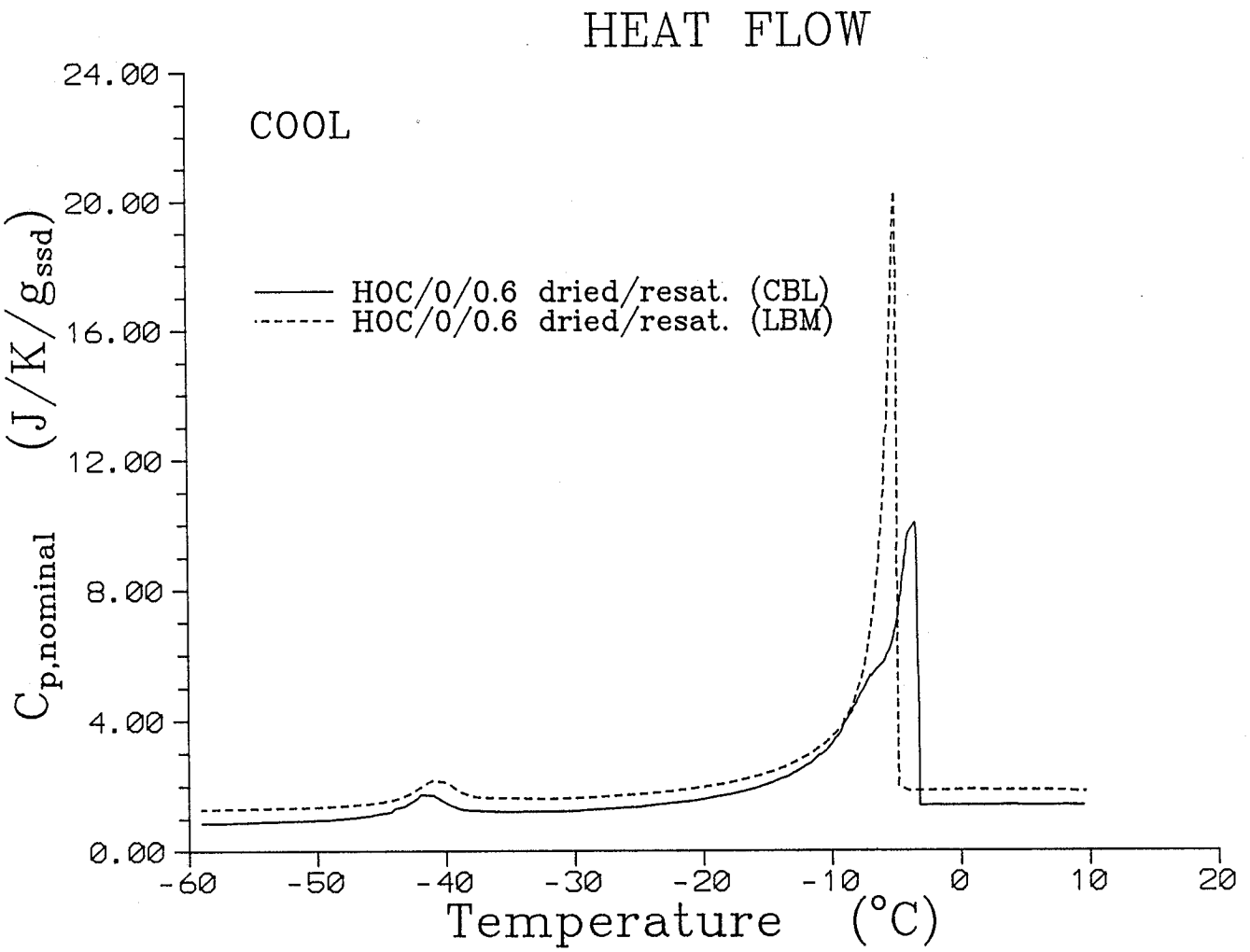

Figure 4.2.1D: Heat capacity during cooling for very mature, dried/ resaturated 0.6 W/C HOC-paste. Cocalibration of CAL at CBL and LBM.

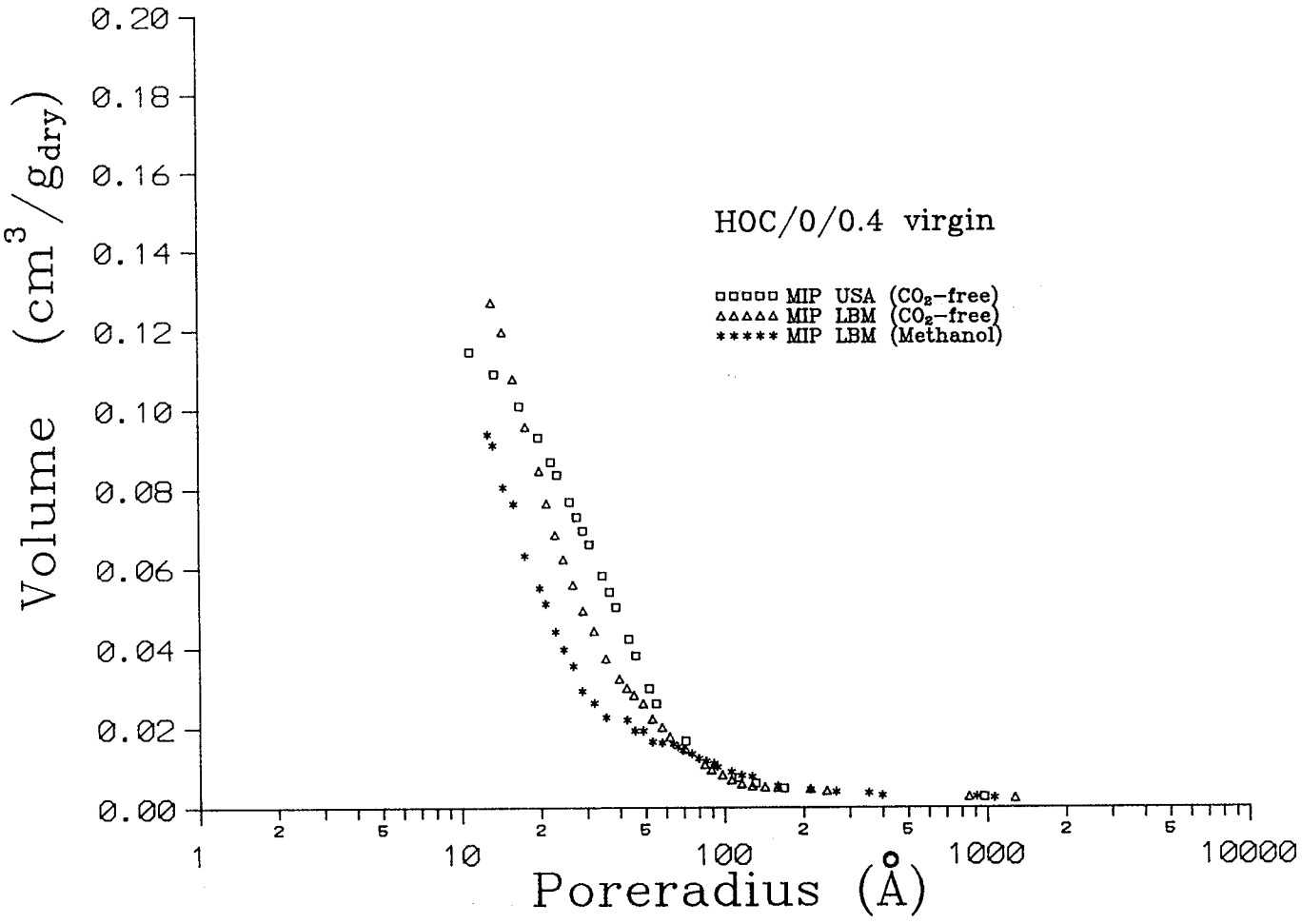

Figure 4.2.2A: Cumulative pore size distribution from MIP performed at LBM (dried by CO_2-free drying and methanol-replacement), USA (CO_2-free drying) and at CZE (CO_2-free drying) for very mature, virgin cured 0.4 W/C HOC-pastes. A contact angle of 117° has been used. Data from CZE are not yet available.

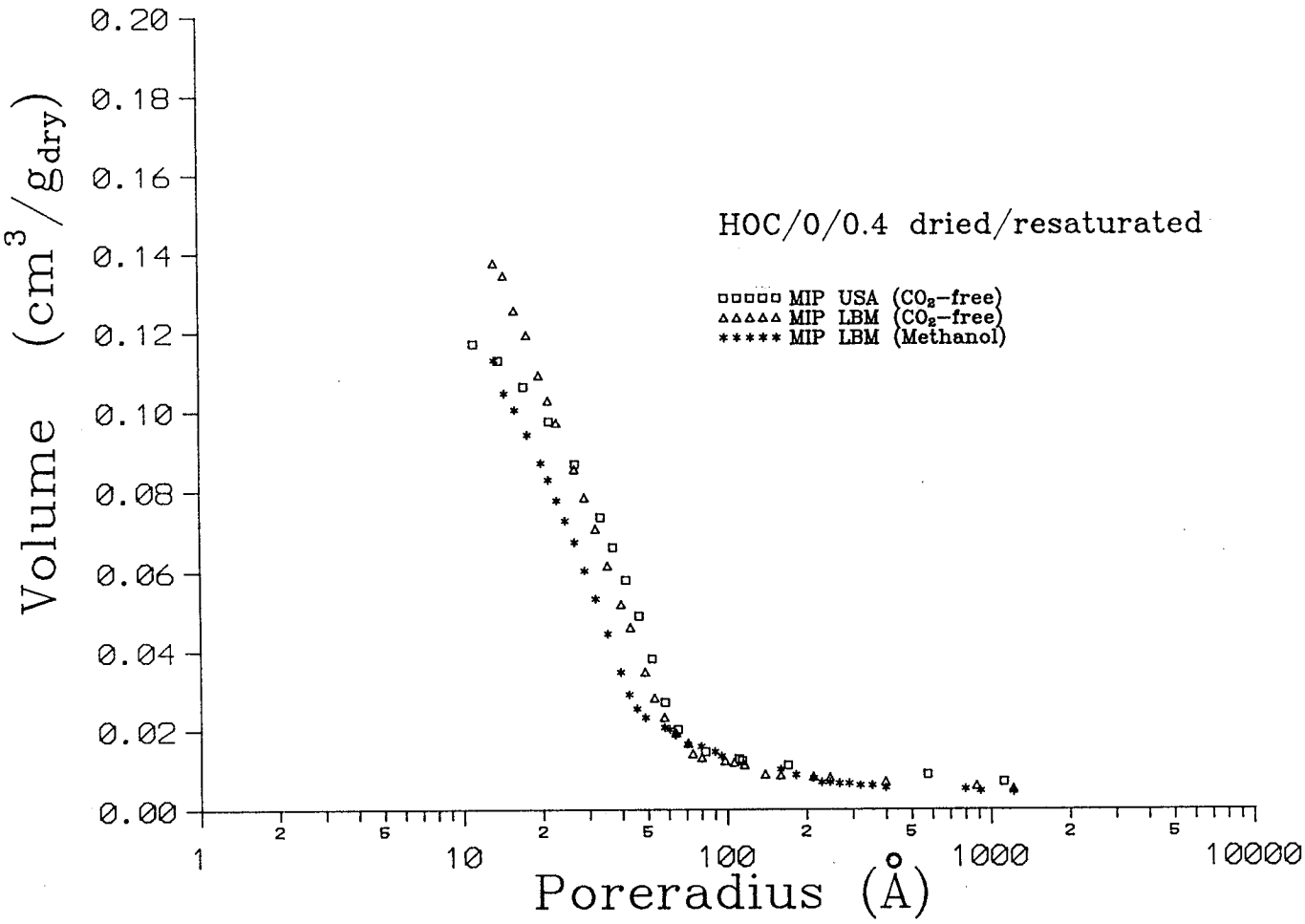

Figure 4.2.2B: Cumulative pore size distribution from MIP performed at LBM (dried by CO_2-free drying and methanol-replacement), USA (CO_2-free drying) and at CZE (CO_2-free drying) for very mature, conditioned (dried/resaturated) 0.4 W/C HOC-pastes. A contact angle of 117° was used. Data from CZE are not yet available.

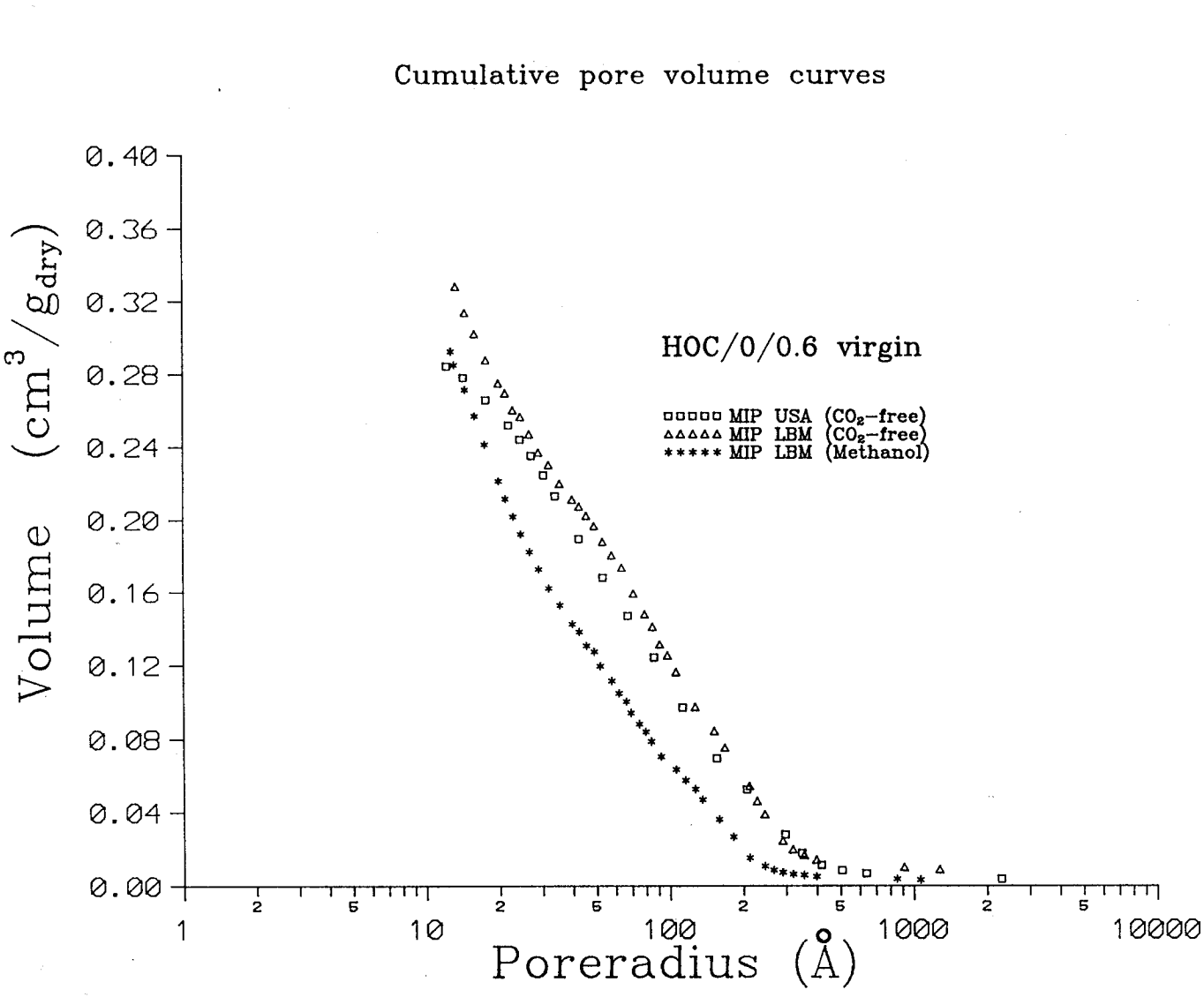

Figure 4.2.2C: Cumulative pore size distribution from MIP performed at LBM (dried by CO_2-free drying and methanol-replacement), USA (CO_2-free drying) and at CZE (CO_2-free drying) for very mature, virgin cured 0.6 W/C HOC-pastes. A contact angle of 117° has been used. Data from CZE are not yet available.

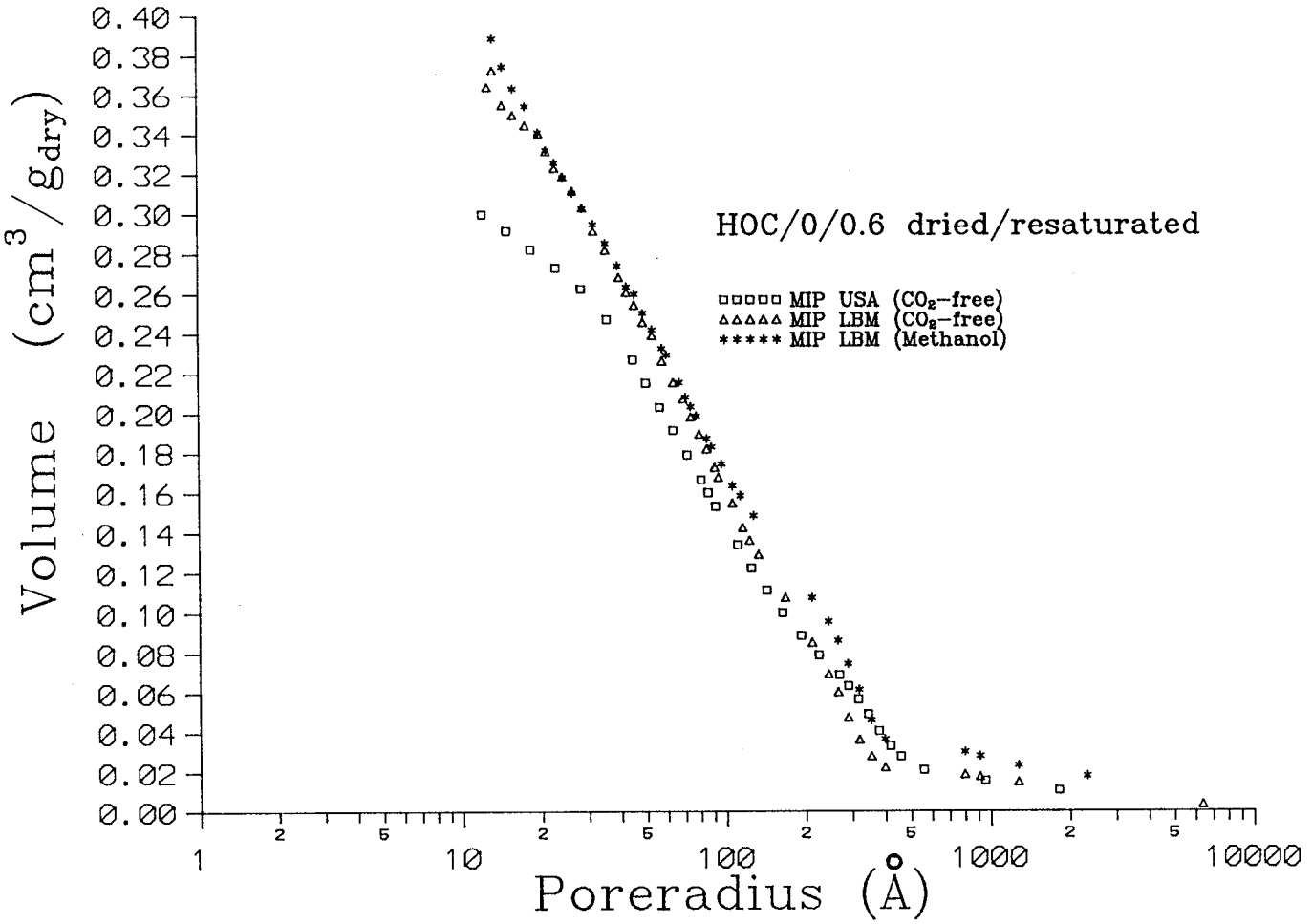

Figure 4.2.2D: Cumulative pore size distribution from MIP performed at LBM (dried by CO_2-free drying and methanol-replacement), USA (CO_2-free drying) and at CZE (CO_2-free drying) for very mature, conditioned (dried/resaturated) 0.6 W/C HOC-pastes. A contact angle of 117° was used. Data from CZE are not yet available.

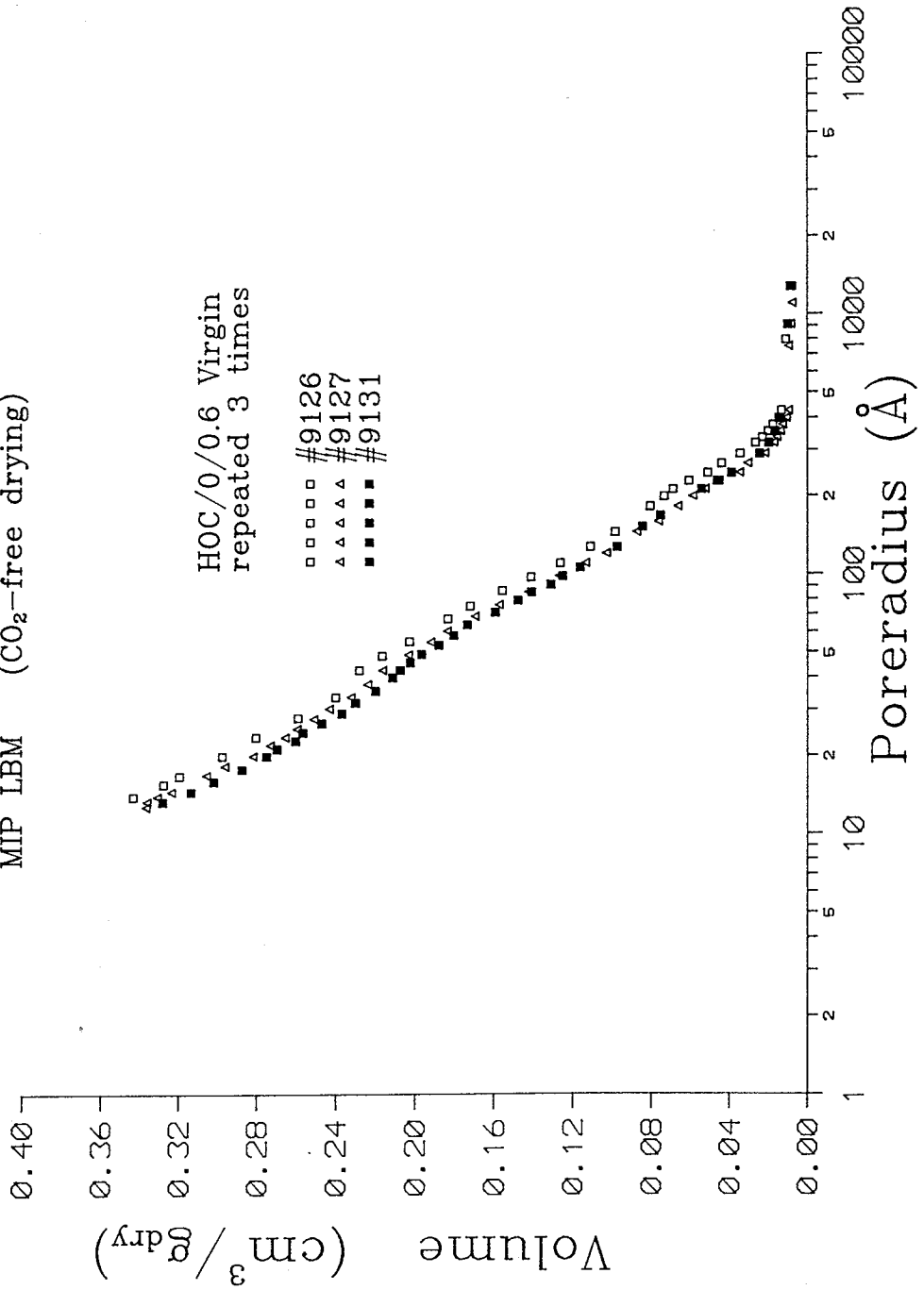

Figure 4.2.2E: Cumulative pore size distibution from MIP performed at LBM (dried by CO_2-free drying) for very mature, virgin cured 0.6 W/C HOC-paste. The paste was analysed by 3 independent repetitions.

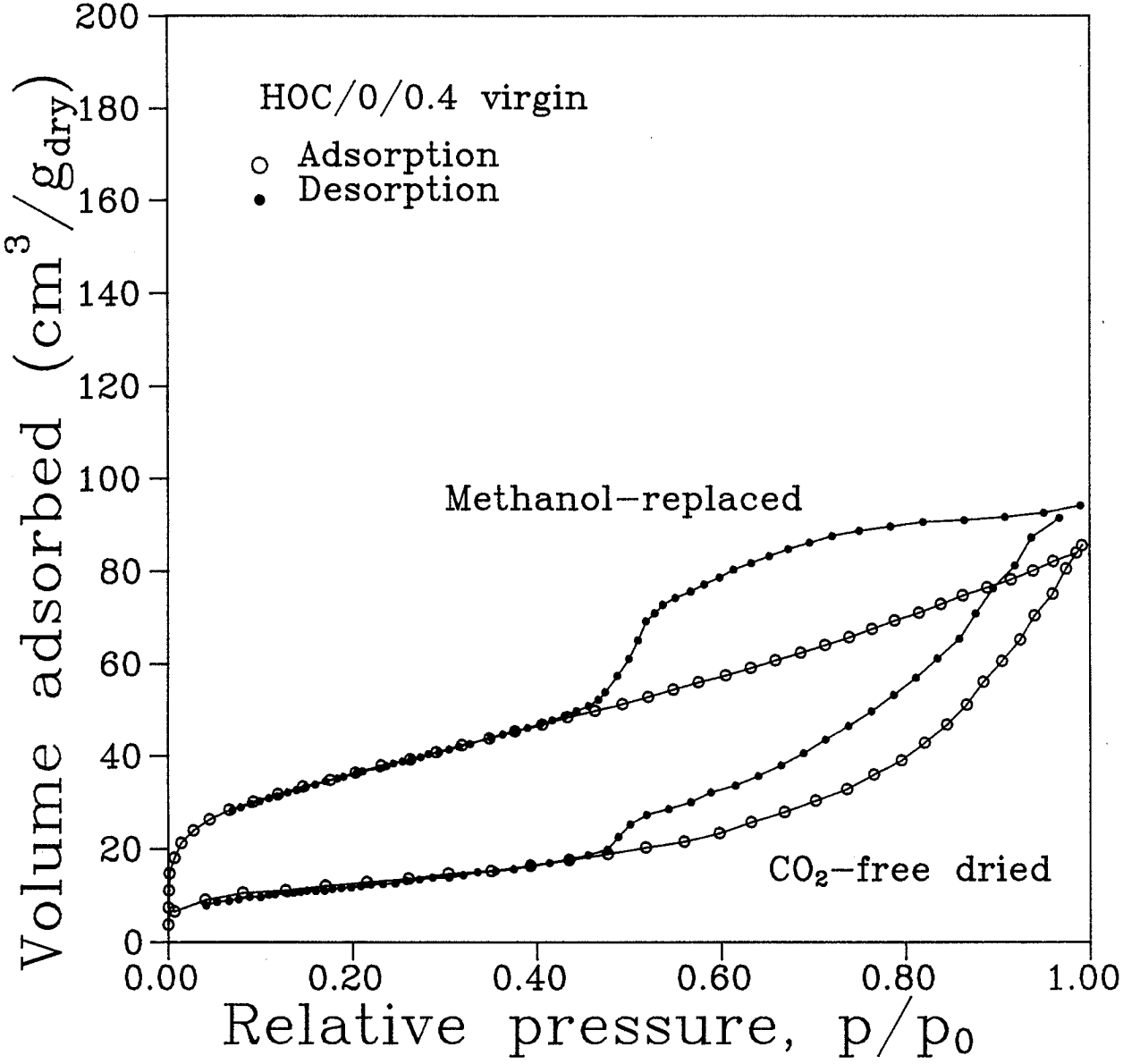

Figure 4.2.3A:

Nitrogen sorption isotherms for very mature, virgin cured 0.4 W/C HOC-pastes. The effect of drying method is shown.

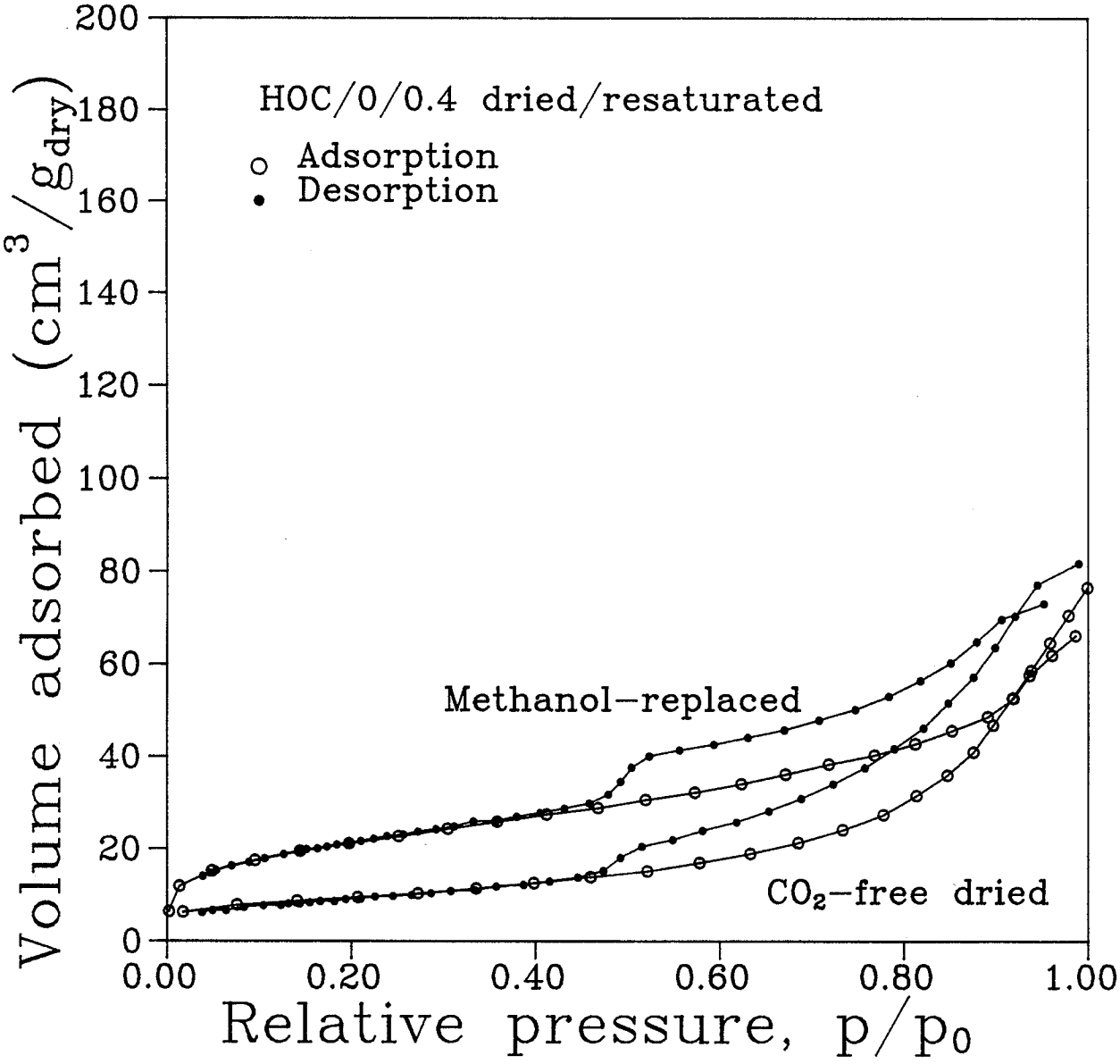

Figure 4.2.3B:

Nitrogen sorption isotherms for very mature, conditioned (dried/ resaturated) 0.4 W/C HOC-pastes. The effect of drying method is shown.

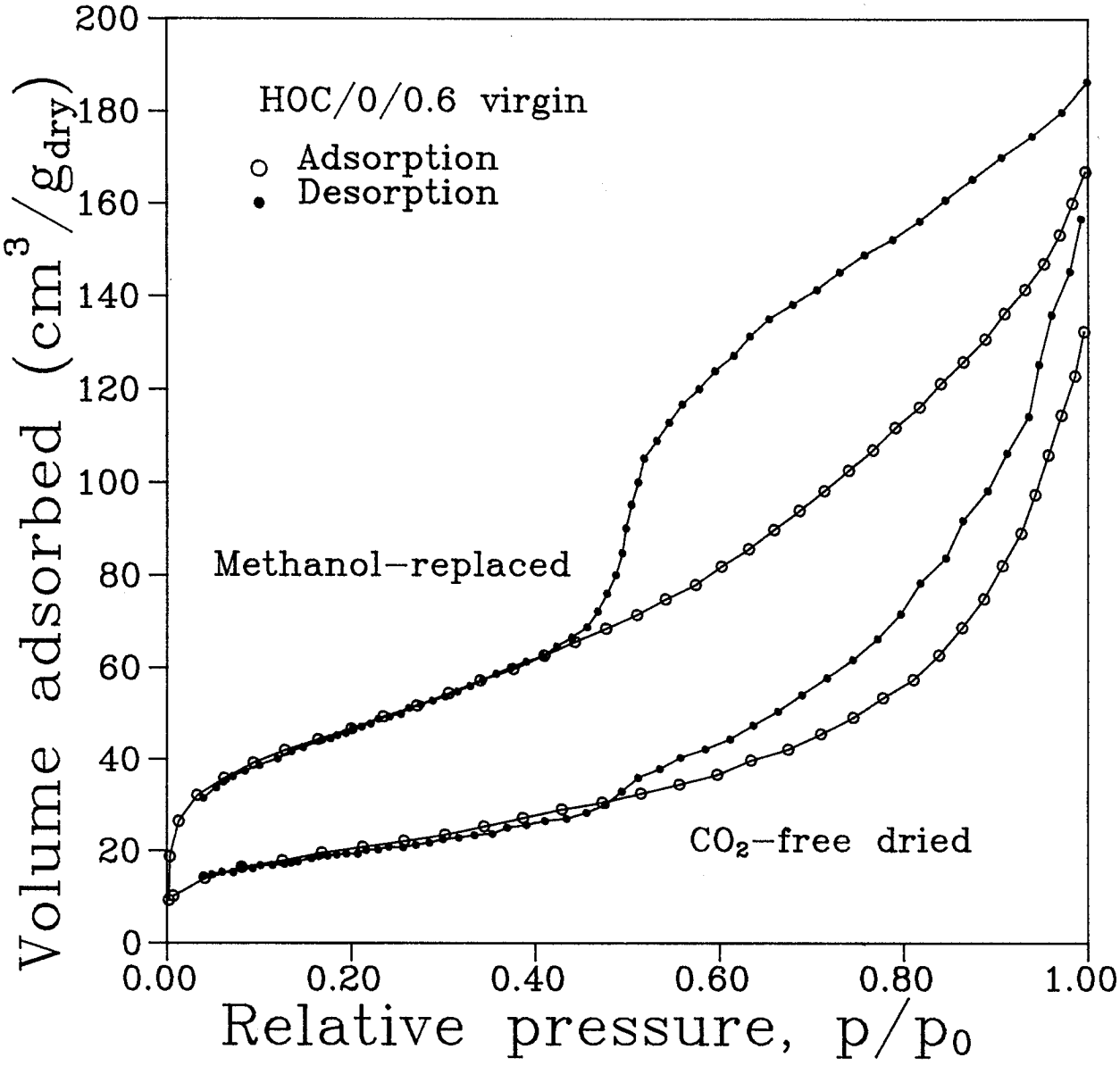

Figure 4.2.3C:

Nitrogen sorption isotherms for very mature, virgin cured 0.6 W/C HOC-pastes. The effect of drying method is shown.

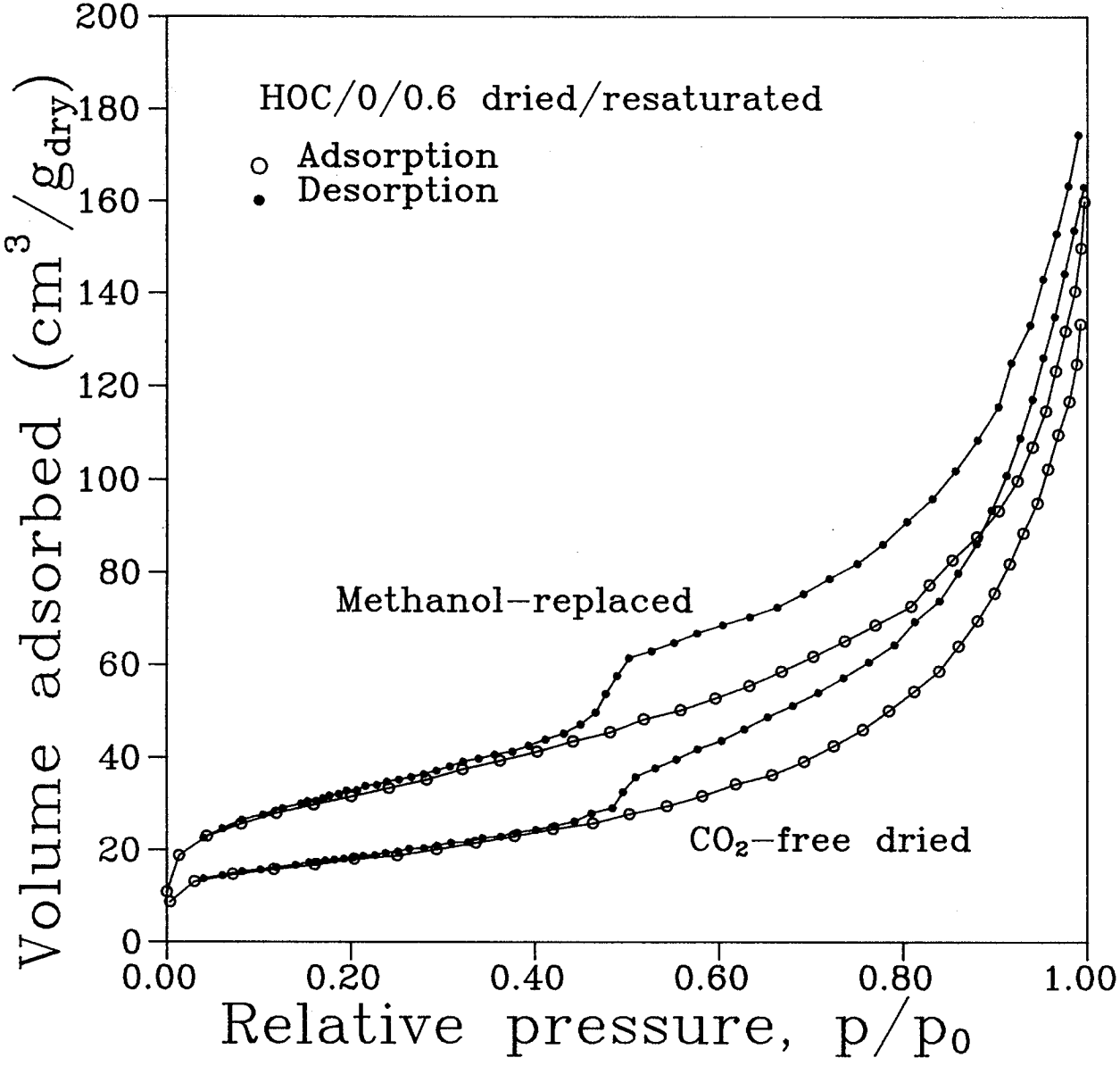

Figure 4.2.3D:

Nitrogen sorption isotherms for very mature, conditioned (dried/resaturated) 0.6 W/C HOC-pastes. The effect of drying method is shown.

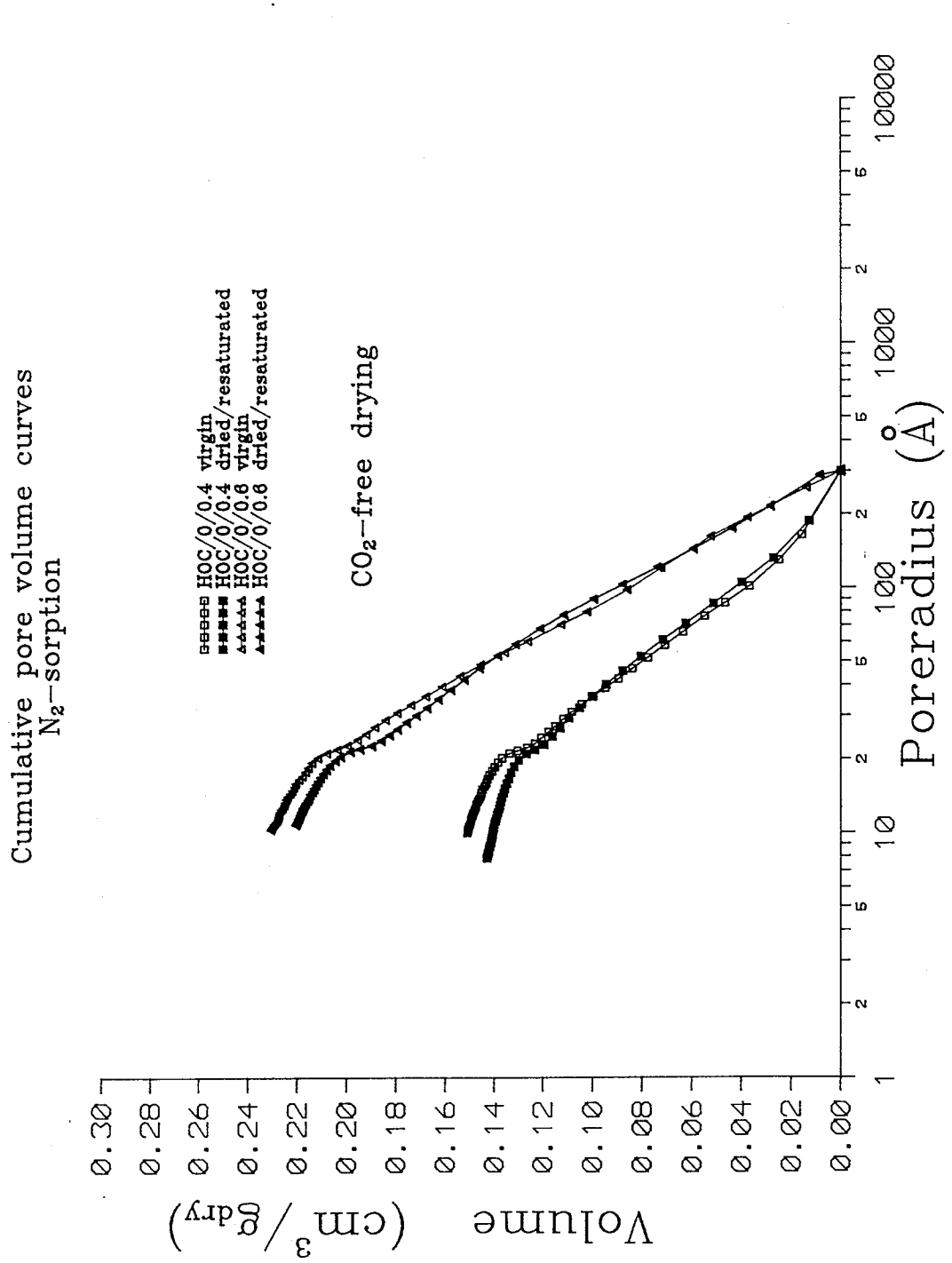

Figure 4.2.4: Cumulative pore size distributions calculated from the desorption branch of the nitrogen isotherm for very mature HOC-pastes. The specimens have been CO_2-free dried before analysis. The effect of W/C and conditioning is shown.

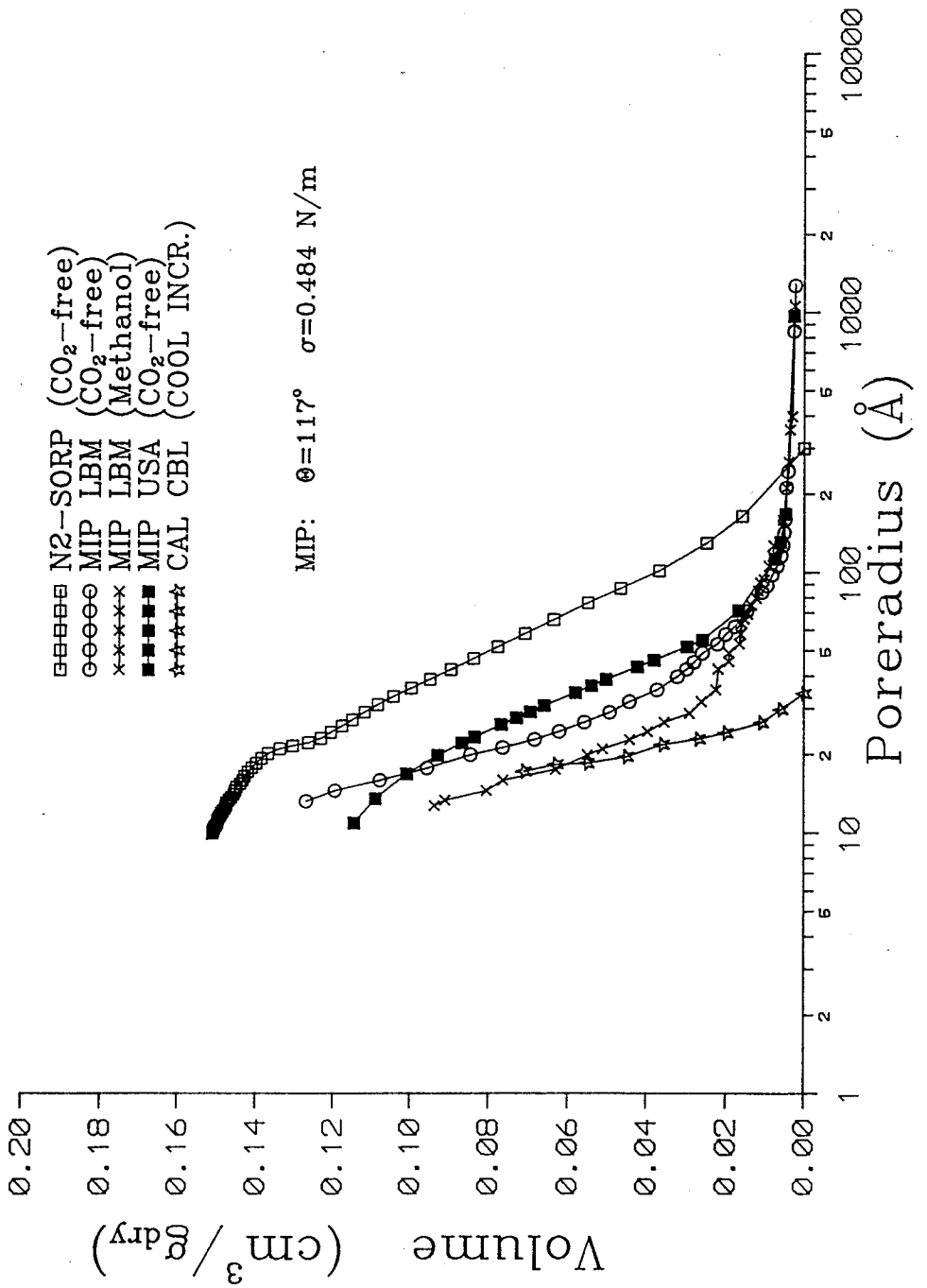

Figure 4.2.6A: Cumulative pore size distributions calculated from N2-SORP, MIP and CAL for very mature, virgin cured 0.4 W/C HOC-paste.
A contact angle of 117° was used for MIP.

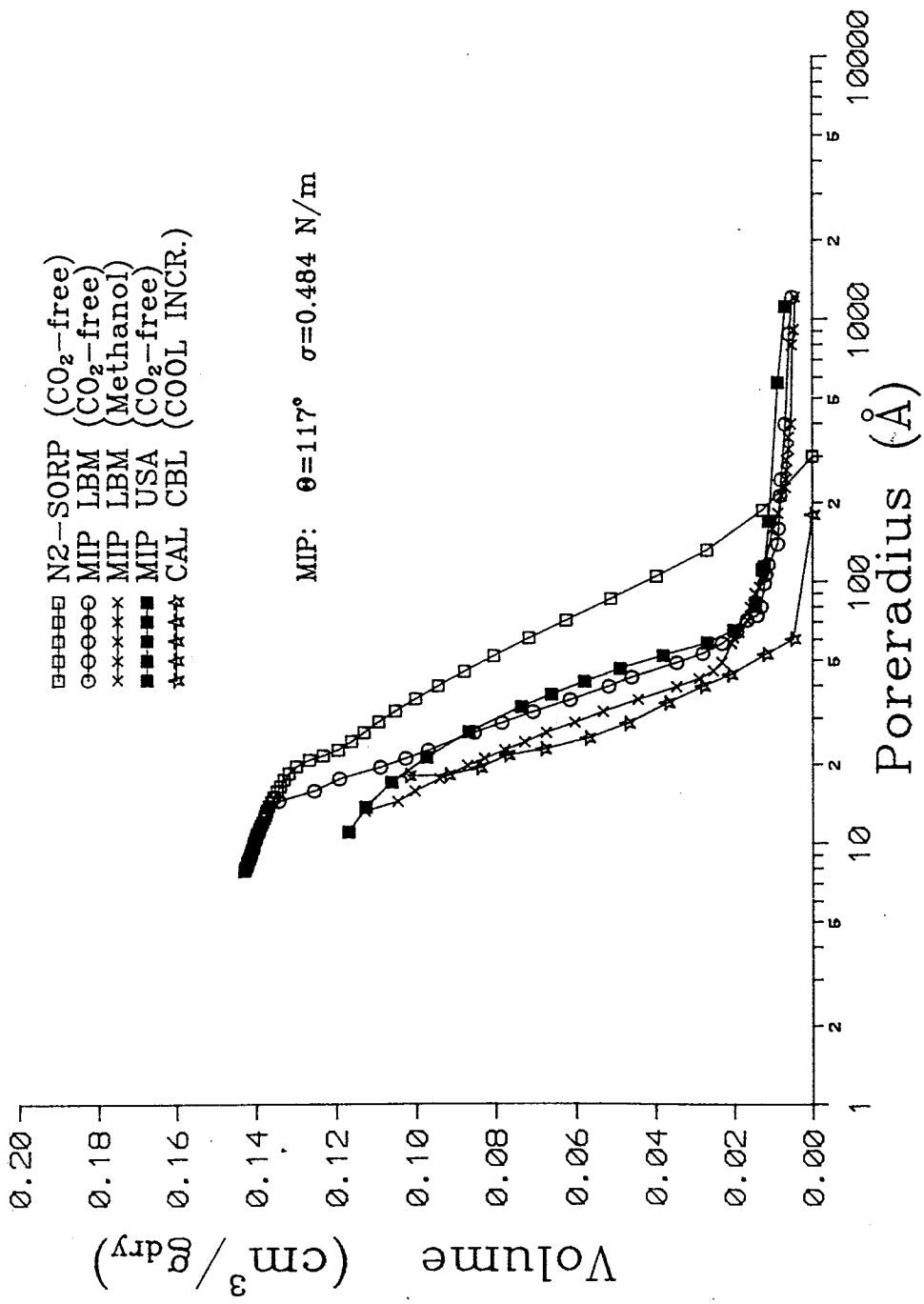

Figure 4.2.68: Cumulative pore size distributions calculated from N2-SORP, MIP and CAL for very mature, conditioned (dried/resaturated) 0.4 W/C HOC-paste. A contact angle of 117° was used for MIP.

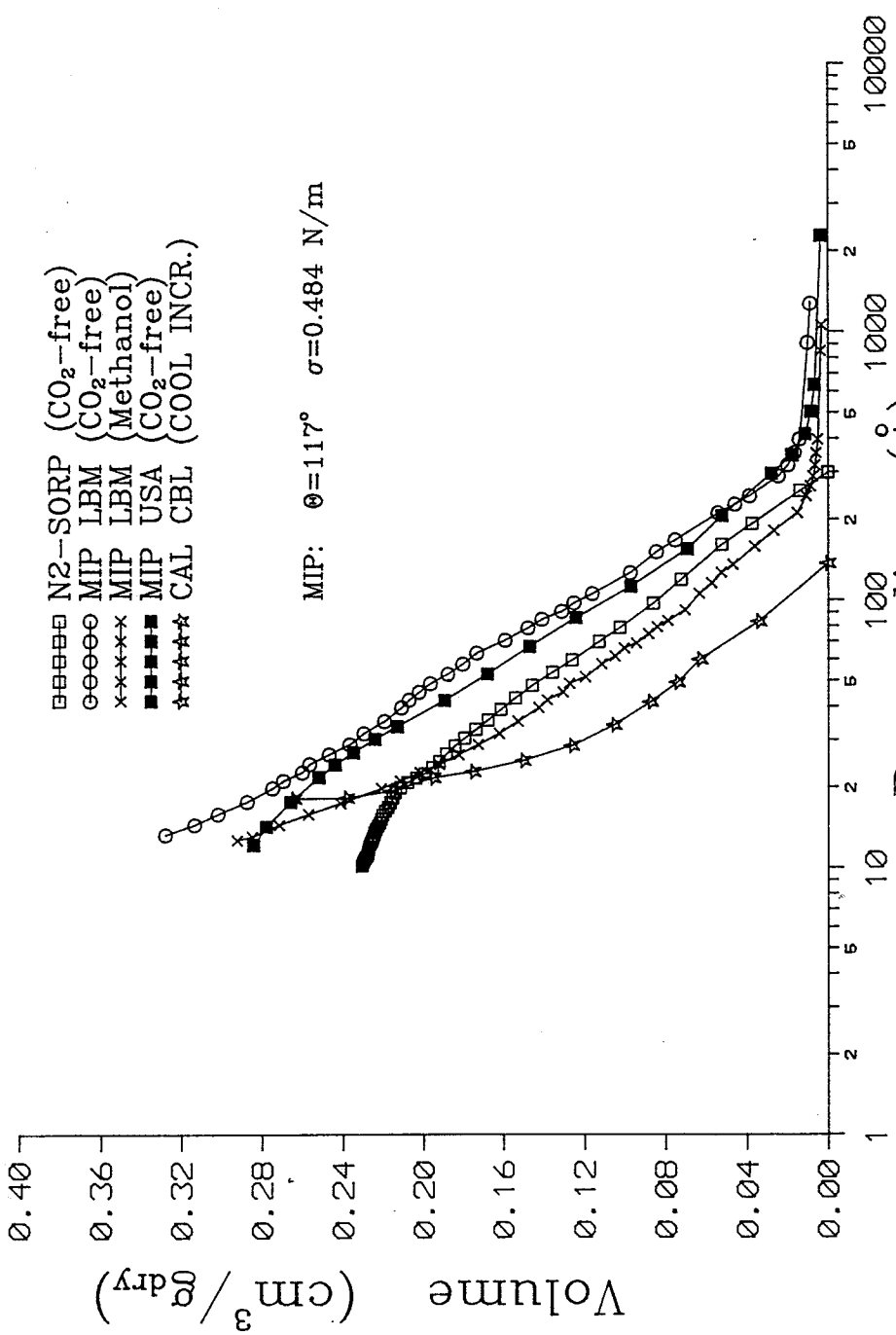

Figure 4.2.6C: Cumulative pore size distributions calculated from N2-SORP, MIP and CAL for very mature, virgin cured 0.6 W/C HOC-paste.
A contact angle of 117° was used for MIP.

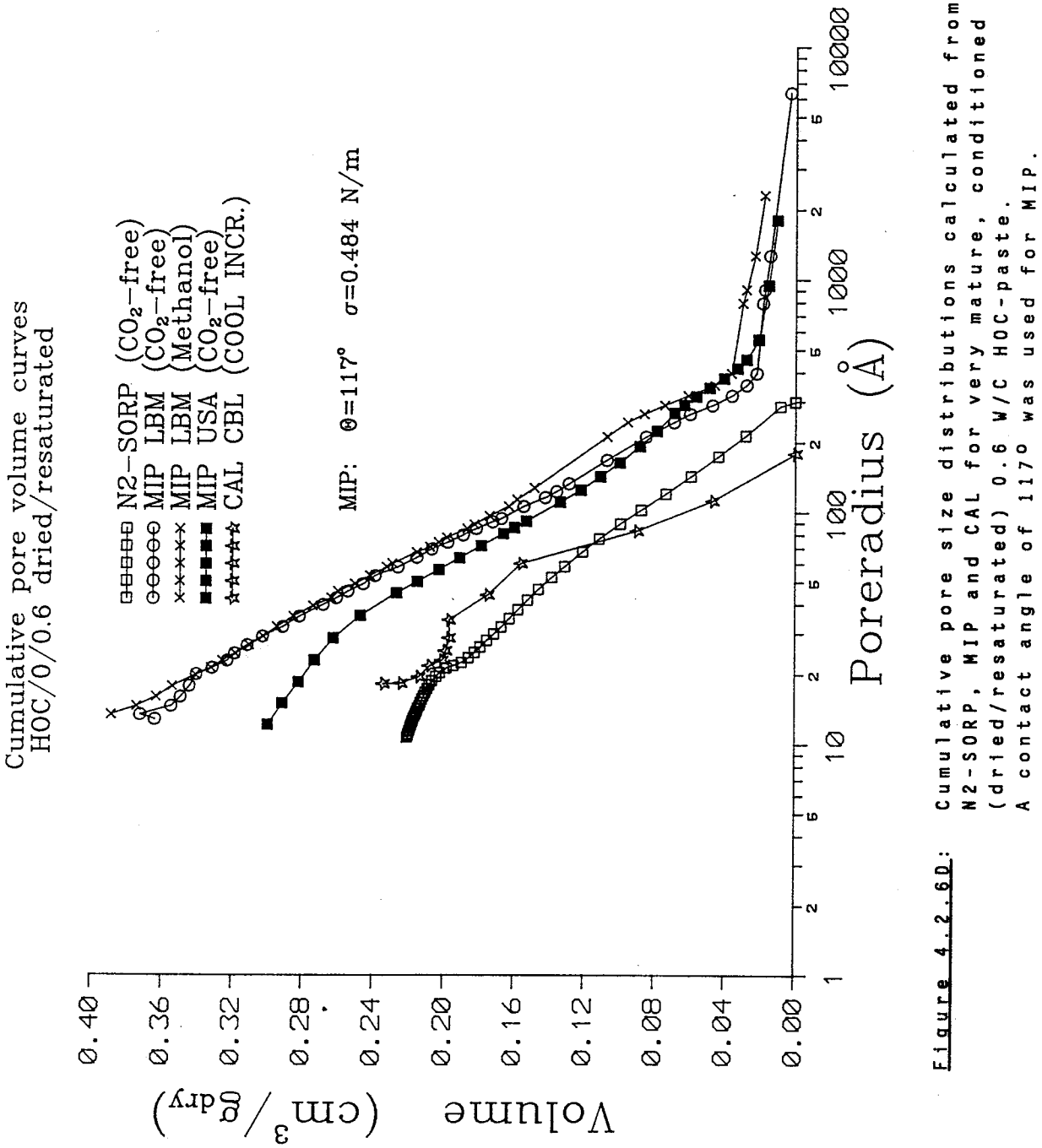

Figure 4.2.60: Cumulative pore size distributions calculated from N2-SORP, MIP and CAL for very mature, conditioned (dried/resaturated) 0.6 W/C HOC-paste. A contact angle of 117° was used for MIP.

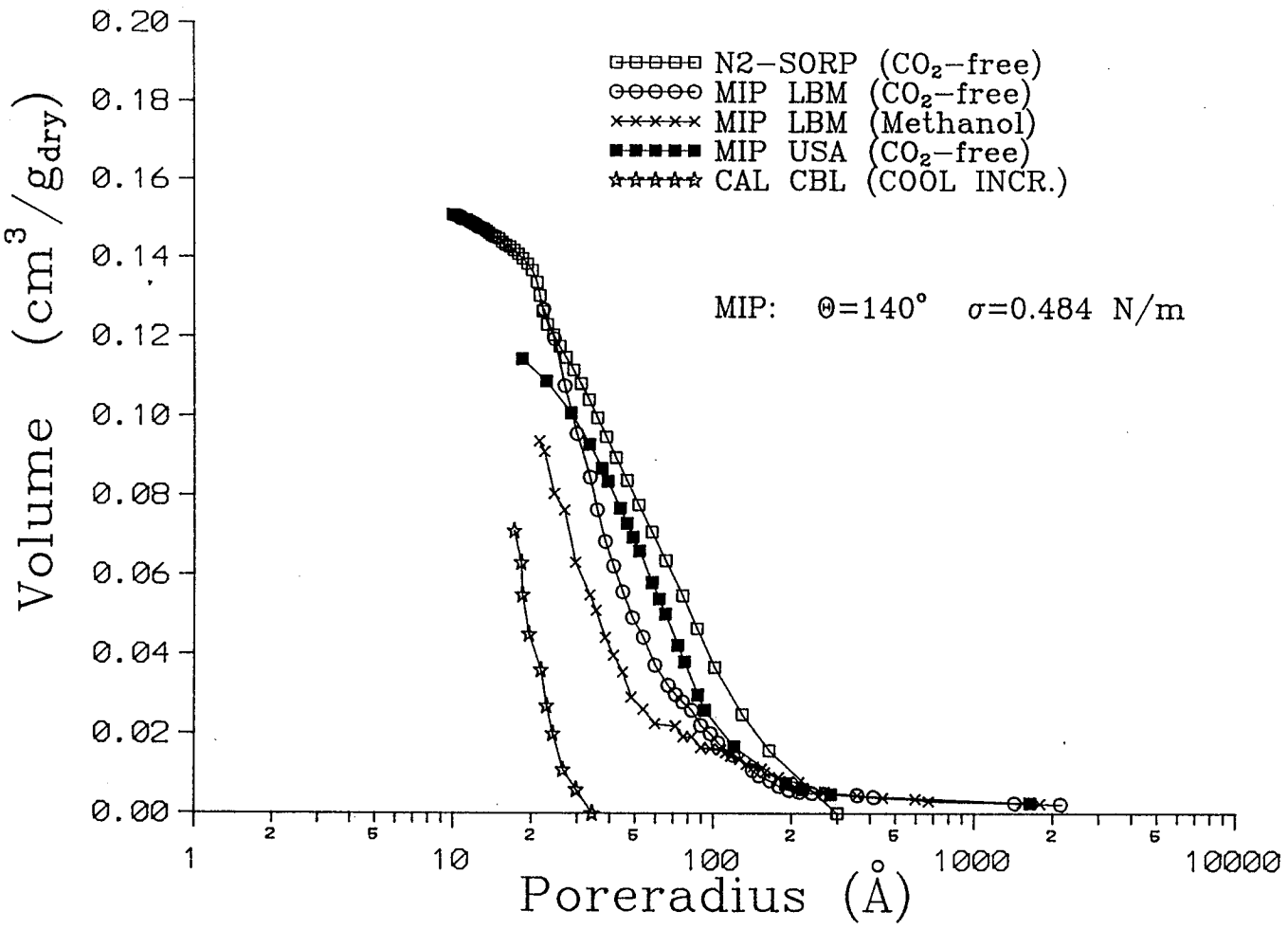

Figure 4.2.7A: Cumulative pore size distributions calculated from N2-SORP, MIP and CAL for very mature, virgin cured 0.4 W/C HOC-paste.
A contact angle of 140° was used for MIP.

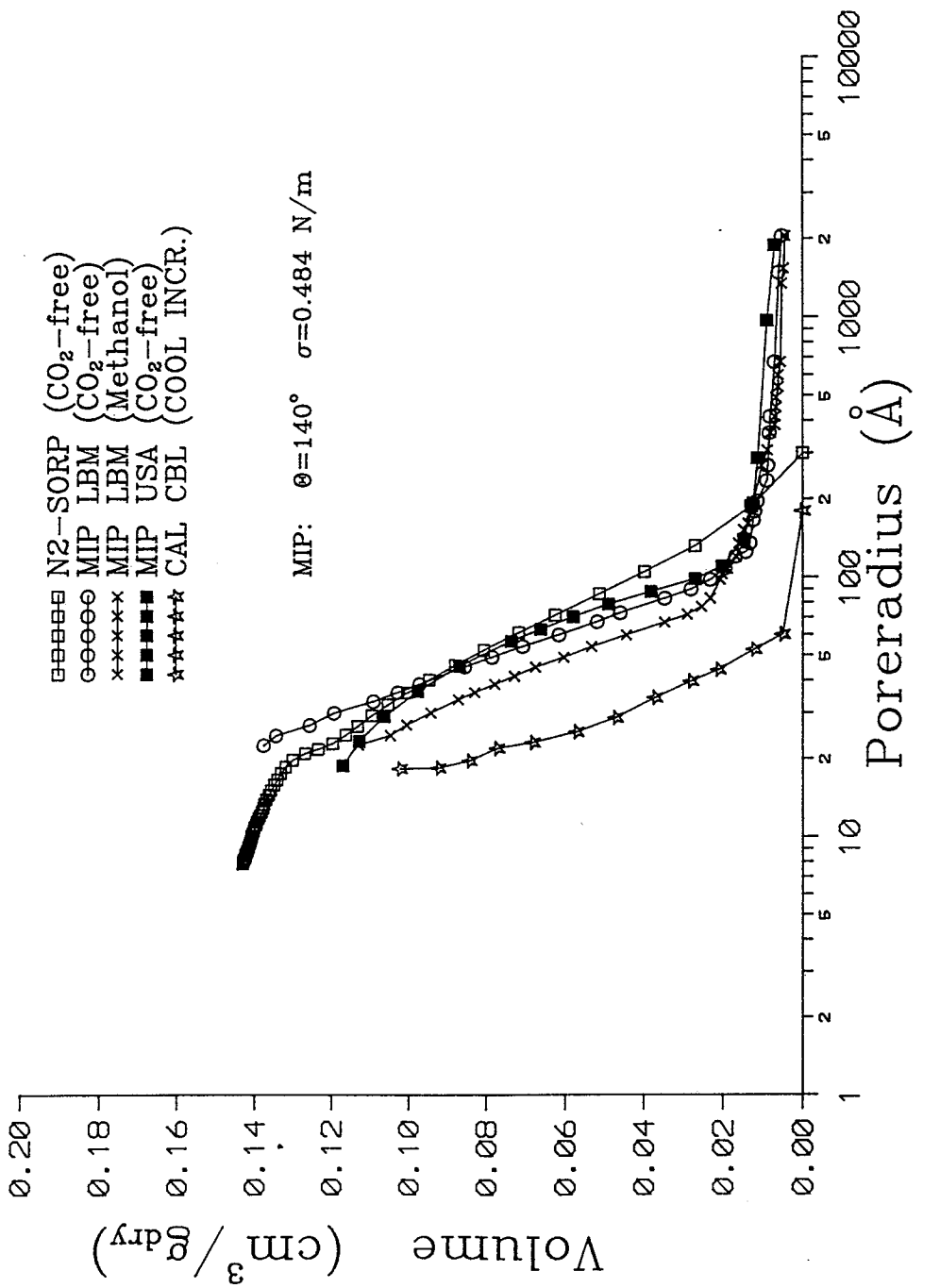

Figure 4.2.7B: Cumulative pore size distributions calculated from N2-SORP, MIP and CAL for very mature, conditioned (dried/resaturated) 0.4 W/C HOC-paste. A contact angle of 140° was used for MIP.

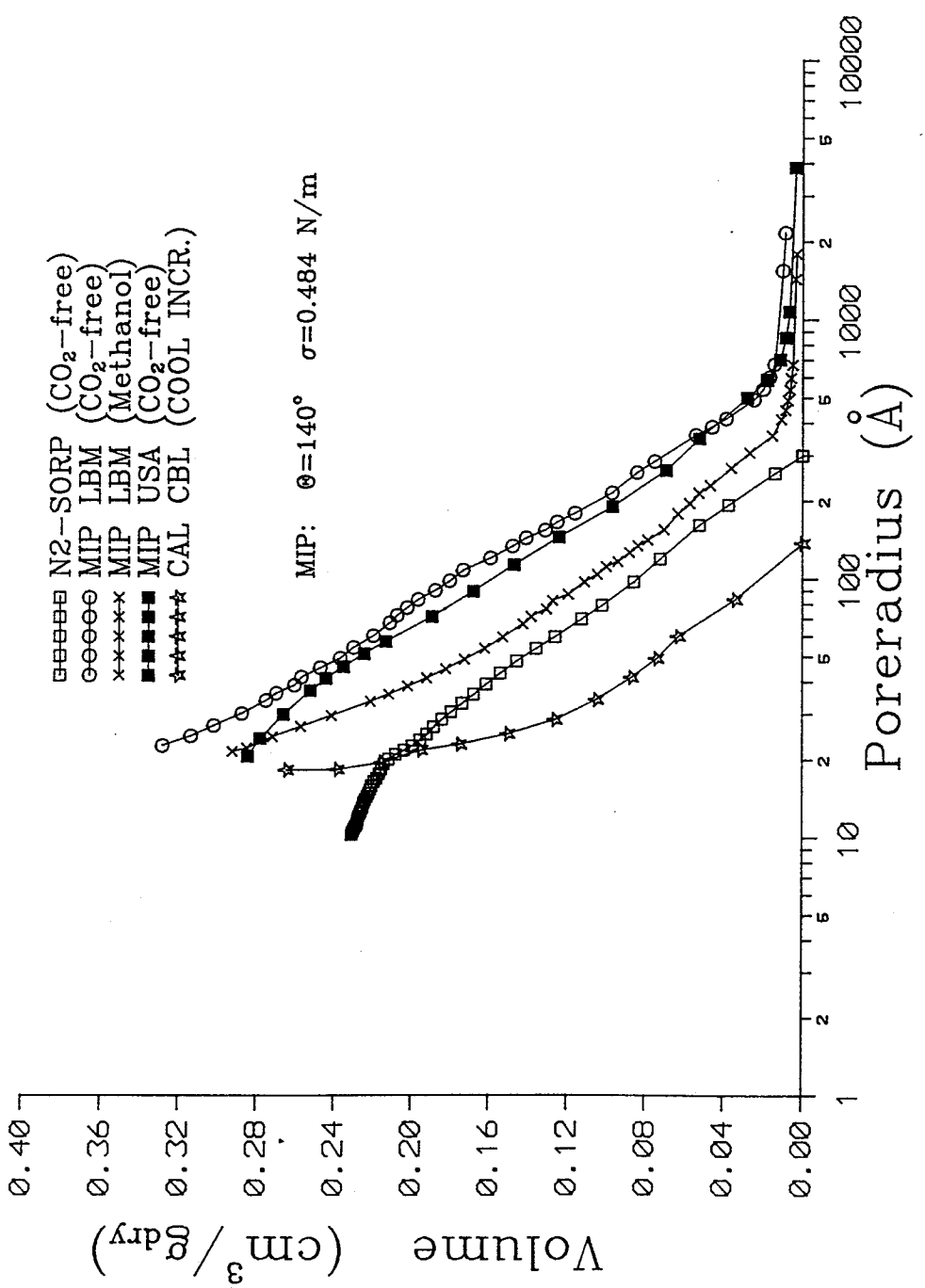

Figure 4.2.7C: Cumulative pore size distributions calculated from N2-SORP, MIP and CAL for very mature, virgin cured 0.6 W/C HOC-paste.
A contact angle of 140° was used for MIP.

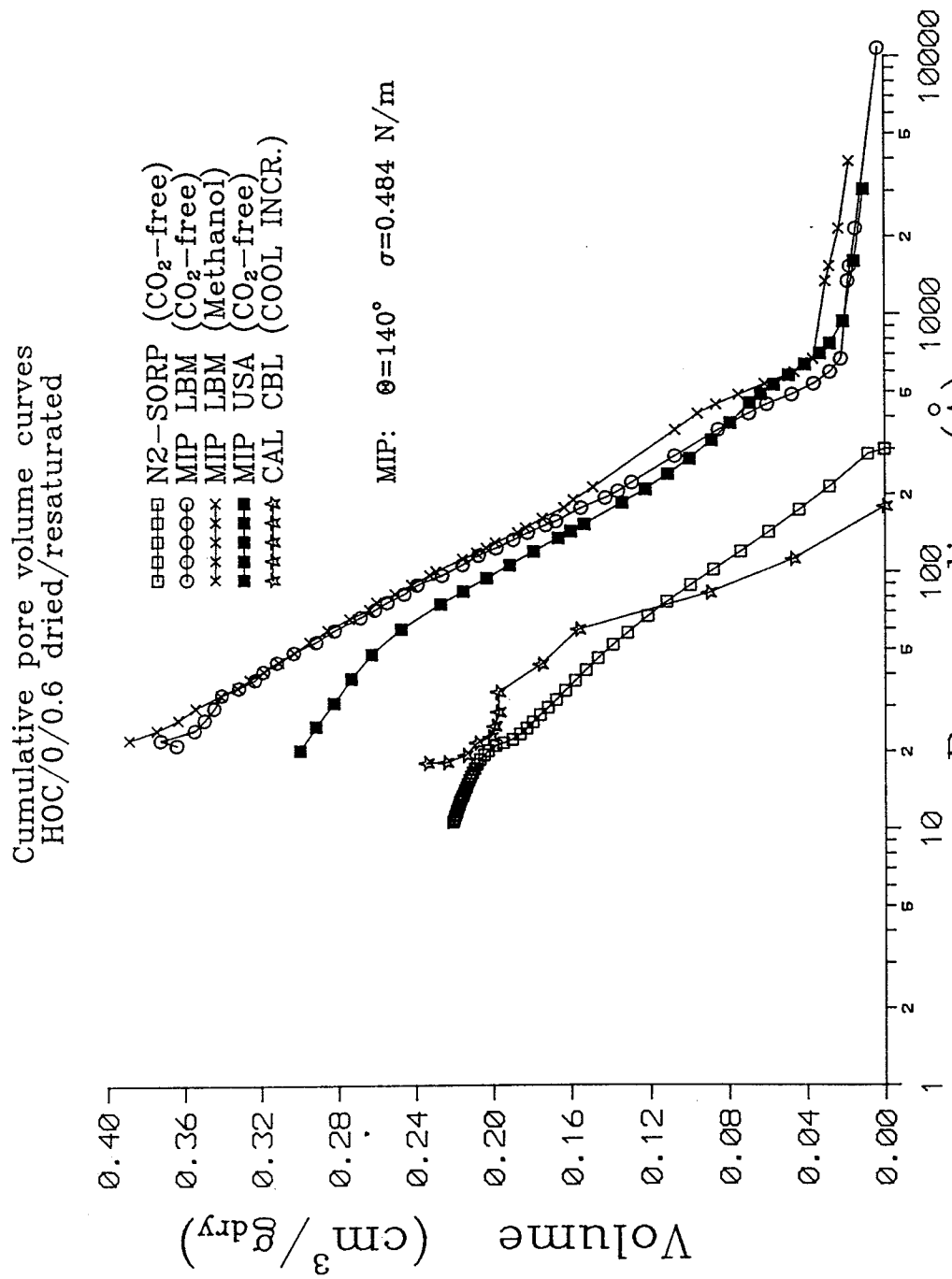

Figure 4.2.7D: Cumulative pore size distributions calculated from N2-SORP, MIP and CAL for very mature, conditioned (dried/resaturated) 0.6 W/C HOC-paste. A contact angle of 140° was used for MIP.

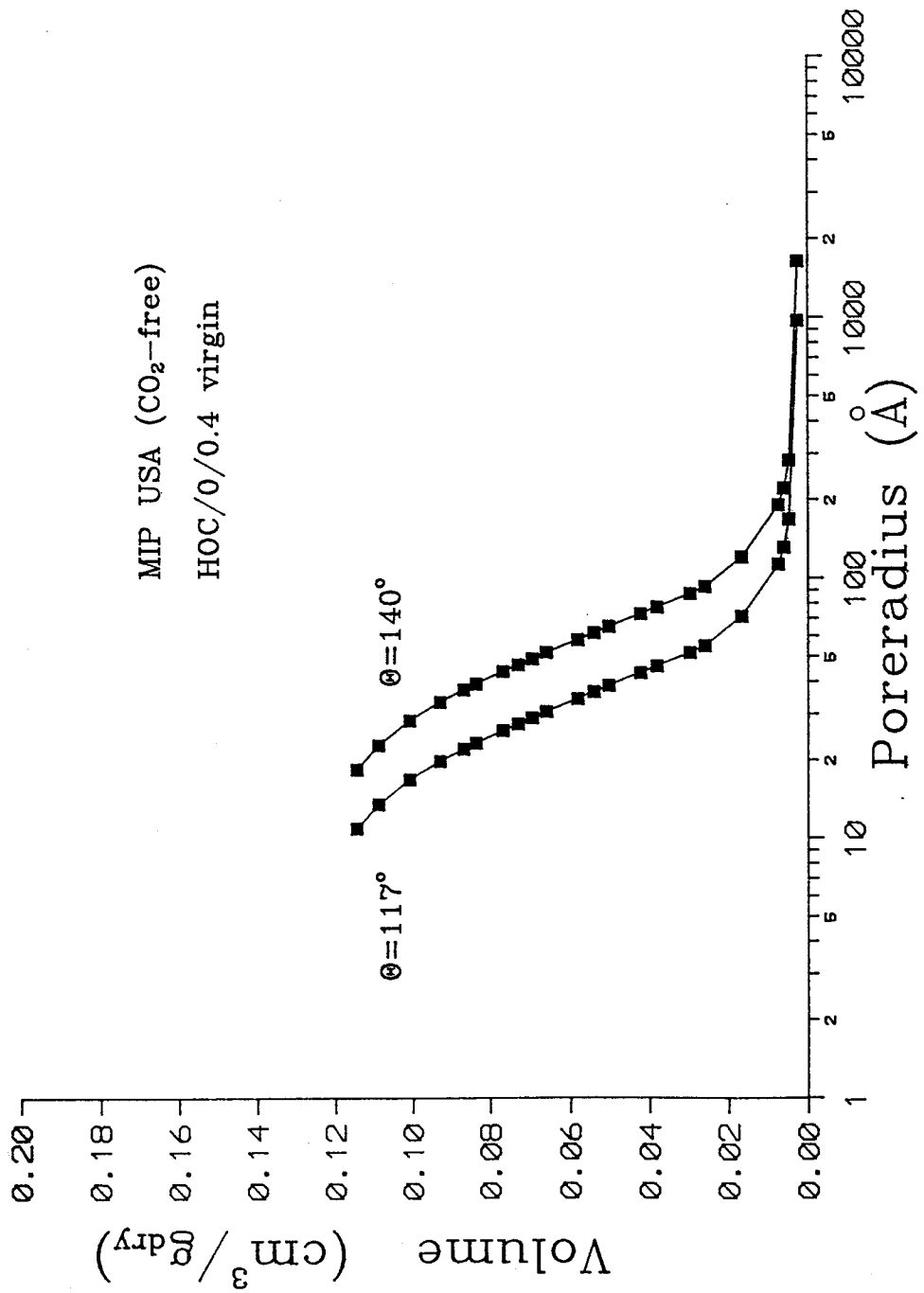

Figure 4.2.8: Cumulative pore size distribution from MIP at USA for very mature 0.4 W/C HOC-paste. The effect of changing the contact angle, Θ, from 117° to 140° is shown.

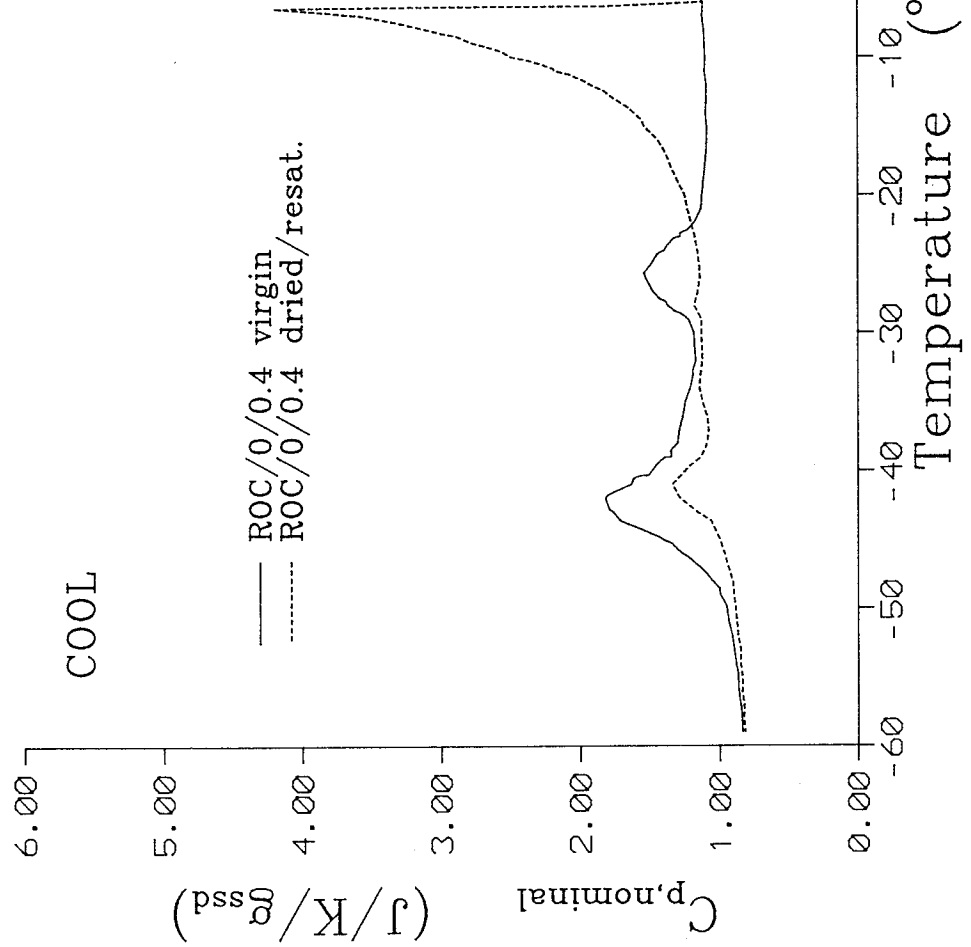

Figure 4.3.1A: Heat capacity during cooling for mature 0.4 W/C ROC-paste. The effect of drying/resaturation is shown.

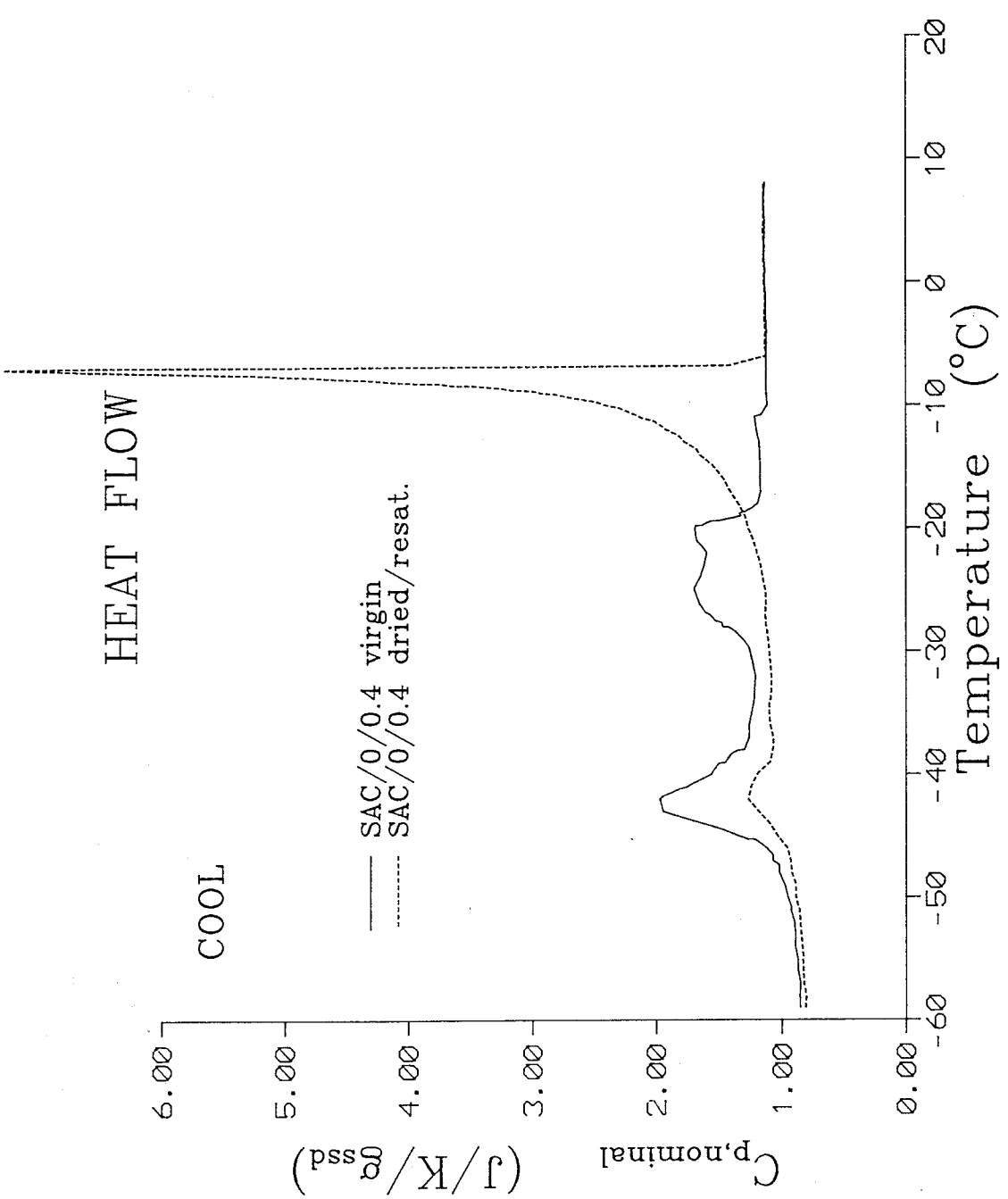

Figure 4.3.18: Heat capacity during cooling for mature 0.4 W/C SAC-paste. The effect of drying/resaturation is shown.

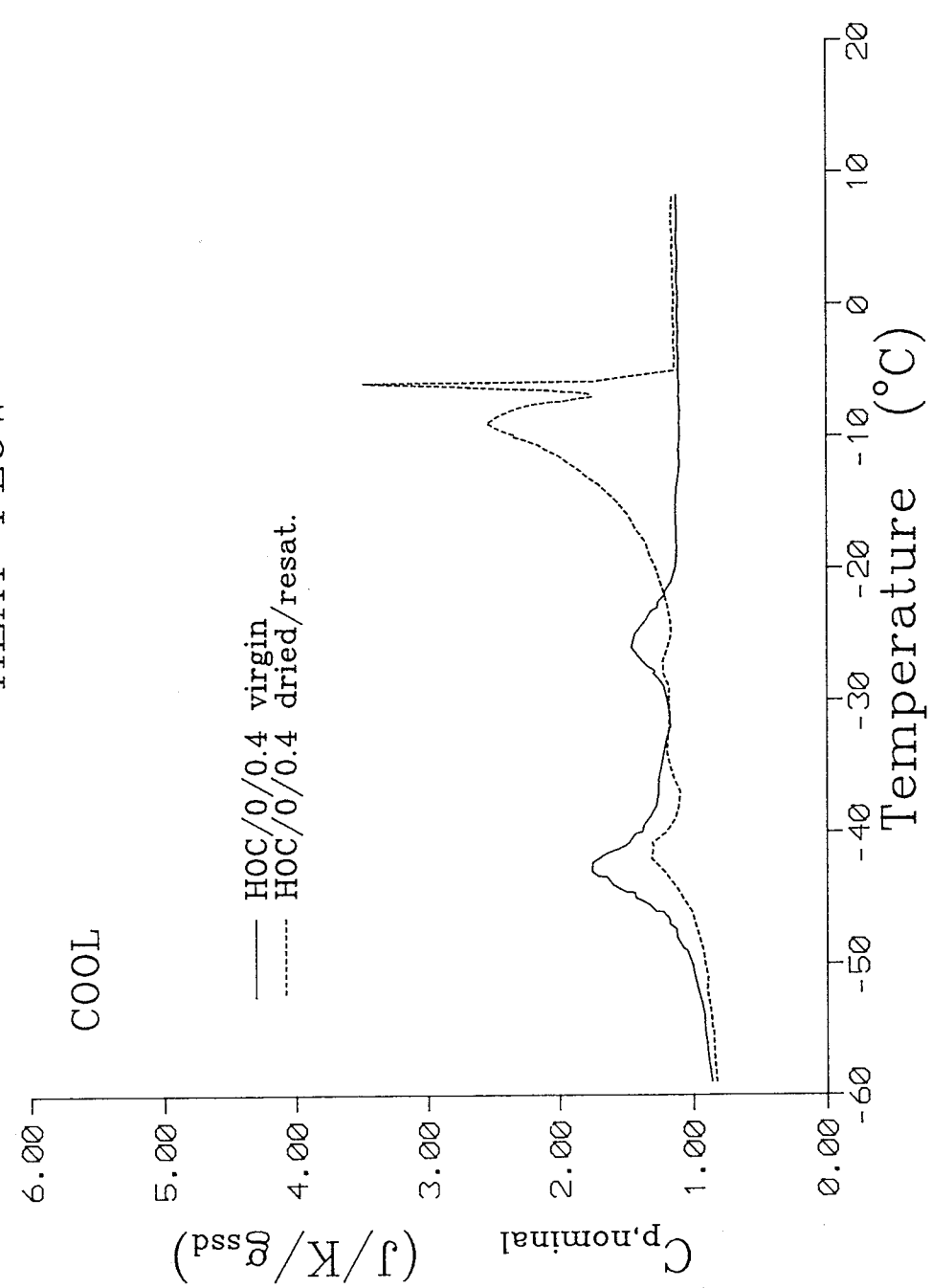

Figure 4.3.1C: Heat capacity during cooling for mature 0.4 W/C HOC-paste. The effect of drying/resaturation is shown.

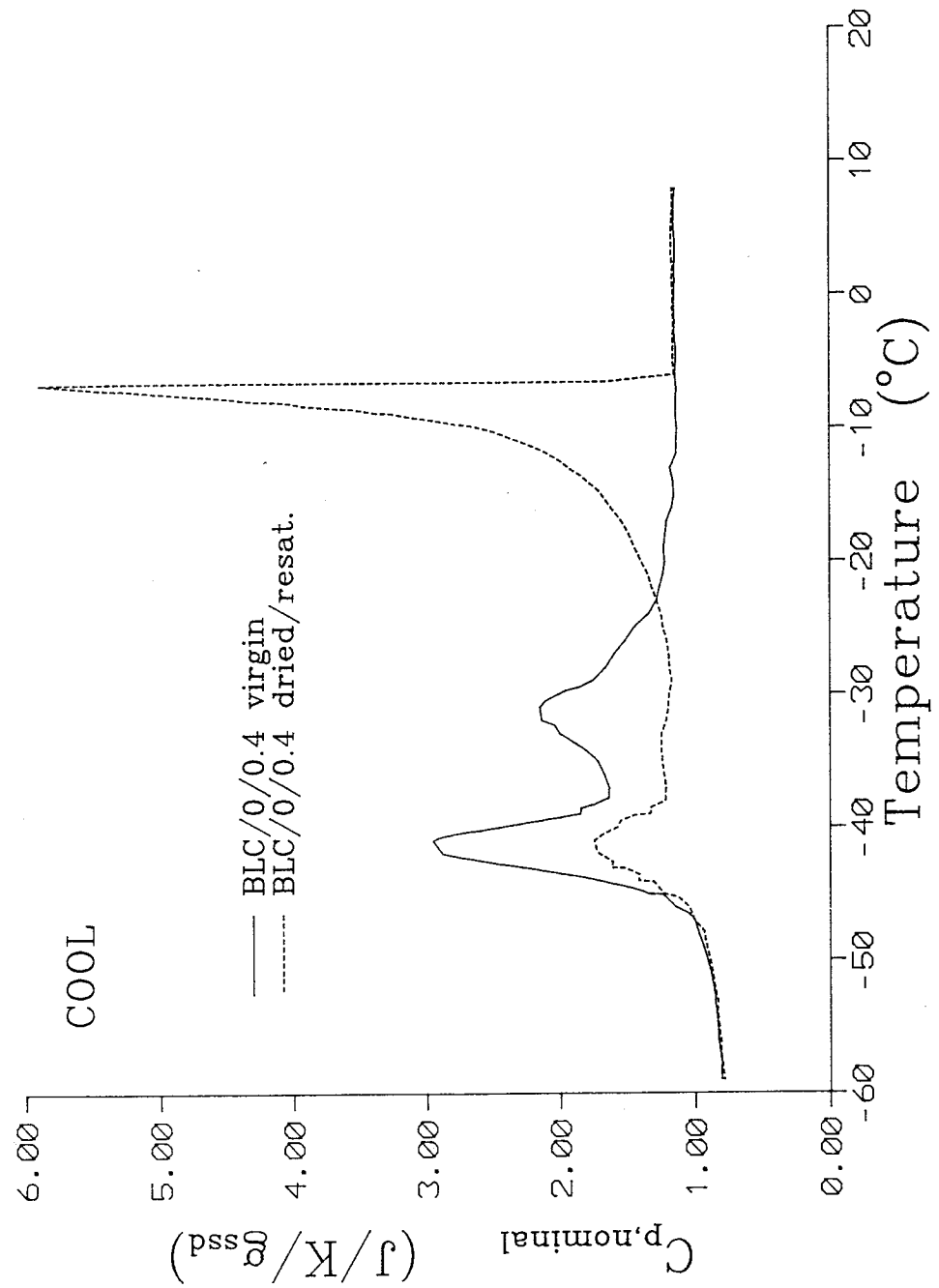

Figure 4.3.1D: Heat capacity during cooling for mature 0.4 W/C BLC-paste. The effect of drying/resaturation is shown.

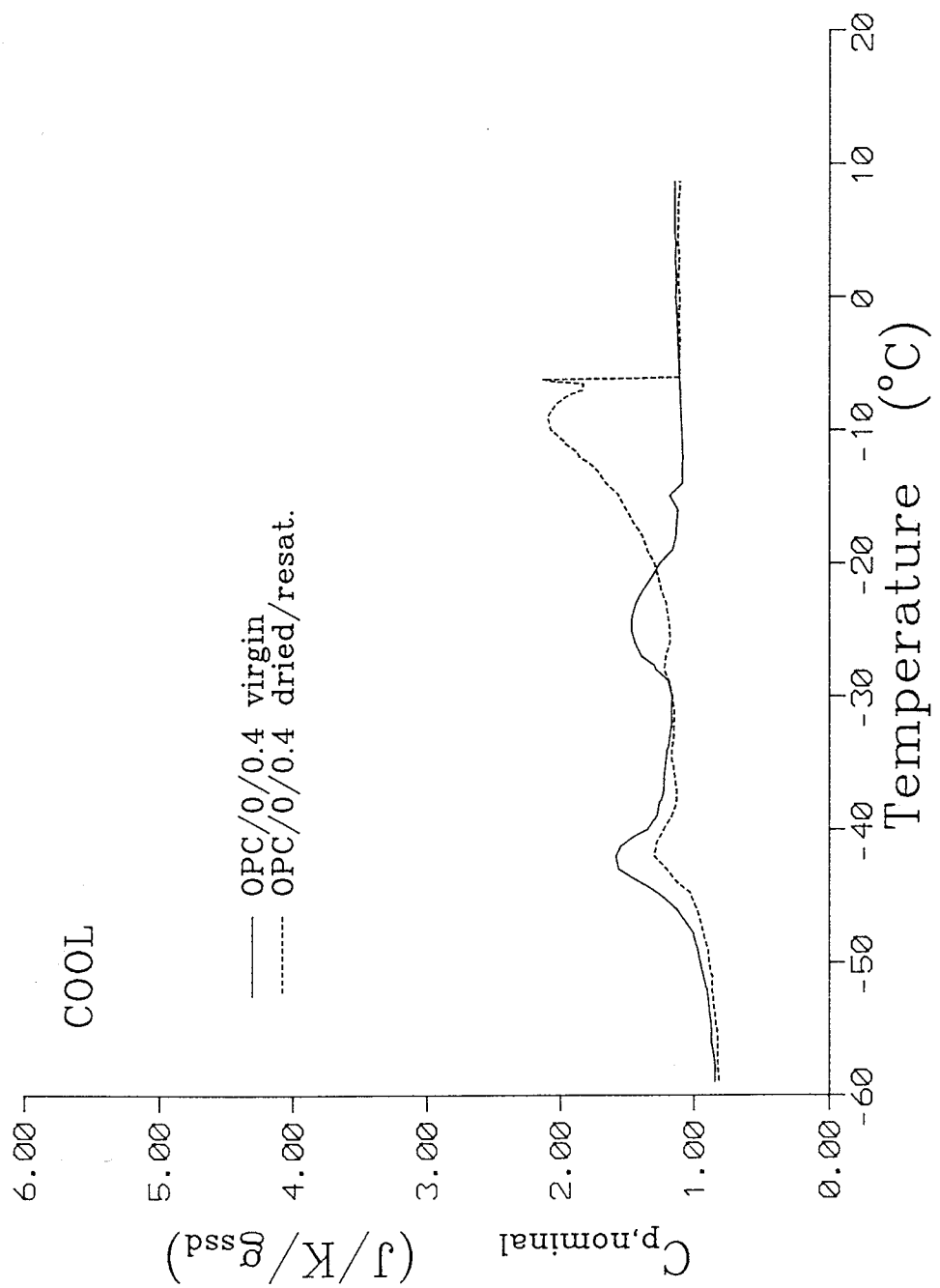

Figure 4.3.1E: Heat capacity during cooling for mature 0.4 W/C OPC-paste. The effect of drying/resaturation is shown.

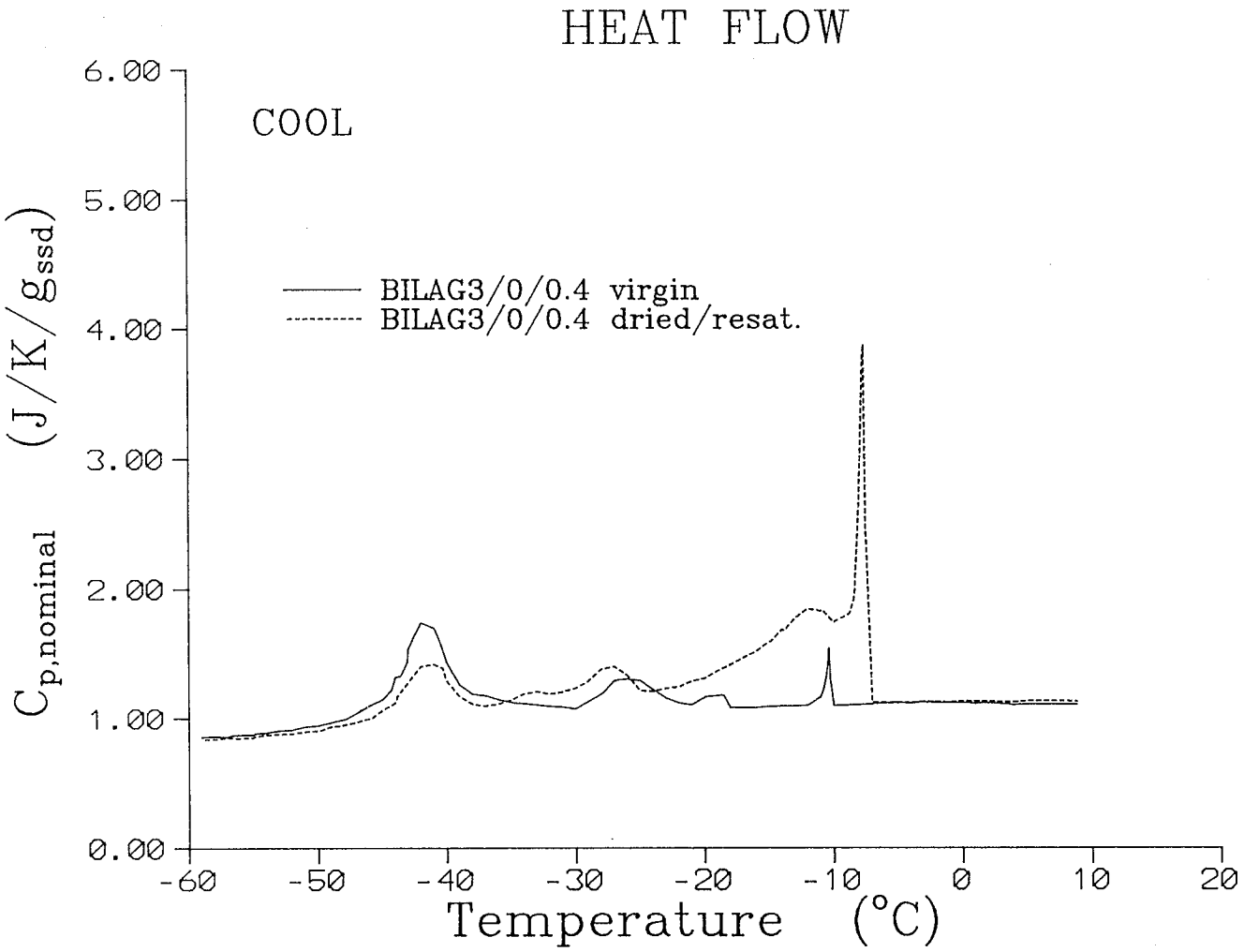

Figure 4.3.1F: Heat capacity during cooling for mature 0.4 W/C BILAG3-paste. The effect of drying/resaturation is shown.

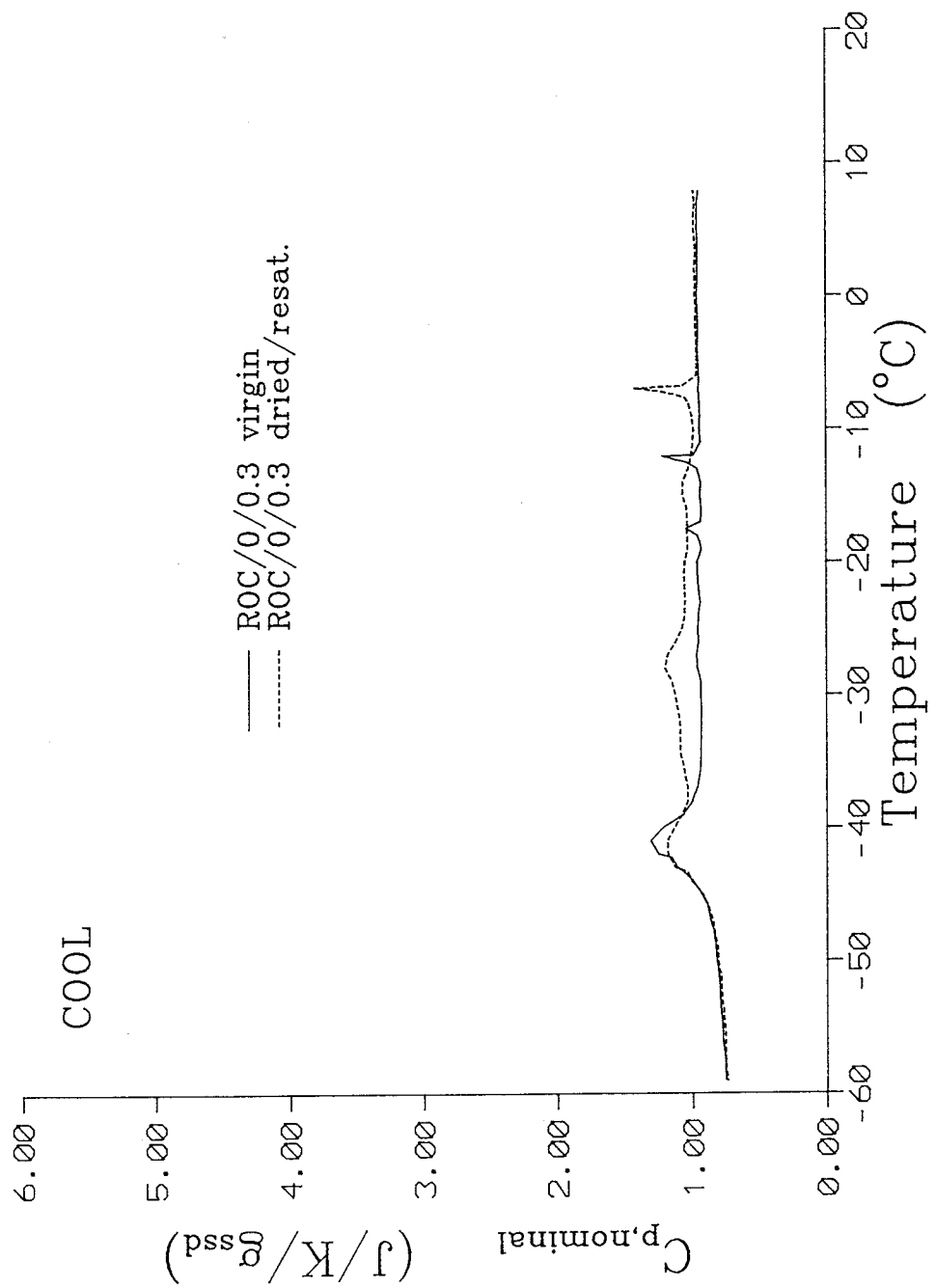

Figure 4.3.1G: Heat capacity during cooling for mature 0.3 W/C ROC-paste. The effect of drying/resaturation is shown.

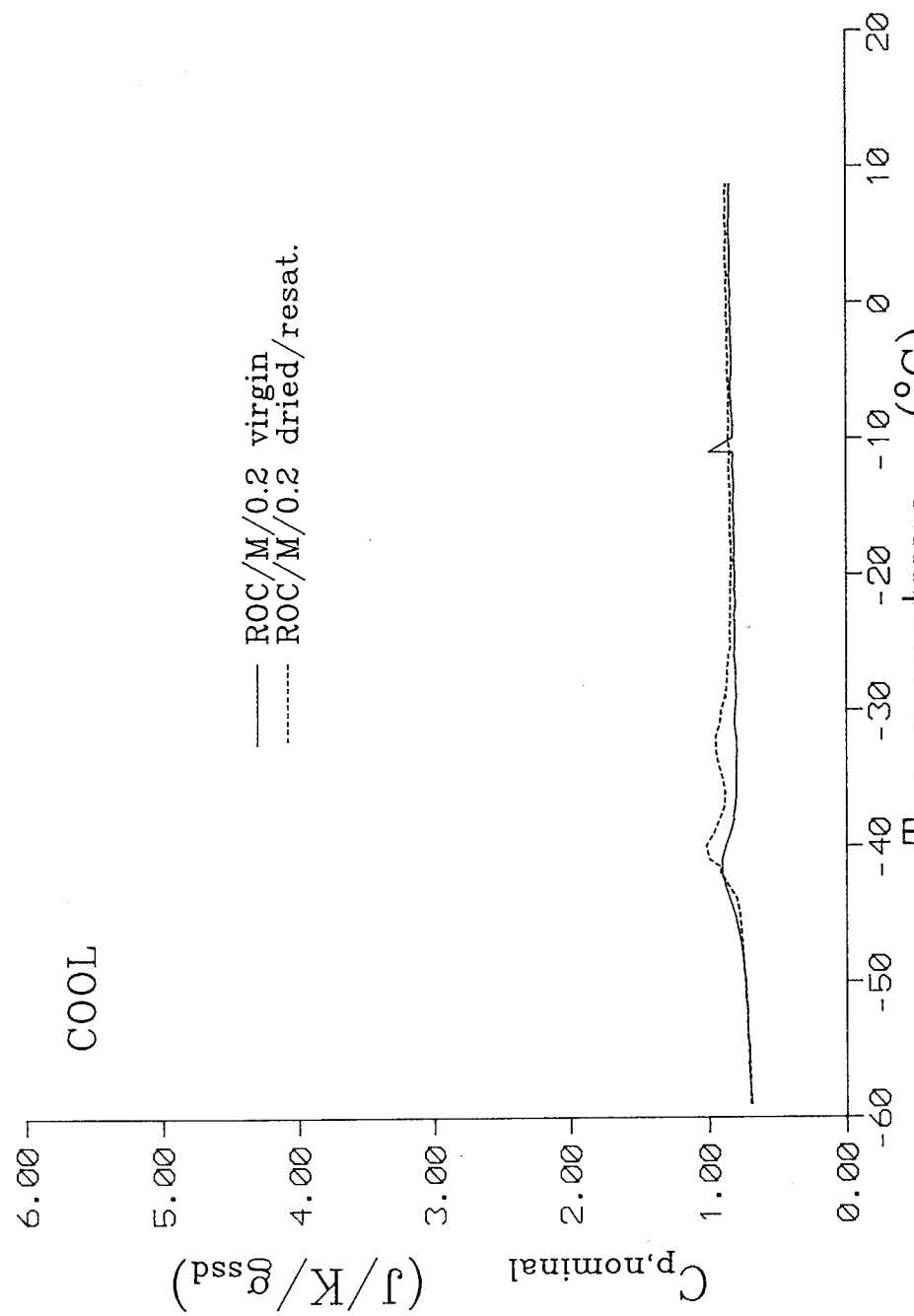

Figure 4.3.1H: Heat capacity during cooling for mature 0.2 W/C ROC-paste. The effect of drying/resaturation is shown.

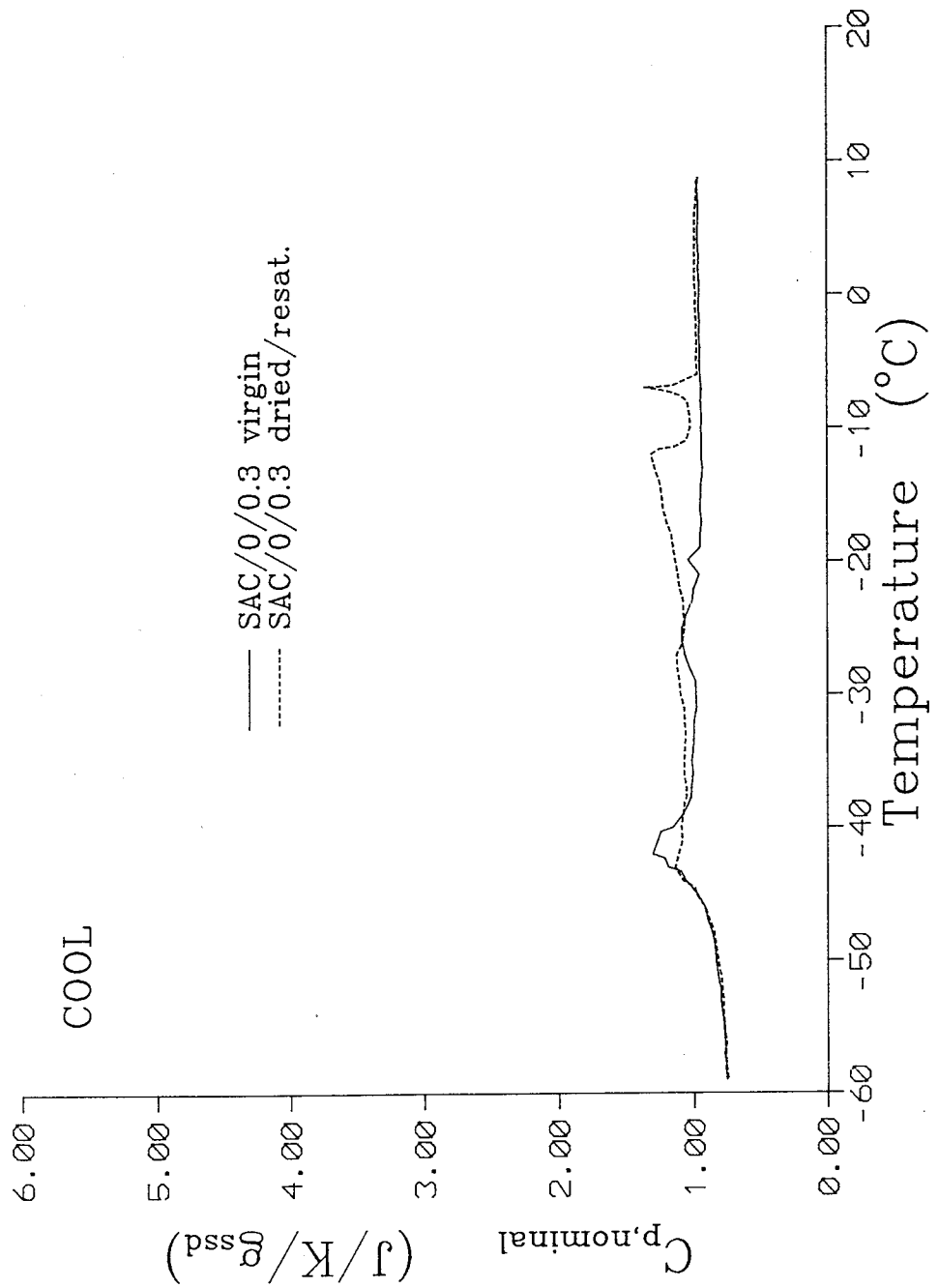

Figure 4.3.11: Heat capacity during cooling for mature 0.3 W/C SAC-paste. The effect of drying/resaturation is shown.

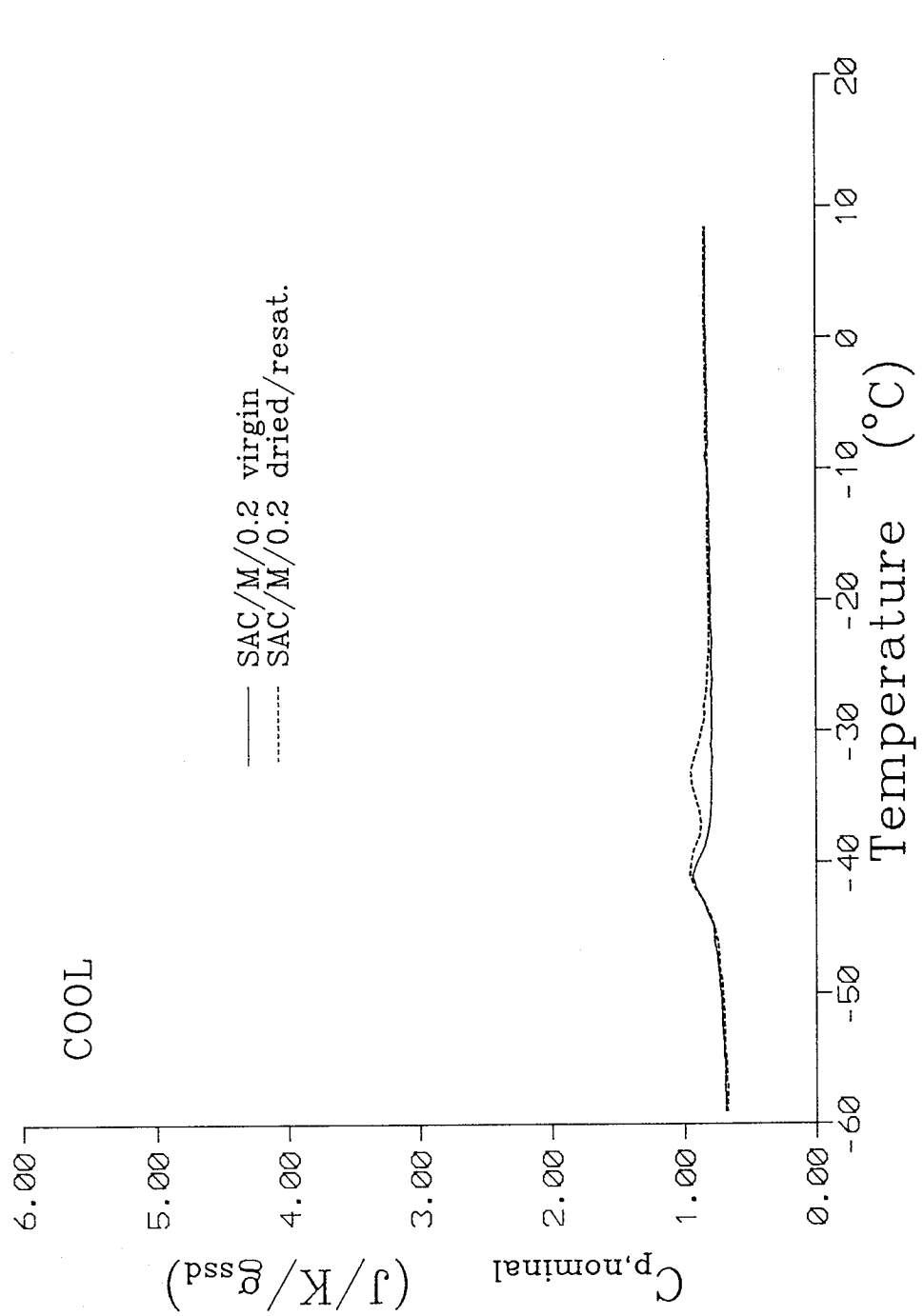

Figure 4.3.1J: Heat capacity during cooling for mature 0.2 W/C SAC-paste. The effect of drying/resaturation is shown.

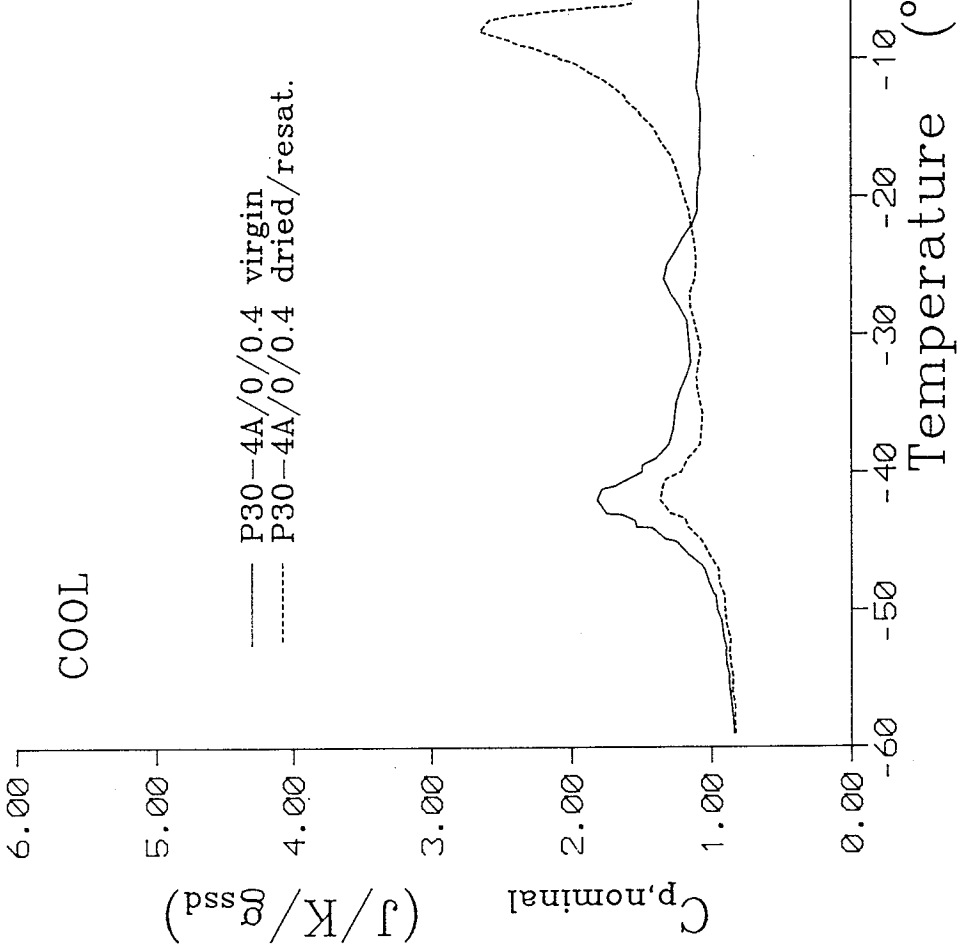

Figure 4.3.1L: Heat capacity during cooling for mature 0.4 W/C P304A-paste. The effect of drying/resaturation is shown.

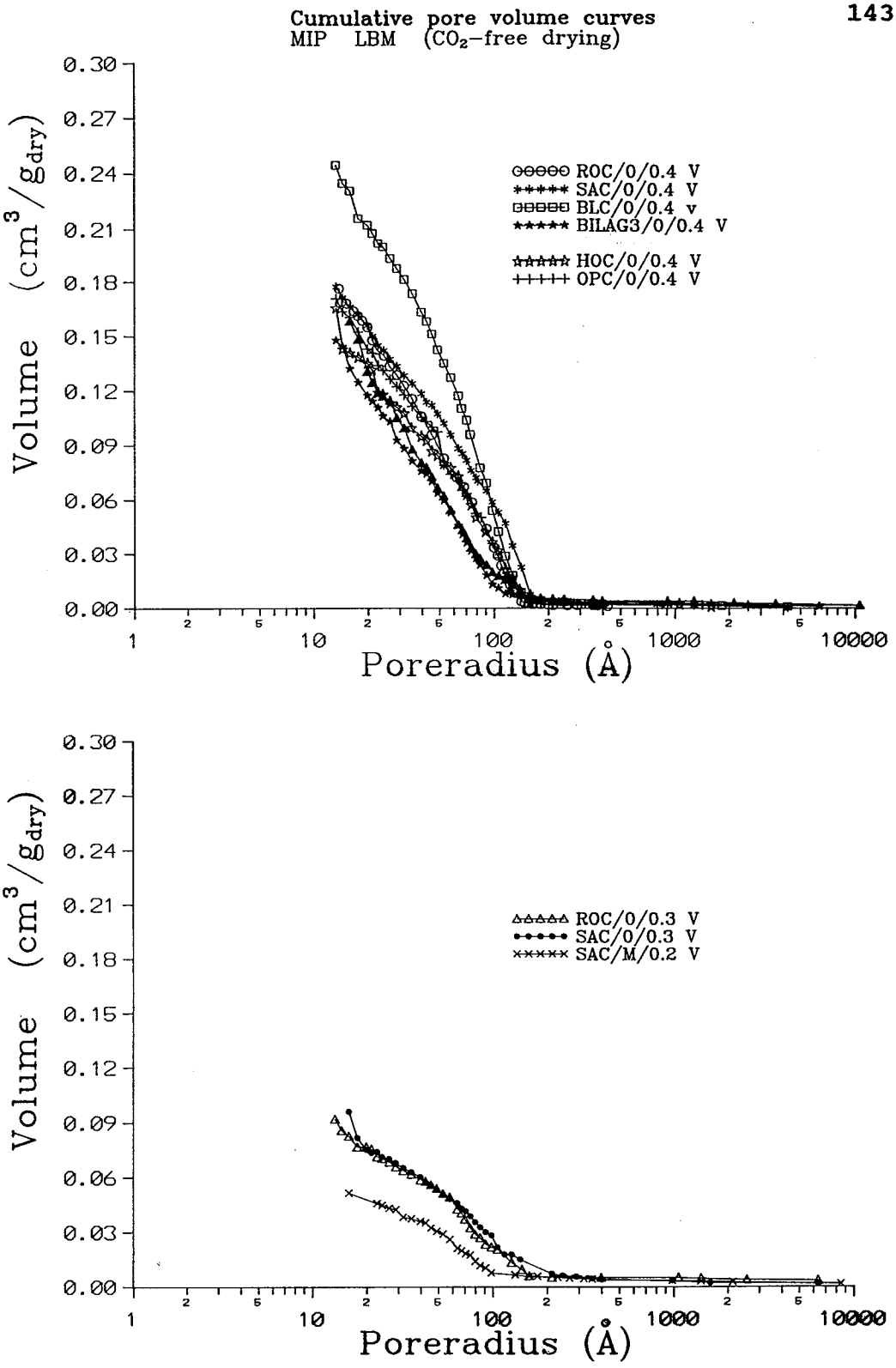

Figure 4.3.2A: Cumulative pore size distibutions from MIP at LBM for different mature, virgin cured HCP-blends.

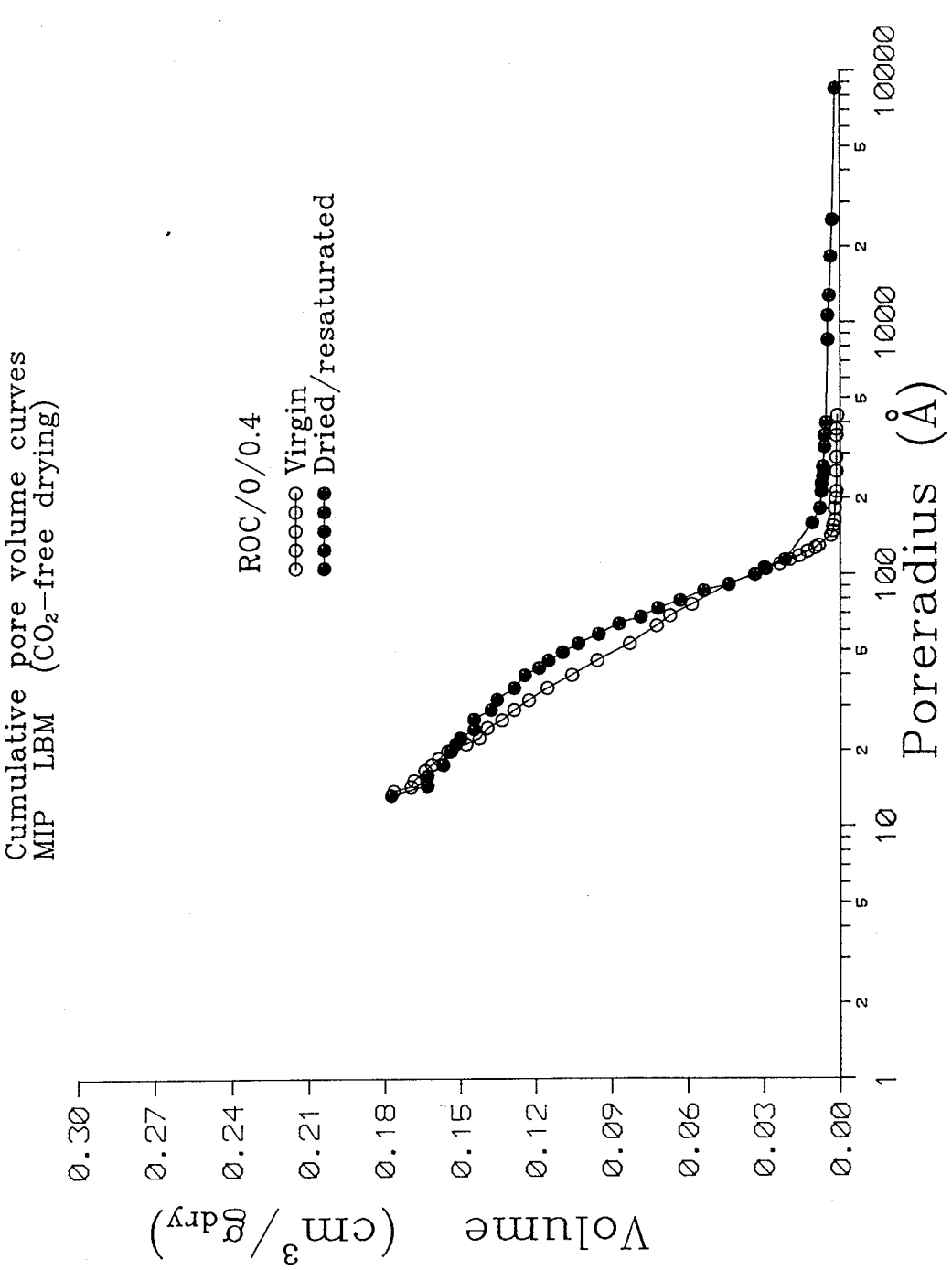

Figure 4.3.2B: Cumulative pore size distribution from MIP at LBM for mature 0.4 W/C ROC-paste. The effect of conditioning (drying/resaturation) is shown. Specimens have been dried by CO_2-free drying prior to MIP.

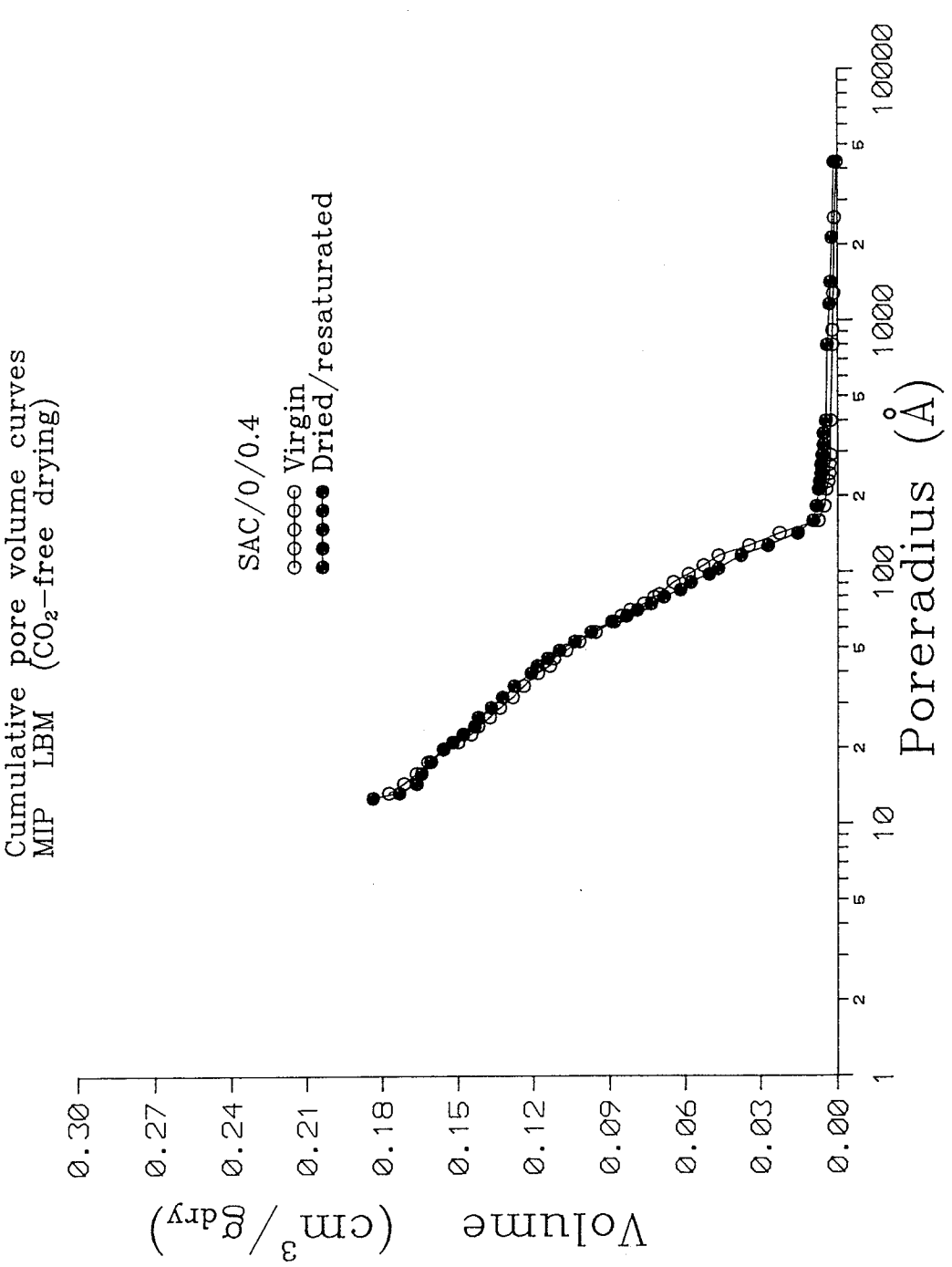

Figure 4.3.2C: Cumulative pore size distribution from MIP at LBM for mature 0.4 W/C SAC-paste. The effect of conditioning (drying/resaturation) is shown. Specimens have been dried by CO_2-free drying prior to MIP.

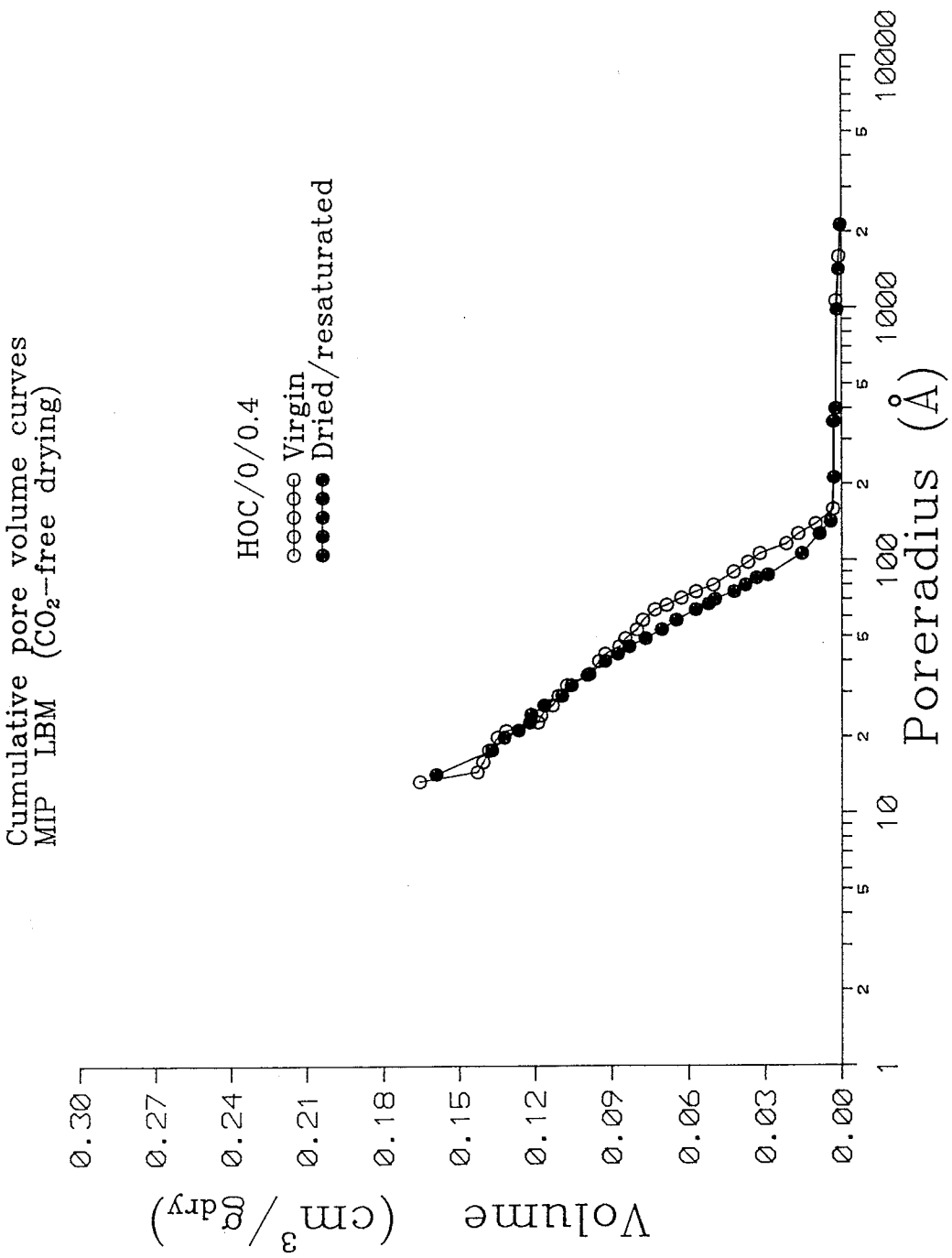

Figure 4.3.2D: Cumulative pore size distribution from MIP at LBM for mature 0.4 W/C HOC-paste. The effect of conditioning (drying/resaturation) is shown. Specimens have been dried by CO_2-free drying prior to MIP.

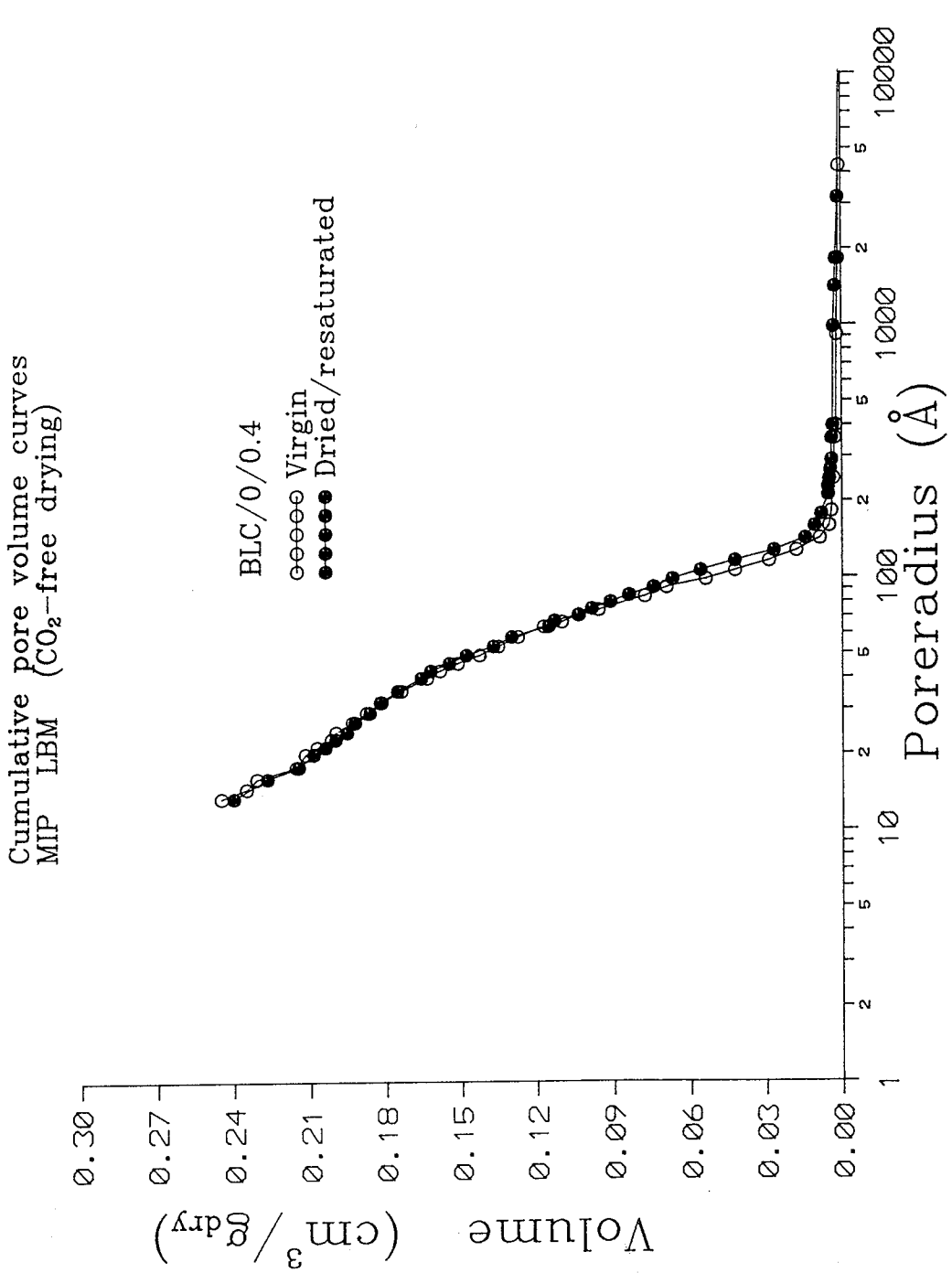

Figure 4.3.2E: Cumulative pore size distribution from MIP at LBM for mature 0.4 W/C BLC-paste. The effect of conditioning (drying/resaturation) is shown. Specimens have been dried by CO_2-free drying prior to MIP.

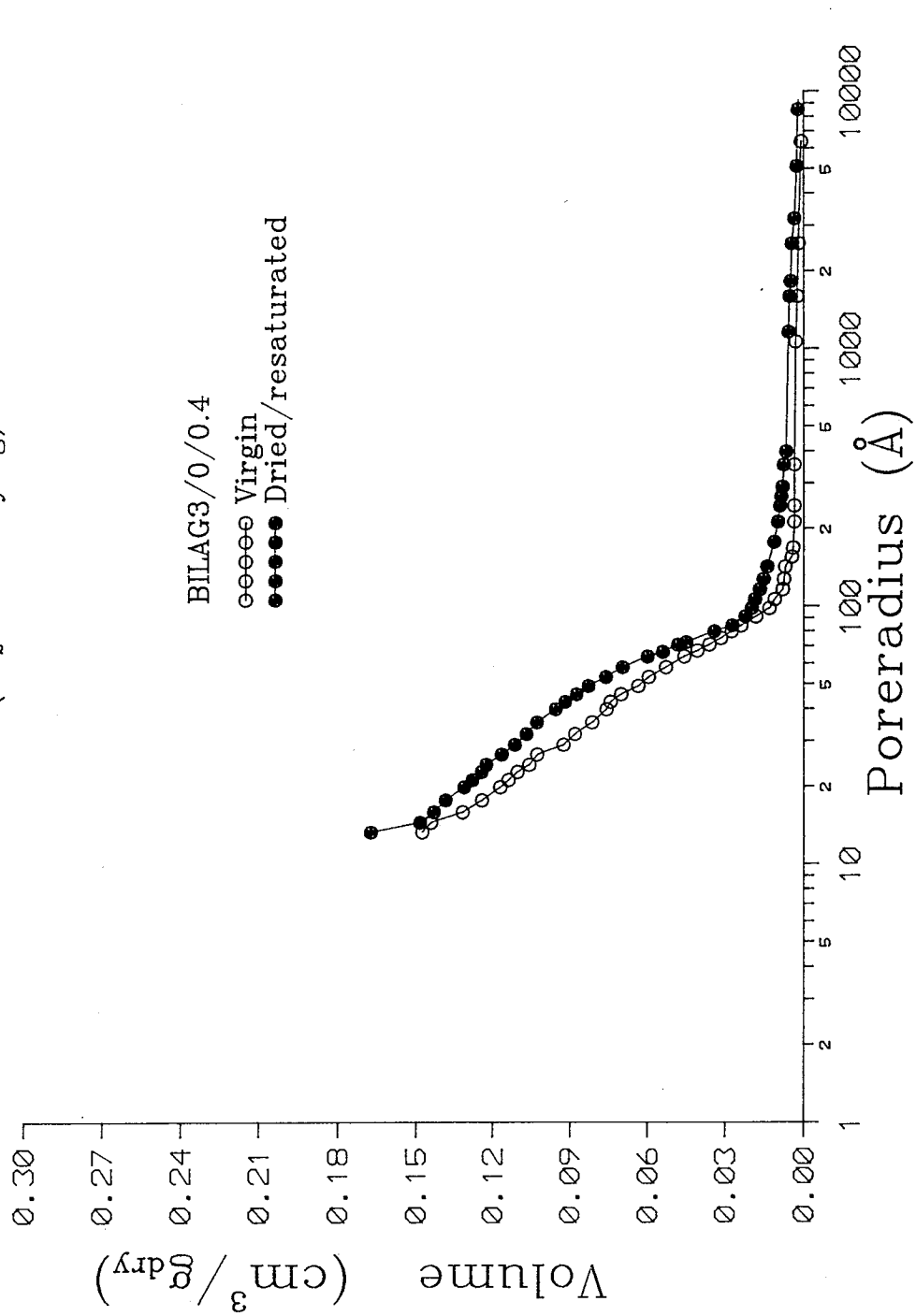

Figure 4.3.2F: Cumulative pore size distribution from MIP at LBM for mature 0.4 W/C BILAG3-paste. The effect of conditioning (drying/resaturation) is shown. Specimens have been dried by CO_2-free drying prior to MIP.

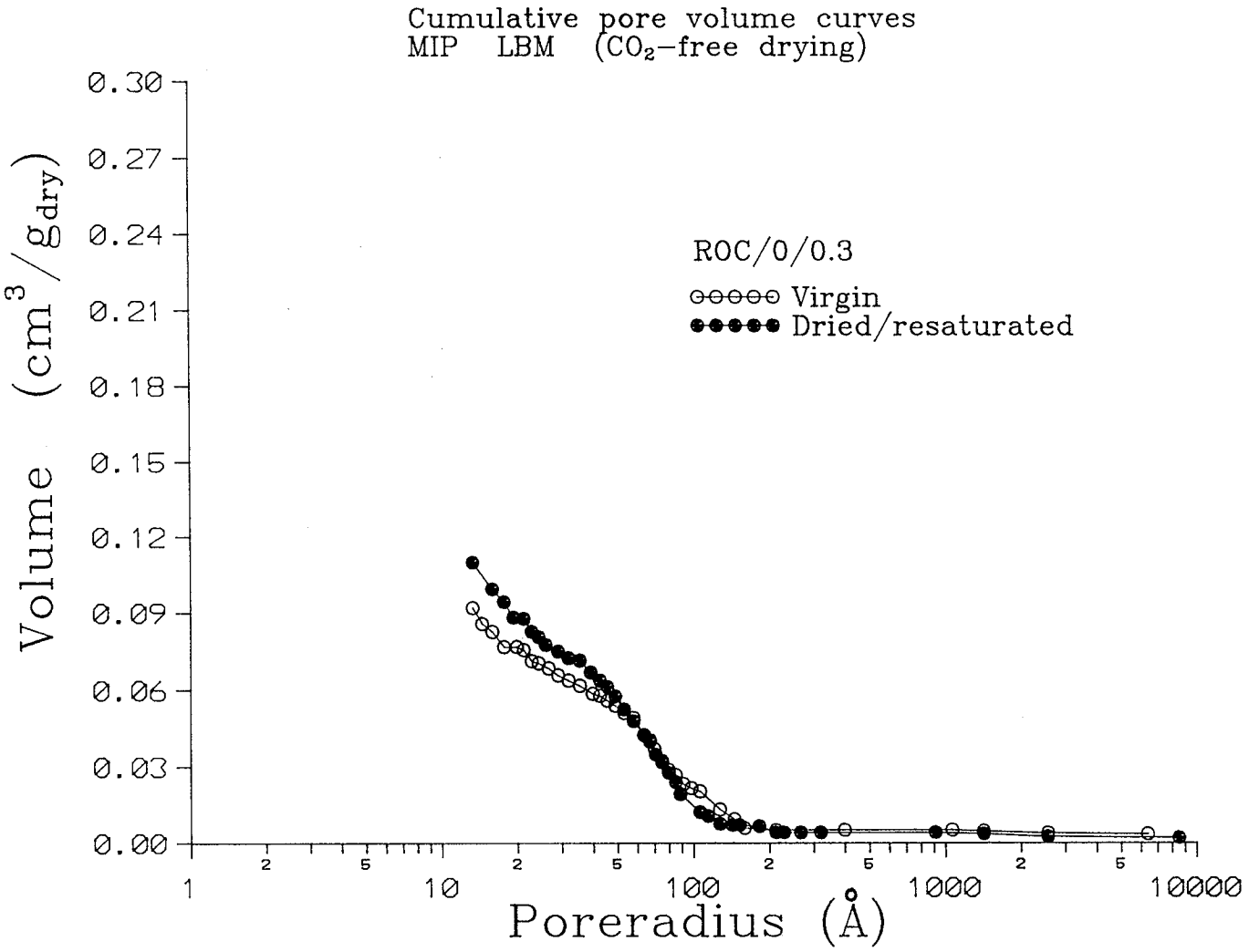

Figure 4.3.2G: Cumulative pore size distribution from MIP at LBM for mature 0.3 W/C ROC-paste. The effect of conditioning (drying/resaturation) is shown. Specimens have been dried by CO_2-free drying prior to MIP.

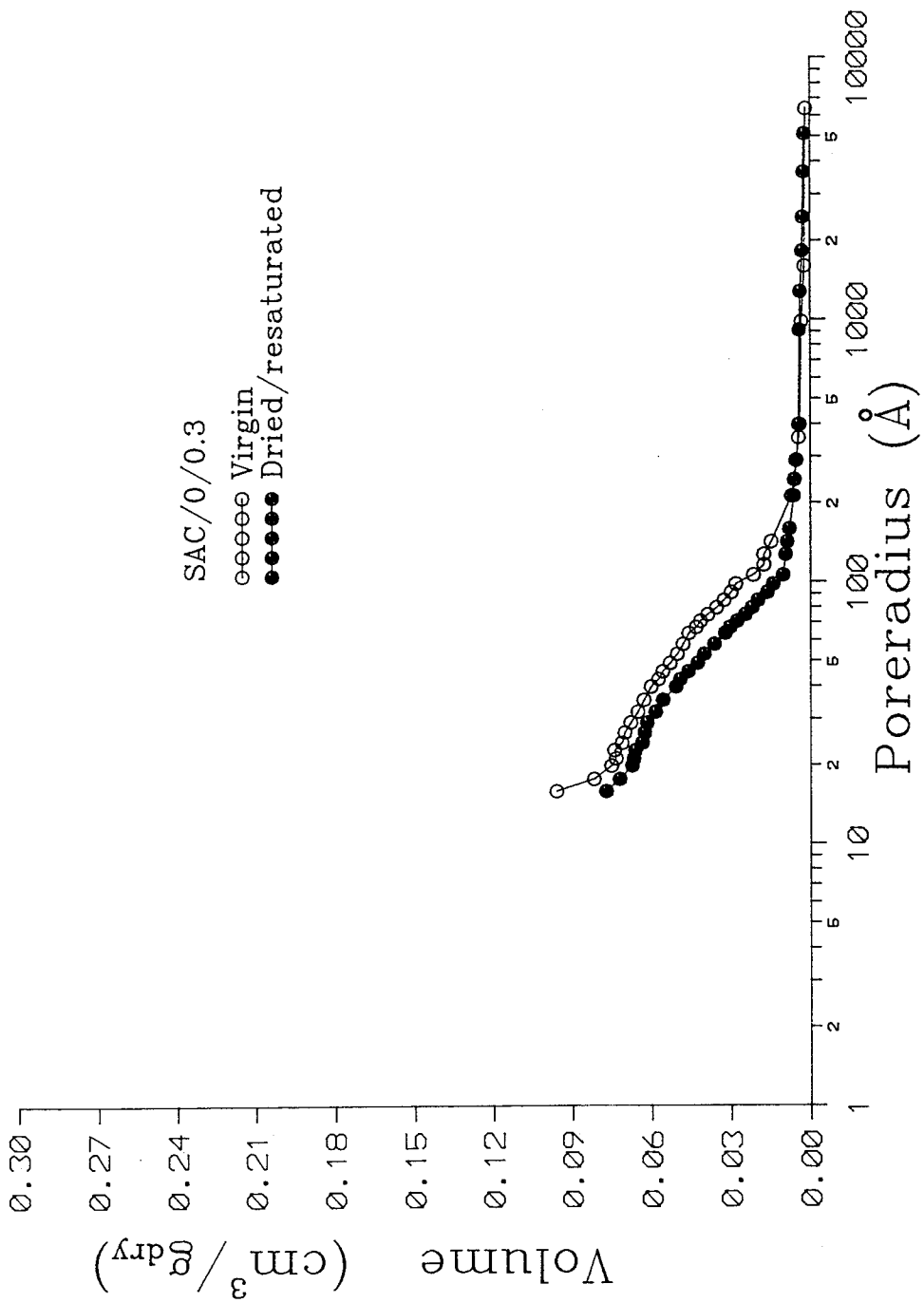

Figure 4.3.2H: Cumulative pore size distribution from MIP at LBM for mature 0.3 W/C SAC-paste. The effect of conditioning (drying/resaturation) is shown. Specimens have been dried by CO_2-free drying prior to MIP.

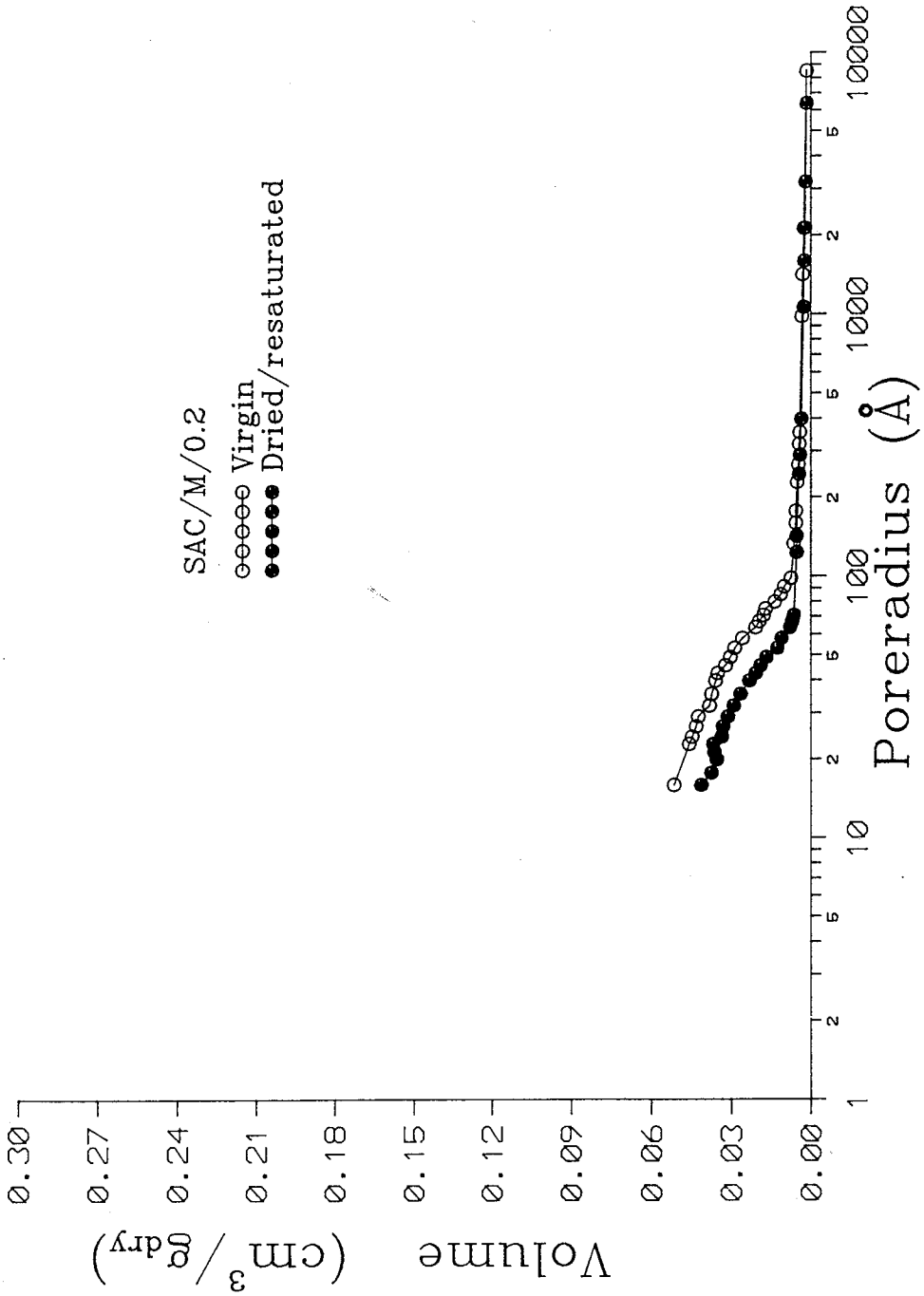

Figure 4.3.21: Cumulative pore size distribution from MIP at LBM for mature 0.2 W/C SAC-paste. The effect of conditioning (drying/resaturation) is shown. Specimens have been dried by CO_2-free drying prior to MIP.

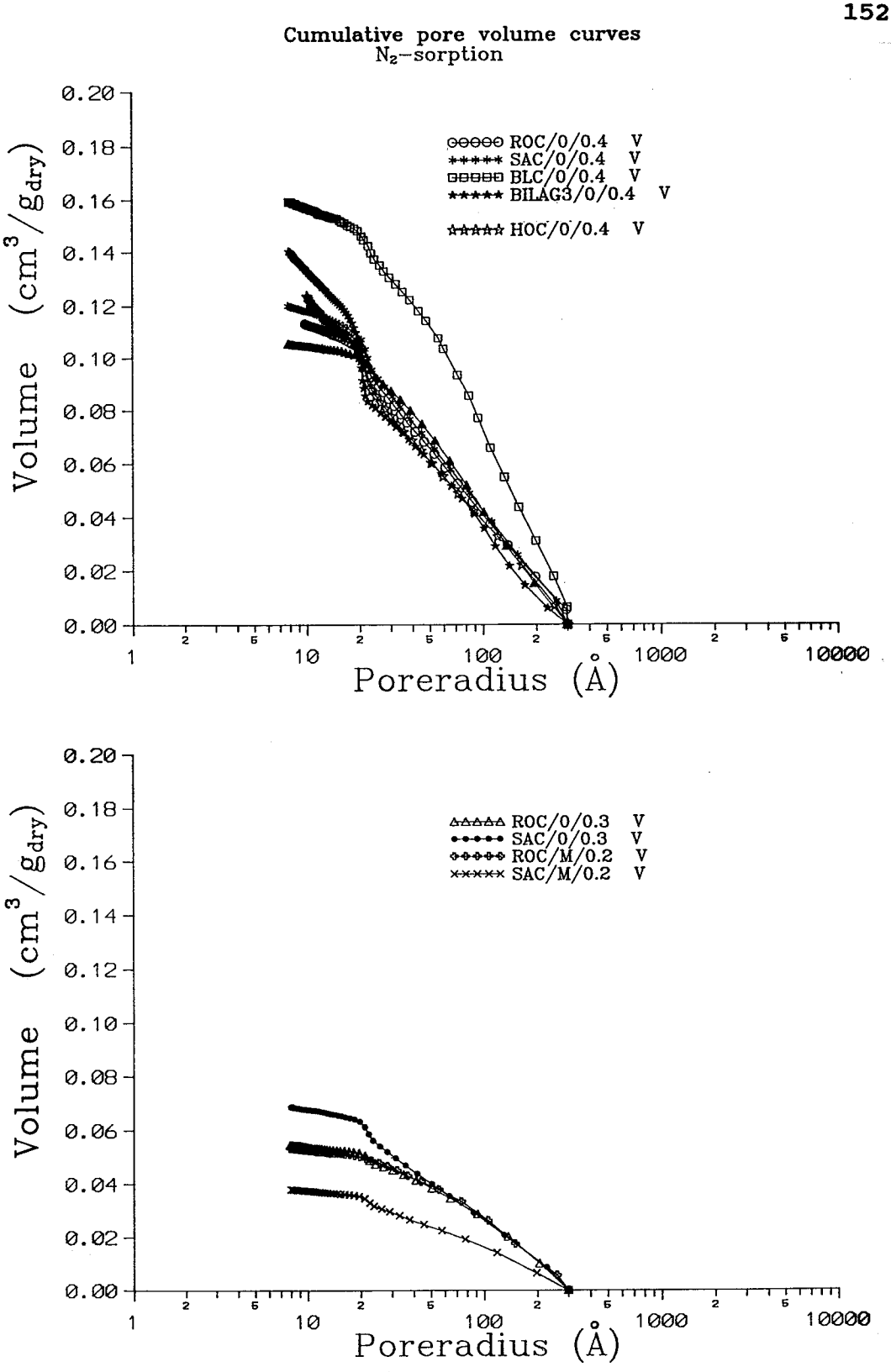

Figure 4.3.3A: Cumulative pore size distributions calculated from the desorption branch of the nitrogen isotherm for different mature, virgin cured HCP blends.

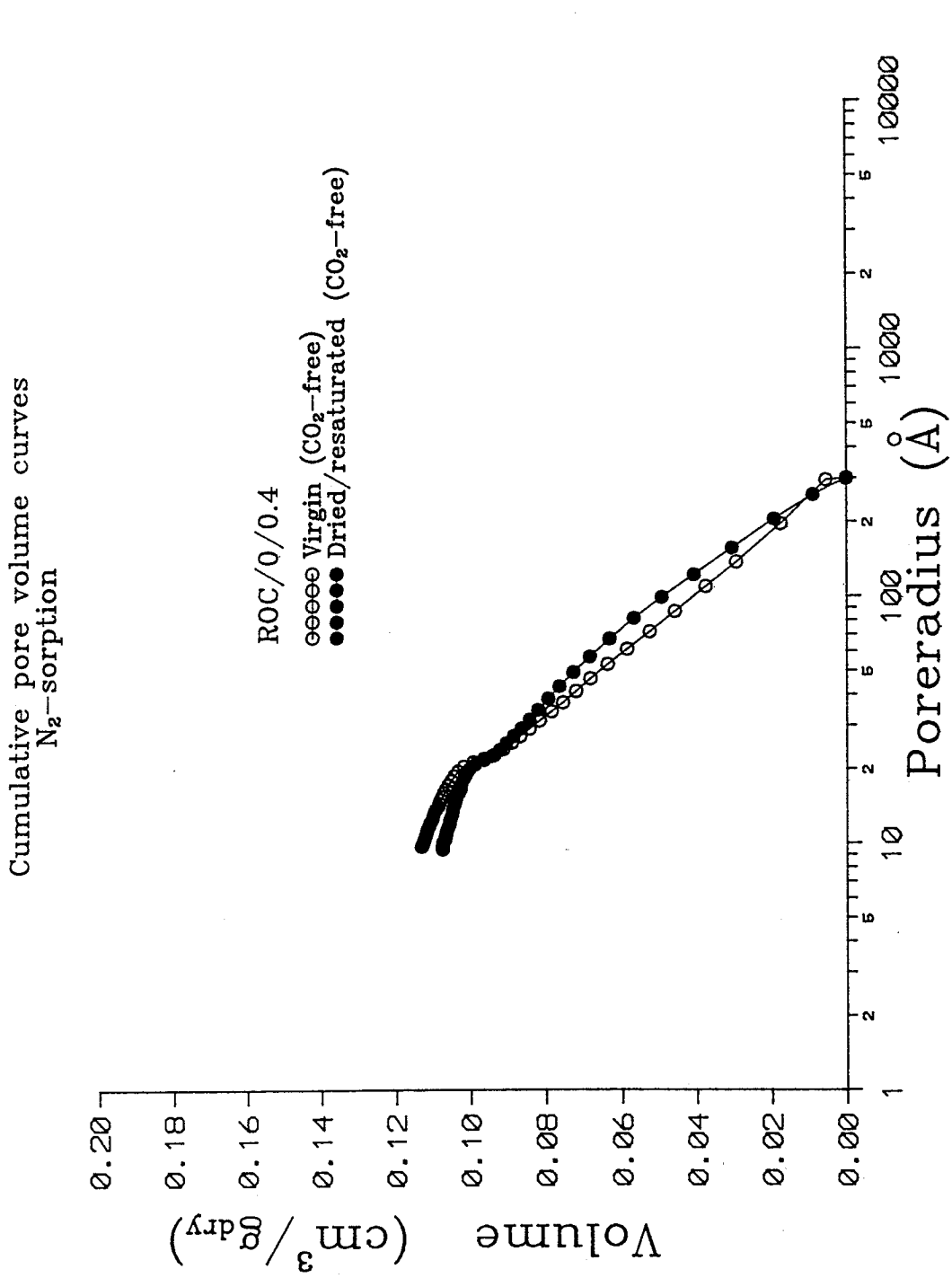

Figure 4.3.38: Cumulative pore size distributions calculated from the desorption branch of the nitrogen isotherm for mature 0.4 W/C ROC-paste. The effect of conditioning (drying/resaturation) is shown.

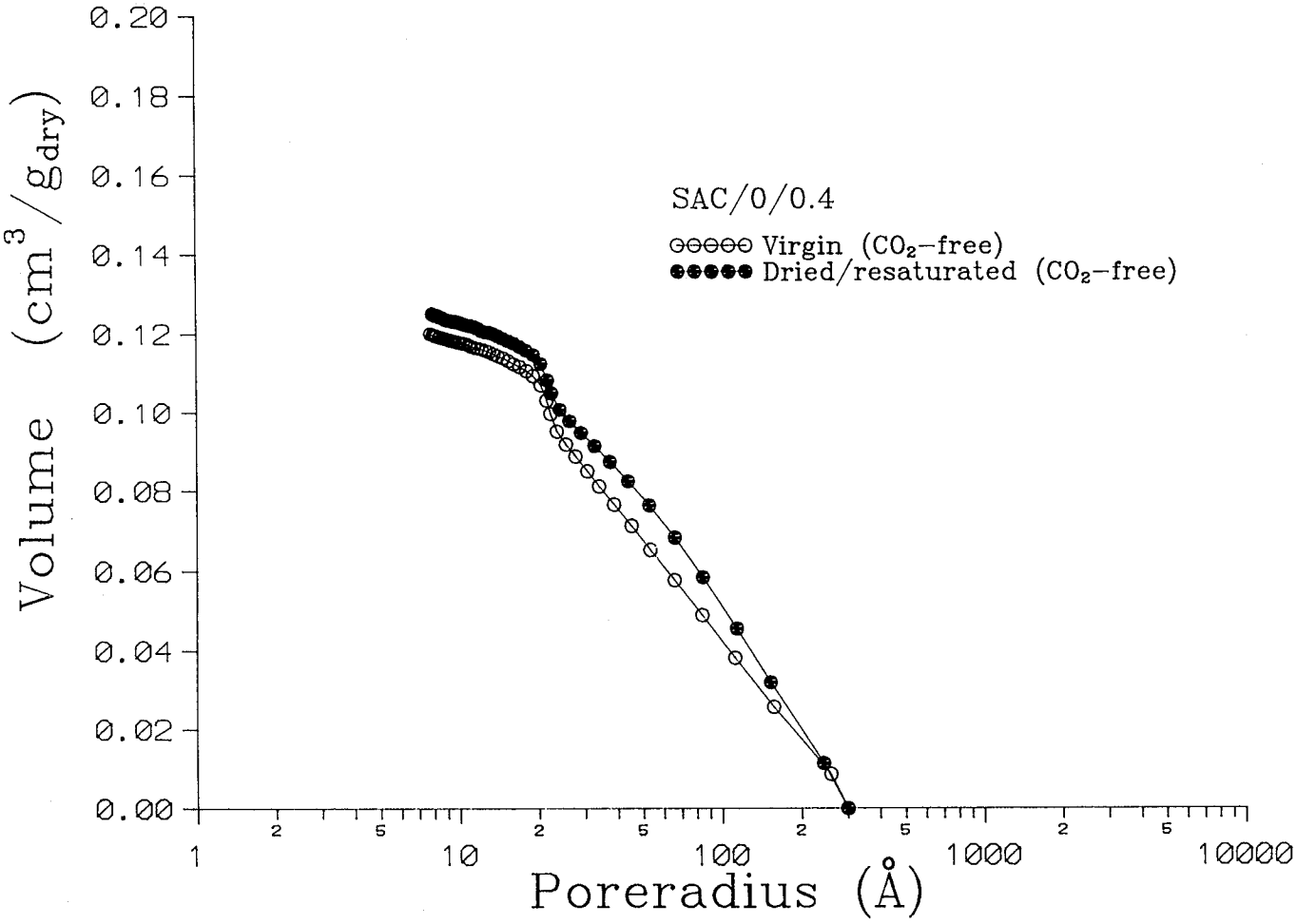

Figure 4.3.3C: Cumulative pore size distributions calculated from the desorption branch of the nitrogen isotherm for mature 0.4 W/C SAC-paste. The effect of conditioning (drying/ resaturation) is shown.

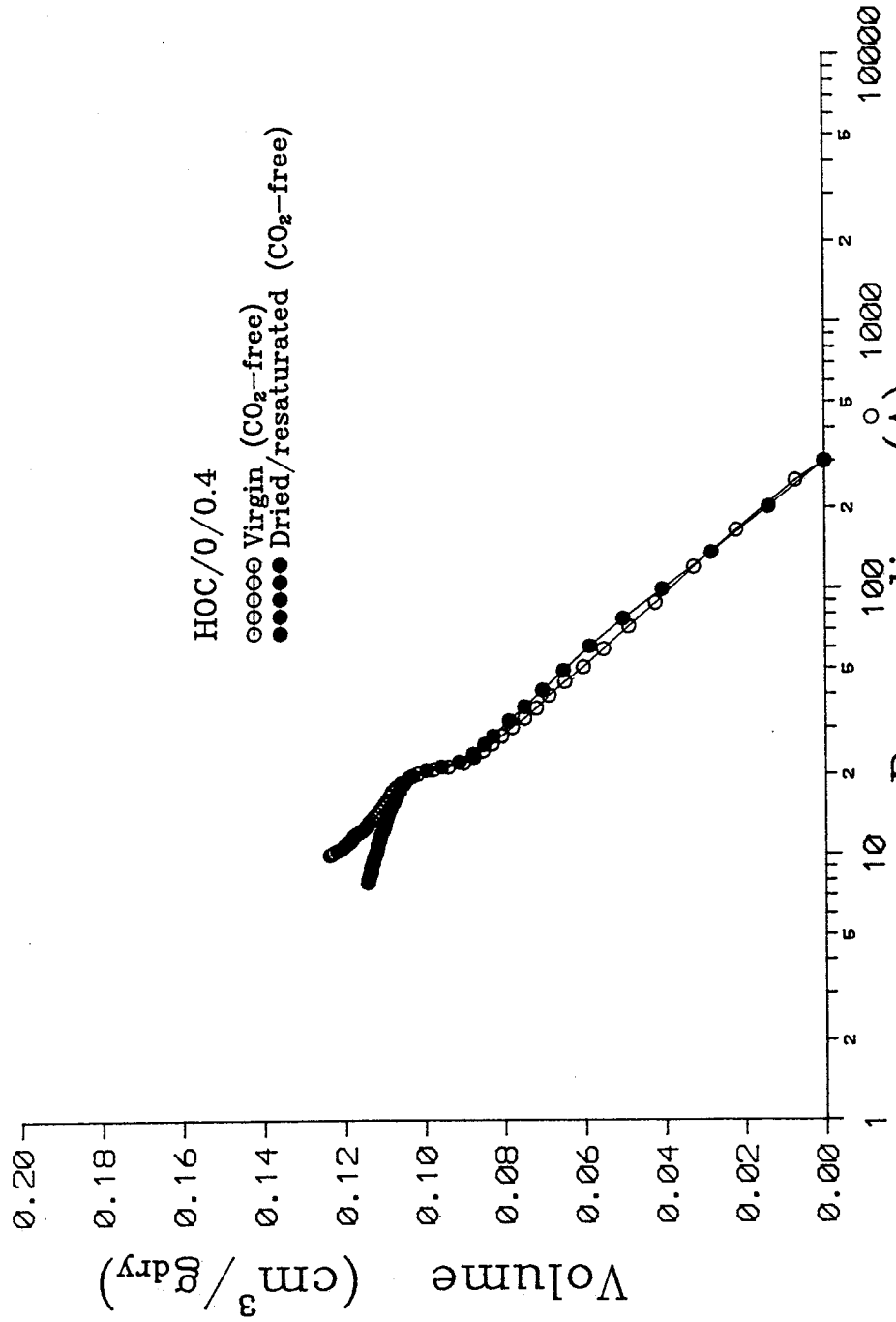

Figure 4.3.3D: Cumulative pore size distributions calculated from the desorption branch of the nitrogen isotherm for mature 0.4 W/C HOC-paste. The effect of conditioning (drying/resaturation) is shown.

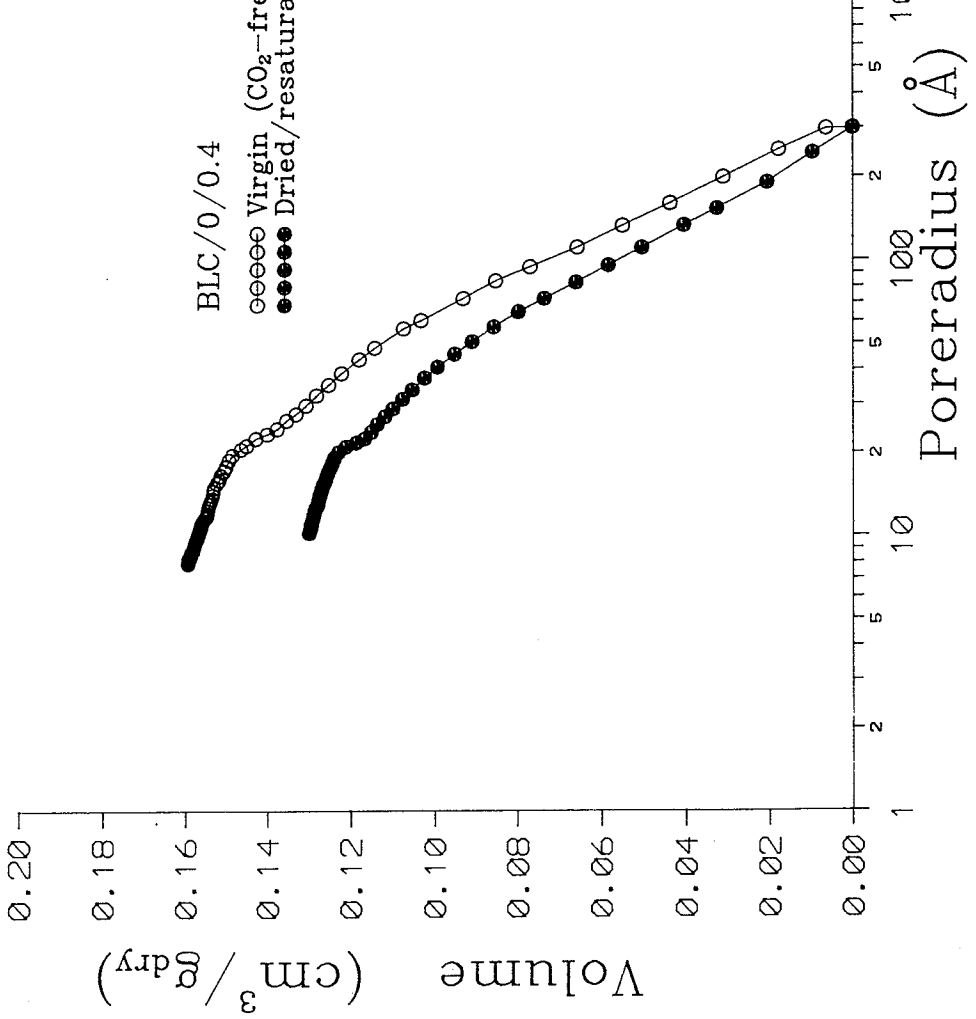

Figure 4.3.3E: Cumulative pore size distributions calculated from the desorption branch of the nitrogen isotherm for mature 0.4 W/C BLC-paste. The effect of conditioning (drying/resaturation) is shown.

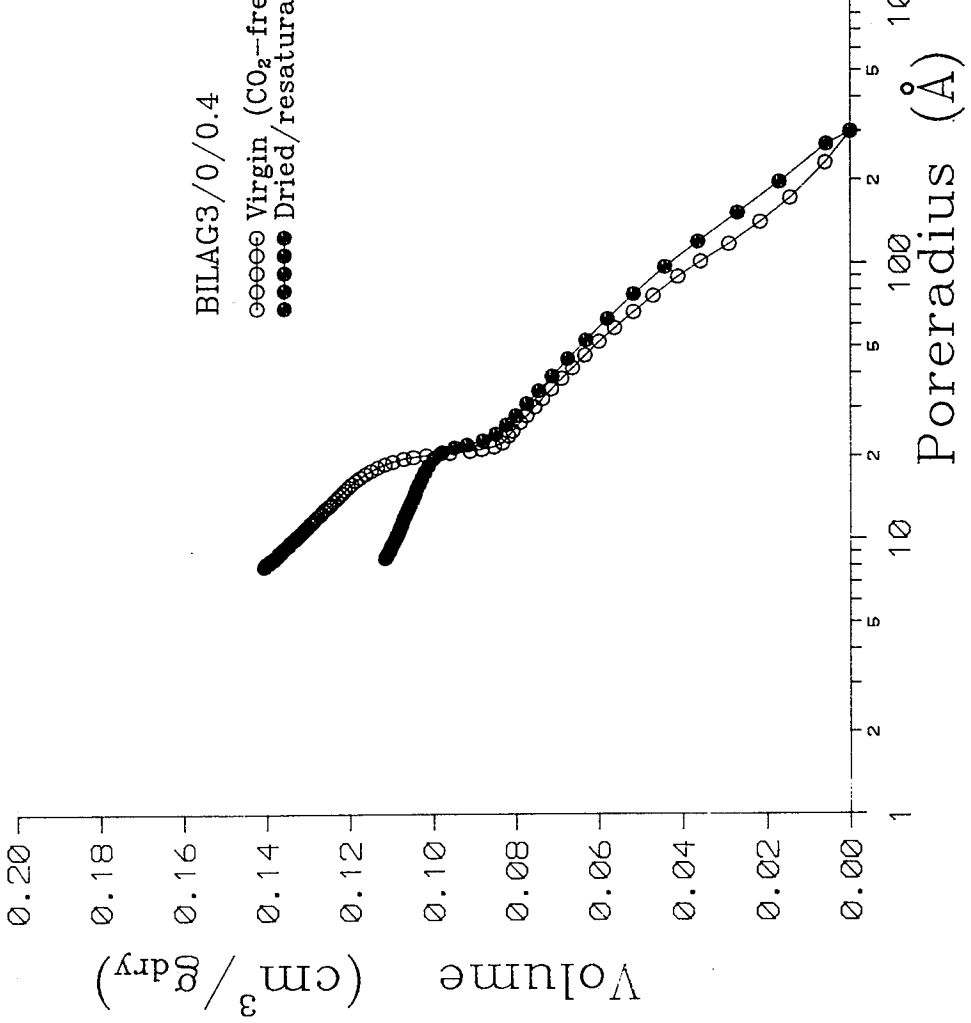

Figure 4.3.3F: Cumulative pore size distributions calculated from the desorption branch of the nitrogen isotherm for mature 0.4 W/C BILAG3-paste. The effect of conditioning drying/resaturation) is shown.

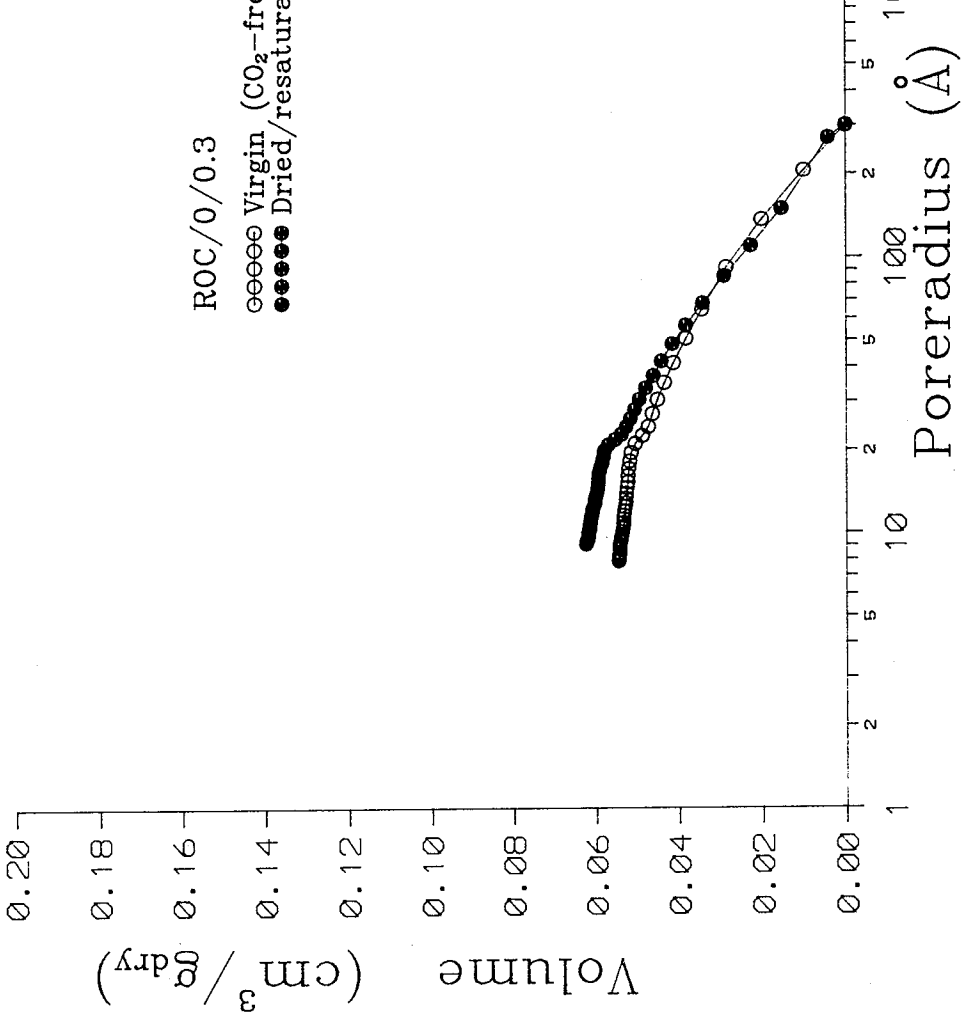

Figure 4.3.36: Cumulative pore size distributions calculated from the desorption branch of the nitrogen isotherm for mature 0.3 W/C ROC-paste. The effect of conditioning (drying/resaturation) is shown.

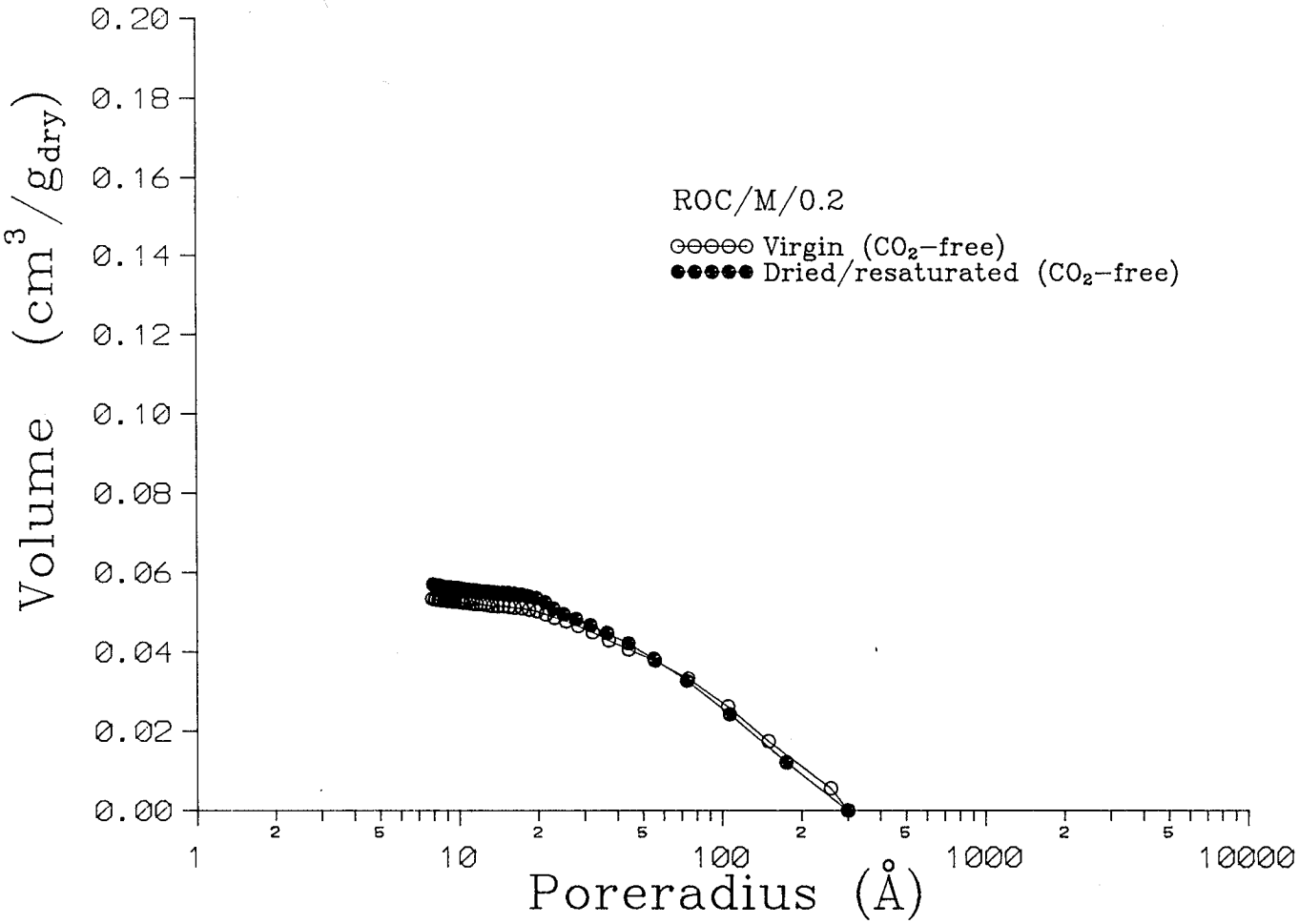

Figure 4.3.3H: Cumulative pore size distributions calculated from the desorption branch of the nitrogen isotherm for mature 0.2 W/C ROC-paste. The effect of conditioning (drying/ resaturation) is shown.

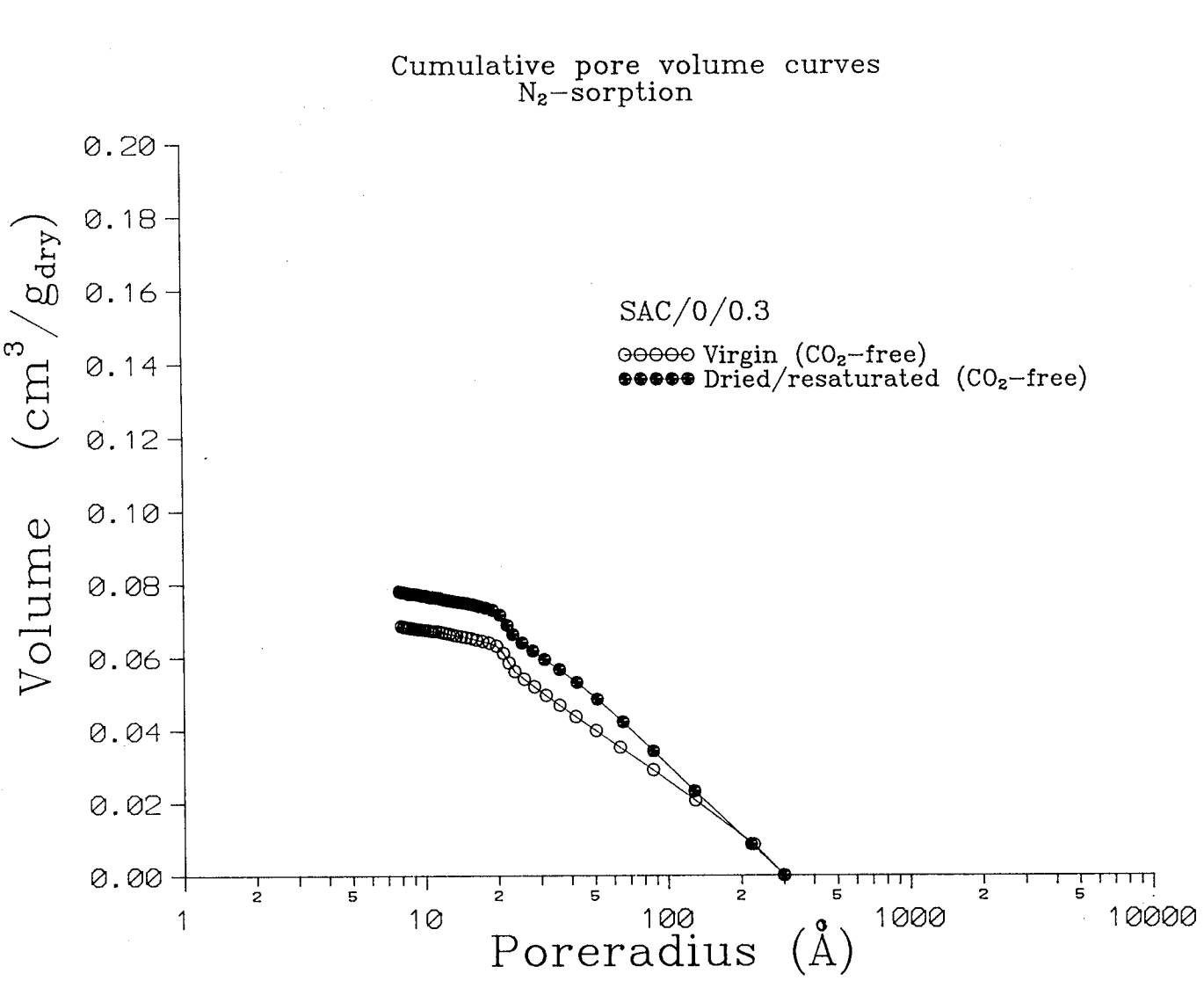

Figure 4.3.31: Cumulative pore size distributions calculated from the desorption branch of the nitrogen isotherm for mature 0.3 W/C SAC-paste. The effect of conditioning (drying/ resaturation) is shown.

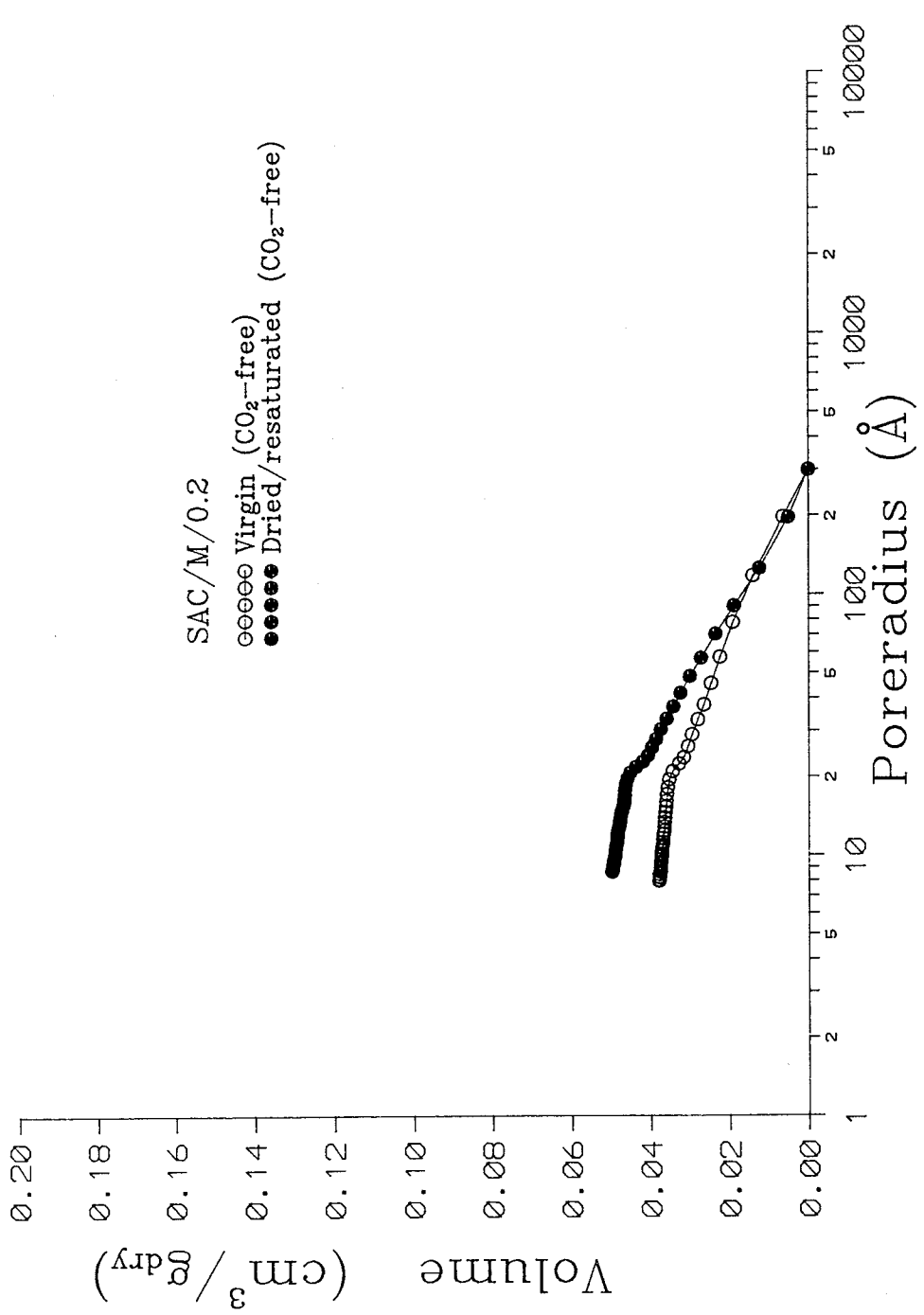

Figure 4.3.3J: Cumulative pore size distributions calculated from the desorption branch of the nitrogen isotherm for mature 0.2 W/C SAC-paste. The effect of conditioning (drying/resaturation) is shown.

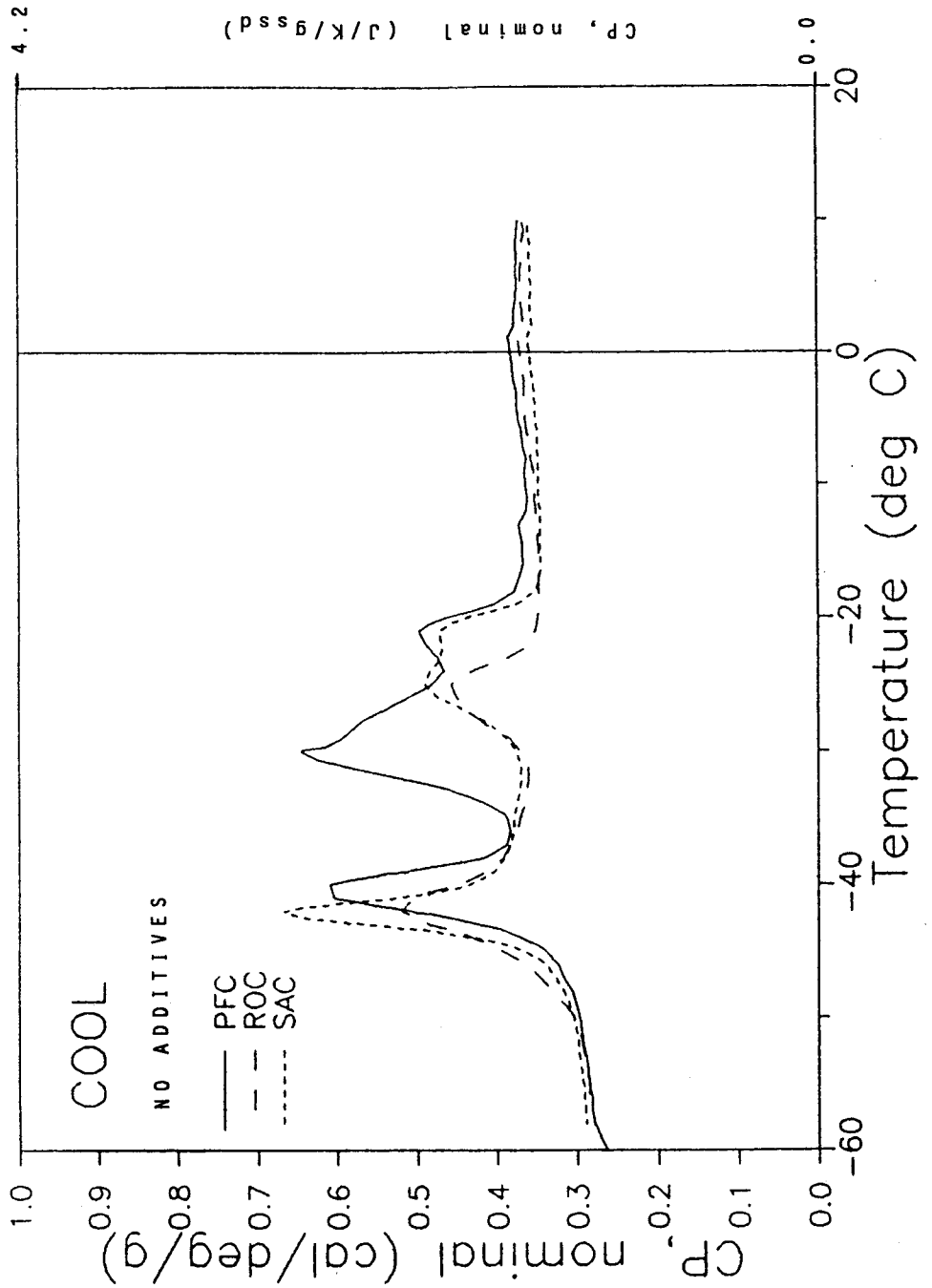

Figure 4.4.1: Heat capacity during cooling for mature, virgin cured 0.4 W/C hardened cement pastes. Effect of cementtype is shown.

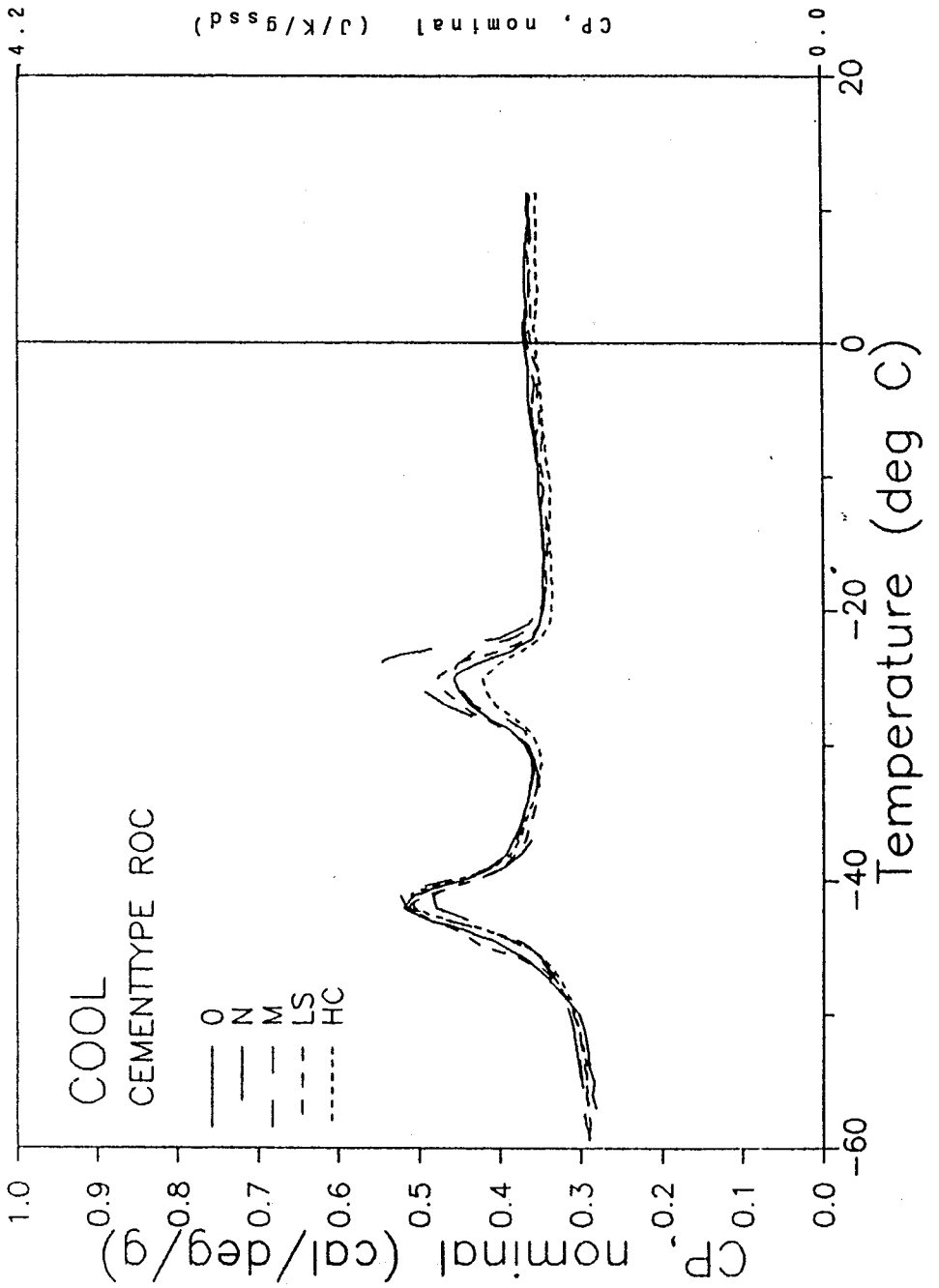

Figure 4.4.2A: Heat capacity during cooling for mature, virgin cured 0.4 W/C ROC-paste. Effect of different additives is shown.

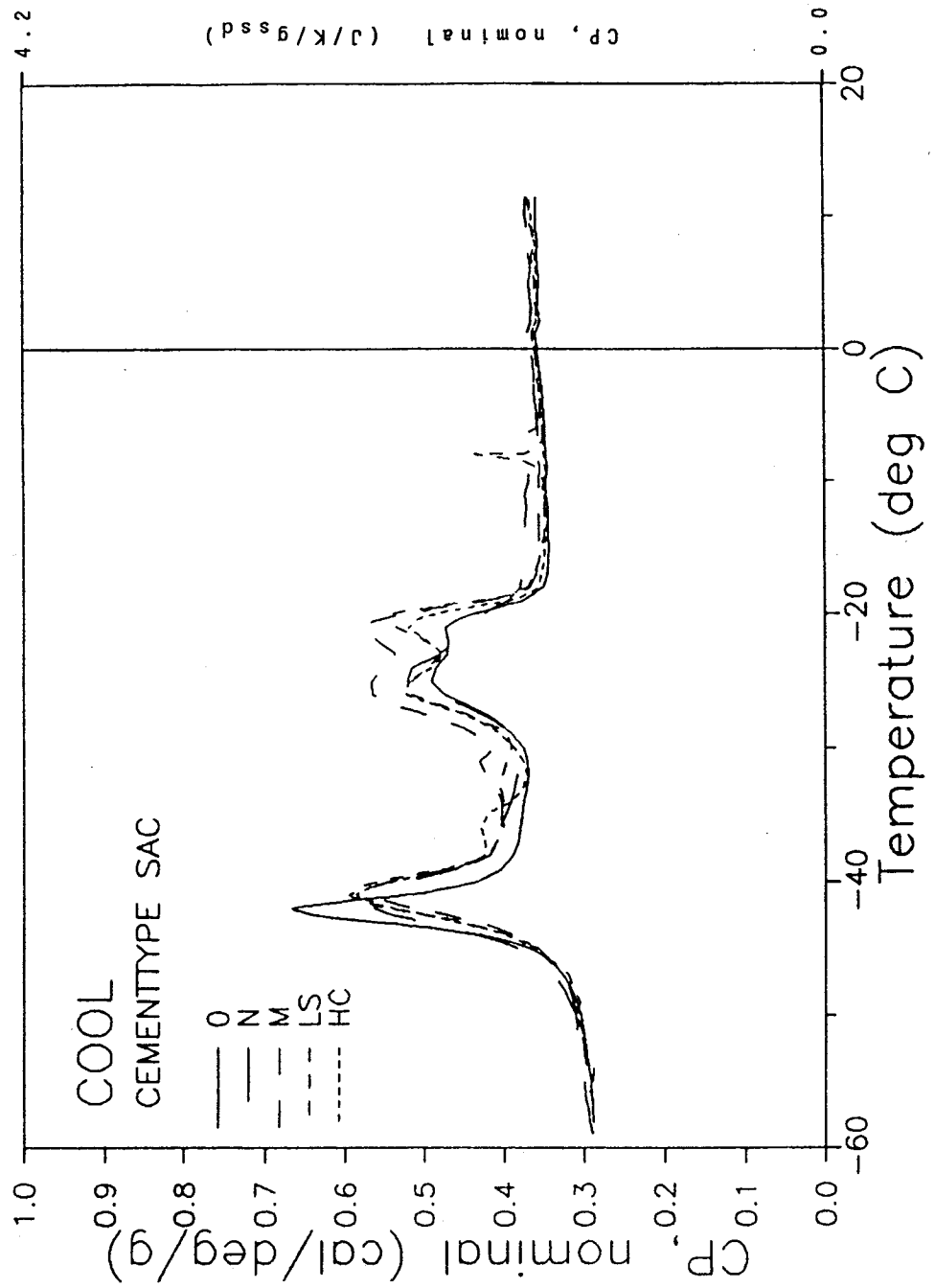

Figure 4.4.2B: Heat capacity during cooling for mature, virgin cured 0.4 W/C SAC-paste. Effect of different additives is shown.

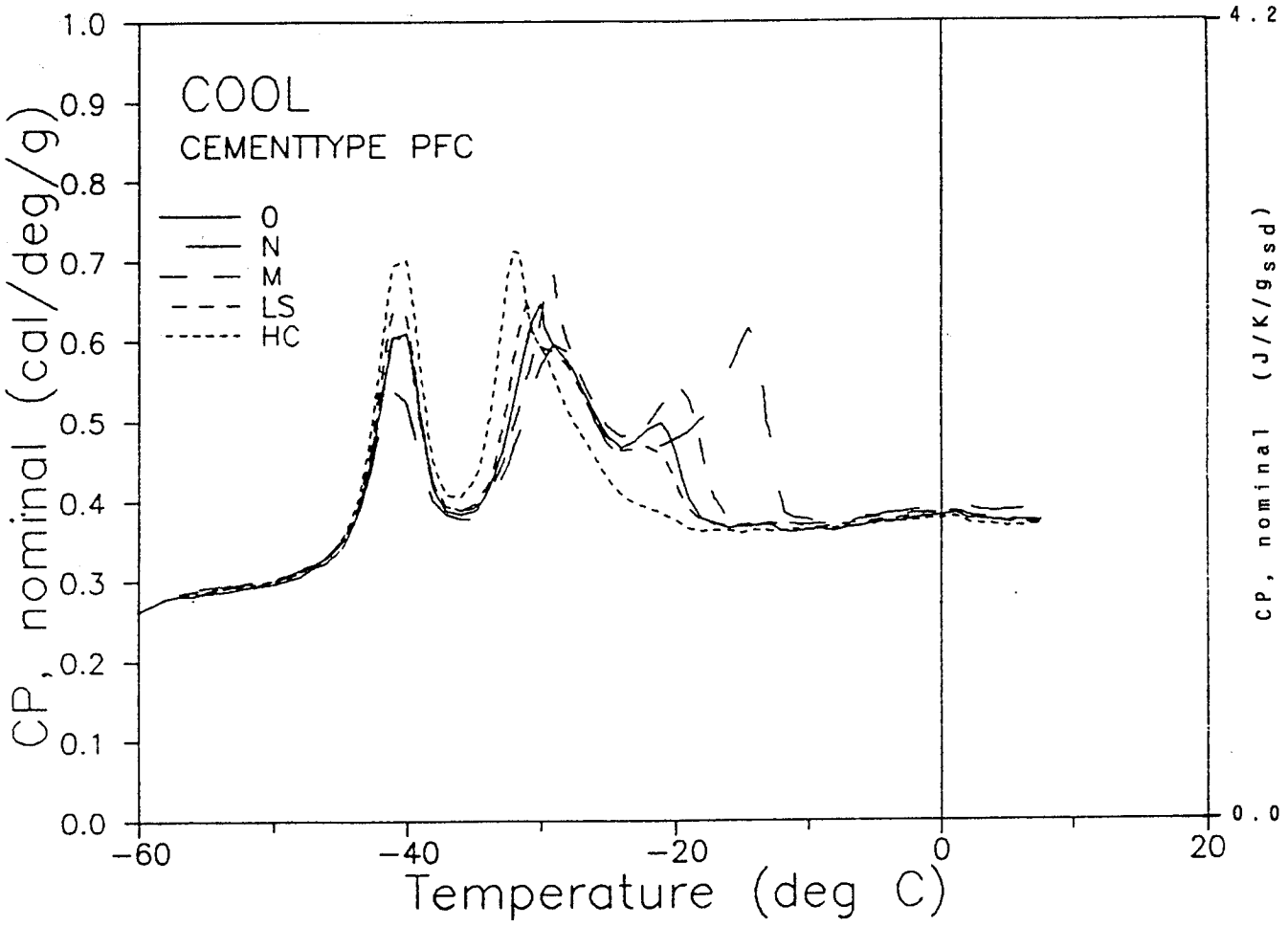

Figure 4.4.2C: Heat capacity during cooling for mature, virgin cured 0.4 W/C PFC-paste. Effect of different additives is shown.

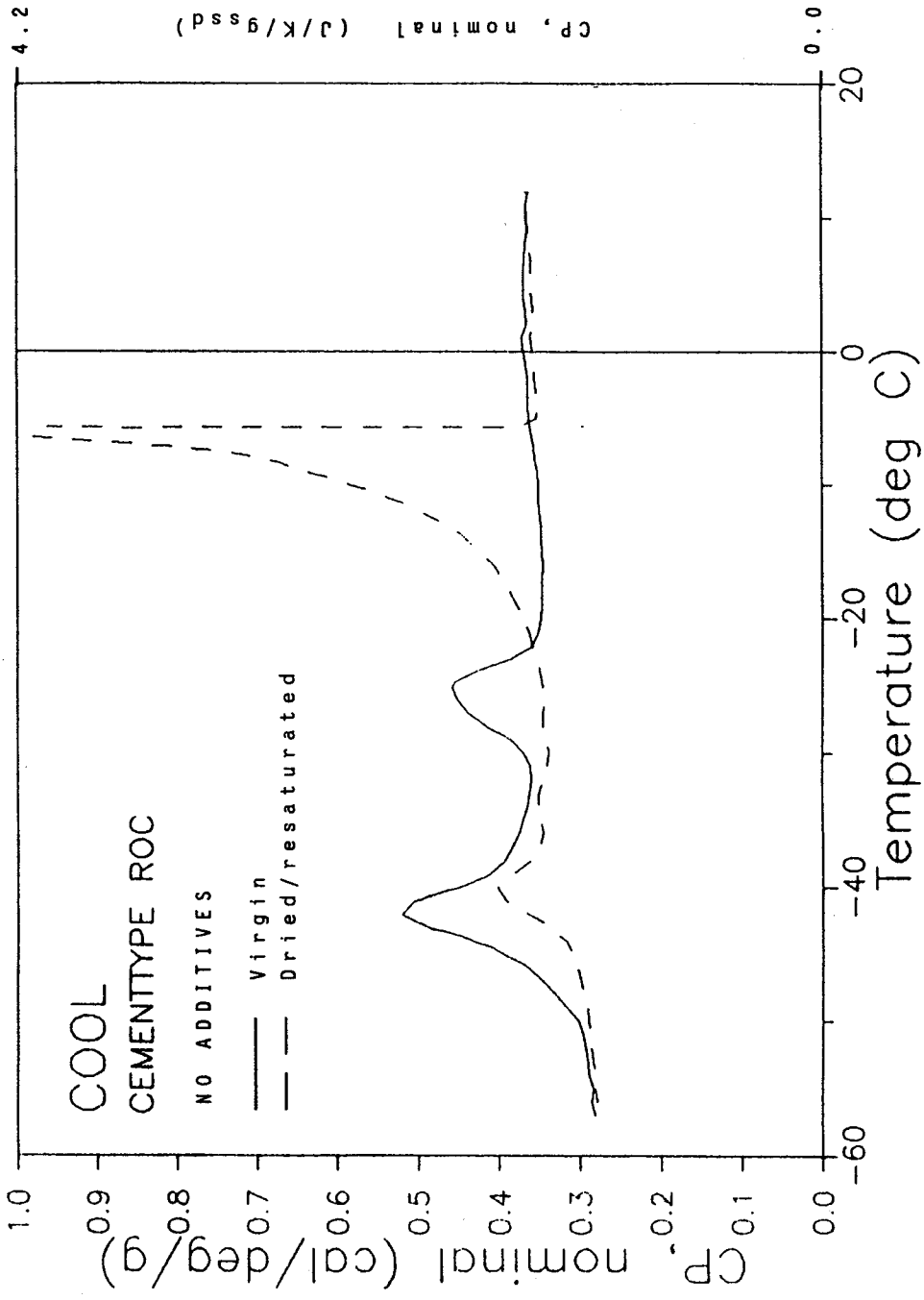

Figure 4.4.3A: Heat capacity during cooling for mature, 0.4 W/C ROC-paste. Effect of conditioning (drying/resaturation) is shown.

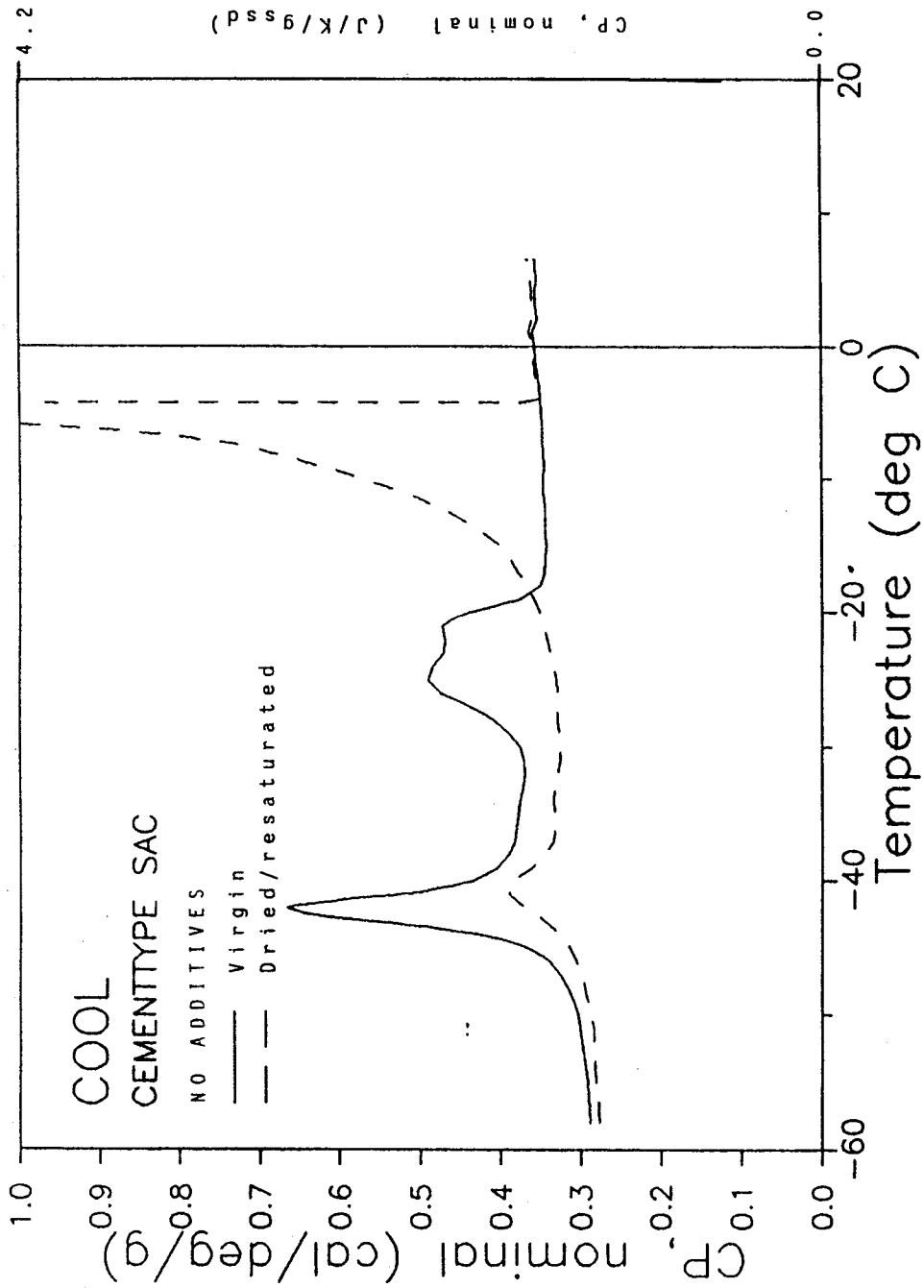

Figure 4.4.3B: Heat capacity during cooling for mature, 0.4 W/C SAC-paste. Effect of conditioning (drying/resaturation) is shown.

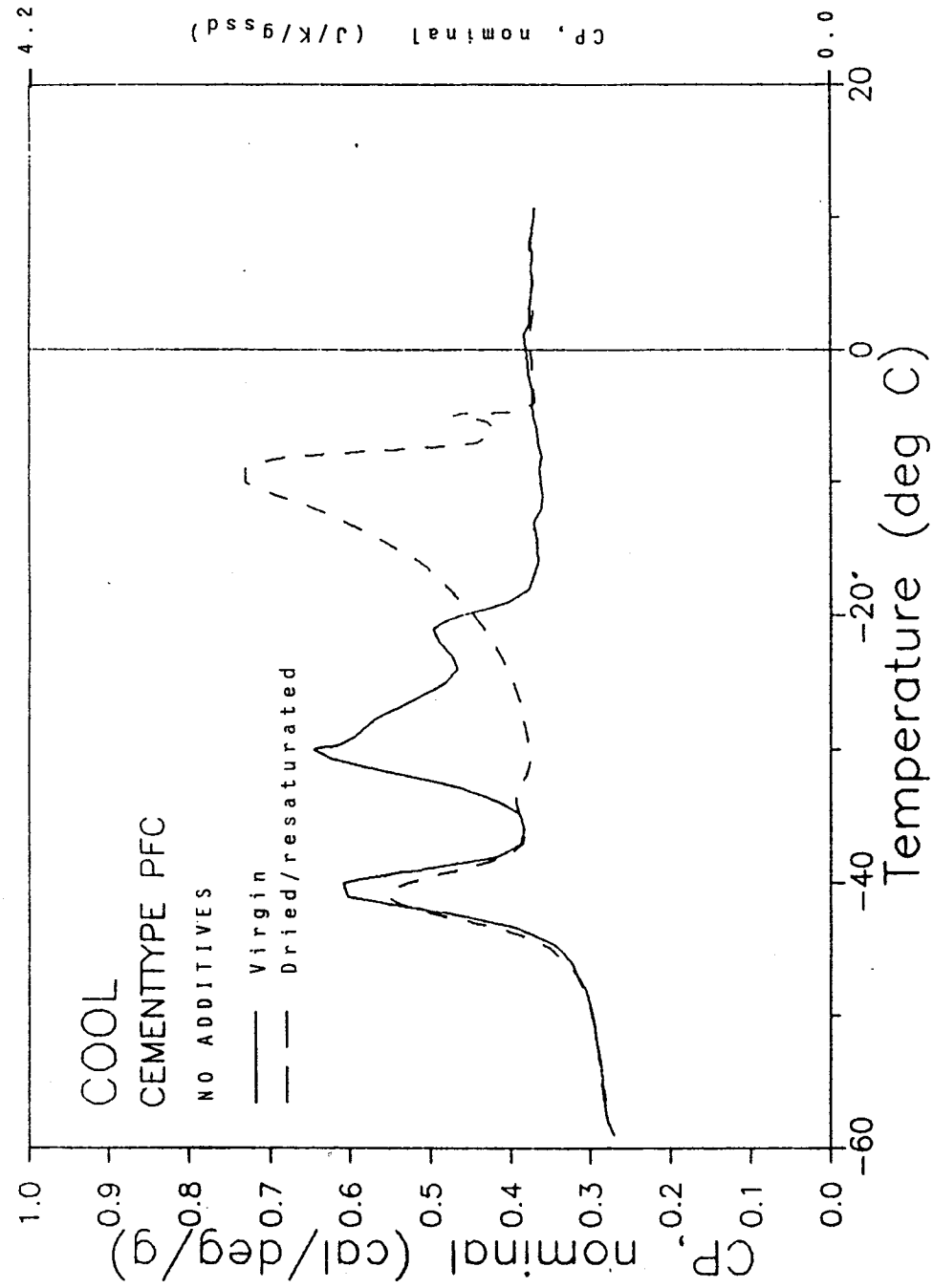

Figure 4.4.3C: Heat capacity during cooling for mature, 0.4 W/C PFC-paste. Effect of conditioning (drying/resaturation) is shown.

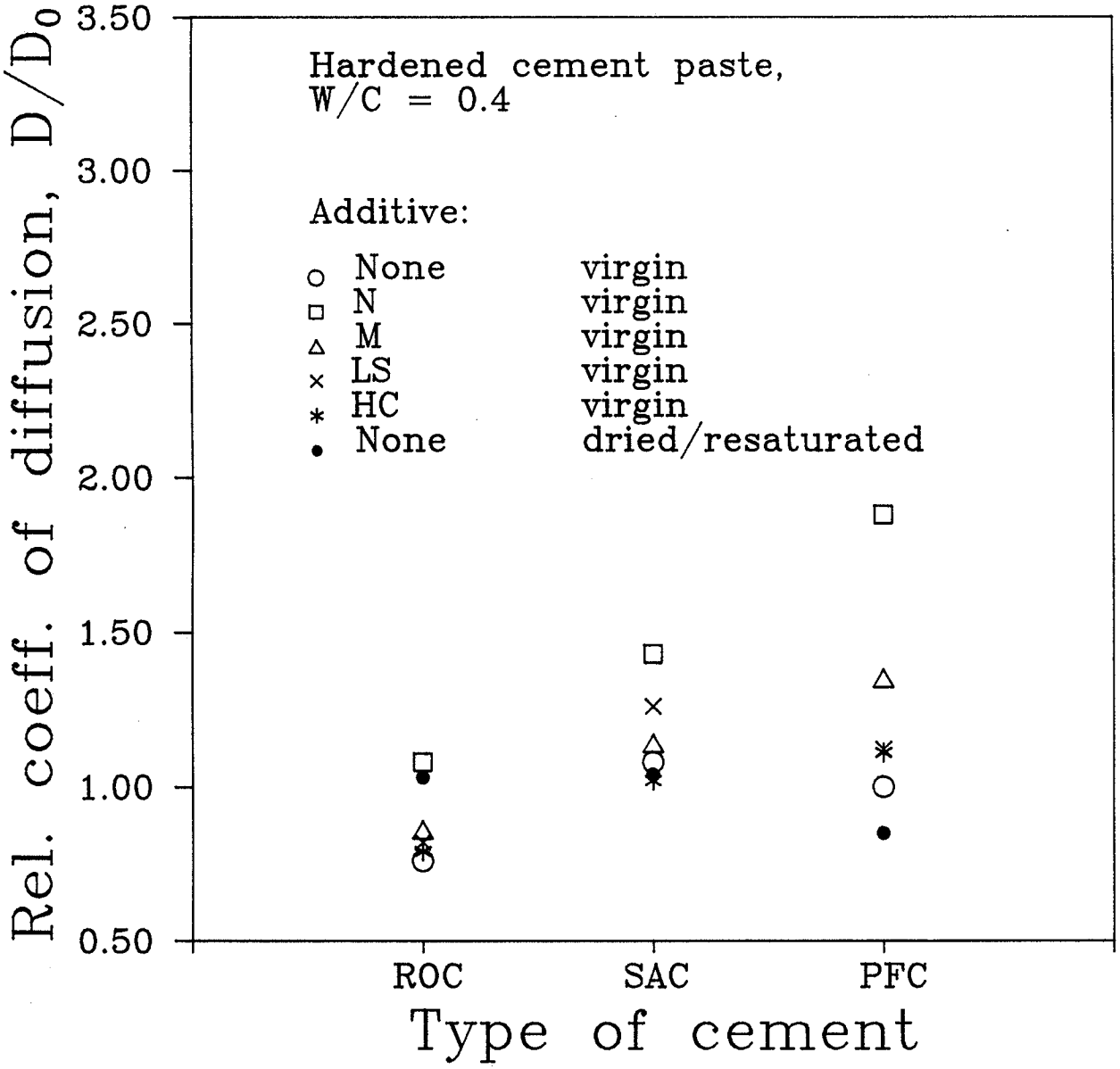

Figure 4.4.4:

Relative water vapour diffusion coefficients calculated from drying test results at 11 % r.h. performed on mature 0.4 W/C cement pastes. Effect of cementtype, additive and conditioning (drying/resaturation) is shown.

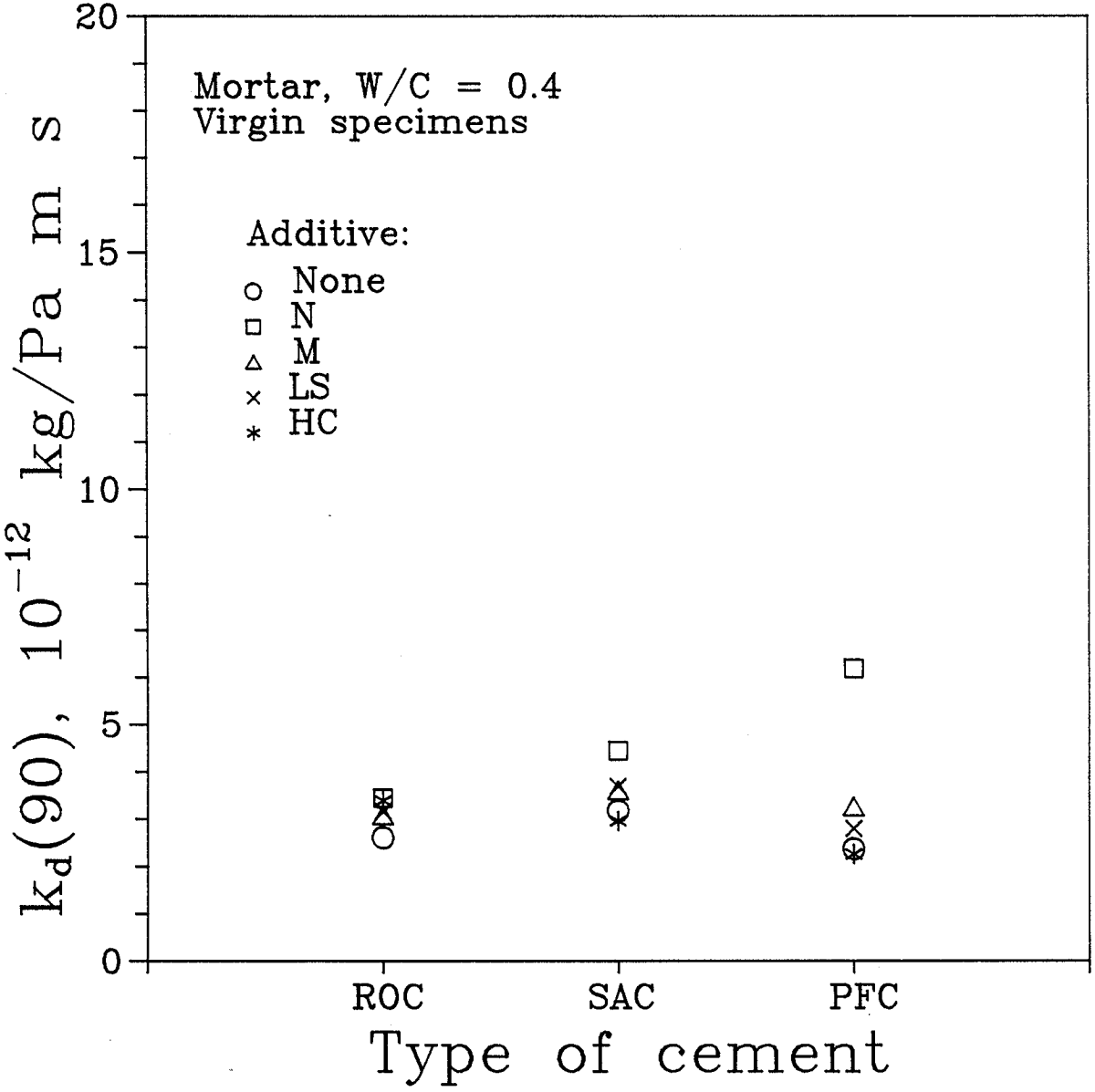

Figure 4.5.1A:

Water vapour diffusion coefficients, $k_d(90)$, calculated from CUP-results. The effect of cementtype and additive is shown. Data from /12/.

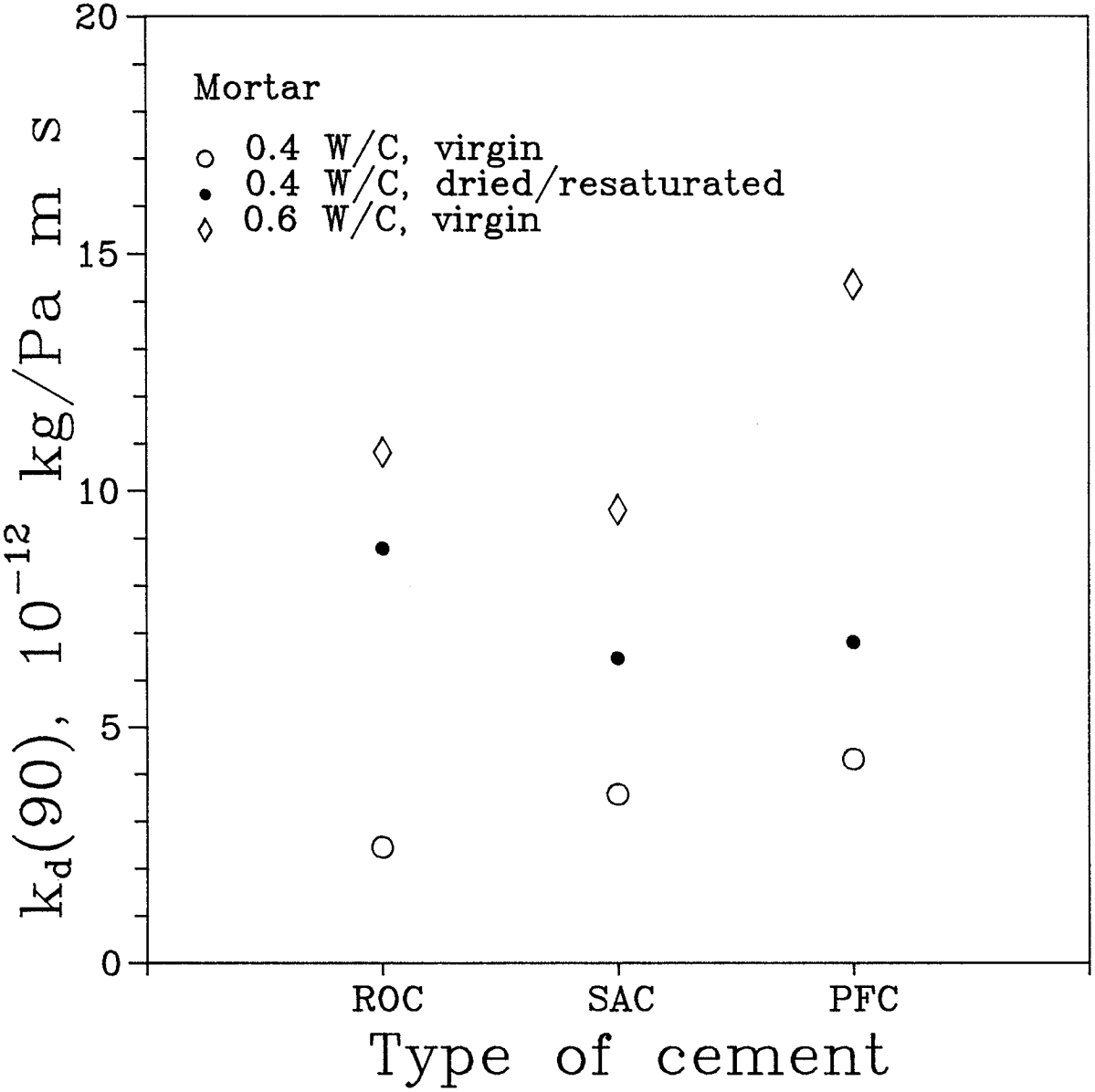

Figure 4.5.1B:

Water vapour diffusion coefficients, $k_d(90)$, calculated from CUP-results. The effect of cementtype, W/C and conditioning (drying/resaturation) is shown. Data from /13/.

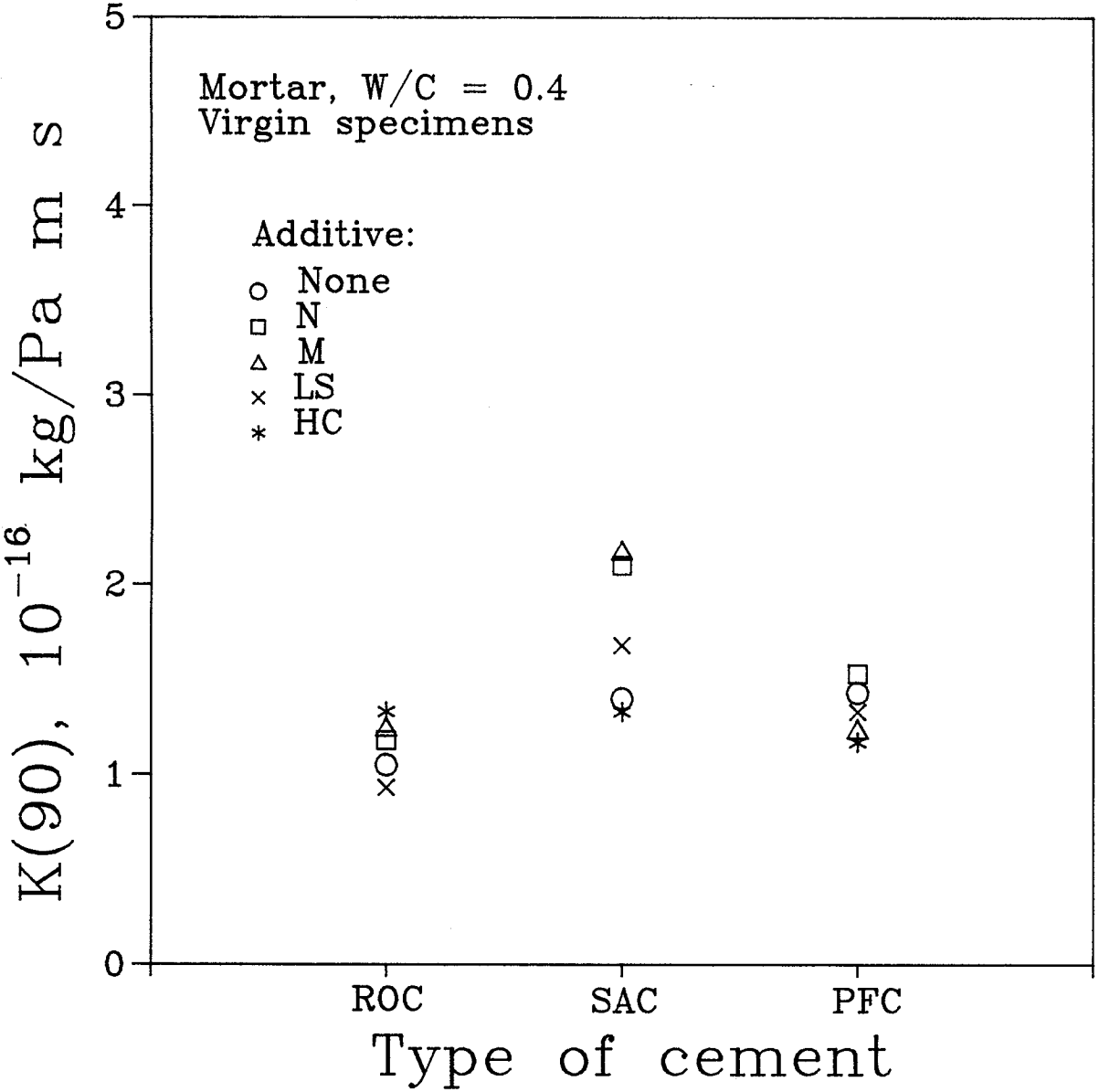

Figure 4.5.2A:

Water permeability coefficients, K(90), calculated from CUP-results. The effect of cementtype and additive is shown. Data from /12/.

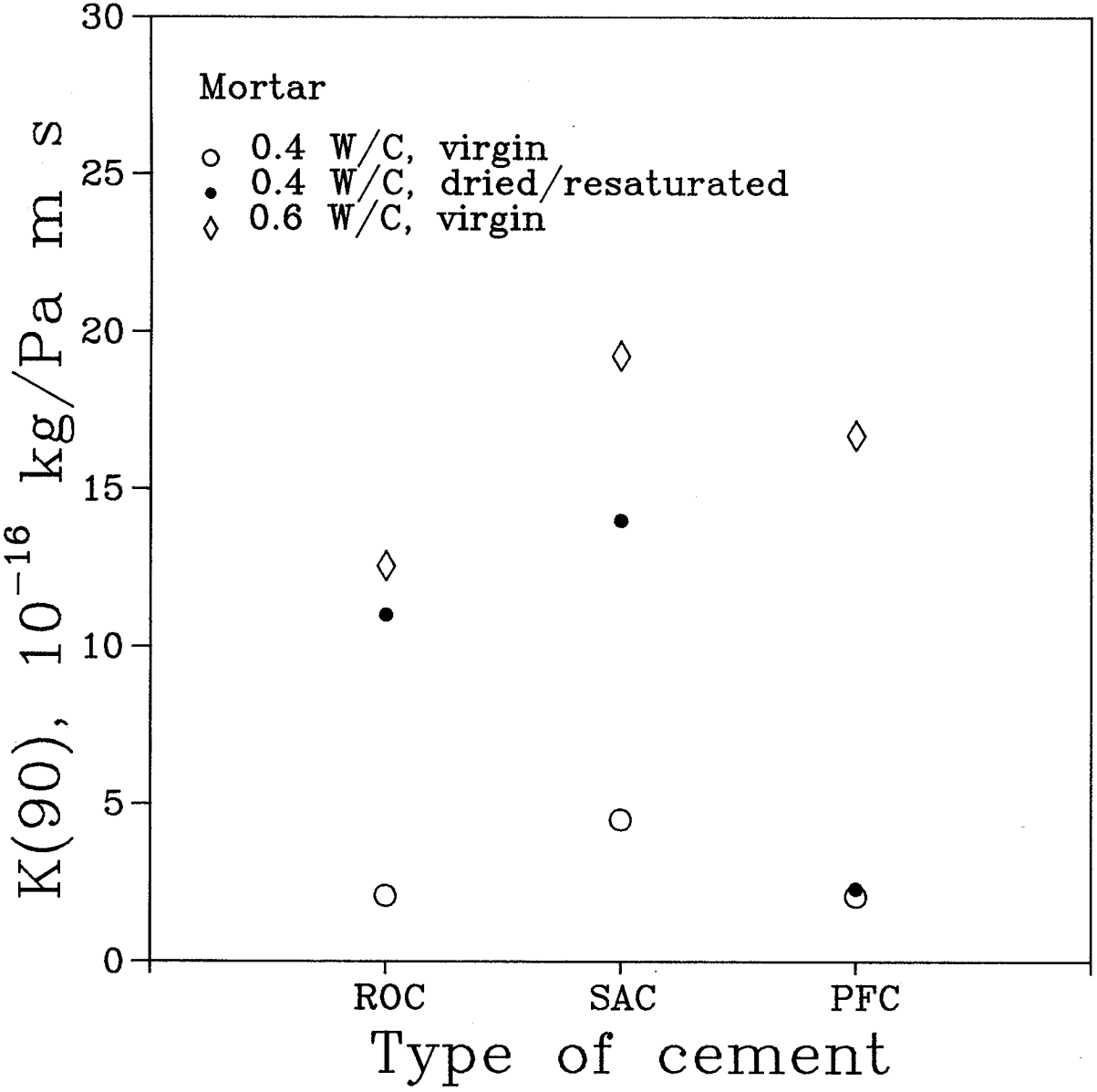

Figure 4.5.2B:

Water permeability coefficients, K(90), calculated from CUP-results. The effect of cement type, W/C and conditioning (drying/resaturation) is shown. Data from /13/.

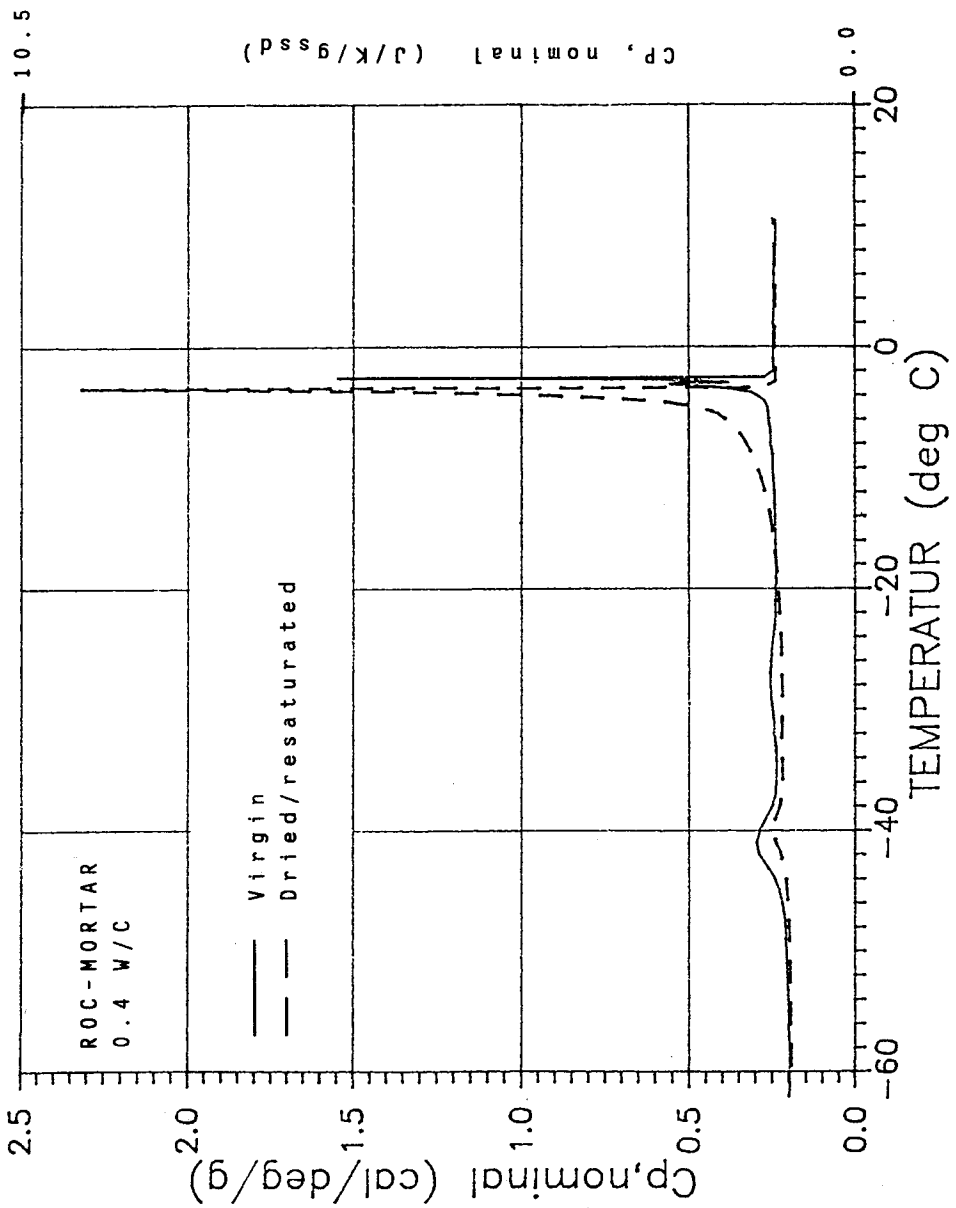

Figure 4.5.3A: Heat capacity during cooling for mature, 0.4 W/C ROC-mortar. Effect of conditioning (drying/resaturation) is shown. Data from /13/.

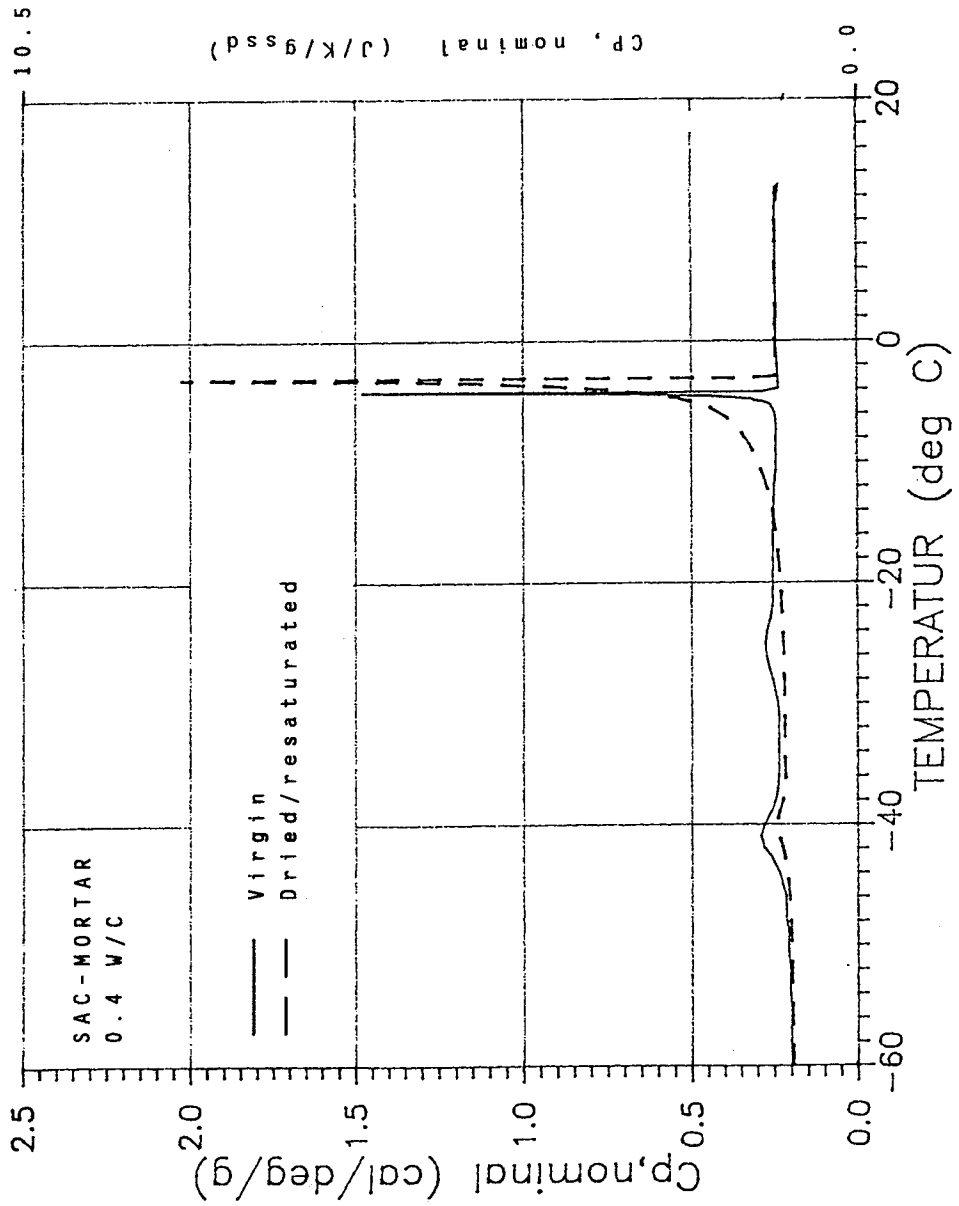

Figure 4.5.38: Heat capacity during cooling for mature, 0.4 W/C SAC-mortar. Effect of conditioning (drying/resaturation) is shown. Data from /13/.

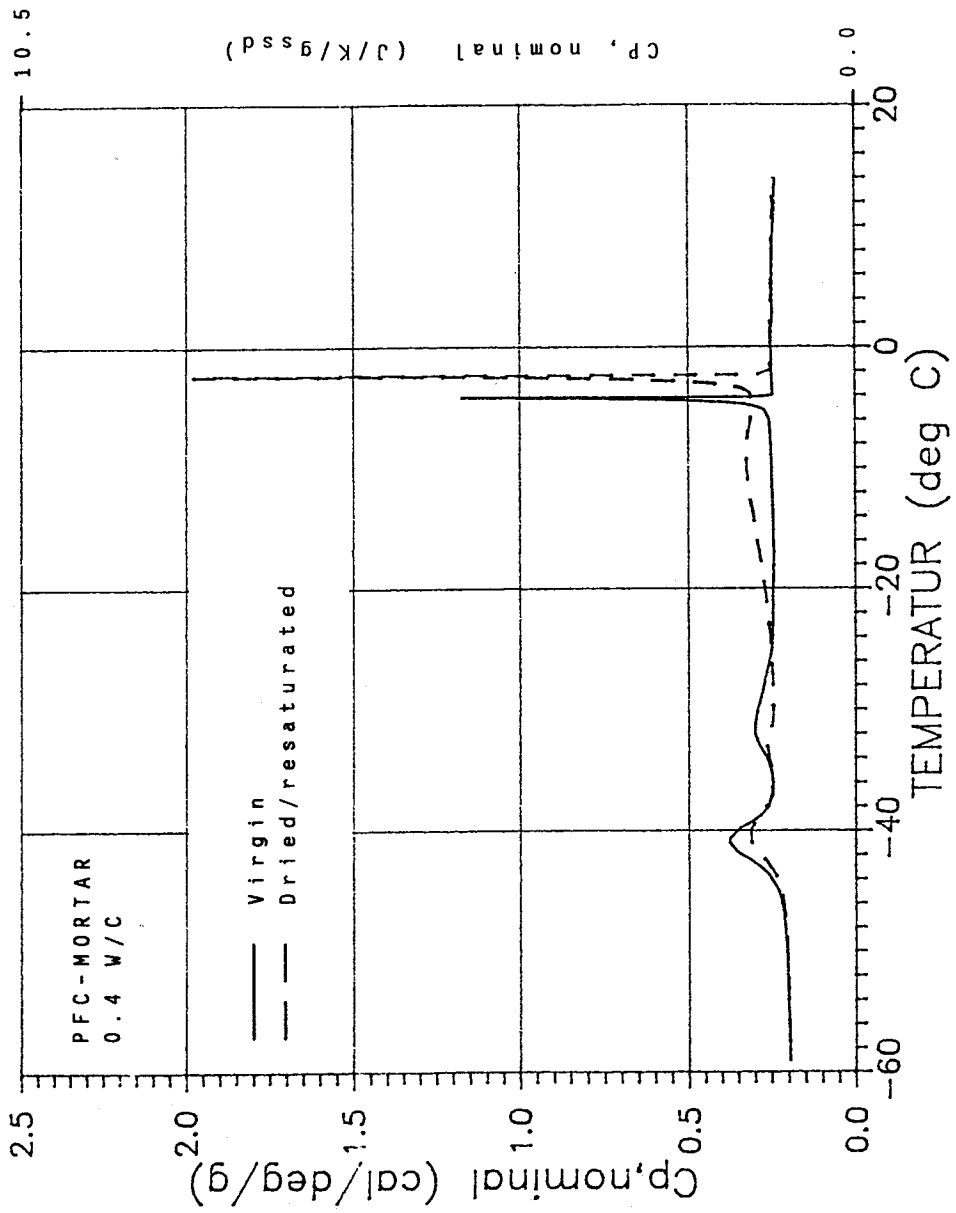

Figure 4.5.3C: Heat capacity during cooling for mature, 0.4 W/C PFC-mortar. Effect of conditioning (drying/resaturation) is shown. Data from /13/.

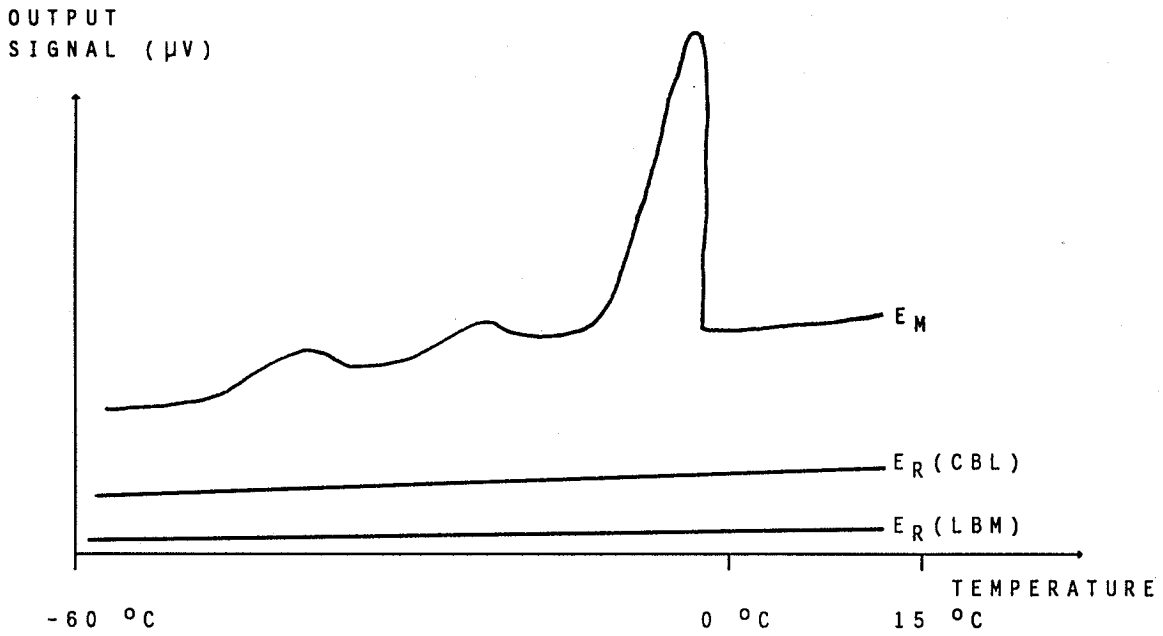

Figure 5.1.1.1: Explanation for differences in heat capacity levels at LBM and CBL.

E_M: output signal from measurement cell
E_R: output signal from reference cell
E_i: differential output signal = E_M - E_R, proportional to the heat capacity.

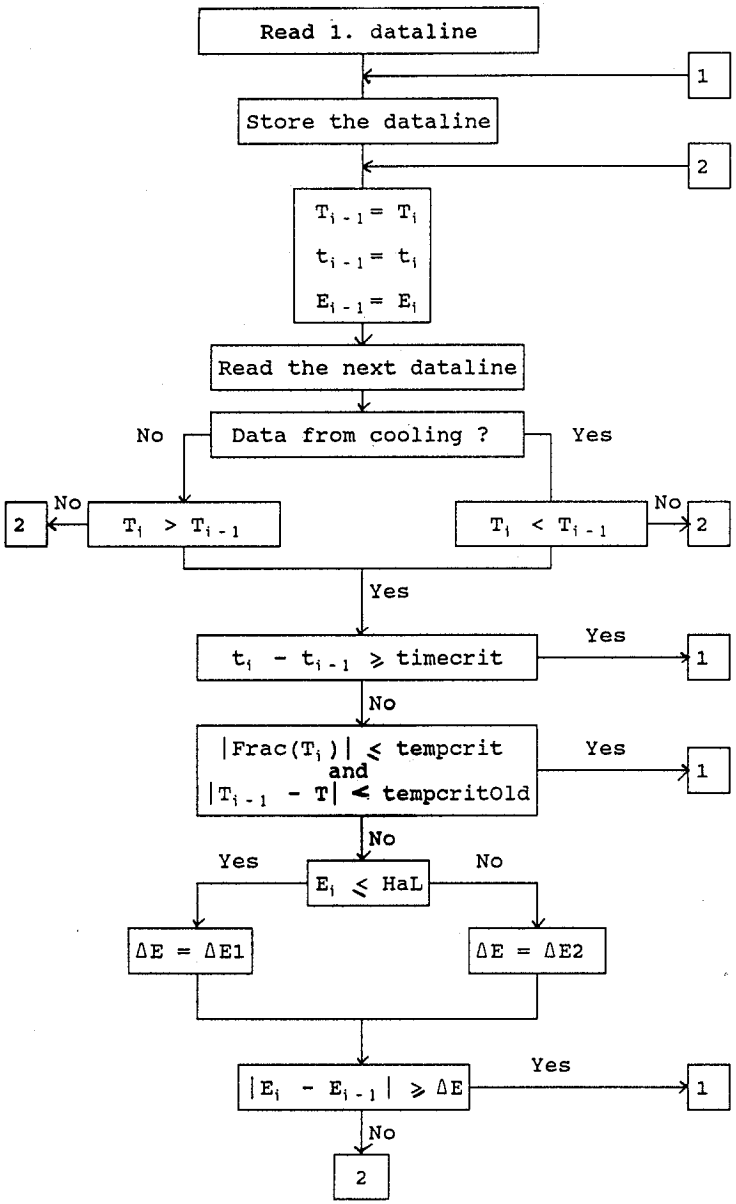

Figure 5.1.1.2A: Procedure and criteria for sorting data from CAL at CBL.

T_i = temperature (°C)
t_i = time (sec)
E_i = 1/10 of the differential output signal (μV)

Standard values (optional):

timecrit	=	1200 sec
tempcrit	=	0.02 °C
tempcritOld	=	0.10 °C
HaL	=	450 μV
$\Delta E1$	=	10 μV
$\Delta E2$	=	17 μV

[a]) **Time criterion:**
More than 1200 seconds ("timecrit") has elapsed since the last set of data was stored.

[b]) Temperature criterion:
The temperature is an integer. Integer temperature is defined when the numerical, fractional value of the actual temperature is less than 0.02 °C ("tempcrit"). Furthermore, this criterion should only be decisive if the numerical temperature change from the previous stored temperature is more than 0.10 °C ("tempcritOld").

[c]) Output signal criterion:
In regions of normal activity ($E_i \leq$ 450 μV ("HaL")):
E_i changes at least 10 μV ("ΔE1").
In regions of high activity ($E_i >$ 450 μV):
E_i changes at least 17 μV ("ΔE2").
At CBL, the differential output signal is diminished by 10, electrically. Accordingly, the values used by Fontenay /18/ to establish the output signal criterion are **divided by 10.**

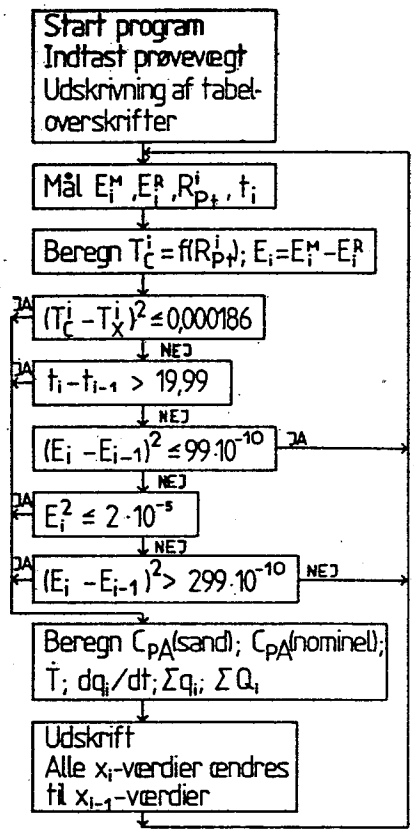

Figure 5.1.1.2B: Procedure and criteria for sorting data from CAL at LBM (Fontenay /18/).

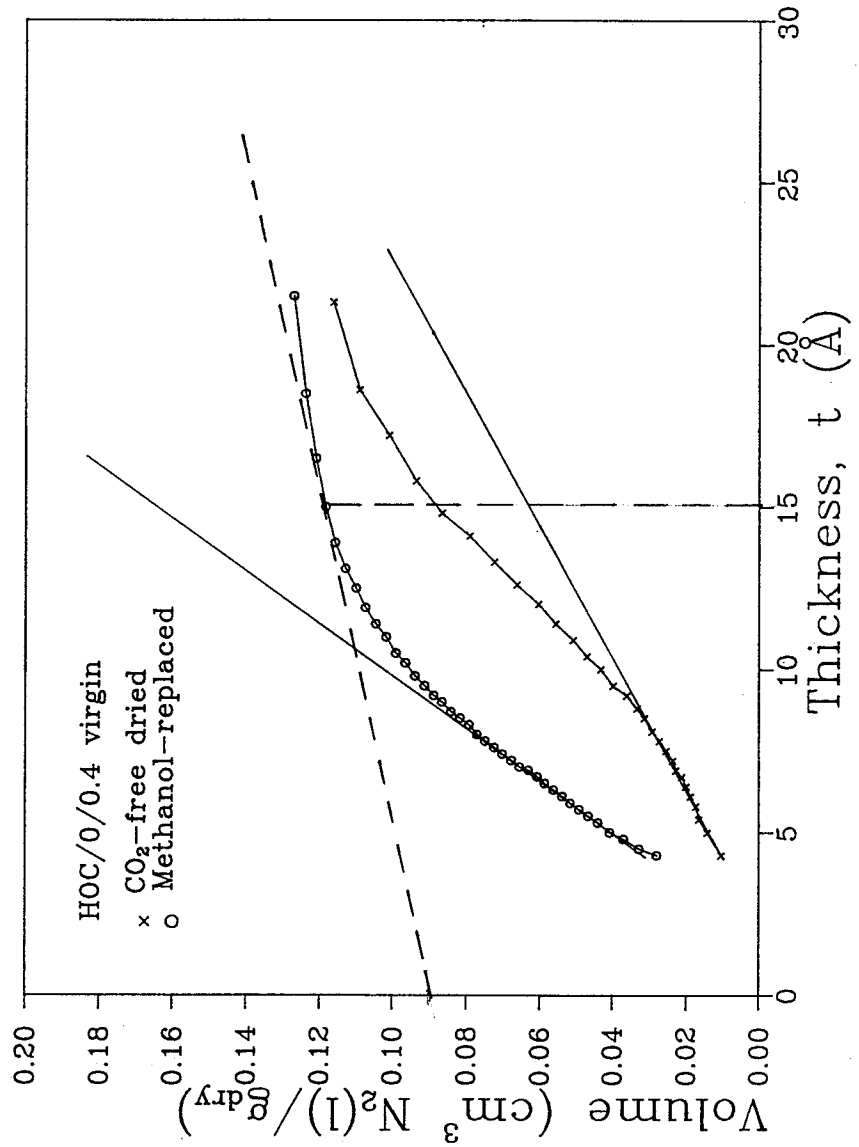

Figure 5.1.3.1A: Nitrogen volume-thickness (V-t) curves from the adsorption branch of the isotherm for very mature, virgin cured 0.4 W/C HOC-pastes. The effect of drying method is shown.

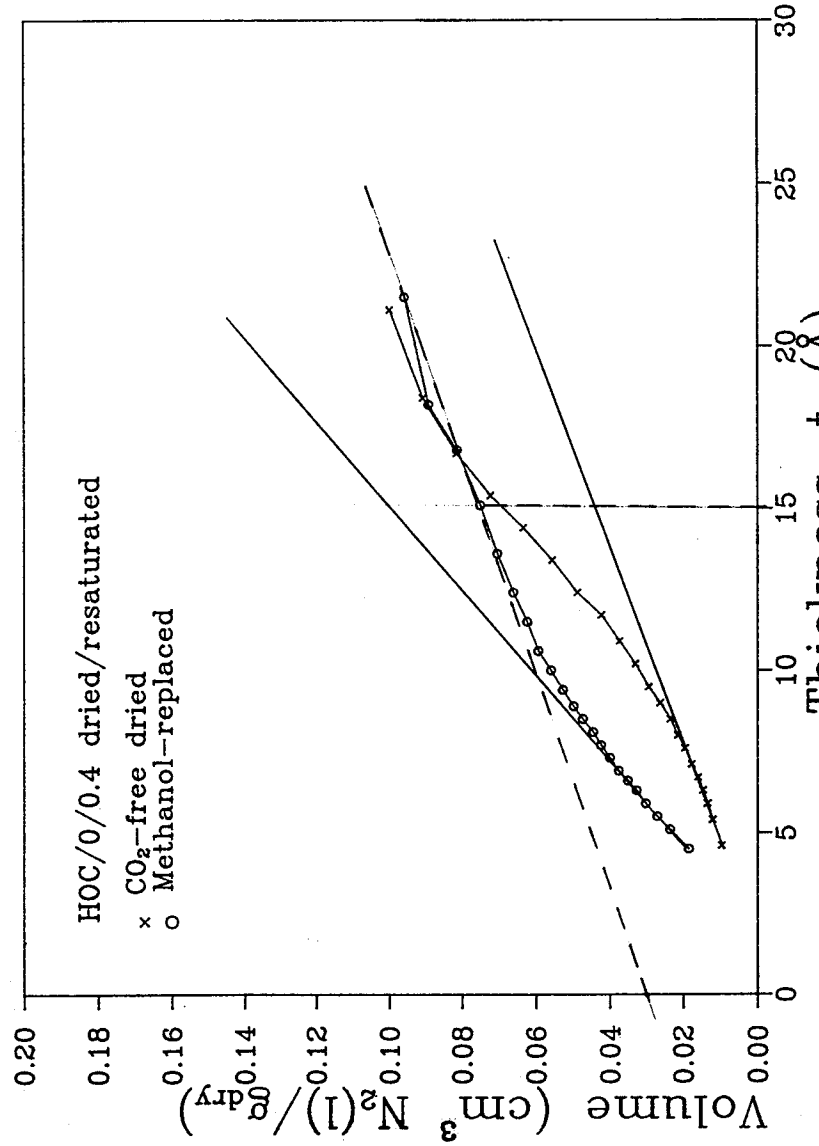

Figure 5.1.3.1B: Nitrogen volume-thickness (V-t) curves from the adsorption branch of the isotherm for very mature, conditioned (dried/resaturated) 0.4 W/C HOC-pastes. The effect of drying method is shown.

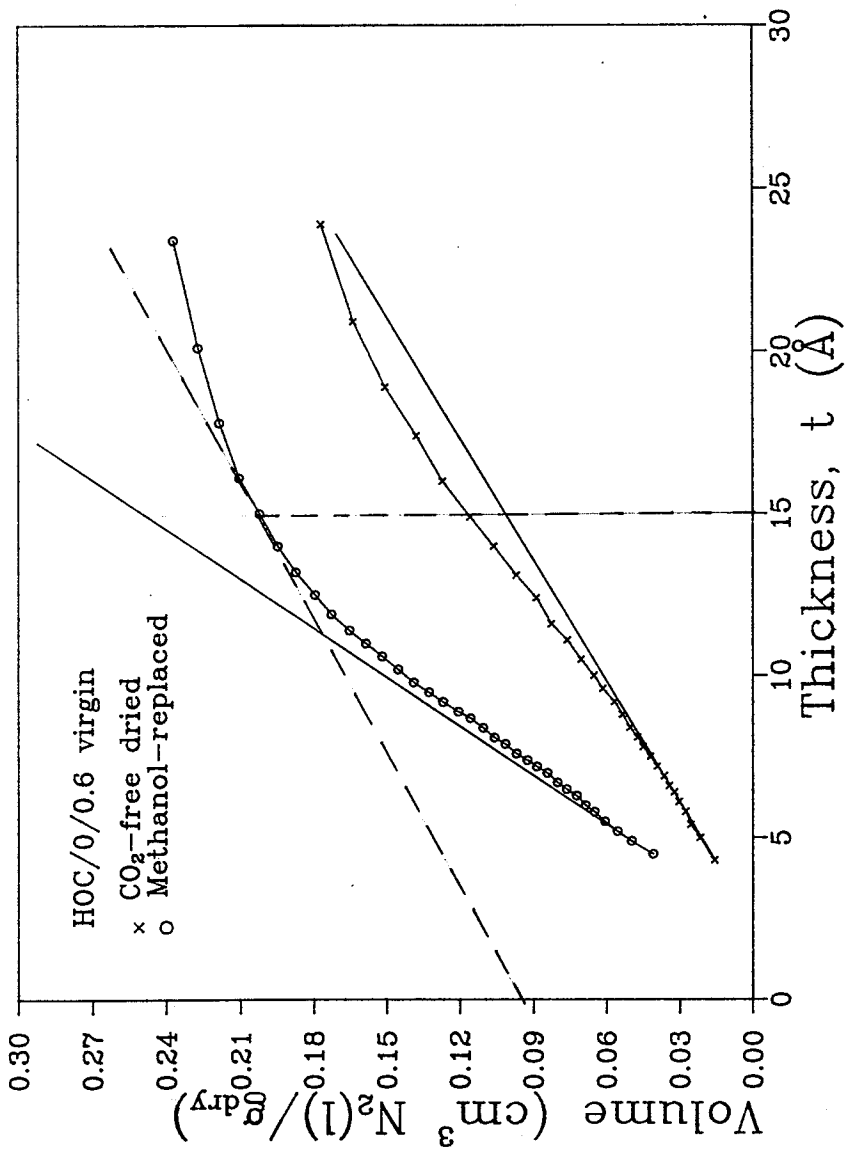

Figure 5.1.3.1C: Nitrogen volume-thickness (V-t) curves from the adsorption branch of the isotherm for very mature, virgin cured 0.6 W/C HOC-pastes. The effect of drying method is shown.

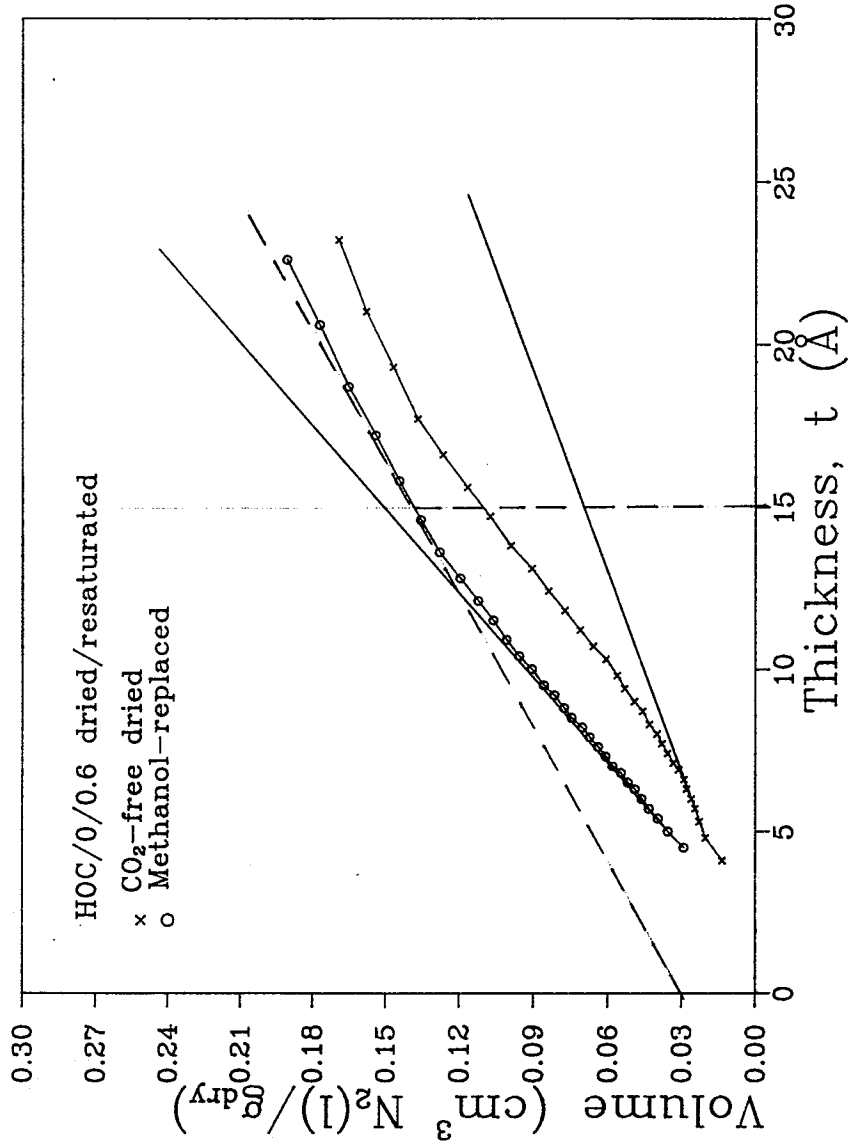

Figure 5.1.3.1D: Nitrogen volume-thickness (V-t) curves from the adsorption branch of the isotherm for very mature, conditioned (dried/resaturated) 0.6 W/C HOC-pastes. The effect of drying method is shown.

Figure 5.1.3.2:

a) Representative Volume-thickness (V-t) plots. Curves A, B and C.

b) Definition of micropore volume

The adsorbate can exist:

- as monolayer/multilayers on the free surface of othervise empty pores (FS)
- in filled micropores (MP)
- as capillary condensate (KCC)

Non-intersecting, open-ended pores.

Only sequential - not simultaneous - micropore filling and capillary condensation is acceptable.

The slope of the initial straight line is equal to total surface area (S_{Vt}).

a)

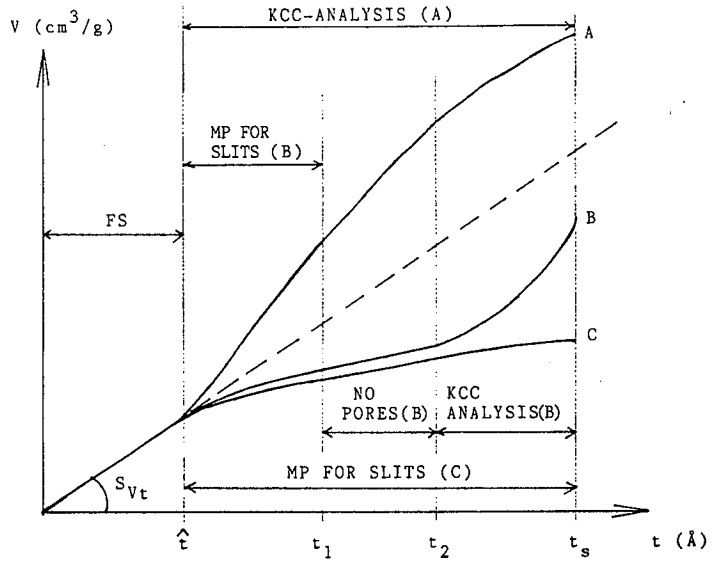

b)

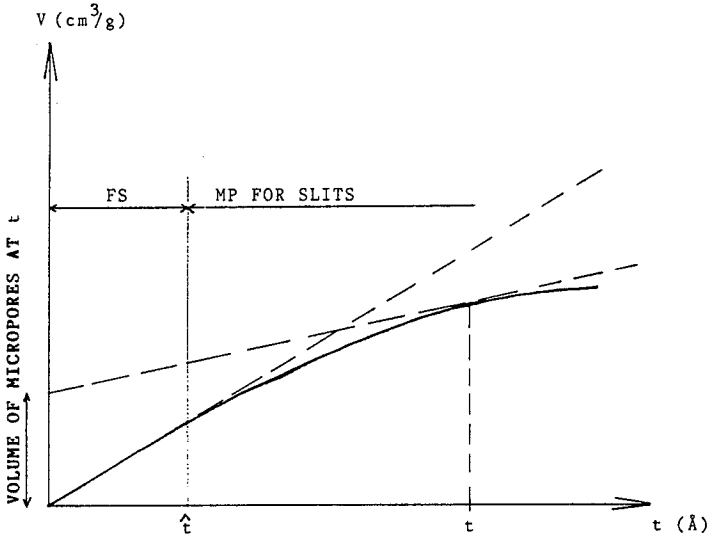

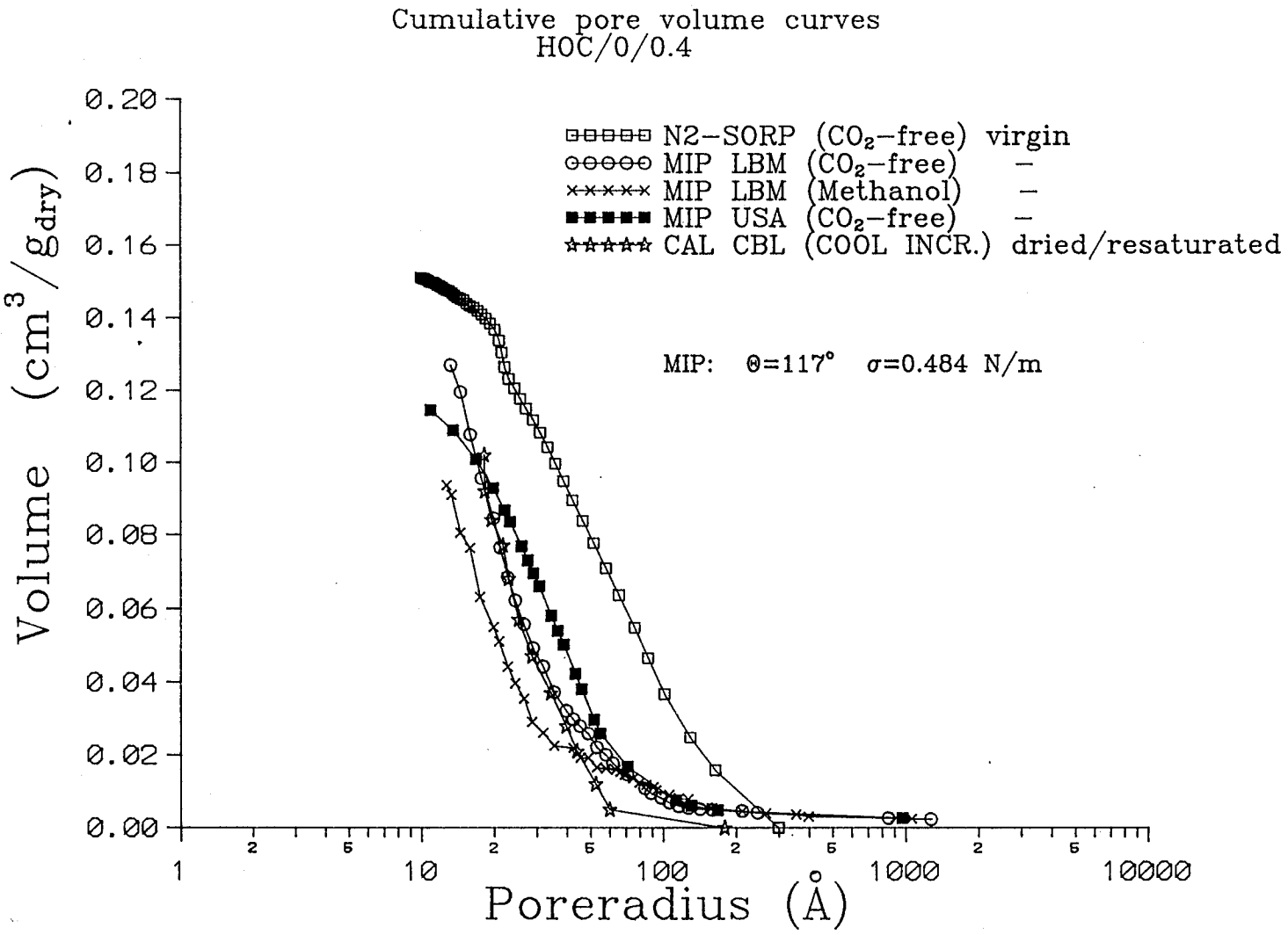

Figure 5.5.1A: Cumulative pore size distributions calculated from N2-SORP, MIP and CAL for very mature 0.4 W/C HOC-paste. A contact angle of 117° was used for MIP. N2-SORP- and MIP-specimens were CO_2-free dried from water- or methanol-saturated state. CAL-specimen was dried (50 °C and 11 % RH for 3 days) and resaturated.

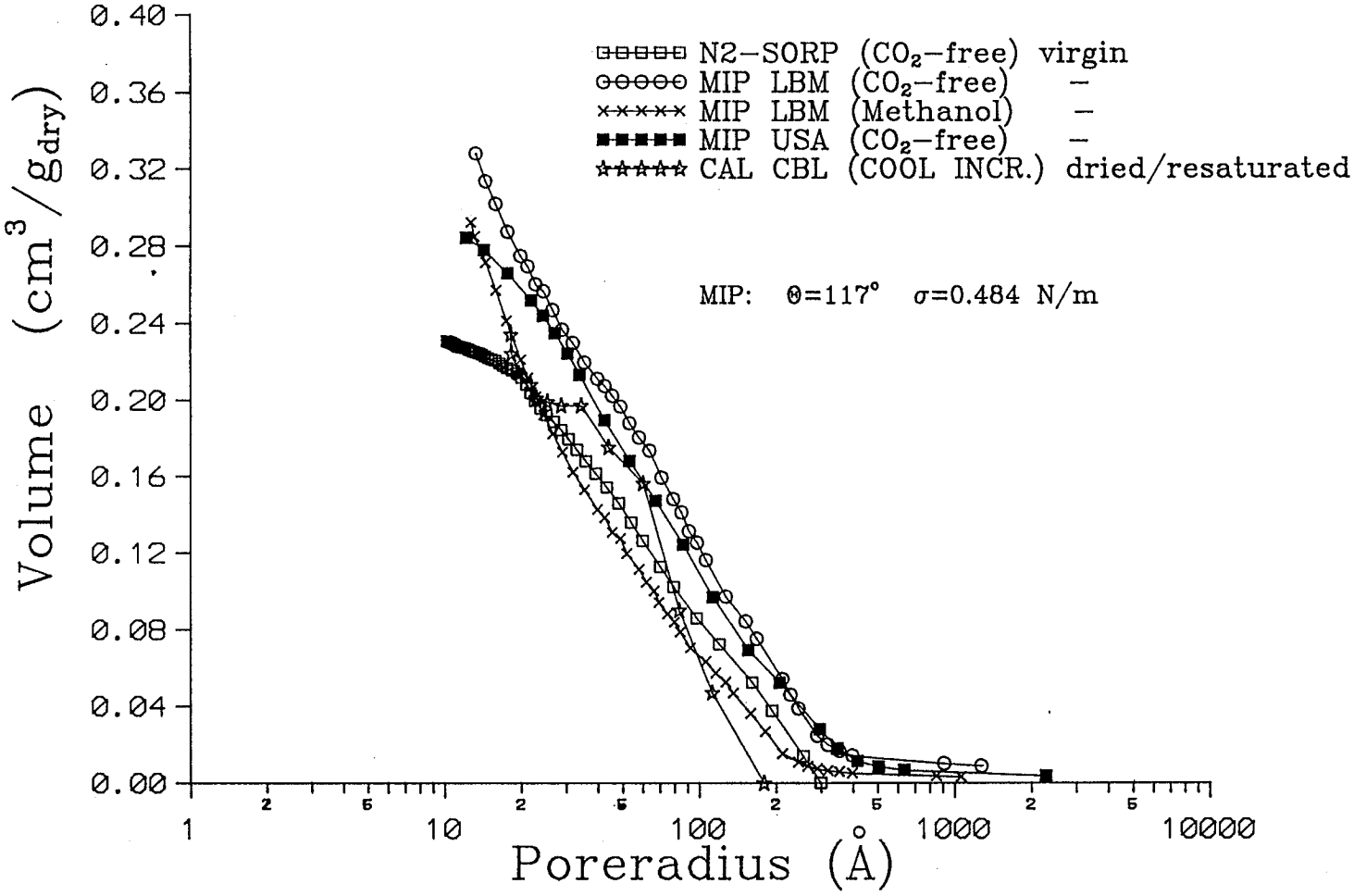

Figure 5.5.1B: Cumulative pore size distributions calculated from N2-SORP, MIP and CAL for very mature 0.6 W/C HOC-paste
A contact angle of 117° was used for MIP.
N2-SORP- and MIP-specimens were CO_2-free dried from water- or methanol-saturated state.
CAL-specimen was dried (50 °C and 11 % RH for 3 days) and resaturated.